

# Implementation and Thickness Optimization of Perpetual Pavements in Ohio

Shad Sargand, Issam Khoury, Ben Jordan, Matthew Scheer, and Paul Cichocki



for the Ohio Department of Transportation  
Office of Statewide Planning and Research

and the  
United States Department of Transportation  
Federal Highway Administration

State Job Number 465970

June 2015

*Final Report*



**OHIO**  
UNIVERSITY



**Ohio Research Institute for  
Transportation and the Environment**

<b>1. Report No.</b> FHWA/OH-2015/17	<b>2. Government Accession No.</b>	<b>3. Recipient's Catalog No.</b>	
<b>4. Title and Subtitle</b> Implementation and Thickness Optimization of Perpetual Pavements in Ohio		<b>5. Report Date</b> June 2015	
		<b>6. Performing Organization Code</b>	
<b>7. Author(s)</b> Shad Sargand, Issam Khoury, Ben Jordan, Matthew Scheer, and Paul Cichocki		<b>8. Performing Organization Report No.</b>	
<b>9. Performing Organization Name and Address</b> Ohio Research Institute for Transportation and the Environment (ORITE) 151 Stocker Center 1 Ohio University Athens OH 45701-2979		<b>10. Work Unit No. (TRAIS)</b>	
		<b>11. Contract or Grant No.</b> State Job No. 465970	
<b>12. Sponsoring Agency Name and Address</b> Ohio Department of Transportation Office of Statewide Planning and Research 1980 West Broad St. Columbus OH 43223		<b>13. Type of Report and Period Covered</b> Final Report	
		<b>14. Sponsoring Agency Code</b>	
<b>15. Supplementary Notes</b> Prepared in cooperation with the Ohio Department of Transportation (ODOT) and the U.S. Department of Transportation, Federal Highway Administration			
<b>16. Abstract</b> <p>This report documents the performance of perpetual pavement structures constructed by the Ohio Department of Transportation. Three perpetual pavement test sections on U.S. Route 23 in Delaware, Ohio (DEL-23) were constructed with AC thicknesses 11 in (28 cm), 13 in (33 cm), 15 in (38 cm) and instrumented to detect strains in Fatigue Resistant Layer (FRL) and base layers, deflections, temperatures, and subgrade pressures. Strains at bottom of FRL during Controlled Vehicle Load (CVL) testing in summer indicated the 13 in (33 cm) section on stabilized subgrade and 15 in (38 cm) section on compacted subgrade met perpetual criteria, while 11 in (28 cm) section on stabilized subgrade did not. Computer simulation of DEL-23 sections with PerRoad confirmed these findings, but also indicated the 11 in (28 cm) section would meet perpetual pavement criteria.</p> <p>Test pavements were built in the Accelerated Pavement Load Facility (APLF) and instrumented similarly to DEL-23. The sections were thinner, but included Highly Modified Asphalt (HiMA) with Kraton polymer binder in sections of depth 8 in (20 cm), 9 in (23 cm), 10 in (25 cm), and 11 in (28 cm), the last using conventional asphalt in the base as a control with HiMA in upper layers. There was no FRL. The 10 in (25 cm) and 11 in (28 cm) sections met perpetual criteria even when heated through to 100°F (37.8°C). After enduring 10,000 passes of 9000 lb (40 kN) load at 5 mph (8 km/h), the surface rutting was measured with a profilometer and was considerably below even the ODOT threshold for "low rutting" (0.125 in or 0.32 cm). An extrapolation of the curve fit suggested the HiMA surface would remain under the low rutting threshold much longer than conventional or WMA surfaces. Note these sections were built under ideal conditions, so field experience may differ.</p> <p>Fatigue endurance limit was computed using parameters measured in the laboratory asphalt mixture performance tester from samples collected from DEL-23 and APLF. Endurance limits computed following the NCHRP Project 9-44A method and MEPDG guide (<math>E_0=E^*</math>) provided a good fit with field results.</p> <p>Ten high-performing existing AC pavements from a previous forensic study (Sargand and Edwards, 2010) were further evaluated as potential perpetual pavements. Follow-up field investigations at each site included distress surveys, falling weight deflectometer (FWD) measurements, dynamic cone penetrometer (DCP) data, and Portable Seismic Property Analyzer (PSPA) measurements. Strains at the bottom of the asphalt were back calculated from FWD deflections using the elastic modulus program Evercalc. AC cores were collected and tested for indirect tensile strength and resilient modulus. The pavements were modeled using finite element software Abaqus, which confirmed the Evercalc strain computations. Of the ten pavements, seven appeared to meet conservative perpetual pavement strain criteria, one could be upgraded to meet perpetual pavement criteria by adding an additional asphalt layer, and two clearly did not meet perpetual pavement standards. A brief report on the status of previous perpetual pavement designs built in Stark County (STA-77) and Wayne County (WAY-30) is given.</p>			
<b>17. Key Words</b> Perpetual Pavement, asphalt endurance limit, accelerated pavement testing, pavement instrumentation		<b>18. Distribution Statement</b> No Restrictions. This document is available to the public through the National Technical Information Service, Springfield, Virginia 22161	
<b>19. Security Classif. (of this report)</b> Unclassified	<b>20. Security Classif. (of this page)</b> Unclassified	<b>21. No. of Pages</b> 308	<b>22. Price</b>

# SI\* (MODERN METRIC) CONVERSION FACTORS

APPROXIMATE CONVERSIONS TO SI UNITS				APPROXIMATE CONVERSIONS FROM SI UNITS			
Symbol	When You Know	Multiply By	To Find	Symbol	When You Know	Multiply By	To Find
<b>LENGTH</b>							
in	inches	25.4	millimeters	mm	millimeters	0.039	inches
ft	feet	0.305	meters	m	meters	3.28	feet
yd	yards	0.914	meters	m	meters	1.09	yards
mi	miles	1.61	kilometers	km	kilometers	0.621	miles
<b>AREA</b>							
in <sup>2</sup>	square inches	645.2	square millimeters	mm <sup>2</sup>	square millimeters	0.0016	square inches
ft <sup>2</sup>	square feet	0.093	square meters	m <sup>2</sup>	square meters	10.764	square feet
yd <sup>2</sup>	square yards	0.836	square meters	m <sup>2</sup>	square meters	1.195	square yards
ac	acres	0.405	hectares	ha	hectares	2.47	acres
mi <sup>2</sup>	square miles	2.59	square kilometers	km <sup>2</sup>	square kilometers	0.386	square miles
<b>VOLUME</b>							
fl oz	fluid ounces	29.57	milliliters	mL	milliliters	0.034	fluid ounces
gal	gallons	3.785	liters	L	liters	0.264	gallons
ft <sup>3</sup>	cubic feet	0.028	cubic meters	m <sup>3</sup>	cubic meters	35.71	cubic feet
yd <sup>3</sup>	cubic yards	0.765	cubic meters	m <sup>3</sup>	cubic meters	1.307	cubic yards
NOTE: Volumes greater than 1000 L shall be shown in m <sup>3</sup> .							
<b>MASS</b>							
oz	ounces	28.35	grams	g	grams	0.035	ounces
lb	pounds	0.454	kilograms	kg	kilograms	2.202	pounds
T	short tons (2000 lb)	0.907	megagrams (or "metric ton")	Mg (or "t")	megagrams (or "metric ton")	1.103	short tons (2000 lb)
<b>TEMPERATURE (exact)</b>							
°F	Fahrenheit temperature	5(°F-32)/9 or (°F-32)/1.8	Celsius temperature	°C	Celsius temperature	1.8°C + 32	Fahrenheit temperature
<b>ILLUMINATION</b>							
fc	foot-candles	10.76	lux	lx	lux	0.0929	foot-candles
fl	foot-Lamberts	3.426	candela/m <sup>2</sup>	cd/m <sup>2</sup>	candela/m <sup>2</sup>	0.2919	foot-Lamberts
<b>FORCE and PRESSURE or STRESS</b>							
lbf	poundforce	4.45	newtons	N	newtons	0.225	poundforce
lbf/in <sup>2</sup>	poundforce per square inch	6.89	kilopascals	kPa	kilopascals	0.145	poundforce per square inch

\* SI is the symbol for the International Symbol of Units. Appropriate rounding should be made to comply with Section 4 of ASTM E380. (Revised September 1993)

# Implementation and Thickness Optimization of Perpetual Pavements in Ohio

Prepared by

Shad Sargand, Issam Khoury, Ben Jordan, Matthew Scheer, and Paul Cichocki

Ohio Research Institute for Transportation and the Environment  
Russ College of Engineering and Technology  
Ohio University  
Athens, Ohio 45701-2979

Prepared in cooperation with the  
Ohio Department of Transportation  
and the  
U.S. Department of Transportation, Federal Highway Administration

*The contents of this report reflect the views of the authors who are responsible for the facts and the accuracy of the data presented herein. The contents do not necessarily reflect the official views or policies of the Ohio Department of Transportation or the Federal Highway Administration. This report does not constitute a standard, specification or regulation.*

Final Report  
June 2015

## **Acknowledgements**

The researchers would like to thank the ODOT Research Section for sponsoring this research and facilitating its progress. In particular, the assistance of the technical panel, Mr. Aric Morse and Mr. Adam Au of the Office of Pavement Engineering, was very important. Thanks are also extended to the project partners, Flexible Pavements of Ohio, particularly Mr. Clifford Ursich, and to Kraton Polymers, particularly Mr. Bob Kluttz, for help with the APLF study. At Ohio University, the support of ORITE technicians Mike Krumlauf and later Joshua Jordan is acknowledged. The cooperation of the Shelly Co., especially Mr. Larry Shively during the construction of test sections was crucial and greatly appreciated.

# Table of Contents

1	Introduction.....	1
2	Objectives .....	2
3	Background and Significance of Work.....	2
4	Literature Review.....	4
	4.1.1 Pavement Response .....	5
	4.1.2 Perpetual Pavement Design .....	6
4.2	Fatigue Endurance Limits.....	7
	4.2.1 Fatigue Endurance Limit Research in the Field.....	9
	4.2.2 NCAT Test Track .....	9
	4.2.3 Texas.....	10
	4.2.4 Oregon.....	10
	4.2.5 Advanced Transportation Research and Engineering Laboratory .....	11
	4.2.6 Kansas .....	12
	4.2.7 New York.....	12
	4.2.8 Accelerated Pavement Load Facility .....	13
	4.2.9 Interstate 77, Canton, Ohio .....	14
	4.2.10 U.S. Route 30, Wayne County, Ohio.....	14
	4.2.11 Summary .....	15
5	DEL-23 Project Background.....	16
	5.1 Project Site Description .....	16
	5.2 Design of Test Sections .....	17
	5.3 Instrumentation of Test Sections .....	18
	5.3.1 Strain Gage Installation.....	18
	5.3.2 Pressure Cell Installation .....	19
	5.3.3 Thermocouple Installation .....	20
	5.3.4 Linear Variable Differential Transducer (LVDT) Installation .....	20
	5.3.5 Strain Gage Rosette Hole Installation.....	21
	5.4 Controlled Vehicle Load Testing.....	25
6	CVL Testing Pavement Response in Late Autumn .....	26
	6.1 Strain Response of the Pavement.....	29
	6.2 Longitudinal Strain in the FRL.....	35
	6.2.1 Influence of Speed on Longitudinal Strain in the FRL.....	37
	6.2.2 Influence of Tire Pressure on Longitudinal Strain in the FRL .....	39
	6.3 Longitudinal Strain in the Base Layer .....	41
	6.3.1 Influence of Speed on Longitudinal Strain in the Base Layer .....	42
	6.3.2 Influence of Tire Pressure on Longitudinal Strain in the Base Layer.....	45
	6.4 Transverse Strain in the Base Layer .....	47
	6.4.1 Influence of Speed on Transverse Strain in the Base Layer .....	48
	6.4.2 Influence of Tire Pressure on Transverse Strain in the Base Layer.....	51
	6.5 Comparisons Between Strain Responses .....	53
7	CVL Testing Pavement Response in Summer.....	56
	7.1 Longitudinal Strain in the FRL .....	58
	7.1.1 Influence of Speed on Longitudinal Strain in the FRL.....	59
	7.1.2 Influence of Tire Pressure on Longitudinal Strain in the FRL .....	61
	7.2 Longitudinal Strain in the Base Layer .....	63

7.2.1	Influence of Speed on Longitudinal Strain in the Base Layer .....	64
7.2.2	Influence of Tire Pressure on Longitudinal Strain in the Base Layer.....	66
7.3	Transverse Strain in the Base Layer .....	68
7.3.1	Influence of Speed on Transverse Strain in the Base Layer .....	69
7.3.2	Influence of Tire Pressure on Transverse Strain in the Base Layer.....	71
7.4	Comparisons Between Strain Responses .....	73
8	PerRoad Analysis.....	76
8.1	Loading Conditions.....	76
8.1.1	Vehicle Classification Distribution.....	77
8.2	Structural and Seasonal Information.....	79
8.3	Performance Criteria.....	80
8.4	Results.....	81
9	Material Properties.....	84
9.1	DEL-23 Asphalt Concrete Material Properties.....	84
9.2	APLF Asphalt Concrete Material Properties .....	85
9.3	Dynamic Modulus of AC Materials.....	87
9.4	Aggregate Base and Subgrade Properties .....	106
10	Evaluation of Highly Modified Asphalt .....	107
10.1	The Accelerated Pavement Load Facility .....	107
10.2	Instrumentation of pavements in the APLF .....	108
10.2.1	Strain Gage Installation.....	108
10.2.2	Thermocouple Installation .....	109
10.2.3	Linear Variable Differential Transformer (LVDT) Installation .....	109
10.2.4	Profilometer Measurements .....	110
10.3	APLF Testing Pavement Responses .....	112
10.3.1	Strain Responses in the HiMA Pavement.....	113
10.3.2	Longitudinal Strain in HiMA Base Caused by Adjusted Load.....	114
10.3.3	Influence of Temperature on Strain in HiMA Base.....	117
10.3.4	Rutting in APLF.....	118
11	Estimating the Fatigue Endurance Limit .....	123
11.1	Effect of the Initial Flexural Stiffness.....	124
11.2	Endurance Limits Based on Laboratory Tested Temperatures .....	125
11.3	Comparison of Endurance Limits and Strain Results from Field Testing.....	125
12	Mechanistic-Empirical Pavement Design.....	131
12.1	MEPDG Inputs.....	131
12.2	MEPDG Results.....	132
12.3	Summary.....	143
13	Asphalt Perpetual Pavement Design: Utilizing Existing Pavement Systems .....	145
13.1	Pavements selected for further analysis as perpetual pavement candidates .....	145
13.2	Site Investigations .....	151
13.2.1	PIK 32-15W .....	152
13.2.2	GRE 35-21E.....	153
13.2.3	LUC 25-10S .....	154
13.2.4	CLA 41-3N .....	156
13.2.5	BUT 129-22E.....	157
13.3	Coring .....	159

13.4	Field Testing .....	160
13.4.1	Falling Weight Deflectometer (FWD) .....	160
13.4.2	FWD Results .....	161
13.4.3	Dynamic Cone Penetrometer (DCP).....	162
13.4.4	Portable Seismic Property Analyzer (PSPA).....	164
13.5	Laboratory Testing.....	167
13.5.1	Indirect Tensile Strength (ITS).....	167
13.5.2	Laboratory Resilient Modulus Testing .....	168
13.6	Modeling Asphalt Pavement Response .....	170
13.7	Other FWD Techniques for Estimating Pavement Response .....	173
13.7.1	Liao Model.....	173
13.7.2	N.C. State University FWD Model.....	174
13.8	Finite Element Modeling of Asphalt Pavement.....	178
13.9	AC Pavement Testing Relationships .....	181
13.10	Summary and Observations on Existing Pavements .....	190
14	Status Update on Previous Perpetual Pavement Test Roads .....	191
14.1	US Route 30 Wayne County (WAY-30) .....	191
14.2	I77 Stark County (STA-77) .....	195
15	Conclusions and Recommendations .....	197
15.1	Major Conclusions .....	197
15.1.1	DEL-23 .....	197
15.1.2	Existing pavements .....	197
15.1.3	APLF.....	198
15.1.4	Additional major conclusions .....	198
15.2	Detailed Conclusions from Various Tasks .....	198
15.3	Recommendations.....	199
15.4	Implementation .....	201
16	References.....	202
Appendix A:	LVDT calibration on DEL-23.....	208
Appendix B:	LVDT enclosure and reference rod diagrams for DEL-23.....	211
Appendix C:	Strain gage rosette hole diagrams for DEL-23.....	214
Appendix D:	Pavement instrumentation diagrams for DEL-23. ....	218
Appendix E:	Truck loads and dimensions for CVL tests on DEL-23 .....	220
Appendix F:	Test day temperatures during CVL testing on DEL23. ....	222
Appendix G:	Strain gauge data from CVL tests on DEL-23.....	228
Appendix H:	LVDT and pressure cell data from CVL tests on DEL-23.....	254
Appendix I:	Lateral tire offset data from CVL testing on DEL-23. ....	290
Appendix J:	PerRoad input values for DEL-23.....	294



# List of Figures

Figure 1. Location of SHRP Test Road (DEL-23), indicated by the green dot (Geology, 2013). .....	16
Figure 2. View of SHRP test road with arrows showing location of DEL-23 Test Sections (picture by ODOT)......	17
Figure 3. Surface layer strain gage orientations.....	19
Figure 4. LVDT enclosure and reference rod diagram (1 in = 2.54 cm). ....	21
Figure 5. Strain gage rosette square hole diagram (1 in = 2.54 cm). ....	22
Figure 6. Strain gage rosette installation: 1. Drilling hole; 2. Grinding square hole; 3. Attaching gage to round hole; 4. Gages arrayed for installation; 5. Balloon used to hold gages in place while adhesive dried; 6. Gages in square hole with lead wires attached.....	23
Figure 7. Instrumentation layout for 13 in (33 cm) and 15 in (38 cm) sections (1 ft = 0.305 m).24	
Figure 8. Measurement of lateral offset from tire track after loaded truck has passed over the sensors.....	25
Figure 9. An ODOT truck loaded for CVL testing.....	25
Figure 10. Axle configurations used in CVL tests: Left, tandem axle; right, single axle with wide base tire. ....	26
Figure 11. 11 in (28 cm) section temperature profile during CVL testing December 18, 2012..	27
Figure 12. 13 in (33 cm) section temperature profile during CVL testing, December 19, 2012.	28
Figure 13. 15 in (38 cm) section temperature profile during CVL testing, November 29, 2012.	29
Figure 14. Longitudinal strain response measured from passing single axle truck with wide-base tire. ....	30
Figure 15. Transverse strain response measured from passing single axle truck with wide-base tire. ....	31
Figure 16. Longitudinal strain in the FRL measured from tandem axle truck passing at 5 mph (8 km/h). ....	32
Figure 17. Longitudinal strain in the FRL measured from tandem axle truck passing at 55 mph (89 km/h).....	33
Figure 18. Strain response from tandem axle truck where steer axle produced maximum strain. .....	34
Figure 19. Strain response above the neutral axis of the pavement. ....	35
Figure 20. Maximum longitudinal strain in FRL versus speed (1 in = 2.54 cm, 1 mph = 1.6 km/h). Solid lines indicate single axle wide-based tire, and dashed lines indicate tandem axle. 38	
Figure 21. Maximum longitudinal strain in FRL versus tire pressure (1 in = 2.54 cm, 1 psi = 6.89 kPa). Solid lines indicate single axle wide-based tire, and dashed lines indicate tandem axle.....	40
Figure 22. Maximum longitudinal strain in base layer versus speed (1 in = 2.54 cm, 1 mph = 1.6 km/h). Solid lines indicate single axle wide-based tire, and dashed lines indicate tandem axle. 44	
Figure 23. Maximum longitudinal strain in the base layer versus tire pressure (1 in = 2.54 cm, 1 psi = 6.89 kPa). Solid lines indicate single axle wide-based tire, and dashed lines indicate tandem axle. ....	46
Figure 24. Maximum transverse strain in the base layer versus speed (1 in = 2.54 cm, 1 mph = 1.6 km/h). Solid lines indicate single axle wide-based tire, and dashed lines indicate tandem axle.....	50

Figure 25. Maximum transverse strain in in the base layer vs. tire pressure (1 in = 2.54 cm, 1 psi = 6.89 kPa). Solid lines indicate single axle wide-based tire, and dashed lines indicate tandem axle.....	52
Figure 26. 11 in (28 cm) section temperature profile during CVL testing July 10, 2013.....	56
Figure 27. 13 in (33 cm) section temperature profile during CVL testing, July 11, 2013.....	57
Figure 28. 15 in (38 cm) section temperature profile during CVL testing, July 1, 2013.....	57
Figure 29. Maximum longitudinal strain in FRL versus speed (1 in = 2.54 cm, 1 mph = 1.6 km/h). Solid lines indicate single axle wide-based tire, and dashed lines indicate tandem axle. 60	
Figure 30. Maximum longitudinal strain in FRL versus tire pressure (1 in = 2.54 cm, 1 psi = 6.89 kPa). Solid lines indicate single axle wide-based tire, and dashed lines indicate tandem axle.....	62
Figure 31. Maximum longitudinal strain in base layer versus speed (1 in = 2.54 cm, 1 mph = 1.6 km/h). Solid lines indicate single axle wide-based tire, and dashed lines indicate tandem axle. 65	
Figure 32. Maximum longitudinal strain in the base layer versus tire pressure (1 in = 2.54 cm, 1 psi = 6.89 kPa). Solid lines indicate single axle wide-based tire, and dashed lines indicate tandem axle. ....	67
Figure 33. Maximum transverse strain in the base layer versus speed (1 in = 2.54 cm, 1 mph = 1.6 km/h). Solid lines indicate single axle wide-based tire, and dashed lines indicate tandem axle.....	70
Figure 34. Maximum transverse strain in in the base layer versus tire pressure (1 in = 2.54 cm, 1 psi = 6.89 kPa). Solid lines indicate single axle wide-based tire, and dashed lines indicate tandem axle. ....	72
Figure 35. WIM Scales on DEL 23. ....	76
Figure 36. WIM Scales on DEL 23. ....	77
Figure 37. Vehicle type distribution as entered into PerRoad. ....	78
Figure 38. Loading conditions as entered into PerRoad. ....	79
Figure 39. Structural and seasonal information as entered into PerRoad. ....	80
Figure 40. Dynamic modulus master curve for 424 surface layer on DEL 23. ....	97
Figure 41. Shift factor vs. temperature for 424 surface layer on DEL 23. ....	98
Figure 42. Dynamic modulus master curve for 442 intermediate layer on DEL 23.....	98
Figure 43. Shift factor vs. temperature for 442 intermediate layer on DEL 23.....	99
Figure 44. Dynamic modulus master curve for 302 AC base layer on DEL 23.....	99
Figure 45. Shift factor vs. temperature for 302 AC base layer on DEL 23. ....	100
Figure 46. Dynamic modulus master curve for 302 FRL on DEL 23. ....	100
Figure 47. Shift factor vs. temperature for 302 FRL on DEL 23.....	101
Figure 48. Dynamic modulus master curve for 442 HiMA surface layer in APLF.....	102
Figure 49. Shift factor vs. temperature for 442 HiMA surface layer in APLF.....	102
Figure 50. Dynamic modulus master curve for 442 HiMA intermediate layer in APLF. ....	103
Figure 51. Shift factor vs. temperature for 442 HiMA intermediate layer in APLF. ....	103
Figure 52. Dynamic modulus master curve for 302 HiMA AC base with Kraton polymer in APLF.....	104
Figure 53. Shift factor vs. temperature for 302 HiMA AC base with Kraton polymer in APLF. ....	104
Figure 54. Dynamic modulus master curve for 302 AC base with control binder in APLF. ....	105
Figure 55. Shift factor vs. temperature for 302 AC base with control binder in APLF. ....	105
Figure 56. Load wheel passing over test pavement in the APLF. ....	107

Figure 57. Gage layout in APLF test lane A, which is similar to the other lanes.....	108
Figure 58. Rolling wheel profiler in use at the APLF.....	110
Figure 59. Overhead view of test pavements in APLF showing placement of profilometer.....	112
Figure 60. Longitudinal strain at bottom of AC base in Lane A, 70°F (21°C), 12 kip (53 kN) load.....	113
Figure 61. Transverse strain at bottom of AC base in Lane C, 70°F (21°C), 12 kip (53 kN) load.....	114
Figure 62. Average max longitudinal strains for APLF test sections at 70°F (21.1°C) (6000 lb = 27 kN, 9000 lb = 40 kN, 12,000 lb = 53 kN) (8 in = 20 cm, 9 in = 23 cm, 10 in = 25 cm, 11 in = 28 cm). .....	116
Figure 63. Average max longitudinal strains for APLF test sections at 100°F (37.8°C) (6000 lb = 27 kN, 9000 lb = 40 kN, 12,000 lb = 53 kN) (8 in = 20 cm, 9 in = 23 cm, 10 in = 25 cm, 11 in = 28 cm). .....	117
Figure 64. Profile history of 8 in (20 cm) section (Lane A) in APLF at 70°F (21.1°C) (1 in = 2.54 cm). .....	118
Figure 65. Profile history of 8 in (20 cm) section (Lane A) in APLF at 100°F (37.8°C) (1 in = 2.54 cm). .....	119
Figure 66. Rut depth vs. number of passes for HiMA at 100°F (37.8°C) (1 in =2.54 cm). .....	120
Figure 67. Comparison of average rut depths between HiMA and WMA mixes at high temperature in APLF (1 in = 2.54 cm).....	121
Figure 68. AC base endurance limit vs. flexural stiffness at various Rest Periods (RP) in seconds for APLF control mix.....	124
Figure 69. Predicted total rutting for Section 39BN803 on DEL-23 (1in = 25.4 mm).....	135
Figure 70. Predicted AC bottom-up cracking for Section 39BN803 on DEL-23.....	136
Figure 71. Predicted total rutting for Section 39BS803 on DEL-23 (1in = 25.4 mm). .....	137
Figure 72. Predicted AC bottom-up cracking for Section 39BS803 on DEL-23. ....	137
Figure 73. Predicted total rutting for Section 39D168 on DEL-23 (1in = 25.4 mm). .....	138
Figure 74. Predicted AC bottom-up cracking for Section 39D168 on DEL-23. ....	139
Figure 75. Predicted total rutting for Section 39P168 on DEL-23 (1in = 25.4 mm).....	140
Figure 76. Predicted AC bottom-up cracking for Section 39P168 on DEL-23.....	140
Figure 77. Predicted total rutting for I77 test section (1in = 25.4 mm). .....	141
Figure 78. Predicted AC bottom-up cracking for I77 test section. ....	142
Figure 79. Predicted total rutting for WAY-30 test section (1in = 25.4 mm). .....	143
Figure 80. Predicted AC bottom-up cracking for WAY-U30 test section.....	143
Figure 81. Geographical distribution of selected asphalt pavements (Edwards & Sargand, 2010). .....	148
Figure 82. General view of PIK 32-15W.....	152
Figure 83. Cracking on PIK 32-15W.....	153
Figure 84. General view of GRE 35-21E site.....	154
Figure 85. Cracking through recent overlay on GRE 35-21E. ....	154
Figure 86. General view of LUC 25-10S.....	155
Figure 87. Cracking on LUC 25-10S.....	155
Figure 88. General view of CLA 41-3N.....	156
Figure 89. Cracking on CLA 41-3N.....	157
Figure 90. General view of BUT 129-22E.....	158
Figure 91. Cracking on BUT 129-22E.....	158

Figure 92. Using a core drill to obtain a sample core of AC pavement.....	159
Figure 93. Core sample obtained from an AC pavement. The surface is at the left. ....	159
Figure 94. Automated DCP in operation. ....	163
Figure 95. PSPA equipment (Geomedia Research & Development, 2007). ....	165
Figure 96. Field operation of the PSPA on asphalt pavement. ....	166
Figure 97. Simplified flowchart for Evercalc (WSDOT, 2005). ....	170
Figure 98. Pavement section mesh.....	178
Figure 99. Pavement section with tire load.....	179
Figure 100. Computed pavement response to load.....	179
Figure 101. AC seismic modulus vs. strain at the bottom of the AC base layer. ....	182
Figure 102. Surface layer ITS vs. strain at the bottom of the AC base layer. ....	185
Figure 103. Intermediate layer ITS vs. strain at the bottom of the AC base layer. ....	185
Figure 104. AC base layer ITS vs. strain at the bottom of the AC base layer. ....	186
Figure 105. AC base ITS vs. strain at the bottom of the AC base layer. ....	187
Figure 106. AC base laboratory resilient modulus vs. strain at the bottom of the AC base layer. .....	188
Figure 107. Surface distress at Station 876 of WAY-30, including test section and WIM. ....	191
Figure 108. Surface distress at Sta. 876 of WAY-30.....	192
Figure 109. Surface distress at Sta.876 of WAY-30.....	192
Figure 110. Test section at Sta. 664 of WAY-30.....	193
Figure 111. Surface distress at Sta. 664 of WAY-30.....	193
Figure 112. Surface distress at Sta. 664 of WAY-30.....	194
Figure 113. Rutting measurement on STA-77.....	195
Figure 114. Longitudinal cracks on STA-77. ....	196
Figure 115. Longitudinal cracks on STA-77. ....	196

# List of Tables

Table 1. Layer specifications for DEL-23 perpetual pavement sections. ....	17
Table 2. Specified layer thicknesses of DEL-23 pavement sections. ....	18
Table 3. Maximum longitudinal strain in the FRL for the 11 in (28 cm) section ( $\mu\epsilon$ ). ....	36
Table 4. Maximum longitudinal strain in the FRL for the 13 in (33 cm) section ( $\mu\epsilon$ ). ....	36
Table 5. Maximum longitudinal strain in the FRL for 15 in (38 cm) section ( $\mu\epsilon$ ). ....	37
Table 6. Maximum longitudinal strain in the base layer for the 11 in (28 cm) section ( $\mu\epsilon$ ). ....	41
Table 7. Maximum longitudinal strain in the base layer for the 13 in (33 cm) section ( $\mu\epsilon$ ). ....	42
Table 8. Maximum longitudinal strain in the base layer for the 15 in (38 cm) section ( $\mu\epsilon$ ). ....	42
Table 9. Maximum transverse strain in the base layer for the 11 in (28 cm) section ( $\mu\epsilon$ ). ....	47
Table 10. Maximum transverse strain in the base layer for the 13 in (33 cm) section ( $\mu\epsilon$ ). ....	48
Table 11. Maximum transverse strain in the base layer for the 15 in (38 cm) section ( $\mu\epsilon$ ). ....	48
Table 12. Longitudinal versus transverse strains in the base layer for the 11 in (28 cm) section ( $\mu\epsilon$ ). ....	53
Table 13. Longitudinal versus transverse strains in the base layer for the 13 in (33 cm) section ( $\mu\epsilon$ ). ....	53
Table 14. Longitudinal versus transverse strains in the base layer for the 15 in (38 cm) section ( $\mu\epsilon$ ). ....	54
Table 15. Maximum longitudinal strain in FRL versus in base layer for single axle wide-base tire truck test with 29 kip (129 kN) axle load for the 11 in (28 cm) section ( $\mu\epsilon$ ). ....	54
Table 16. Maximum longitudinal strain in FRL versus in base layer for single axle wide-base tire truck test with 29 kip (129 kN) axle load for the 13 in (33 cm) section ( $\mu\epsilon$ ). ....	54
Table 17. Maximum longitudinal strain in FRL versus in base layer for single axle wide-base tire truck test with 29 kip (129 kN) axle load for the 15 in (38 cm) section ( $\mu\epsilon$ ). ....	55
Table 18. Maximum longitudinal strain in the FRL for the 11 in (28 cm) section ( $\mu\epsilon$ ). ....	58
Table 19. Maximum longitudinal strain in the FRL for the 13 in (33 cm) section ( $\mu\epsilon$ ). ....	59
Table 20. Maximum longitudinal strain in the FRL for 15 in (38 cm) section ( $\mu\epsilon$ ). ....	59
Table 21. Maximum longitudinal strain in the base layer for the 11 in (28 cm) section ( $\mu\epsilon$ ). ....	63
Table 22. Maximum longitudinal strain in the base layer for the 13 in (33 cm) section ( $\mu\epsilon$ ). ....	63
Table 23. Maximum longitudinal strain in the base layer for the 15 in (38 cm) section ( $\mu\epsilon$ ). ....	64
Table 24. Maximum transverse strain in the base layer for the 11 in (28 cm) section ( $\mu\epsilon$ ). ....	68
Table 25. Maximum transverse strain in the base layer for the 13 in (33 cm) section ( $\mu\epsilon$ ). ....	69
Table 26. Maximum transverse strain in the base layer for the 15 in (38 cm) section ( $\mu\epsilon$ ). ....	69
Table 27. Longitudinal versus transverse strains in the base layer for the 11 in (28 cm) section ( $\mu\epsilon$ ). ....	73
Table 28. Longitudinal versus transverse strains in the base layer for the 13 in (33 cm) section ( $\mu\epsilon$ ). ....	73
Table 29. Longitudinal versus transverse strains in the base layer for the 15 in (38 cm) section ( $\mu\epsilon$ ). ....	74
Table 30. Maximum longitudinal strain in FRL versus in base layer for single axle wide-base tire truck test with 29 kip (129 kN) axle load for the 11 in (28 cm) section ( $\mu\epsilon$ ). ....	74
Table 31. Maximum longitudinal strain in FRL versus in base layer for single axle wide-base tire truck test with 29 kip (129 kN) axle load for the 13 in (33 cm) section ( $\mu\epsilon$ ). ....	74
Table 32. Maximum longitudinal strain in FRL versus in base layer for single axle wide-base tire truck test with 29 kip (129 kN) axle load for the 15 in (38 cm) section ( $\mu\epsilon$ ). ....	75
Table 33. Vehicle type distribution. ....	77

Table 34. Seasonal information for Ohio (The Weather Channel, 2013).....	79
Table 35. Elastic modulus and Poison’s ratio for pavement materials.....	80
Table 36. Perpetual pavement performance criteria used in PerRoad.....	81
Table 37. Fatigue transfer function empirical constants (values from Timm & Priest 2006). ....	81
Table 38. PerRoad results for 11 in (28 cm) section.....	82
Table 39. PerRoad results for 13 in (33 cm) section.....	82
Table 40. PerRoad results for 15 in (38 cm) section.....	83
Table 41. DEL-23 layer thicknesses .....	84
Table 42. AC mix design and volumetrics for DEL-23 sections.....	85
Table 43. DEL-23 binder properties.....	85
Table 44. APLF test section layer thicknesses.....	86
Table 45. AC Mix Design and Volumetrics for HiMA and control materials in APLF.....	86
Table 46. APLF test section binder properties.....	87
Table 47. Average dynamic modulus of the 424 Surface Layer on DEL 23.....	88
Table 48. Average dynamic modulus of the 442 intermediate layer on DEL 23. ....	89
Table 49. Average dynamic modulus of the 302 AC base layer on DEL 23.....	90
Table 50. Average dynamic modulus of the 302 FRL on DEL 23.....	91
Table 51. Average dynamic modulus of the 442 surface layer HiMA.....	92
Table 52. Average dynamic modulus of the 442 intermediate layer HiMA.....	93
Table 53. Average dynamic modulus of the 302 AC base HiMA with Kraton polymer. ....	94
Table 54. Average dynamic modulus of the 302 AC base with no polymer for control section in APLF.....	95
Table 55. Curve fitting parameters and regression coefficients for each AC layer.....	97
Table 56. Average and maximum longitudinal strains in base layer ( $\mu\epsilon$ ). ....	115
Table 57. Percent increase in longitudinal strains due to temperature increase. ....	117
Table 58. Maximum rut depth for APLF lanes at 100°F (37.8°C). ....	119
Table 59. Trendline parameters for HiMA lanes.....	120
Table 60. Maximum rut depth for APLF and WMA surface mixes under high temperature. WMA data from Sargand et al. (2009). ....	121
Table 61. Number of passes of 9000 lb (40kN) load to reach low rutting classification (0.125 in = 0.32 cm). ....	122
Table 62. Estimation of endurance limit when $E_0 = E^*$ , $RP = 5$ seconds, $f = 10$ Hz, $N = 200,000$ , $SR = 1$ . ....	125
Table 63. Estimation of endurance limit when $E_0 = E^*/2$ , $RP = 5$ seconds, $f = 10$ Hz, $N = 200000$ , $SR = 1$ . ....	125
Table 64. Dynamic modulus results at 10 Hz.....	126
Table 65. Second order regression coefficients for each mix. English units at top, metric units at bottom. ....	126
Table 66. DEL-23 fatigue endurance limit at test temperatures $E_0 = E^*$ , $RP = 5$ seconds, $f = 10$ Hz, $N = 200000$ , $SR = 1$ . ....	127
Table 67. DEL-23 stiffness ratio based on the average peak strain measured during the controlled vehicle load tests ( $E_0 = E^*$ ), $RP = 5$ seconds, $f = 10$ Hz, $N = 200000$ . ....	127
Table 68. DEL-23 Fatigue endurance limits at test temperatures ( $E_0 = E^*/2$ ), $RP = 5$ seconds, $f = 10$ Hz, $N = 200000$ , $SR = 1$ . ....	128
Table 69. DEL-23 stiffness ratio based on the average peak strain measured during the controlled vehicle load tests ( $E_0 = E^*/2$ ), $RP = 5$ seconds, $f = 10$ Hz, $N = 200000$ . ....	128

Table 70. APLF fatigue endurance limits at test temperatures ( $E_0 = E^*$ ), $RP = 5$ seconds, $f = 10$ Hz, $N = 200000$ , $SR = 1$ .	128
Table 71. APLF stiffness ratio based on the average peak strain measured during the controlled load tests ( $E_0 = E^*$ ), $RP = 5$ seconds, $f = 10$ Hz, $N = 200000$ .	129
Table 72. APLF fatigue endurance limit at test temperatures ( $E_0 = E^*/2$ ), $RP = 5$ seconds, $f = 10$ Hz, $N = 200000$ , $SR = 1$ .	129
Table 73. APLF stiffness ratio based on the average peak strain measured during the controlled load tests ( $E_0 = E^*/2$ ), $RP = 5$ seconds, $f = 10$ Hz, $N = 200000$ .	129
Table 74. MEPDG traffic input recommendations (Abbas and Frankhouser, 2012).	132
Table 75. Design inputs for Section 39BN803 on DEL-23 (1 in = 25.4 mm).	133
Table 76. Design inputs for Section 39BS803 on DEL-23 (1 in = 25.4 mm).	133
Table 77. Design inputs for Section 39D168 on DEL-23 (1 in = 25.4 mm).	133
Table 78. Design inputs for Section 39P168 on DEL-23 (1 in = 25.4 mm).	134
Table 79. Design inputs for I77 test section (1 in = 25.4 mm).	134
Table 80. Design inputs for US30 test section (1 in = 25.4 mm).	134
Table 81. Distress prediction summary for Section 39BN803 on DEL-23 (1 in/mile = 15.78 mm/km = $1.578 \times 10^{-5}$ ; 1 in = 25.4 mm; 1ft/mile = 18.94 cm/km = $1.894 \times 10^{-4}$ ).	135
Table 82. Distress summary for Section 39BS803 on DEL-23 (1 in/mile = 15.78 mm/km = $1.578 \times 10^{-5}$ ; 1 in = 25.4 mm; 1ft/mile = 18.94 cm/km = $1.894 \times 10^{-4}$ ).	136
Table 83. Distress summary for Section 39D168 on DEL-23 (1 in/mile = 15.78 mm/km = $1.578 \times 10^{-5}$ ; 1 in = 25.4 mm; 1ft/mile = 18.94 cm/km = $1.894 \times 10^{-4}$ ).	138
Table 84. Distress summary for Section 39P168 on DEL-23 (1 in/mile = 15.78 mm/km = $1.578 \times 10^{-5}$ ; 1 in = 25.4 mm; 1ft/mile = 18.94 cm/km = $1.894 \times 10^{-4}$ ).	139
Table 85. Distress summary for I77 test section (1 in/mile = 15.78 mm/km = $1.578 \times 10^{-5}$ ; 1 in = 25.4 mm; 1ft/mile = 18.94 cm/km = $1.894 \times 10^{-4}$ ).	141
Table 86. Distress summary for WAY-30 test section (1 in/mile = 15.78 mm/km = $1.578 \times 10^{-5}$ ; 1 in = 25.4 mm; 1ft/mile = 18.94 cm/km = $1.894 \times 10^{-4}$ ).	142
Table 87. Flexible pavements selected for forensic investigation (Edwards & Sargand, 2010).	146
Table 88. Layer characterization of “Excellent” rated sites (Edwards & Sargand, 2010). For each layer, thickness is given in in (cm) followed by ODOT item number, listed in Table 89.	147
Table 89. ODOT classifications for AC pavement materials (Edwards & Sargand, 2010).	148
Table 90. Test results from forensic investigation (Edwards & Sargand, 2010), English units.	149
Table 91. Test results from forensic investigation (Edwards & Sargand, 2010), metric units.	149
Table 92. Ranking (1-10) of each test for each site in 2010.	150
Table 93. Overall rankings of sites from forensic investigation in 2010.	151
Table 94. Average FWD deflections Normalized to 9000 lb (40 kN). English units at top, metric units below. Metric subscripts for D indicate distance from center of load plate in mm.	161
Table 95. Average modulus of subgrade reaction for each site.	162
Table 96. Summary of resilient moduli obtained from DCP data analysis.	164
Table 97. PSPA seismic modulus test results.	167
Table 98. ITS test results-English units.	168
Table 99. ITS test results-metric units.	168
Table 100. AC base layer resilient modulus test results-English units.	169
Table 101. AC base layer resilient modulus test results-metric units.	169
Table 102. Typical ranges for elastic modulus (Qin, 2010).	171

Table 103. Evercalc 5.0 results. ....	172
Table 104. Average AC temperature vs. air temperature coefficients (Figueroa, 2004). ....	173
Table 105. FWD results using Liao model. ....	174
Table 106. Kim and Park FWD model results. ....	175
Table 107. Average tensile strain at the bottom of the AC base layer from 9000 lb (40 kN) load. .....	175
Table 108. Finite element model results. ....	180
Table 109. Finite element model results using DCP subgrade modulus. ....	180
Table 110. Comparison of DCP vs. FWD based modulus of aggregate base. ....	181
Table 111. Comparison of DCP vs. FWD based modulus of subgrade. ....	181
Table 112. Comparison of seismic modulus and resilient modulus. ....	182
Table 113. ITS of WAY-30 FRL (Kim et al., 2010). ....	184
Table 114. ITS of AC base layers. ....	183
Table 115. Comparison of the ITS and FWD modulus of the AC base layer. ....	186
Table 116. AC base layer modulus comparison (Lab vs. FWD). ....	189
Table 117. Summary of FWD data from WAY-30. ....	194
Table 118. Summary of FWD data from STA-77. ....	195



# 1 Introduction

Increases in traffic volume and loads, demands for longer-lasting pavements that reduce user delays due to reconstruction, and rising costs of energy and asphalt materials are some of the major challenges facing the paving industry and State DOTs in the United States. The concept of perpetual pavements has been identified as an emerging design technique to solve these challenges. Perpetual asphalt pavements are designed to confine distresses to the upper layer of the structure, by eliminating or reducing the potential for fatigue cracking by maintaining the horizontal strains at the bottom of the pavement below a critical fatigue endurance limit (FEL).

While there have been a number of successful installations of perpetual pavements, there are still questions to be answered in order to achieve a comprehensive understanding of the design of such pavements. For example, although various endurance limits have been proposed, none have been determined and field validated for efficient design. The National Center for Asphalt Technology (NCAT) suggested the FEL value for most perpetual pavement designs is in the range of 70 to 100  $\mu\epsilon$ . However, based on the results of different in-service pavement sections, some researchers suggested the Fatigue Resistance Layer (FRL) can withstand up to 150  $\mu\epsilon$  depending on the type of mixture used.

The Ohio Department of Transportation (ODOT) used the US Route 30 bypass of Wooster, Ohio, in Wayne County to demonstrate the concept of perpetual pavement design (Sargand, Figueroa, and Romanello, 2008). The pavement structure in the “WAY-30” pavement, designed to limit the strain at the bottom of the FRL to 70  $\mu\epsilon$ , consisted of four asphalt concrete layers with a total thickness of 16.25 in (41.28 cm) placed on top of a 6 in (15.24 cm) Dense Graded Aggregate Base (DGAB) layer laid over compacted subgrade. The pavement was instrumented with strain gauges to measure transverse and longitudinal strains in the Fatigue Resistance Layer (FRL) and Asphalt Treated Base (ATB) layer, pressure cells to monitor subgrade pressures, and deep and shallow LVDTs to record pavement deflections. A weather station was also used to monitor environmental conditions. Controlled Vehicle Load (CVL) tests were carried out to monitor the responses of the pavement structure under in-service traffic conditions. The results from WAY-30 provided important information about the design and construction of perpetual pavements. It was also concluded the FEL is a function of temperature and traffic speed, as these two parameters dictate the response of asphalt materials (Sargand, Figueroa, and Romanello, 2008).

ODOT then funded a study at the Accelerated Pavement Loading Facility (APLF) at Ohio University to determine if the thickness of an asphalt pavement could be reduced from that of WAY-30 while still meeting perpetual pavement criteria and maintaining performance (Sargand, Figueroa, Edwards, and Al-Rawashdeh, 2009). In this study, four perpetual pavement sections were constructed and tested. The first section had the same asphalt layer structure as the WAY-30 perpetual pavement. In the other sections, the total thickness of the asphalt layers was progressively decreased to 15 in (38 cm), 14 in (35.6 cm), and 13 in (33 cm), respectively. However, the total thickness of the pavement structure was maintained by increasing that of the DGAB layer. The results showed reducing the asphalt layer thickness while increasing the thickness of the DGAB layer did not have a significant effect on the measured pavement response parameters, which suggested the thickness of asphalt layers could be reduced by at least 2 in (5 cm).

This research study was aimed at determining a minimum thickness design for perpetual pavements in Ohio. To achieve this objective, pavement sections were constructed and instrumented on the Strategic Highway Research Program (SHRP) Test Road on US Route 23 in Delaware County, referred to as “DEL-23”. The four test sections were designed with three different total pavement thicknesses of 11 in (28 cm), 13 in (33 cm) (two sections), and 15 in (38 cm). The response of those sections was monitored under controlled vehicle loads to determine if they met the perpetual pavement criteria, with the exception of one 13 in (33 cm) section that did not conform to the design at the location of the instrumentation, as explained below. The data obtained were used to determine the design thickness of perpetual pavements that would minimize their life cycle costs. In this report, the pavement response data collected through the sensors installed in the experimental test sections are analyzed in order to assess the performance of the pavement and the perpetual nature of the various sections. Furthermore, the pavement test sections were analyzed using the computer programs PerRoad and AASHTOWare Pavement-ME Design which modeled and evaluated the sections using realistic conditions.

ODOT must manage its resources as wisely as possible, and the results of this study will not only help ODOT reduce reconstruction costs by implementing the perpetual pavement concept, but to do so in the most effective way possible. Implementing a procedure to determine the minimum thickness required to create a perpetual pavement will save on initial construction costs and resources where conventional perpetual pavement designs exceed this minimum. Additionally, the study examines how to use rehabilitation techniques on existing pavements to bring them to a perpetual pavement standard, minimizing future rehabilitation costs.

## **2 Objectives**

The main objective of this study was to develop a procedure for the selection of the optimal design for perpetual pavements in Ohio. Other specific objectives of this project included:

- Investigate various perpetual pavement structure alternatives through varying the thickness and material properties of pavement layers in field test sections constructed on DEL-23 and in the Accelerated Pavement Load Facility (APLF).
- Use data collected at the field test sections to verify the analysis results.
- Evaluate typical conventional asphalt pavement designs currently used in Ohio and develop an approach to retrofit existing conventional asphalt pavements in good condition to meet perpetual pavement requirements.

## **3 Background and Significance of Work**

The perpetual pavement system, using pavement designs which result in long lasting structures, is a development which could save state and federal departments of transportation (DOTs) tremendous amounts of resources. Perpetual pavements are asphalt concrete (AC) pavement structures designed to carry the heaviest vehicle loadings without the need for major structural rehabilitation or reconstruction for at least 50 years (Asphalt Pavement Alliance, 2002). These pavement structures obtain their longevity from resisting the failure modes of bottom-up fatigue cracking and structural rutting. They achieve this through an increased thickness and a multiple layer system where thickness and stiffness are varied depending on the type of distress the layer is intended to resist. Properly designed perpetual pavement structures

can provide superior engineering performance creating minimal user-delays and economic efficiency.

Fatigue endurance limits are used to evaluate these perpetual pavement systems without requiring the need to wait through the system's entire service life before an analysis can be made. It was discovered that if certain pavement responses remain below specific thresholds, the pavement structure, in theory, can withstand an infinite amount of loading cycles without development of damage. During loading, reactions at critical locations can be monitored and compared with these threshold limits and if the reactions remain below the threshold limit, damages that will transpire during the structure's lifespan will be diminished [Timm and Newcomb, 2006]. Both bottom-up fatigue cracking and structural rutting can be analyzed through fatigue endurance threshold limits and will be the main source for analysis throughout this report.

A review of literature indicates there are studies of individual perpetual pavement projects [e.g. Battaglia, Bischoff, Ryan, and Reichelt, 2010] in addition to those in Ohio [Sargand, Figueroa, and Romanello, 2008; Sargand, et al., 2009; Sargand and Figueroa, 2010; Sargand, et al., 2010], and a synthesis of previous studies [Newcomb, Willis, and Timm, 2010].

Battaglia, Bischoff, Ryan, and Reichelt [2010], report on two test sections of perpetual pavement constructed on a weigh station entrance ramp on I-94 near Kenosha, Wisconsin. Annual performance surveys conducted after 4, 5, and 6 years of service found many instances of alligator cracking and longitudinal cracking in the wheel paths. The cracking was top-down, and had not yet reached the middle layer of HMA. Thus it is believed the observed premature cracking was due to segregation and over-compaction of the upper layers of pavement. Rutting was less than 0.1 in (2.5 mm) and ride quality was good. The authors also noted it is difficult to estimate an expected service life before the first surface layer replacement. The FEL ( $\epsilon_{\text{allowable}}$  at the bottom of the pavement) was recommended to be set to  $70\mu\epsilon$ , and the constructed pavement generally had lower strains during testing.

Park and Kim [2003] proposed a method for predicting the remaining life of flexible pavements from FWD measurements. The performance of pavement undergoing fatigue cracking could be predicted by their method except for sections in wet freeze regions that had experienced high levels of cracking that appear to have been caused by environmental distresses, such as low-temperature cracking.

The synthesis by Newcomb, Willis, and Timm [2010] recommends several areas of continued investigation, such as the development of high-modulus asphalt pavements and mix designs. They also recommend identifying factors that influence the fatigue limit and otherwise refining the determination of the FEL, even though it is the subject of NCHRP Study 9-44A.

Willis [2009] and Willis and Timm [2009] compared laboratory measurements of fatigue thresholds to cumulative strain distributions via a fatigue ratio. Correlating the laboratory fatigue threshold to one point on the cumulative strain distribution was difficult. Instead a ratio was used to quantify the strain distribution by comparing to the 95<sup>th</sup> percentile lower bound of the fatigue threshold confidence interval determined in the laboratory. A table of upper bound fatigue limits is presented by Willis [2009], with the recommendation that with similar mix designs and traffic patterns to those analyzed, sections whose measured cumulative strain distributions remain below the upper bound in the table should withstand fatigue cracking. The authors recommend further research to develop the links between laboratory fatigue thresholds, measured field strains, and pavement performance.

The above studies indicated there was a great need for developing a comprehensive understanding of the design of perpetual pavements. The main deficiency with pre-existing perpetual pavement design method is it does not ensure an optimum structure and/or layers that will last for a 50-year design life.

Perpetual pavement systems can also be analyzed using the computer software program PerRoad. PerRoad performs a layered elastic analysis with a Monte Carlo Simulation on pavement structures. It was developed by the Asphalt Pavement Alliance to estimate stresses, strains, and deflections within the pavement structure using loading conditions, seasonal temperatures, pavement layer thicknesses and properties, and limiting pavement responses. Pavement responses are compared with threshold limits in order to predict if they will be detrimental to the pavement's structure. Fatigue transfer functions can also be applied to estimate accumulating damages and, therefore, lifespan. Finally, a cost analysis can also be performed. The PerRoad program is useful for analyzing pavement structures under the likely conditions they will experience during their service lives.

## 4 Literature Review

The Asphalt Pavement Alliance defines perpetual pavements as “an asphalt pavement designed and built to last longer than 50 years without requiring major structural rehabilitation or reconstruction, and needing only periodic surface renewal in response to distresses confined to the top of the pavement” (Asphalt Pavement Alliance, 2002, p. 5). These innovative pavement structures are designed to provide an infinite structural life under the heaviest vehicle loadings. Only surface layers would intermittently require milling and replacement to reduce surface distresses, a quick repair with minimal delays and restoration costs (Sargand, Figueroa, & Romanello, 2008).

Perpetual pavement designs have become practical because of their engineering performance and economic efficiency. The maintenance required incorporates minimal user-delays. When designed appropriately, perpetual asphalt pavements can be more economical than conventionally designed asphalt concrete pavements (Newcomb et al., 2010). Sargand et al. (2008) estimated perpetual pavements can save state and federal DOTs billions of dollars.

Although not recognized until recently, long-life asphalt pavements have been around since the 1960s (Newcomb & Hansen, 2006). Many sections of pavement have received perpetual pavement awards for having extended service lives. These sections had thicker designs, whether full-depth or deep-strength, and were well-constructed resulting in successful performances (Estes, 2005). Asphalt pavements built directly on the subgrade soil are called full-depth pavements while asphalt pavements that are built on a thin granular base course are deemed deep-strength pavements (Buchner, Newcomb, & Huddleston, 2000). Using the same concepts, pavement systems are now purposefully designed to be perpetual.

Deterioration of perpetual pavements typically consists of cracking or rutting in the surface layer (Nunn & Ferne, 2001). Traffic and weathering will cause damage to appear in the surface layer every 15 to 20 years (Hatch, 2008). This damage includes top-down fatigue cracking, thermal cracking, rutting, and surface wear (Asphalt Pavement Alliance, 2002). The surface layer should be replaced once these distresses reach critical levels. If distresses in the surface extend down into the structural layers of the pavement, major rehabilitation of the entire structure will be necessary (Buchner et al., 2000). Resurfacing may also be essential when improvements are needed for noise, driving comfort, or safety (Newcomb et al., 2010). Replacing the surface layer can be done overnight with minimal traffic disturbance.

Perpetual pavements are especially applicable for higher traffic volume roadways due to their ability to extend service life and minimize user delays, usually with little increase in design thickness. They are also valid design considerations for major airports where delays due to construction are extremely costly (Asphalt Pavement Alliance, 2002). Perpetual pavements are typically only used for high volumes of traffic, but designs for roads with lower traffic volumes can be vindicated as well (Buchner et al., 2000).

#### **4.1.1 Pavement Response**

Most approaches for designing perpetual pavement structures are focused on limiting the pavement's response to bottom-up fatigue cracking and structural rutting (Newcomb et al., 2010).

##### **4.1.1.1 Fatigue Cracking**

One of the major components instigating structural deterioration of pavements is fatigue cracking. Bottom-up fatigue cracking is the process where heavy traffic loading repeatedly creates high tensile strains in the bottom of the asphalt layer due to bending. (Newcomb et al., 2010; Retrepo-Velez, 2011; Willis, 2009). These repeated strains eventually exceed the fatigue resistance of the asphalt concrete and result in cracking. This cracking eventually propagates through the asphalt structure to the surface. Fatigue life is ultimately determined by the frequency and severity of horizontal strains experienced at the base of the asphalt layer (Newcomb et al., 2010).

Fatigue cracking is detrimental to a pavement structure. Once initiated, fatigue cracking will accelerate pumping, rutting, and overall deterioration of the asphalt layer (Willis, 2009). If the pavement's environment includes freezing and thawing cycles, water that has seeped into crack voids will expand under freezing conditions causing the crack to expand and eventually produce a pot hole.

Although fatigue cracking occurs in the asphalt layer of the pavement structure it ultimately affects all the other components of the structure as well. Fatigue cracking provides openings for water and moisture to seep into the unbound layers of the pavement structure, thus altering their material properties (Willis, 2009; Willis & Timm, 2009). Once a pavement structure has a cracked asphalt layer and a weakened subgrade or bases from moisture damage, major rehabilitation or reconstruction will be necessary.

Fatigue cracking is prevented in perpetual pavement by either increasing the thickness of the pavement structure or developing a more flexible base layer which can better resist strain repetitions (Newcomb et al., 2010). By reducing the strain at the base of the asphalt, the critical location becomes the surface where deep structural maintenance is avoided. This does not mean surface cracks can be overlooked due to their effect on ride quality and noise, but it does mean rehabilitation costs will be significantly reduced (Newcomb et al., 2010).

##### **4.1.1.2 Rutting**

Structural rutting is a permanent deformation that develops when the strength of the pavement structure is inadequate (Newcomb et al., 2010). Rutting deformation can present itself in one or multiple layers. Structural rutting occurs in the aggregate base or subgrade while surface rutting occurs in the surface layer of the asphalt layer.

Rutting potential can be minimized using different techniques. Studies have shown a threshold effect where rutting potential due to compressive strains on the subgrade significantly decreases after a certain thickness is reached (Nunn & Ferne, 2001). Structural rutting can be

prevented not only by designing a thicker pavement structure but also by increasing the stiffness in portions of the structure as well (Newcomb et al., 2010).

#### **4.1.2 Perpetual Pavement Design**

Perpetual pavement requires proper structural design as well as the use of appropriate materials. The main difference between perpetual pavements and conventional pavements is the design methodology used with perpetual pavements. Perpetual pavements are designed specifically to resist deep structural rutting and fatigue cracking (Newcomb et al., 2010). The optimal pavement structure is obtained by using a multiple layer system where thickness and mix design are varied depending on the type of distress the layer is intended to diminish (Tarefder & Bateman, 2012).

The material selection involved with perpetual pavements is important. Because each layer is designed to resist various distresses, the materials considered, mix design, and laboratory testing should be unique for each layer (Buchner et al., 2000). When developing the surface layer, it is important to consider shear strains (Newcomb & Hansen, 2006). All layers of the pavement system should possess good constructability characteristics as well as, to the greatest extent, be impermeable to avoid stripping damage along with other moisture problems (Newcomb & Hansen, 2006). The pavement structure must also be thick enough to provide the structural integrity needed to prevent structural rutting, fatigue cracking, and permanent deformation while also having the durability to resist damage from the environment (Willis & Timm, 2009).

##### **4.1.2.1 Fatigue Resistant Layer**

The structural adequacy of perpetual pavement relies on the fatigue behavior of the fatigue resistant layer (FRL). The main function of the FRL is to provide durability and resistance to fatigue cracking. The FRL is the bottom layer of the asphalt structure, so if damages occur, total reconstruction is unavoidable.

Cracking tendencies need to be mitigated in the bottom layer. Increasing the asphalt content of the bottom layer provides further protection against fatigue cracking (Buchner et al., 2000; Newcomb et al., 2010). Carpenter and Shen (2006) estimate the FRL should have a half percent of asphalt binder content increase. Although the asphalt content can become too high, additional asphalt, up to a certain point, impedes the development and progression of fatigue cracks (Asphalt Pavement Alliance, 2002). The increased amount of binder avoids the initiation of cracks by making the layer more flexible and, thus, more resistant to repeated loading. Since the layer is designed to reduce fatigue cracking through flexibility, rut-testing of the material should be performed to ensure the equipment driving directly on the layer during construction does not cause permanent damage (Asphalt Pavement Alliance, 2002). The FRL should be between three and four inches to avoid extending base material properties into higher portions of the asphalt system (Newcomb et al., 2010).

Although increasing the binder content in the bottom layer of the asphalt structure provides additional fatigue protection, Newcomb and Hansen (2006) suggest increasing the total pavement thickness is considerably more beneficial than solely relying on increasing the binder content. Furthermore, Tarefder and Bateman (2012) report the necessity for a rich bottom fatigue layer diminishes once the total pavement thickness starts to exceed 12 in (30.5 cm). They also report when using an FRL, the layer does not have the stiffness required to make contributions to the pavement's rutting strength and using an FRL layer is not economical.

Higher air voids in the FRL will result in reduced fatigue life. The FRL should have a max in-place density of between 96% and 98% or 2% to 4% air voids (Buchner et al., 2000).

Typical standard designs are only compacted to between 6 and 7% air voids (Carpenter & Shen, 2006). Newcomb and Hansen (2006) suggest using a fine graded mix to permit for lower air voids. This was also a consideration made by Willis (2009) while he analyzed data collected from Phase III of the NCAT Test Track. He discovered fine graded mixtures, when compared to coarse graded mixtures, seemed to be more resistant to cracking. The reduction in air voids allows the layer to be further compacted, thus increasing its resistance to fatigue and improving durability (Newcomb et al., 2010). Increasing the volume of voids filled with binder (VMA) is a critical component to the pavement's durability and flexibility.

Moisture susceptibility problems can be of concern with the FRL because the layer is likely to have extended periods of contact with water (Newcomb et al., 2010). Moisture can lead to stripping, a decrease in bond strength between the aggregate and binder, which will gradually decrease the strength of the pavement. Proper mix designs and compaction during construction are essential to combatting moisture susceptibility. It is also important to realize the stiffness of the base layer will increase with time which will intensify its bottom-up fatigue cracking potential (Nunn & Ferne, 2001). Engineers should take both of these factors into account when designing perpetual pavement structures.

#### **4.1.2.2 Perpetual Pavement Structural Trends**

In 2012, Tarefder and Bateman compiled a prominent amount of perpetual pavement research reports from around the country to analyze and determine the optimal perpetual pavement structure for New Mexico. When analyzing structures of perpetual pavement test sections, they discovered surface layers had thicknesses, on average, of 2 in (5.1 cm) with a 2.5 in (6.3 cm) transitional layer. Intermediate layers were, on average, eight inches thick and FRLs, if they were used, were five inches. Aggregate bases were also not always used but when they were they had an eight inch average thickness. Tarefder and Bateman also discovered that researchers used an FRL 60% of the time and aggregate bases were used 80% of the time. When considering the surface layer, an SMA surface course was used approximately 30% of the time while an OGFC surface was used 15% of the time.

## **4.2 Fatigue Endurance Limits**

A perpetual pavement system is often analyzed using some threshold level. During loading, if reactions at critical localities within the pavement remain below this threshold, damages occurring during the pavement's life will be eliminated or minimized (Timm & Newcomb, 2006). Tensile strain produced at the bottom of the asphalt is typically used for this threshold.

The fatigue endurance limit (FEL) is a strain limit for the bottom of the asphalt layer researchers have been using to make assumptions at early stages of the pavement's life on whether or not the pavement will be perpetual. The FEL has become an important consideration for any multi-layered perpetual pavement design. Many researchers suggest that involving an FEL while designing a perpetual pavement system is the utmost important aspect (Thompson & Carpenter, 2006a). The Asphalt Pavement Alliance (2002) alleged the FEL is the classification of an ideal pavement system that will not involve reconstruction.

Carpenter, Ghuzlan, and Shen (2003) performed laboratory research in order to discover whether or not an FEL exists, possibly determine its precise value, and analyze different variables that might alter the FEL. Their testing included ten mixtures with varying gradations, asphalt contents, and air voids. The samples were obtained directly from the truck, were reheated and compacted, and then tested using an IPC fatigue machine. A dissipated energy

ratio analysis was performed which quantifies the amount of energy a mixture is capable of handling.

Carpenter, Ghuzlan, and Shen made several significant discoveries. First and foremost, they noticed that the rate at which damage was accumulated began to diminish around 100  $\mu\epsilon$ . They predicted the FEL to be in the range of 70  $\mu\epsilon$  to 90  $\mu\epsilon$ . They discovered the FEL was different for different mixes but as long as strain in the bottom of the asphalt layer remained below 70  $\mu\epsilon$ , material variability would have no effect on fatigue life. Distinct differences were found between higher and lower strain levels regardless of the mix being tested and accumulated damage was disproportionately less than traditional theoretical strain level fatigue testing extrapolations.

At the November, 2007 Hot Mix Endurance Limit Workshop in Washington DC, the FEL was defined as the “level of strain below which there is no cumulative damage over an indefinite number of load cycles” (Advanced Pavement Technologies, 2008).

At lower strain levels, the damage produced by each loading cycle is low enough to allow the pavement’s healing process to replace all of the energy lost while being deformed (Carpenter et al., 2003). Thus, if strains are kept small enough, sufficient time will be available during rest periods for damages to recover. NCHRP project 9-38 supported the existence of a FEL for the asphalt mixes evaluated (National Cooperative Highway Research Program, 2010). As with most properties of flexible pavement, the FEL is not a constant. Modifiers within the binder, the aggregate used as well as its gradation, the grade of the binder, and volumetric properties of the mixture all have an effect on the FEL value (National Cooperative Highway Research Program, 2010). An extensive lab testing program was developed under NCHRP project 9-44 (Advanced Pavement Technologies, 2008) to relate the FEL determined in the laboratory to asphalt mixture properties. This testing program was modified and completed under NCHRP project 9-44A (Witczak et al., 2013). The following model was developed, based on beam fatigue testing, for inclusion in the AASHTOWare Pavement ME Design software:

$$SR = 2.0844 - 0.1386*\log(E_0) - 0.4846*\log(\epsilon_i) - 0.2012*\log(N) + 1.4103*\tanh(0.8471*RP) + 0.0320*\log(E_0)*\log(\epsilon_i) - 0.0954*\log(E_0)*\tanh(0.7154*RP) - 0.4746*\log(\epsilon_i)*\tanh(0.6574*RP) + 0.0041*\log(N)*\log(E_0) + 0.0557*\log(N)*\log(\epsilon_i) + 0.0689*\log(N)*\tanh(0.259*RP)$$

Where:

$SR$  = stiffness ratio = stiffness measured at any load cycle during beam fatigue testing to the initial stiffness of the specimen

$E_0$  = initial flexural stiffness (ksi)

$\epsilon_i$  = applied tensile strain ( $\mu\epsilon$ )

$RP$  = rest period (sec)

$N$  = number of load cycles

The FEL is the tensile strain value which results in a stiffness ratio of one in the above equation.

Fatigue limits can be established for more than just horizontal strain located at the bottom of the asphalt layer. Engineers typically design perpetual pavement structures to limit vertical compressive strain located at the top of the subgrade or aggregate base layer to 200 microstrain ( $\mu\epsilon$ ) (Willis & Timm, 2009). Furthermore, Romanello suggested (2007) that, in order to evaluate the pavement’s potential for structural rutting, the subgrade should not exceed 20 mil (0.5 mm)



of deflection and that, in order to monitor the strain distribution throughout the depth of the pavement, the base layer should not exceed 50  $\mu\epsilon$  of horizontal strain.

#### **4.2.1 Fatigue Endurance Limit Research in the Field**

Little understanding of HMA performance is known at lower levels of strain because fatigue testing is typically performed at higher strain levels in the lab. Furthermore, a report by the Advanced Asphalt Technologies (2008) suggests further field research is needed on the FEL because current fatigue damage models do not incorporate healing or damage recovery taking place between loading cycles. Fatigue curves developed by current AASHTO models have misrepresented field conditions when strains produced are limited (Carpenter et al., 2003). In other words, fatigue behavior, when subjected to low strain levels, does not follow typical model relationships. Lab testing also leaves out factors such as the environment, loading variation, and rest periods which can alter estimated FEL values.

#### **4.2.2 NCAT Test Track**

Willis and Timm (2009) wrote a report on field-based strain thresholds using instrumented perpetual pavement test section on the NCAT Test Track in Alabama. They wanted to discover if there was a relationship between field measured and laboratory strain thresholds. They also sought to recommend an FEL based on both experimental methods. Their testing included data recorded from 2006 NCAT Test Track sections, lab tests performed on samples obtained from the same test sections, and a PerRoad analyses.

Willis and Timm (2009) discovered sections of the test track failed due to fatigue when experiencing strains greater than 125  $\mu\epsilon$  at the bottom of the asphalt layer. While some sections eventually failed due to fatigue even while experiencing strains lower than 70  $\mu\epsilon$ , this information was deemed to be irrelevant because the sections were constructed on poor subgrades. Sections experiencing strain below 10  $\mu\epsilon$  were considered to be overdesigned and thus 10  $\mu\epsilon$  was set as a lower bound value for the FEL. Lab testing resulted in strain thresholds higher than thresholds revealed from the test track, with lab tests resulting in strain thresholds as high as 220  $\mu\epsilon$ . Willis and Timm found no clear correlation between lab and field testing.

Prowell and Brown (2006) performed a small study in order to determine a field-based FEL at the NCAT Test Track. After analyzing field measurements, they supported the concept of an FEL and found fatigue cracking was prevented when strains at the bottom of the asphalt layer were kept below 100  $\mu\epsilon$ .

Willis (2009) composed his thesis centered on an analyses of field based strain thresholds in perpetual pavement test sections at the NCAT Test Track. He found some sections had received strain readings at the base of the asphalt layer greater than 70  $\mu\epsilon$  without fatigue damage even after being exposed to 19 million ESALs. He concluded perpetual pavements could possibly withstand strains greater than 70  $\mu\epsilon$  or even 100  $\mu\epsilon$ .

As part of Phase III testing at the NCAT Test Track, eleven perpetual pavement test sections were constructed in order to evaluate the structural performance effects of thickness and polymer additions. Six sections were constructed with three varying thicknesses, 17 in (43 cm), 15 (38 cm), and 13 in (33 cm). Each thickness incorporating a section using unmodified binder and a section using polymer modified binder (Timm, 2009; Willis, 2009). Timm mentions two additional sections were built, one with an FRL and one without. These additional sections also incorporated an SMA surface course. The final three sections included two with total pavement thicknesses of 15 in (38 cm) and one with a total pavement thickness of 13 in (33 cm) with an SMA surface course (Willis, 2009).

A report composed by Robbins and Timm (2008) illustrated the instrumentation used for Phase III. Pressure cells were installed on the surface of the subgrade and base layer. Twelve strain gages, both in the longitudinal and transverse orientations, were placed at the base of the asphalt layer both along the wheel path and offset to both sides. Three temperature probes were installed to monitor pavement temperature on the surface, at mid-depth, and base of the asphalt layer along with the granular base.

Robbins and Timm (2008) described testing performed on four different dates. They reported loading was applied to the sections by a 12 kip steer axle, a 40 kip tandem axle, and a 20 kip single axle. Testing was performed at speeds of 15 mph (24 km/h), 25 mph (40 km/h), 35 mph (56 km/h), 45 mph (72 km/h), and 55 mph (89 km/h). Included in the report was surface temperature data which ranged between 70°F (21°C) and 125°F (52°C) during testing.

According to Robbins and Timm (2008), longitudinal and transverse strain decreased in a logarithmic fashion with increasing speeds. They discovered the rate at which the strain changed due to speed amplified as the temperature increased. Hence, at higher temperatures, speed was more influential on the strain induced at the bottom of the asphalt layer. This trend existed for both axle types. Robbins and Timm also revealed strain exponentially increased with pavement temperature increases for both the transverse and longitudinally oriented gages. Equations to represent the relationship between temperature and strain were developed and resulted in high correlations between equations and experimental data. This was also reported in Willis's (2009) thesis along with documentation stating that the two 15 in (38 cm) sections had still experienced no fatigue cracking after receiving over 19 million ESALs. Additionally, although all sections had recorded strains above 70  $\mu\epsilon$ , the 14 in (35.6 cm) section utilizing the SMA surface course and the FRL was experiencing the lowest strain values.

### **4.2.3 Texas**

A field study was performed by Quintus (2006) by utilizing field performance data of existing pavement structures. Quintus analyzed existing pavement structures by comparing their survival rates to the amount of loading, thus strain, they were receiving. He wanted to determine if field performance data supported the concept of an FEL and determine a reasonable FEL. Quintus revealed survival rates began to dramatically increase as 100  $\mu\epsilon$  and below thresholds levels were seen. He predicted the FEL to be 65  $\mu\epsilon$  with a 95% confidence level.

### **4.2.4 Oregon**

The Oregon Department of Transportation (DOT) along with Oregon State University performed a field study in 2005 of a perpetual pavement test section constructed on Interstate 5. A journal article on the project written by Estes (2005) revealed the section was not originally intended to be perpetual but after analysis was performed by Oregon State it was discovered the section possessed perpetual qualities. The objectives of the field study were to gain valuable information to further guidelines for future designs of perpetual pavement systems (Estes, 2005).

Scholz (2006) described the section as having a total asphalt thickness of 12 in (30 cm). He further defined the section as being built on top of an eight inch rubblized joint reinforced concrete pavement (JRCP) as well as a nine inch aggregate base. The section was compared to a standard 12 in (30 cm) section constructed directly on 16 in (41 cm) of aggregate (Scholz et al., 2006).

A large quantity of instrumentation was installed in the pavement section. Scholz (2006) illustrated the instrumentation as 12 strain gages placed directly on the aggregate base, 6 longitudinal and 6 transverse, and 12 placed on the rubblized JRCP, also 6 longitudinal and 6

transverse. He described the gages as being located along the wheel path and having an orientation of four rows of three with 2 ft (61 cm) spacings between them. Four temperature probes were used to record pavement temperature and a WIM sensor along with a classifier loop were installed before the instrumentation in order to record loading information and location (Scholz et al., 2006).

Estes (2005) disclosed data were collected from the section for a year and Scholz (2006) discovered the following results. Longitudinal strain gages experienced compressive strain directly before and after being loaded during which they experienced tensile strain. Transverse strain gages did not experience any compressive strain. Longitudinal strains magnitude was discovered to be greater in the standard section. Pavement seemed to be behaving elastically in the longitudinal direction but had a more viscous response transversely. Longitudinal and transverse strains recorded have been less than the 70  $\mu\epsilon$  threshold.

#### **4.2.5 Advanced Transportation Research and Engineering Laboratory**

The Advanced Transportation Research and Engineering Laboratory (ATREL) at the University of Illinois Urbana-Champaign branch campus has an Accelerated Transportation Loading Assembly (ATLAS) for evaluating pavement systems under realistic loading conditions. The loading facility is capable of inducing 10,000 loading cycles on an experimental pavement test pad per day (Al-Qadi, Wang, Yoo, & Dessouky, 2008). The assembly is capable of producing various loads along with multiple tire configurations.

Al-Qadi et al. (2008) wrote a report containing an evaluation of testing performed on two perpetual pavement test sections built at the ATREL. They described the test sections as having total pavement thicknesses of approximately of 16.5 in (42 cm). One of the test sections utilized an SMA surface course and an FRL with an increased binder content of 5.1%. The second test section incorporated a standard superpave surface layer and a base layer with a binder content of 4.5%. Moreover, two control sections were tested as well; one had a total pavement thickness of about 10 in (25 cm) and the other had 6 in (15 cm). Al-Qadi detailed that all four sections were constructed on top of a lime modified subgrade. Instrumentation of the test sections, as illustrated by Al-Qadi, included H-type strain gages located on the top of the subgrade, both in the longitudinal and transverse directions, and thermocouples throughout the thickness of the asphalt layer and subgrade.

Testing of the sections at the ATREL was performed using a load of approximately ten kips with two tire configurations including a dual-tire and a wide-base tire (Al-Qadi et al., 2008). Al-Qadi stated the tires were filled to a tire pressure of 100 psi (689 kPa) and two speeds of 5 mph (8 km/h) and 10 mph (16 km/h) were implemented in the study. Although test sections were outside and exposed to various temperatures, strain measurements were normalized to 77°F (25°C).

Al-Qadi et al. (2008) reported longitudinal strain included both a compressive and tensile zone unlike the transverse gages which only experienced tensile strain. Longitudinal strain was also greater in magnitude than transverse strain. This difference seemed to decrease as the thickness of the pavement increased. Strains recorded in the perpetual test sections were lower than those found in the standard sections although strain in the perpetual sections were only slightly lower than strains in the 10 in (25 cm) standard section. When comparing differences between the three pavement thicknesses, Al-Qadi et al. found tensile strain was strongly influenced by the thickness of the asphalt layer.

#### 4.2.6 Kansas

In order to investigate the practical use of perpetual pavement structures, the Kansas DOT constructed and instrumented four perpetual pavement structures on U.S. Route 75. The four sections were constructed in 2005 on top of a subgrade consisting of a high plasticity clay with a resilient modulus of 2,500 psi (17 MPa) (Portillo, 2008). Total pavement thickness of the sections ranged from 11 in (28 cm) to 16 in (41 cm). Thickness differences were implemented in the base layer and a variety of binder grades were used in the intermediate and base layers. Each section was constructed on top of 6 in (15 cm) of lime stabilized subgrade.

Each test section included the following instrumentation as described by Portillo (2008). Strain gages were positioned on top of the lime treated subgrade. Four longitudinal and transverse strain gage pairs were installed directly on the wheel path while four pairs were installed 6 in (15 cm) to the right of the wheel path. One pressure cell was positioned directly on the wheel path. Temperature probes were located at mid-depth of each asphalt layer.

Testing was conducted seven times between July 2005 and October 2007 using a class five single axle dump truck. For each testing session, three sets of five passes were accomplished for each pavement section consisting of three different speeds; 20-25 mph (32-40 km/h), 40-45 mph (64-72 km/h), and 55-60 mph (89-97 km/h). Wheel loads ranged within approximately a kip (4.4 kN) of ten kip (44 kN) for each session (Portillo, 2008).

Portillo (2008) discovered speed and temperature had large effects on strain readings. The highest strains were recorded in August while the lowest strains were recorded in October. Additionally, there seemed to be a linear relationship between strain and temperature. Romanoschi (2006) noted strains did not seem to have a linear relationship with speed. As speed decreased the rate at which strains increased intensified. Abnormally, as described by Portillo, transverse strains were greater in magnitude than longitudinal strains. Although strains were typically lower than 70  $\mu\epsilon$ , sections with pavement thickness's less than 16 in (41 cm) experienced some longitudinal strains greater than 70  $\mu\epsilon$  when the truck was traveling at 20 mph (32 km/h) along with transverse strain exceeding 70  $\mu\epsilon$  at all three speed increments (Portillo, 2008). Strain measurements produced by the steering axle were typically between 50% and 70% of the strains produced by the rear axles suggesting that assessing damages caused by the steering axles ought to be considered (Romanoschi, Gisi, Portillo, & Dumitru, 2008).

#### 4.2.7 New York

In 2008, Ohio University and the New York State DOT instrumented a perpetual pavement test section in hopes of validating New York State DOT designs and to further investigate the concept of perpetual pavements. Sargand, Khoury, and Morrison (2012) describe the test section as a 7.5 in (19 cm) asphalt layer constructed on top of 9 in (23 cm) of rubblized Portland cement concrete (PCC).

Sargand et al. (2012) explains the instrumentation as three transverse and five longitudinal strain gages in the base layer and two transverse and six longitudinal strain gages in the intermediate layer. Moreover, two pressure cells were installed on the subgrade surface and two deep and shallow linear variable displacement transducers (LVDT) were installed to reference subgrade displacement and total pavement system displacement. Finally, thermocouples were placed in the base and intermediate layers to monitor pavement temperature. CVL testing was conducted in October of 2008 and May of 2009 (Bendana et al., 2009).

Overall, Sargand et al. (2012) found that strain results were typically below 70  $\mu\epsilon$ . Sargand et al. commented that during visual inspection between 2008 and 2011, no damage requiring reconstruction was noted even after the pavement had been subjected to heavy truck

loading and weathering. Sargand et al. also mentions that during FWD testing strain resulting in the base layer was around  $100 \mu\epsilon$  when using a 16 kip (71 kN) impact load. The pavement temperature was recorded at  $84^{\circ}\text{F}$  ( $29^{\circ}\text{C}$ ) during FWD testing.

#### **4.2.8 Accelerated Pavement Load Facility**

The Accelerated Pavement Load Facility (APLF) is an indoor pavement testing facility located at the Ohio University Lancaster branch campus. The facility is capable of representing tire loading and environmental effects. Tire loading can be simulated at speeds less than or equal to 5 mph (8 km/h) and at loads of up to 30 kip (133 kN) (Hernandez, 2010). The facility is unique in that it can simulate various environmental effects including air temperatures ranging between  $10^{\circ}\text{F}$  ( $-12^{\circ}\text{C}$ ) and  $130^{\circ}\text{F}$  ( $54^{\circ}\text{C}$ ) in addition to any percentage of humidity. The APLF also incorporates the use of underground pipes to allow the subgrade moisture to be manipulated. Ohio University evaluated four perpetual pavement sections at the APLF.

The perpetual pavement sections built at the APLF were used to evaluate the impact of various perpetual pavement thicknesses. Sargand, Figueroa, Edwards, and Al-Rawashdeh (2009) describe the sections as including an A6-A7 subgrade soil, a 6 in (15 cm) DGAB, and the use of FRLs. The total pavement thicknesses of the sections were 13 in (33 cm), 14 in (35.6 cm), 15 in (38 cm), and 16 in (40.6 cm), which was accomplished by following the WAY-30 design and altering the thickness of the intermediate layer and adjusting the DGAB to make the surface level. Different types of Warm-Mix Asphalt (WMA) were used in the surface layer but had negligible effects on the perpetual pavement behavior.

Instrumentation was installed in the sections in order to experimentally investigate the sections. Hernandez (2010) explains the instrumentation as including two longitudinal and two transverse strain gages spaced 18 in (46 cm) apart located at the bottom of the asphalt layer. Additionally, one pressure cell was placed on top of the subgrade and deep and shallow LVDTs were used.

Testing was performed at various temperatures using multiple loads. The pavement sections were subjected to loadings of 6 kip (27 kN), 9 kip (40 kN), and 12 kip (53 kN) at temperatures of  $40^{\circ}\text{F}$  ( $4.4^{\circ}\text{C}$ ),  $70^{\circ}\text{F}$  ( $21^{\circ}\text{C}$ ), and  $104^{\circ}\text{F}$  ( $40^{\circ}\text{C}$ ) (Hernandez, 2010). Sargand et al. (2009) state the test sections were tested before and after being subjected to 10,000 loading cycles of a 9 kip (40 kN) wheel load. Both the loading cycles and testing were performed at 5 mph (8 km/h).

Many response trends were discovered by Sargand et al. (2009) as a result of their experiment. Transverse and longitudinal strains in the FRL were only slightly higher as the thickness of the structure decreased independent of temperature and loading. These facts lead them to believe that similar effects would be seen by increasing the base structure as increasing the asphalt structure. Longitudinal strains remained below  $70 \mu\epsilon$  except for a few outliers during test runs with 12 kip (53 kN) of loading at  $104^{\circ}\text{F}$  ( $40^{\circ}\text{C}$ ). Increases in longitudinal strain were seen when increasing either load or temperature. Hernandez's (2010) report made additional observations by adding that the longitudinal strain went from compressive to tensile and back to compressive again while being loaded whereas the transverse strain was only subjected to tensile strain. Also, longitudinal strain seemed to increase more rapidly as temperature increased while the transverse strain had a linear relationship with temperature creating an increased difference between the two at higher temperatures. Finally, he added temperature had less effect on strain as pavement thickness was increased.

#### **4.2.9 Interstate 77, Canton, Ohio**

The first instrumented perpetual pavement section constructed in Ohio was located in Canton, Ohio on Interstate 77. Sargand and Figueroa (2010) recounted the section had a total pavement thickness of 16.25 in (41.3 cm), which included an FRL and an SMA surface course. The section was reported to have been instrumented with three longitudinal and three transverse strain gages at the bottom of the FRL, two pressure cells located on the subgrade surface, and thermocouples installed near the strain gages.

CVL testing of the section took place on December 15 of 2003 (Sargand & Figueroa, 2010). Sargand and Figueroa (2010) denoted the testing as a single axle dual tire producing a 13.5 kip load at speeds of 5 mph (8 km/h), 30 mph (48 km/h), 40 mph (64 km/h), and 50 mph (80 km/h). The pavement temperature that evening was measured at 36°F (2.2°C). No further testing has been completed because of high traffic volumes on the section.

Due to minimal testing only a few conclusions could be made by Sargand and Figueroa (2010). The first was an increase in strain with decreasing speeds. The maximum longitudinal and transverse strains, 35.6  $\mu\epsilon$  and 24.4  $\mu\epsilon$  respectively, were recorded at a creep speed of 5 mph (8 km/h). Strains received at 50 mph (80 km/h) were slightly lower at 28.7  $\mu\epsilon$  and 20.0  $\mu\epsilon$  for longitudinal and transverse respectively. Pressures measured by the pressure cells were minimal for all increments of speed.

#### **4.2.10 U.S. Route 30, Wayne County, Ohio**

In the fall of 2005, the Ohio DOT constructed a perpetual pavement test section on U.S. Route 30 in Wayne County, Ohio, also known as WAY-30. Sargand, Houry, Romanello, and Figueroa (2006) label the route as being a rural freeway. Three identical test sections were instrumented in order to analyze performance and design assumptions.

Sargand, Romanello, and Figueroa (2008) made the following descriptions on the three instrumented test sections. The sections had total pavement thicknesses of 16.25 in (41.3 cm) including a 4 in (10 cm) FRL and an SMA surface course. The asphalt layer was constructed on a 6 in (15 cm) crushed DGAB all of which was supported by a compacted subgrade with a CBR of between four and six. Strain gages were installed in the FRL in order to monitor fatigue resistance as well as in the intermediate layer to evaluate the pavement's potential for cracking. Strain gages were oriented in the longitudinal and transverse directions. Shallow and deep LVDTs were used to measure displacement of the total pavement system or subgrade. Subgrade pressure was measured through the use of pressure cells installed on the subgrade surface. An automated weather station was constructed to monitor air temperature, precipitation, wind speed and direction, relative humidity, and incoming solar radiation.

CVL testing was conducted in December of 2005, July of 2006, and May of 2008. Testing performed in December of 2005 was done prior to the roadway being opened to traffic. A standard Ohio DOT single and tandem axle truck were the testing vehicles (Sargand et al., 2008). Sargand et al. reported pavement temperatures of 30°F (-1.1°C) to 35°F (1.7°C) were experienced in December and 95°F (35°C) to 126°F (52 °C) in July. Pavement temperatures ranging between 56°F (13°C) and 74°F (23°C) were reported by Restrepo-Velez (2011) for the May testing. Varying between approximately 20 kip (89 kN) to 30 kip (133 kN) and 35 kip (156 kN) to 50 kip (222 kN) were axle loadings used for the tandem and single axle, respectively (Restrepo-Velez, 2011; Sargand et al., 2008). Testing was conducted in a similar fashion during all three sessions.

A large amount of quality results were obtained on WAY-30 since testing was conducted at various speeds, temperatures, loads, and axle configurations. Although the tandem axle truck

carried a greater load than the single axle truck, strains were found to be higher for the single axle truck than for the tandem axle truck while both axle types produced higher strains at lower speeds as depicted by Restrepo-Velez (2011). However, this was not the case for transverse strains recorded in the intermediate layer. She discovered strains were higher in the FRL than the intermediate layer. Also, Restrepo-Velez found longitudinal strains experienced tension and compression while transverse strain experienced only tension. Sargand et al. (2006) reported pressures in the subgrade were higher due to the tandem axle than the single axle. Furthermore, pressures typically decreased with increasing truck speeds. Although no deflections were recorded exceeding 20 mil (0.5 mm), greater deflections were produced as temperature was increased (Romanello, 2007; Sargand et al., 2008). Romanello (2007) added this effect was less profound in the subgrade. Sargand et al. (2008) concluded although some strains were recorded above the 70  $\mu\epsilon$  threshold, they were produced at abnormally slow speeds and heavy loads and therefore under typical conditions the pavement would rarely be subjected to strain values in the FRL exceeding the FEL.

#### **4.2.11 Summary**

Many common discoveries and trends can be discerned in the research reviewed in this chapter. Instrumentation almost always included strain gages located at the bottom of the asphalt layer along with pressure cells installed on the subgrade surface. Furthermore, temperature probes were used to monitor pavement temperature. Some researchers also installed strain gages in the intermediate layer and/or displacement sensors. All of the research showed an increase in pavement strain, pressure, and displacement with increasing pavement temperatures. Additionally, many findings reported an exponential relationship between strain and temperature. Researchers tended to find an increase in strain with a decrease in speed as well with some researchers denoting a linear relationship. Strain results typically decreased with decreasing loads as well as an increase in total pavement thickness. If multiple axle configurations were used, tandem axles, even when carrying higher loads, typically generated lower strains. This was not necessarily the case when analyzing pressure and displacement data.

## 5 DEL-23 Project Background

### 5.1 Project Site Description

As part of the ODOT's Partnered Research Exploration Program, ODOT and the Ohio Research Institute for Transportation and the Environment (ORITE) continued research with intentions of developing optimized perpetual pavement designs in Ohio through the instrumentation of four pavement test sections with varying thicknesses during reconstruction of test sections on the Strategic Highway Research Program (SHRP) Test Road on U.S. Route 23 in Delaware County, Ohio, near the town of Waldo, henceforth referred to as "DEL-23". The project was focused on analyzing the impact of varying total pavement thicknesses by monitoring data obtained during CVL testing. Research findings should help provide further understanding of the optimal design thickness for perpetual pavements in order to minimize their life cycle costs. The location of DEL-23 is indicated with a green dot in the map of Ohio in Figure 1.

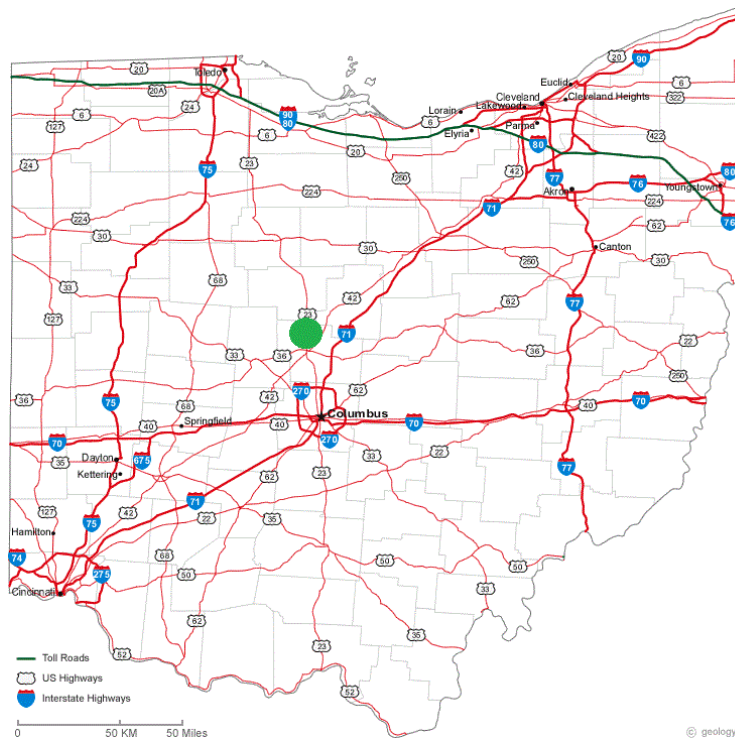


Figure 1. Location of SHRP Test Road (DEL-23), indicated by the green dot (Geology, 2013).

In this project, DEL-23 included four asphalt concrete perpetual test sections. Two of the test sections were constructed on North Waldo Road as indicated by the red arrow in Figure 2. The two sections were constructed adjacent to each other, section 39BN803 in the northbound lane and section 39BS803 in the southbound lane. The two remaining test sections were constructed on the northbound lanes of the U.S. Route 23 mainline, indicated by the green arrow in Figure 2. These sections were also adjacent to each other with section 39D168 residing in the driving lane and section 39P168 in the passing lane.





Figure 2. View of SHRP test road with arrows showing location of DEL-23 Test Sections (picture by ODOT).

## 5.2 Design of Test Sections

The pavement thicknesses were selected to validate results previously obtained from existing sections on WAY-30 and the Accelerated Pavement Load Facility (APLF). A practical perpetual pavement design was ultimately used. Sections with a total asphalt thickness of 15 in (38 cm) and 13 in (33 cm) were similar to sections constructed in the APLF and were expected to have strains of  $70 \mu\epsilon$  or less at the bottom of the FRL. The section with a total asphalt thickness of 11 in (28 cm) was expected to have a strain of  $70 \mu\epsilon$  or more. Table 1 lists specifications for each layer used.

Table 1. Layer specifications for DEL-23 perpetual pavement sections.

Layer	Description	PG Binder Grade	Binder Content
Surface	Fine Graded Polymer Asphalt Concrete	PG 76-22M	7.6%
Intermediate	Asphalt Concrete, 19 mm	PG 64-28	4.9%
Base	Asphalt Concrete	PG 64-22	4.2%
Fatigue Resistant	Fatigue Resistant Base Layer	PG 64-22	4.6%

Table 2 provides the specified layer thicknesses for each section. Each section was constructed on a six inch DGAB. The subgrade for all four sections had a soil classification of

A-6. In addition, the subgrade for sections 39BS803 and 39BN803 had been chemically stabilized through lime treatment during a previous construction project. Testing conducted by Ohio University revealed the subgrade beneath sections 39D168 and 39P168 had an average resilient modulus of 20 ksi (138 MPa) while the stabilized subgrade for section 39BS803 and 39BN803 had an average resilient modulus of 40 ksi (276 MPa). After construction of the test sections, core samples obtained revealed Section 39P168 had been constructed with a total pavement thickness of 16 in (41 cm), a 3 in (7.6 cm) increase from what had been specified. Due to this discrepancy, data obtained from this section are not presented in this report.

**Table 2. Specified layer thicknesses of DEL-23 pavement sections.**

Layer	39D168		39P186		39BS803		39BN803	
	(in)	(cm)	(in)	(cm)	(in)	(cm)	(in)	(cm)
Surface Layer	1	2.5	1	2.5	1	2.5	1	2.5
Intermediate Layer	2	5.1	2	5.1	2	5.1	2	5.1
Base Layer	8	20.3	6	15.2	6	15.2	4	10.2
Fatigue Resistant Layer	4	10.2	4	10.2	4	10.2	4	10.2
Total Pavement Thickness	15	38.1	13	33.0	13	33.0	11	27.9

### 5.3 Instrumentation of Test Sections

In order to evaluate pavement responses while being exposed to dynamic loading and various environmental conditions, numerous sensors were installed throughout the pavement structure. ORITE developed a comprehensive instrumentation plan including the use of thermocouples to measure pavement temperature throughout the depth of the pavement and air temperature. Linear Variable Differential Transformers (LVDT) were installed in order to measure deflections of the pavement structure as well as the subgrade exclusively and strain gages to monitor horizontal pavement strains. Pressure cells recorded subgrade and FRL pressures. Horizontal strain gages were installed in every asphalt layer in the longitudinal, transverse, and 45° positions. Furthermore, for each section excluding 39BN803, a square and round hole were cored through the entire depth of the pavement along the instrumentation line and strain gage rosettes were bonded to their walls to acquire additional strain measurements including the vertical direction. A detailed layout of the entire instrumentation plan is presented at the conclusion of this section.

#### 5.3.1 Strain Gage Installation

Two different strain gages were used to measure pavement strains on DEL-23. A majority of the gages were embedment strain gages of type KM-100HAS, provided by Tokyo Sokki Kenkyujo Co. These gages had a 350 Ω full bridge resistance. The second type of strain gages used were asphalt strain gages of type PMFLS-60, also provided by Tokyo Sokki Kenkyujo Co. In contrast, these gages had a 120Ω quarter bridge resistance.

For all of the sections excluding section 39BN803, four longitudinal, one transverse, and one 45° diagonally-oriented strain gage were installed at the bottom of the FRL. Also, the base layer was instrumented with three longitudinal and transverse strain gages accompanied by two 45° strain gages. Finally, the intermediate layer contained two sets of a longitudinal, transverse, and 45° strain gage. Section 39BN803 utilized six longitudinal strain gages in the FRL and three longitudinal and three transverse strain gages in the base layer. It did not contain any gages in

the intermediate layer.

Preceding the paving of the asphalt layer receiving instrumentation, strain gage location layouts were painted using LVDT stakes as reference points. Lead wires were stretched to their pull boxes on the side of the road and buried in the DGAB when instrumenting the FRL, or taped to the asphalt surface when instrumenting the base and intermediate layers. In order to prevent the paver from damaging or shifting the strain gages they were embedded and buried by hand in a thin layer of asphalt before paving equipment laid down the entire lift. Asphalt used to embed and bury the strain gages was attained directly from the truck and sifted in order to remove large aggregates that might have punctured the strain gages or lead wires. For further protection of the instrumentation, during compaction, two passes of the compaction rollers were made before vibratory roller compaction was used. All of the strain gages installed were found to be working properly after the pavement had cooled.

Due to the thin nature of the surface layer, a slightly different approach was used when installing gages in this layer. In all of the sections except for section 39BN803, one longitudinal, transverse, and 45° oriented strain gage was installed. This was accomplished by leaving a thin piece of metal approximately the size of the strain gage in the proper location and orientation while the surface layer was paved. Figure 3 illustrates the metal plates after the surface layer had been paved. After the paving was complete and the asphalt had cooled, these metal plates were removed and a strain gage was bonded in its place. The gages used for the surface layer were 120Ω, quarter-bridge, type WFLM-60, provided by Tokyo Sokki Kenkyujo Co.



Figure 3. Surface layer strain gage orientations.

### 5.3.2 Pressure Cell Installation

For DEL-23, pressure cells were utilized to monitor vertical pressure in the subgrade. Two Geokon 3500 pressure cells were installed on the subgrade surface for each section. These pressure cells are created to measure changes in stress applied to their surface (Hornyak, Crovetti, Newman, & Schabelski, 2007). These pressure cells measure pressure through the use of a pressure transducer connected to liquid, a high stiffness oil, confined between two steel plates (Portillo, 2008). When a load is applied to the flat circular surface, the plates deflect causing the fluid pressure to increase.

In order to avoid construction equipment driving directly over the pressure cells, they were installed after the DGAB had been graded. At this point, holes were excavated down to the subgrade along with trenches leading off the road large enough to encompass the earth pressure

cells and their lead wires. The pressure cells were installed using a layer of sand above and below them to provide a uniform surface before being buried by the aggregate base.

In addition to the subgrade pressure cells, two pressure cells were installed on the surface of the FRL in every section except for 39BN803. These pressure cells were different from those used on the subgrade. They were Total Earth Pressure Cells purchased from RST Instruments. A unique feature of these pressure cells was a kink in the tube allowing the cell to lie flat on the hard, DGAB surface while their handles were buried in the DGAB. Similarly, the pressure cells were first surrounded by sand to provide them with a uniform surface. Then, directly before paving took place, the pressure cells were hand compacted in a thin layer of sifted asphalt in a similar fashion as the strain gages. Their lead wires were installed similar to that of the strain gages as well.

### **5.3.3 Thermocouple Installation**

Two thermocouples were installed in the instrumentation line of every asphalt layer receiving instrumentation. Single point thermocouples purchased from Measurement Instruments were used to measure pavement temperature of the various asphalt layers. An additional thermocouple was used to measure air temperature. Thermocouples were installed in the same way as strain gages.

### **5.3.4 Linear Variable Differential Transducer (LVDT) Installation**

Linear Variable Differential Transducers (LVDTs) from Trans-Tek were used to measure vertical deflections. Before the LVDTs were installed, they were calibrated. Calibration data can be found in Appendix A.

A diagram of the LVDT enclosure and reference rod for the 13 in (33 cm) section is displayed in Figure 4. Diagrams of the LVDT enclosures and reference rods for all sections can be found in Appendix B. As shown in the Figure, the LVDT was connected to a plate inside the LVDT enclosure. The LVDT enclosure was installed in the asphalt concrete so that when the surface of the pavement displaced in the vertical direction, the LVDT enclosure and thus the LVDT displaced as well. During these vertical displacements the LVDTs measured off of deep and shallow reference rods. Deep LVDT reference rods extended 11 ft (3.4 m) below the subgrade surface where displacements from the load were insignificant. Displacements measured by deep reference rods represented the displacement of the entire pavement system. Shallow reference rods, as shown in Figure 3.16, extended to the subgrade surface. By subtracting displacements measured from the shallow reference rods from displacements measured from the deep reference rods displacement of the subgrade was obtained.

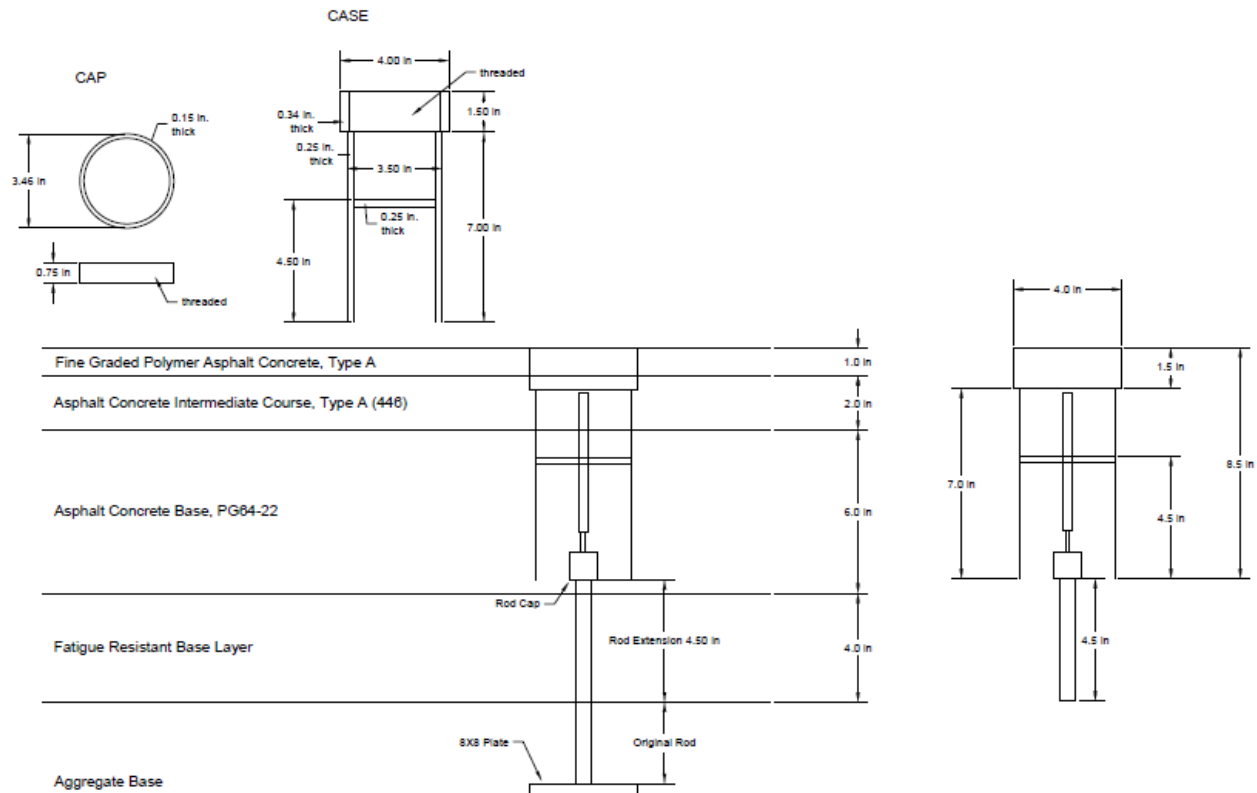


Figure 4. LVDT enclosure and reference rod diagram (1 in = 2.54 cm).

LVDT installation began after the DGAB had been placed. At this point, the LVDT locations were surveyed and holes were bored approximately 10 ft (3 m) deep in the subgrade in order to install the deep LVDT reference rods. PVC piping was used to prevent the hole from collapsing and reference rods were driven another foot or two (0.3-0.6 m) into the bottom of the hole. Next, the deep reference rods were grouted into place. Holes were then excavated down to the subgrade surface and shallow LVDT plates and reference rods were placed. Surveys were then made so that the location of the LVDT reference rods could be located after the completion of paving.

After the completion of paving, cores were made through the pavement in order to gain access to the LVDT reference rods. Then, rod extensions and caps were connected to the existing rods to elevate them to the proper height. LVDTs were housed in cases that were connected using bolts and Pro-proxy adhesive in the core holes. The caps of the LVDT enclosures were flush with the pavement surface.

### 5.3.5 Strain Gage Rosette Hole Installation

A unique feature installed in DEL-23 were vertical rosettes installed along the walls of a round and square hole in section 39BS803, 39P168, and 39D168. The round holes had diameters of 6 in (15 cm) and the square holes had widths of 6 in (15 cm). Strain gage rosettes were installed in the holes on the walls parallel and perpendicular with traffic. Two strain gages rosettes per wall were placed in the base layer while one strain gage rosette was placed in the intermediate and surface layers. Surface layer strain gage rosettes were not implemented in the round holes. A diagram for the square rosette hole in the 13 in (33 cm) section is displayed in

Figure 5. Dimensions of the base layer strain gage rosettes varied depending on the thickness of the base layer. Diagrams for square and round rosette holes for all sections containing them can be found in Appendix C. The gages used for the rosette holes were 120 $\Omega$ , quarter-bridge, type WFLM-30, provided by Tokyo Sokki Kenkyujo Co. Due to limitations involved with the thickness of the surface layer, type WFLM-10 gages were used for the surface layer.

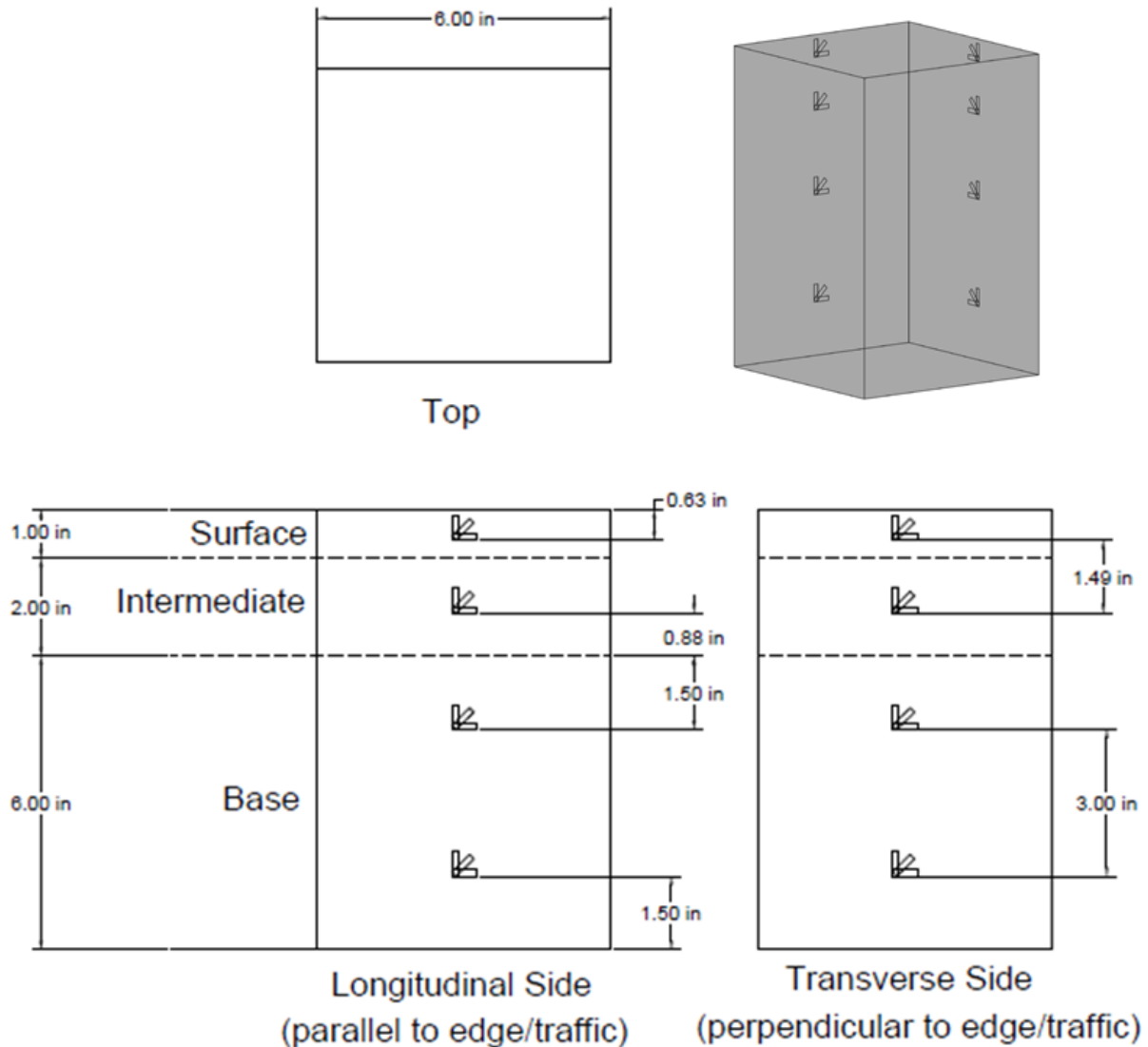


Figure 5. Strain gage rosette square hole diagram (1 in = 2.54 cm).

The rosette hole installation process began after the DGAB was placed. At this point, PVC pipes were buried in the DGAB from the location of the rosette holes to the edge of the road so strain gage wires could be snaked underneath the pavement after the rosette holes were constructed. Next, after the completion of paving, six inch cores were made in the locations of the rosette holes (Item 1 of Figure 6). A grinder was used to square off the square rosette holes as shown in Item 2 of Figure 6. Then, strain gage rosettes were bonded to the walls of the holes in their proper locations through the use of a rubber mat (Items 3 and 4 of Figure 6). For the

square holes the strain gage rosettes were held in place with a clamp while the adhesive dried while a balloon was used to keep pressure on the strain gage rosettes in the round holes (Item 5 of Figure 6). Finally, lead wires were snaked through the PVC piping.



**Figure 6. Strain gage rosette installation: 1. Drilling hole; 2. Grinding square hole; 3. Attaching gage to round hole; 4. Gages arrayed for installation; 5. Balloon used to hold gages in place while adhesive dried; 6. Gages in square hole with lead wires attached.**

A diagram illustrating the entire instrumentation layout for the 13 in (33 cm) and 15 in (38 cm) sections is presented in Figure 7. Instrumentation diagrams for the 11 in (28 cm) section are shown in Appendix D. Yellow represents strain gages which can be found in the fatigue resistant, base, and intermediate layers. Beneath the strain gage locations in the profile view an L, T, or 45 is given indicating the orientation of the strain gage with L, T, and 45 representing longitudinal, transverse, and 45° respectively. Red represents thermocouples. Two thermocouples were located within each layer's strain gage lineup as shown in Figure 7. Deep and shallow referenced LVDTs can be found in either direction of the strain gages and thermocouples. LVDTs are represented by the color blue. Finally, located at the end of the instrumentation line are the strain gage rosette holes with the round hole preceding the square hole. The strain gage rosette holes are indicated with turquoise. Surface layer strain gages are not presented in Figure 7 but were aligned directly before the first set of LVDTs; all of the sensors reside in the wheel path of the lane.

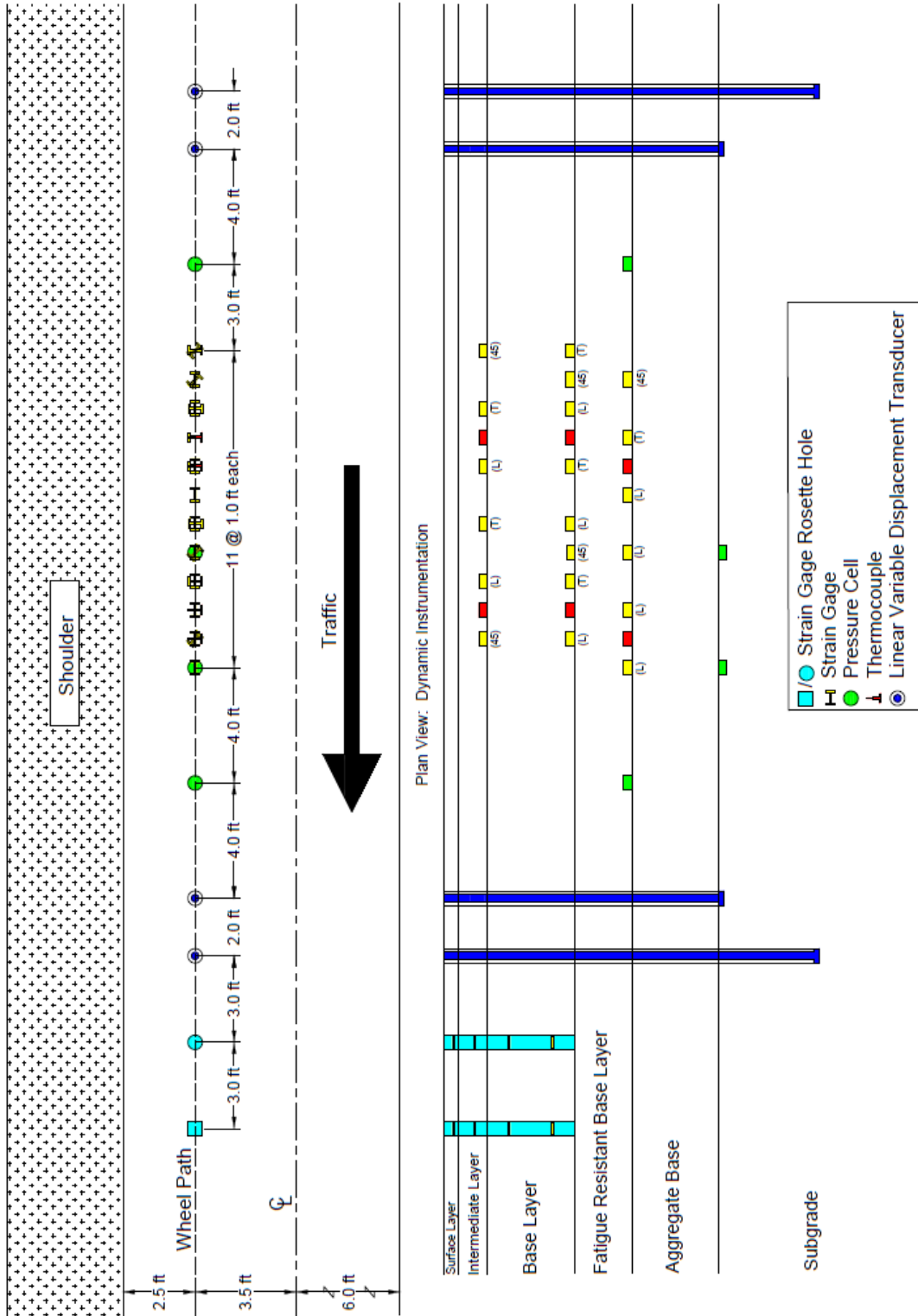


Figure 7. Instrumentation layout for 13 in (33 cm) and 15 in (38 cm) sections (1 ft = 0.305 m).



## 5.4 Controlled Vehicle Load Testing

Controlled vehicle load (CVL) testing was performed to evaluate the various pavement structures under real traffic conditions. Many variables were controlled while performing CVL tests. For example, data was collected from the sensors while being subjected to a known load, axle type, tire pressure, and speed. Although lateral offset of the tire load could not be completely controlled, it was monitored through the use of sand prints as shown in Figure 8. CVL testing was performed using two different drivers driving ODOT dump trucks. Figure 9 is a photo of one ODOT truck utilized. For every variation of load, axle type, tire pressure, and speed, at least five tests were performed and the three tests with the least amount of lateral offset measured were used for analysis. The actual offset measurements are presented in Appendix I.



Figure 8. Measurement of lateral offset from tire track after loaded truck has passed over the sensors.



Figure 9. An ODOT truck loaded for CVL testing.

The first round of CVL testing was conducted during the end of November and throughout December of 2012. For this round of testing, two types of axle configurations were used with the maximum load the ODOT trucks were capable of carrying. The first truck utilized a dual tire, tandem axle while the second truck consisted of a single axle with a single wide-based tire. The two axle configurations are depicted in Figure 10. The maximum loading

resulted in the tandem and single axle types carrying approximately a 37 kip (165 kN) and 29 kip (129 kN) axle load, respectively. The exact loadings and dimensions used can be found in Appendix E. This round of testing consisted of tire pressures of 80 psi (552 kPa), 110 psi (758 kPa), and 125 psi (862 kPa) and truck speeds of 5 mph (8 km/h), 30 mph (48 km/h), and 55 mph (89 km/h).

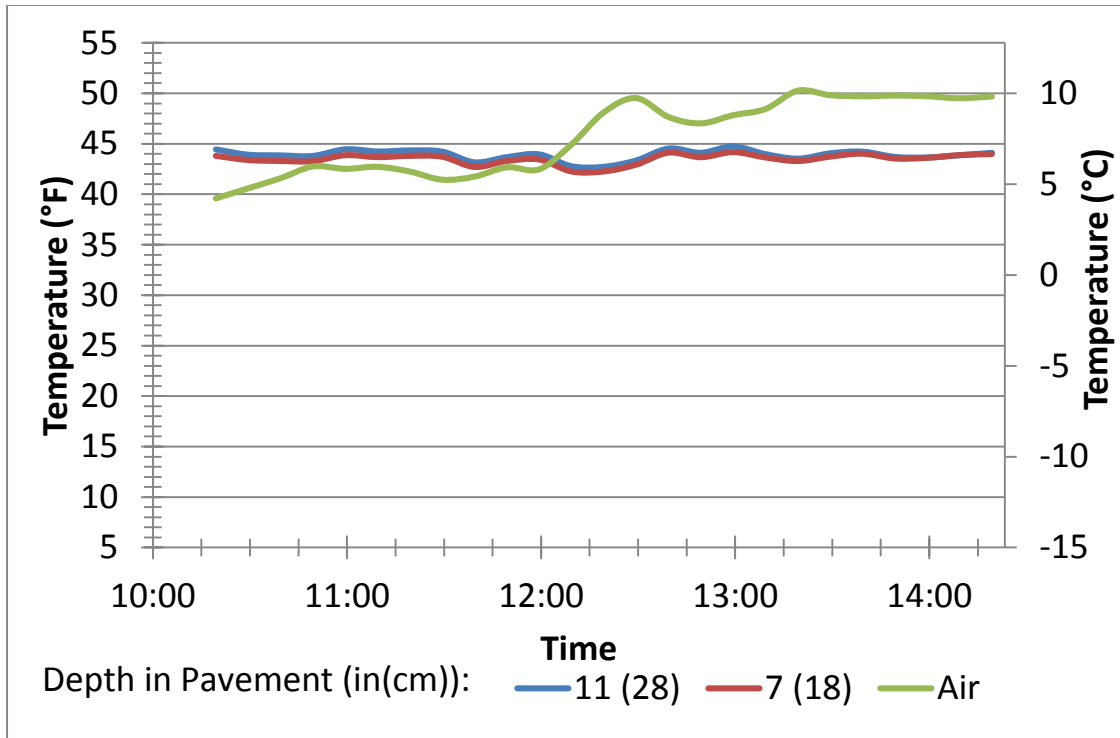


Figure 10. Axle configurations used in CVL tests: Left, tandem axle; right, single axle with wide base tire.

## 6 CVL Testing Pavement Response in Late Autumn

Controlled vehicle load (CVL) testing was conducted on the perpetual pavement test sections during the months of November and December 2012. Three separate days were used for testing of the 11 in (28 cm), 13 in (33 cm), and 15 in (38 cm) sections but testing for each section did not extend to multiple days. Henceforth, sections 39BN803, 39BS803, and 39D168 will be identified as the 11 in (28 cm), 13 in (33 cm), and 15 in (38 cm) sections respectively. Each section was tested throughout the course of a single day, typically between 10:00 AM and 3:00 PM. Although pavement temperatures remained fairly consistent during testing some variations were seen throughout the course of testing for each section and between testing days. The following provides information on air and pavement temperatures measured throughout the course of testing.

The 11 in (28 cm) section was tested on December 18, 2012. Figure 11 displays the air and pavement temperatures recorded during testing. Temperatures were measured every 15 minutes. Testing was conducted throughout the day at a tire pressure of 125 psi (862 kPa), followed by 110 psi (758 kPa), and finally 80 psi (552 kPa). For each tire pressure, testing began at 5 mph (8 km/h), then 30 mph (48 km/h), and finally 55 mph (89 km/h). Tandem and single axle trucks made test runs consecutively. Temperatures recorded during the test days can be found in tabular form in Appendix F.



**Figure 11. 11 in (28 cm) section temperature profile during CVL testing December 18, 2012.**

The 13 in (33 cm) section was tested on December 19, 2012. Figure 12 illustrates the air and pavement temperatures measured during testing. Temperatures were recorded every 15 minutes. Testing was conducted throughout the day at a tire pressure of 125 psi (862 kPa), followed by 110 psi (758 kPa), and finally 80 psi (552 kPa). For each tire pressure, testing began at 5 mph (8 km/h), then 30 mph (48 km/h), and finally 55 mph (89 km/h). Tandem and single axle trucks made test runs consecutively.

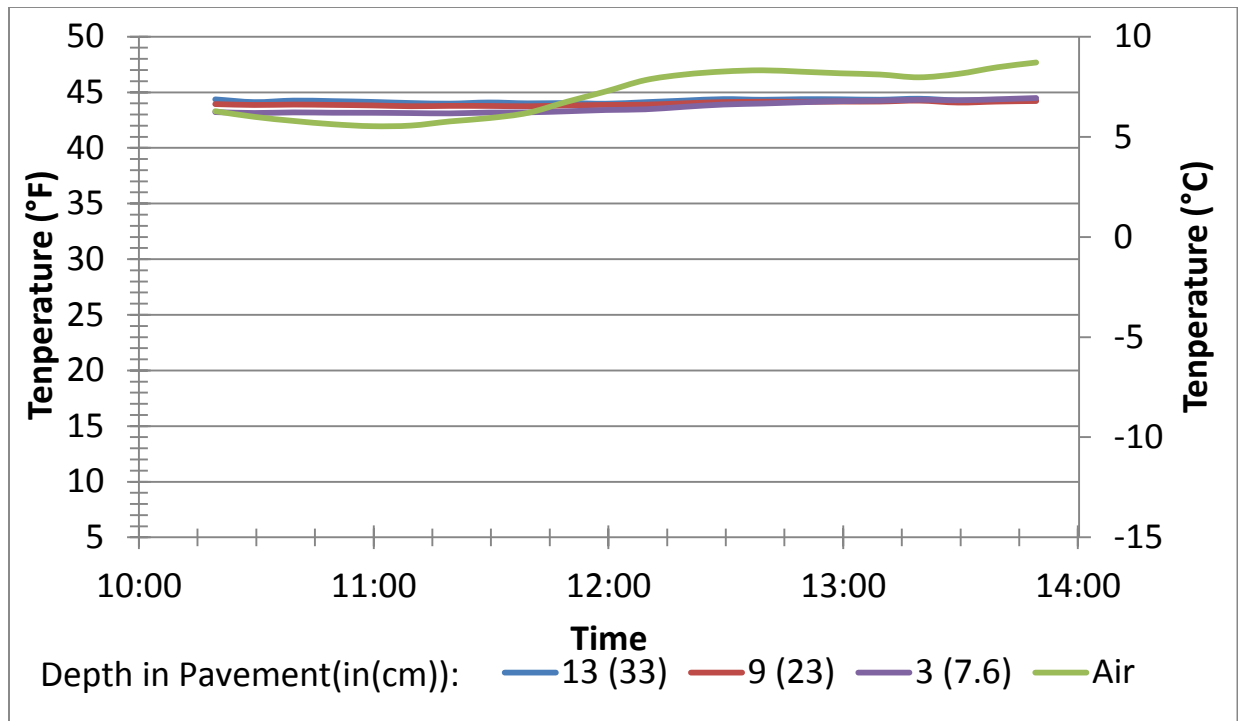


Figure 12. 13 in (33 cm) section temperature profile during CVL testing, December 19, 2012.

The 15 in (38 cm) section was tested on November 29, 2012. Figure 13 shows the air and pavement temperatures measured throughout the progression of testing. Temperatures were, once again, measured every 15 minutes. Testing was conducted throughout the day at a tire pressure of 125 psi (862 kPa), followed by 110 psi (758 kPa), and finally 80 psi (552 kPa). Unlike the 11 in (28 cm) and 13 in (33 cm) sections, for each tire pressure, testing began at 55 mph (89 km/h), then 30 mph (48 km/h), and finally 5 mph (8 km/h). Tandem and single axle trucks made test runs sequentially. Tables containing the full set of strain data are presented in Appendix G, and tables with the measurements collected from the LVDTs and pressure cells are given in Appendix H. The subsequent discussion is based on the maximum and average response values obtained.

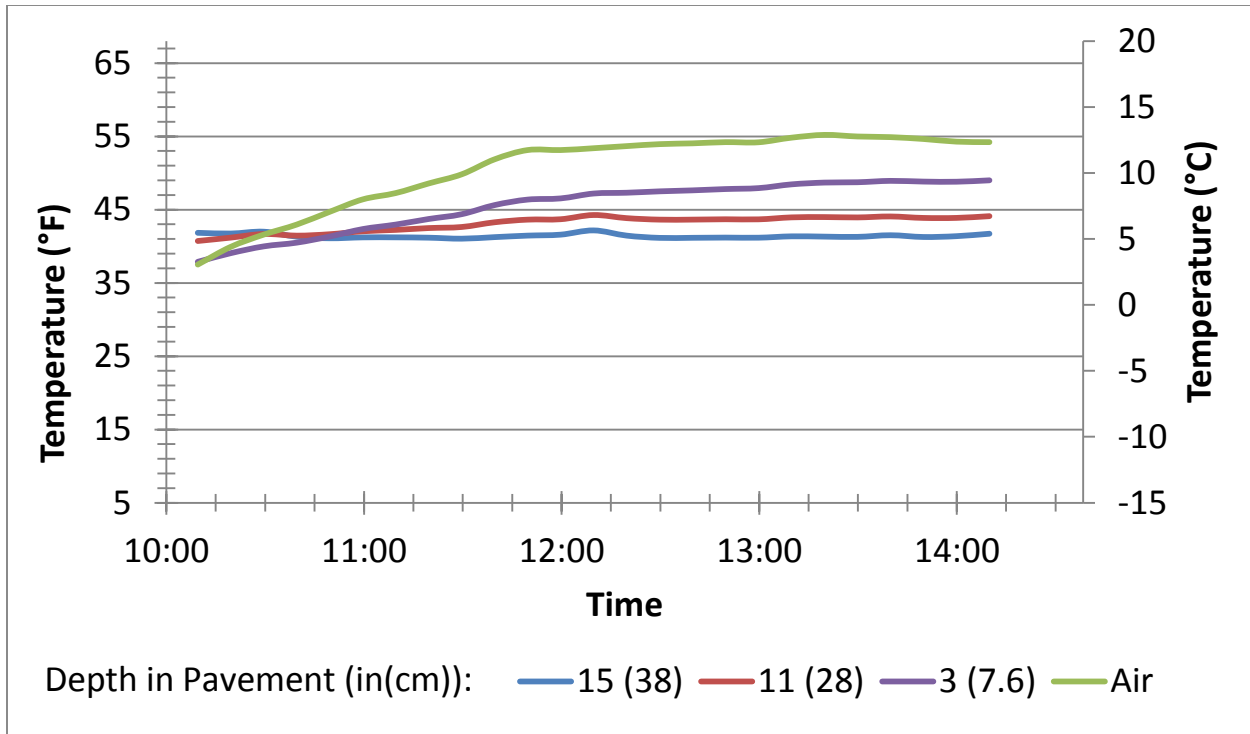
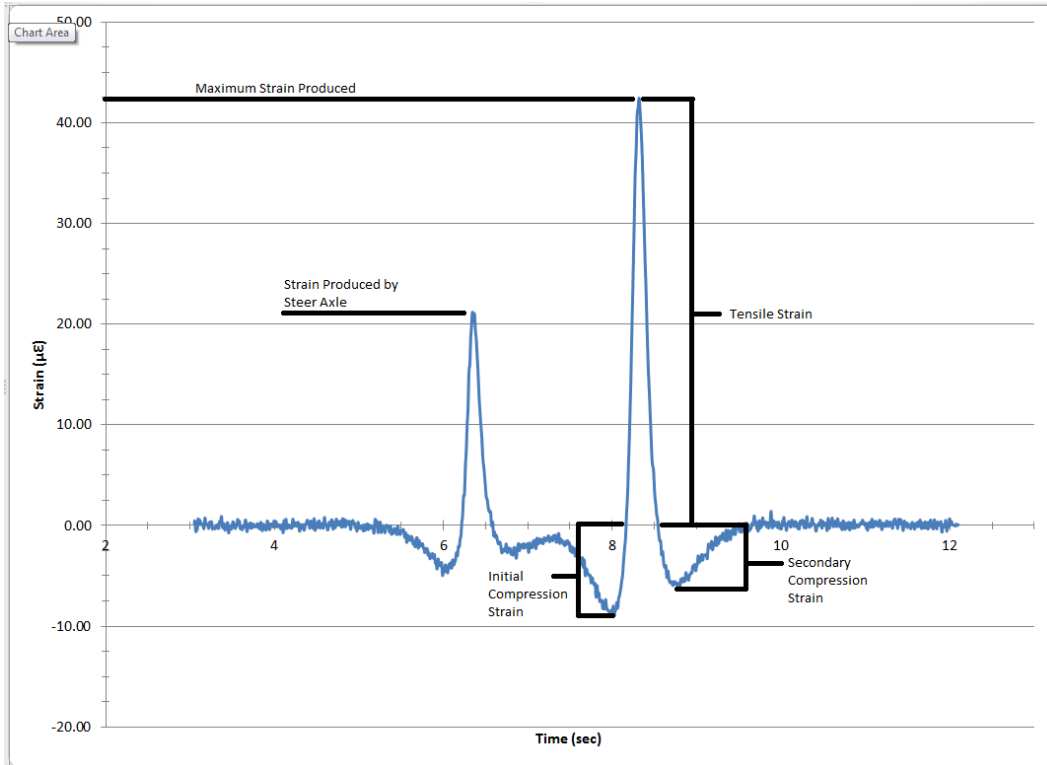


Figure 13. 15 in (38 cm) section temperature profile during CVL testing, November 29, 2012.

### 6.1 Strain Response of the Pavement

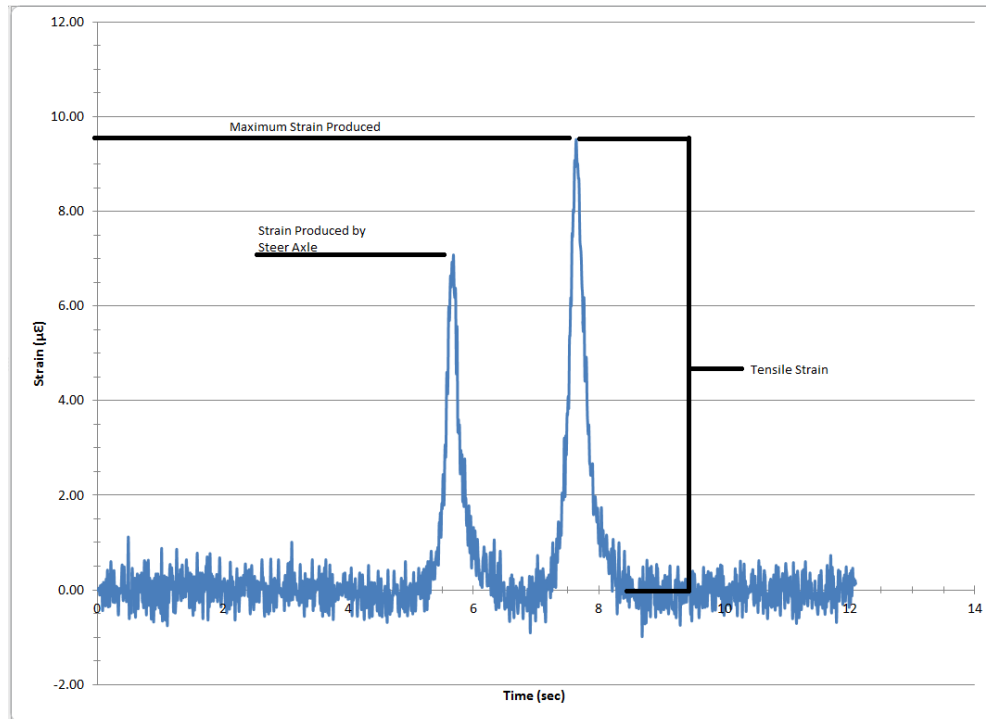
The pavement's strain response was dependent on many factors. One of these factors included the orientation of the strain gage. A strain gage aligned parallel with traffic, or in the longitudinal direction, tended to receive compression strains as the truck tire approached and moved away from the location of the strain gage. However, while the tire load was passing over the longitudinal strain gage it produced a tensile strain. The compression and tensile strains experienced by a longitudinally oriented strain gage are displayed in Figure 14 which represents the longitudinal strains measured in the FRL of the 11 in (28 cm) section during a single axle test run.



**Figure 14. Longitudinal strain response measured from passing single axle truck with wide-base tire.**

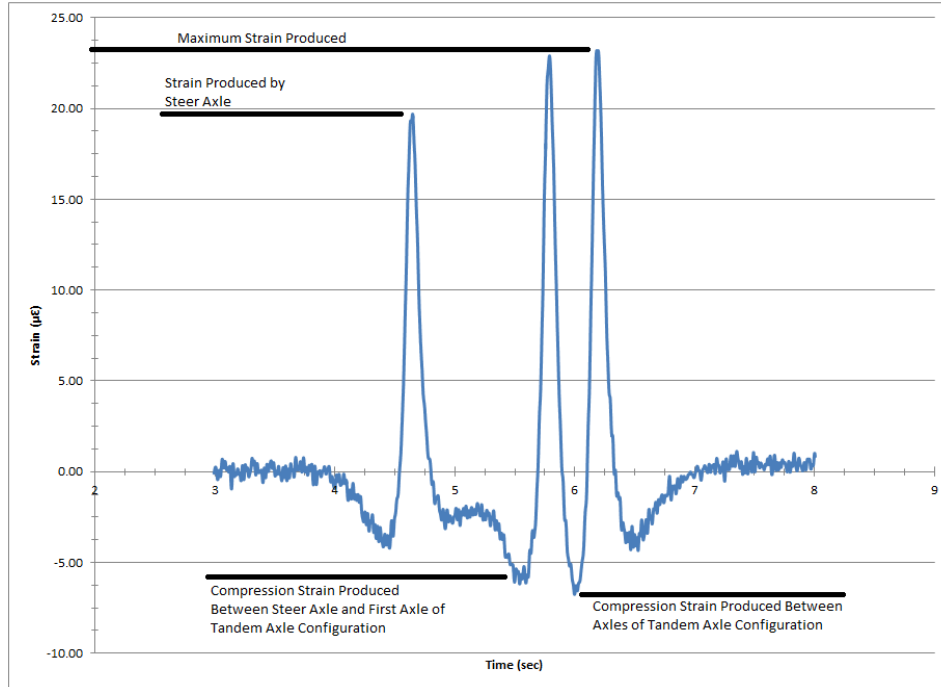
As seen in Figure 14, Compression strains were recorded as negative values whereas tensile strains were recorded as positive values. The first tensile strain peak received by the strain gage was due to the steer axle of the truck while the second tensile strain peak was due to the loading produced by the single axle at the rear of the truck. Figure 14 shows both the steer and single axle tensile strain peaks are preceded and succeeded by smaller but notable compression strain peaks. Although it is important to note the pavement responded with both tensile and compression strains in the longitudinal direction, the critical value, which will be analyzed throughout these results, was the maximum strain recorded. For this scenario, the maximum strain recorded was tensile and was approximately 42  $\mu\epsilon$ . As noted in Figure 14, the maximum strain produced by the steer axle was approximately 22  $\mu\epsilon$ ; about 52% of the maximum tensile strain produced by the rear single axle. The tire load produced by the steer axle, which utilized a regular tire, was measured to be 6.10 kips; about 43% of the tire load produced by the rear single axle wide-base tire configuration which was measured at 14.25 kips.

Conversely, strain gages oriented perpendicular to the flow of traffic, or in the transverse direction, tended to receive only compressive or tensile strains depending on the depth of the gage. The transverse strains measured in the base layer of the 11 in (28 cm) section during a single axle test run are shown in Figure 15. As both the front and single rear axle passed over the strain gage, only a tensile strain peak was recorded by the strain gage.



**Figure 15. Transverse strain response measured from passing single axle truck with wide-base tire.**

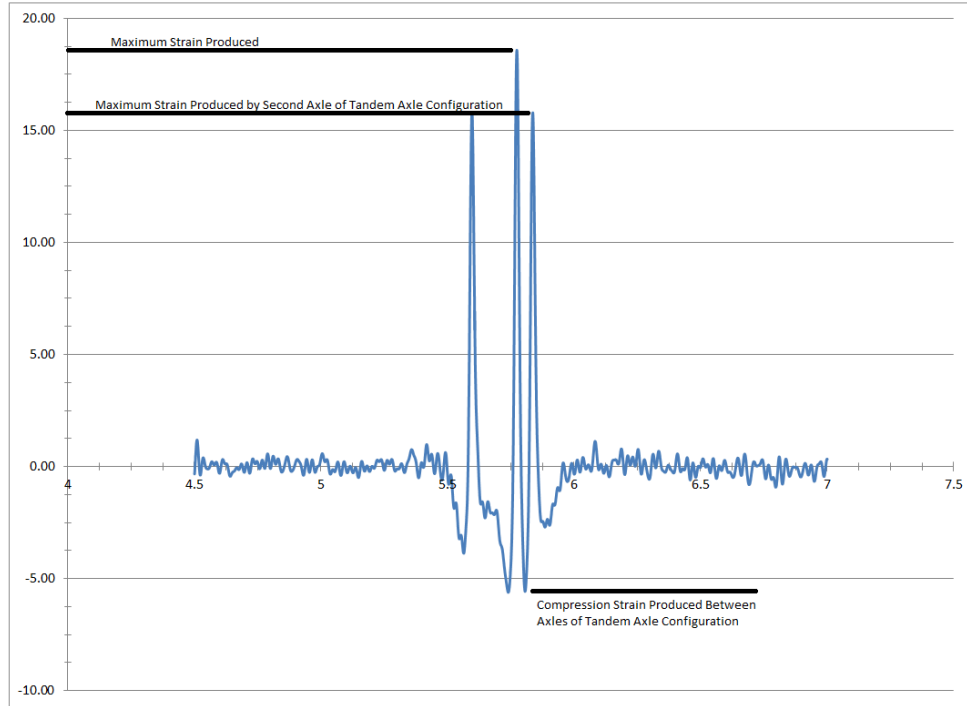
The tandem axle truck was another factor influencing the pavement's strain response. Figure 16 displays the longitudinal strains recorded in the FRL of the 11 in (28 cm) section during a tandem axle test run. It is important to note this test run was performed at 5 mph (8 km/h). As displayed in Figure 16, test runs involving the tandem axle truck resulted in three tensile strain peaks, one for the steer axle and one for each of the axles that comprised the tandem axle. Figure 16 also shows each tensile strain peak, like the tensile peaks produced by the single axle, were led and followed by a compression strain peaks although the compression strain did not return to zero between the tandem axles or between the steer axle and first axle of the tandem axle configuration. The highest value of compression strain measured was for the tandem axle configuration. As noted in Figure 16, the maximum tensile strain produced by the steer axle was approximately 19  $\mu\epsilon$ ; about 83% of the maximum tensile strain produced by the tandem axle, 23  $\mu\epsilon$ . The tire load produced by the steer axle was measured to be 6.60 kip (29.4 kN); about 75% of the dual-tire loads produced by the tandem axle which was measured at 8.8 kip (39.1 kN). The tandem axle truck had dual-tires spreading the load in the rear of the truck between eight tires while the single axle truck used wide based tires spreading the load in the rear of the truck between only two tires.



**Figure 16. Longitudinal strain in the FRL measured from tandem axle truck passing at 5 mph (8 km/h).**

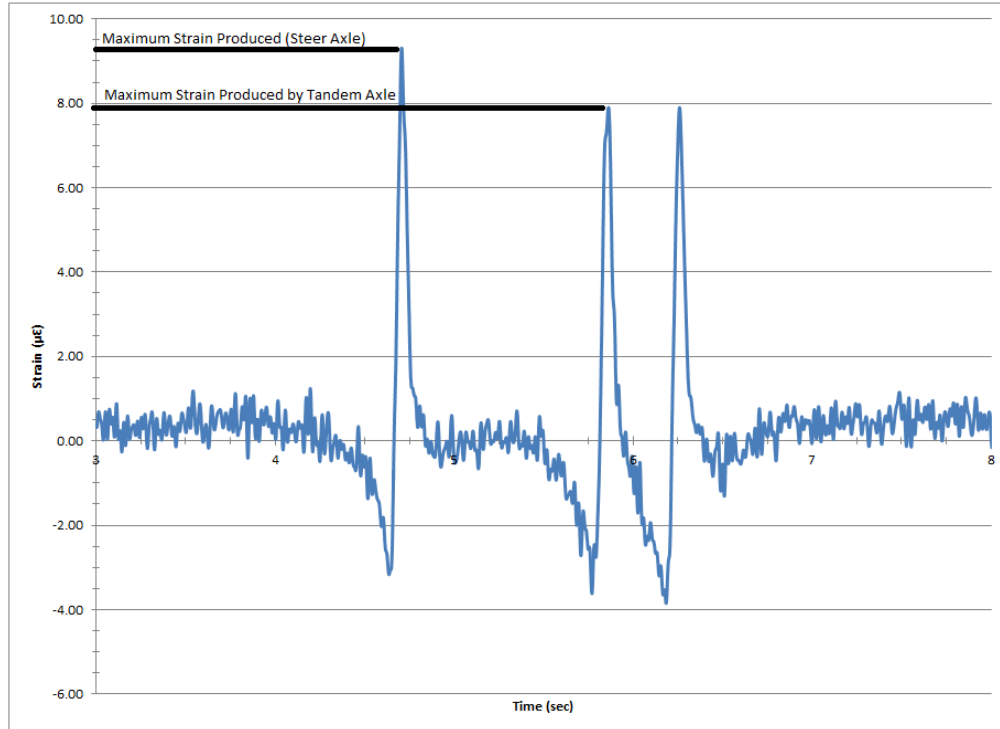
The speed at which the tandem axle truck was traveling during testing had some effects on the pavement's strain response. Figure 17 shows longitudinal strains measured in the FRL of the 11 in (28 cm) section during a tandem axle test run conducted at 55 mph (89 km/h). As displayed in Figure 17, the maximum tensile strain produced by the first axle of the tandem axle configuration was notably higher than the strain produced by the second axle. This difference was also noted for tandem axle testing conducted at 30 mph (48 km/h) but was not as substantial. Surprisingly, even at high truck speeds, a compression strain peak was observed between the axles of the tandem axle configuration. Both of these observations were prevalent for all tandem axle truck testing at higher speeds.





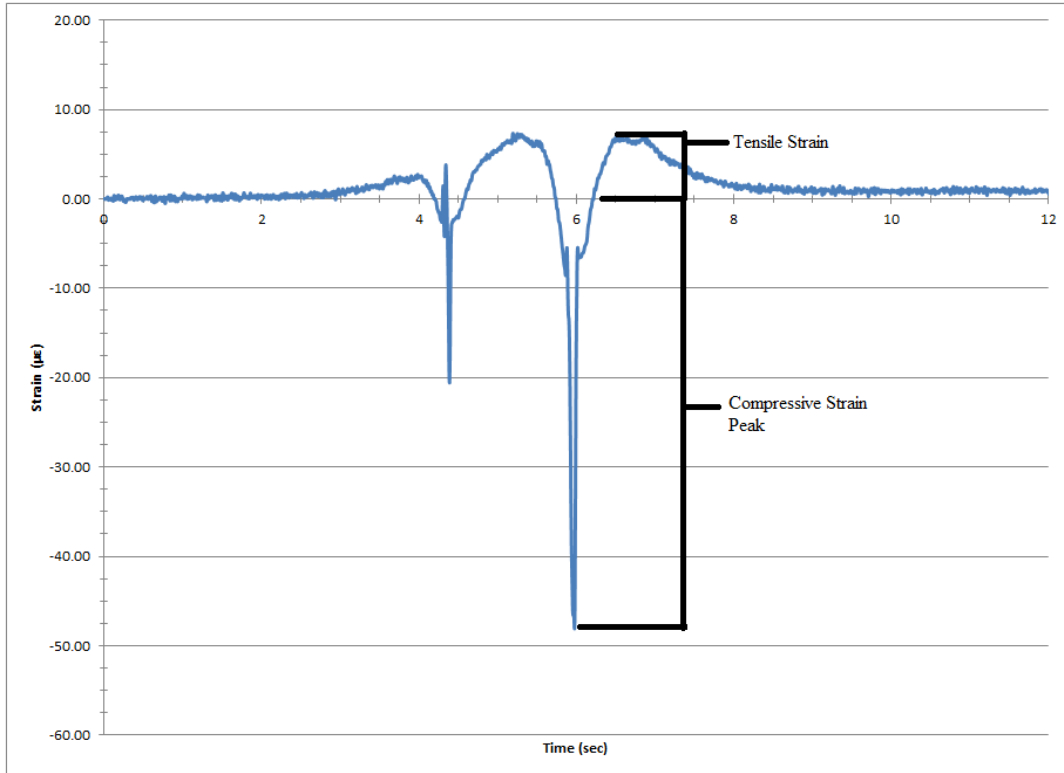
**Figure 17. Longitudinal strain in the FRL measured from tandem axle truck passing at 55 mph (89 km/h).**

Maximum strains measured in the base, intermediate, and surface layers were in some instances produced by the steering or front axle of the tandem axle truck. On the rare occasion, this was also true for maximum longitudinal strains produced in the FRL of the 11 in (28 cm) section. Longitudinal strains recorded in the base layer of the 13 in (33 cm) section for a tandem axle test run are displayed in Figure 18, which shows, for this test run, the maximum strain produced occurred while the steer axle was crossing the location of the gage. This phenomenon only transpired during tandem axle truck testing. Maximum strains during single axle truck testing were always produced by the single axle.



**Figure 18. Strain response from tandem axle truck where steer axle produced maximum strain.**

As the location of the strain gage moves from below (FRL and base layer) to above (intermediate and surface layers) the neutral axis of the pavement the maximum strain switched from being tensile to compressive. Longitudinally oriented strain gages above the neutral axis receive slight tensile strains directly before and after being loaded while receiving a larger compressive strain peak while being loaded. Transversely oriented strain gages above the neutral axis received only compressive strain peaks. Figure 19 displays a chart of strains recorded by a longitudinal strain gage in the surface layer of the 15 in (38 cm) section during a single axle truck test run.



**Figure 19. Strain response above the neutral axis of the pavement.**

## **6.2 Longitudinal Strain in the FRL**

The 11 in (28 cm) section received the highest longitudinal strains in the FRL in comparison with the 13 in (33 cm), and 15 in (38 cm) sections. Table 3 shows the average maximum longitudinal strain and maximum longitudinal strain measured in the FRL for testing conducted on the 11 in (28 cm) section. It compares strains found at various speeds and tire pressures for both the single axle wide-based tire and tandem axle dual tire trucks. As seen in Table 3 the maximum longitudinal strain recorded in the FRL for the 11 in (28 cm) section was 68.49  $\mu\epsilon$ . This value was captured during single axle truck testing at a truck speed of 5 mph (8 km/h) and a tire pressure of 110 psi (758 kPa). Table 3 presents average longitudinal strains in the FRL ranging between 32  $\mu\epsilon$  and 48  $\mu\epsilon$  for tests involving the single axle truck and 19  $\mu\epsilon$  and 25  $\mu\epsilon$  for tandem axle truck testing. Table 3 shows the highest longitudinal strain in the FRL for both axle configurations at every speed was measured during testing at a tire pressure of 110 psi except for testing at 30 mph (48 km/h) with the tandem axle truck where the average and maximum longitudinal strain was observed to be maximized at 80 psi (552 kPa). The highest average and maximum values for the longitudinal strain in the FRL for the 11 in (28 cm) section were consistently seen during 5 mph (8 km/h) testing for each tire pressure.

**Table 3. Maximum longitudinal strain in the FRL for the 11 in (28 cm) section ( $\mu\epsilon$ ).**

Tire Pressure (psi)   (kPa)		Speed (mph (km/h))					
		5 (8)		30 (48)		55 (89)	
		<i>Average</i>	<i>Max</i>	<i>Average</i>	<i>Max</i>	<i>Average</i>	<i>Max</i>
Single Axle Wide-Base Tire (29 Kip (129 kN) Axle Load)							
80	552	46.09	60.85	39.14	50.72	32.92	39.15
110	758	47.17	68.49	41.67	58.82	39.00	48.94
125	862	47.12	61.18	38.19	50.10	36.13	51.81
Tandem Axle Dual Tire (37 Kip (165 kN) Axle Load)							
80	552	24.29	31.98	21.40	27.50	19.24	25.53
110	758	24.90	33.20	21.35	27.15	20.40	30.17
125	862	24.29	32.38	20.72	29.24	19.73	30.18

The 13 in (33 cm) section received significantly lower longitudinal strains in the FRL than the 11 in (28 cm) section. Table 4 presents a summary of longitudinal strains measured in the FRL during testing on the 13 in (33 cm) section. The maximum FRL, longitudinal strain obtained in the 13 in (33 cm) section was 34.53  $\mu\epsilon$  which was considerably less than the 11 in (28 cm) section. The maximum longitudinal strain in the FRL for the 13 in (33 cm) section was discovered when testing at 5 mph (8 km/h) with a tire pressure of 125 psi (862 kPa) and the tandem axle truck. Table 4 shows that average longitudinal strain in the FRL for the 13 in (33 cm) section ranged between 22  $\mu\epsilon$  and 32  $\mu\epsilon$  for the single axle truck and 11  $\mu\epsilon$  and 17  $\mu\epsilon$  for the tandem axle truck. Similar to the 11 in (28 cm) section, Table 4 also shows that strains produced by the single axle truck were consistently higher than strains produced by the tandem axle truck. Longitudinal strain in the FRL were also, once again, highest when testing at 5 mph (8 km/h) for each tire pressure, although, they were maximized between all three tire pressures for each speed.

**Table 4. Maximum longitudinal strain in the FRL for the 13 in (33 cm) section ( $\mu\epsilon$ ).**

Tire Pressure (psi)   (kPa)		Speed (mph (km/h))					
		5 (8)		30 (48)		55 (89)	
		<i>Average</i>	<i>Max</i>	<i>Average</i>	<i>Max</i>	<i>Average</i>	<i>Max</i>
Single Axle Wide-Base Tire (29 Kip (129 kN) Axle Load)							
80	552	31.10	33.46	26.37	28.51	22.05	24.48
110	758	31.07	32.22	25.61	28.44	25.45	27.18
125	862	31.88	34.53	25.57	27.00	23.54	25.50
Tandem Axle Dual Tire (37 Kip (165 kN) Axle Load)							
80	552	15.93	16.82	13.38	14.08	11.72	13.20
110	758	16.07	17.40	13.14	14.19	12.27	13.68
125	862	15.80	16.89	12.97	13.91	12.54	13.29

Surprisingly, the 15 in (38 cm) sections received slightly higher longitudinal strain in the FRL compared to the 13 in (33 cm) section, although, they were still substantially lower than measurements in the 11 in (28 cm) section. One possible explanation for higher resulting strains in the 15 in (38 cm) section compared to the 13 in (33 cm) section could be the difference in subgrade resilient modulus. The 13 in (33 cm) section was constructed on chemically stabilized

subgrade which had a resilient modulus of 40 ksi (276 MPa) while the 15 in (38 cm) section was constructed on a subgrade which had a resilient modulus of 20 ksi (138 MPa). Table 5 displays the maximum and average maximum longitudinal strains recorded in the FRL for the 15 in (38 cm) section. The table shows that the maximum strain discovered was 43.18  $\mu\epsilon$ , measured during 5 mph (8 km/h) testing using the single axle truck at a tire pressure of 80 psi (552 kPa). Average longitudinal strain in the FRL ranged between 24  $\mu\epsilon$  and 43  $\mu\epsilon$  for testing utilizing the single axle truck and 18  $\mu\epsilon$  and 23  $\mu\epsilon$  with the tandem axle truck. Once more, the highest strains were obtained during 5 mph (8 km/h) for each tire pressure, although, a variety of tire pressures acquired the highest strains for each speed as shown in Table 5.

**Table 5. Maximum longitudinal strain in the FRL for 15 in (38 cm) section ( $\mu\epsilon$ ).**

Tire Pressure		Speed (mph (km/h))					
		5 (8)		30 (48)		55 (89)	
(psi)	(kPa)	<i>Average</i>	<i>Max</i>	<i>Average</i>	<i>Max</i>	<i>Average</i>	<i>Max</i>
Single Axle Wide-Base Tire (29 Kip (129 kN) Axle Load)							
80	552	39.53	43.18	31.12	35.30	25.70	28.57
110	758	38.62	40.34	32.21	33.69	25.79	29.74
125	862	35.72	39.30	29.25	33.23	24.39	27.83
Tandem Axle Dual Tire (37 Kip (165 kN) Axle Load)							
80	552	22.21	25.12	18.63	22.81	15.76	18.37
110	758	21.39	23.66	18.23	21.97	17.74	23.08
125	862	20.83	24.18	17.54	20.11	16.81	21.30

### 6.2.1 Influence of Speed on Longitudinal Strain in the FRL

As seen in Table 3, Table 4, and Table 5 along with Figure 20, the longitudinal strain in the FRL typically decreased as speed increased. Figure 20 is a chart of strain versus speed for both axle configurations and all three tire pressures in the 11 in (28 cm), 13 in (33 cm), and 15 in (38 cm) sections. Once again, one run with little lateral tire offset was used to create the results as well as strains produced only by the tandem axle of the tandem axle truck. The figure clearly shows a decrease in longitudinal strain in the FRL as speed increased for all tire pressures, in each section, and for both axle configurations. The influence of speed on strain was most prevalent in the 15 in (38 cm) and 11 in (28 cm) sections while its influence in the 13 in (33 cm) section was slightly less. Longitudinal strain in the FRL decreased more with speed for testing conducted with the single axle truck. Figure 20, when analyzing the 11 in (28 cm) and 13 in (33 cm) sections for both axle configurations and the 15 in (38 cm) section with the tandem axle configuration, shows that at lower tire pressures the longitudinal strain in the FRL appeared to stabilize at higher speeds, thus testing conducted between 30 mph (48 km/h) and 55 mph (89 km/h). For lower tire pressures, specifically the 80 psi (552 kPa) tire pressure, the strain continued to decrease between 30 mph (48 km/h) and 55 mph (89 km/h). This observation was not made for single axle truck testing on the 15 in (38 cm) section where all tire pressures displayed a decrease in strain between 30 mph (48 km/h) and 55 mph (89 km/h).

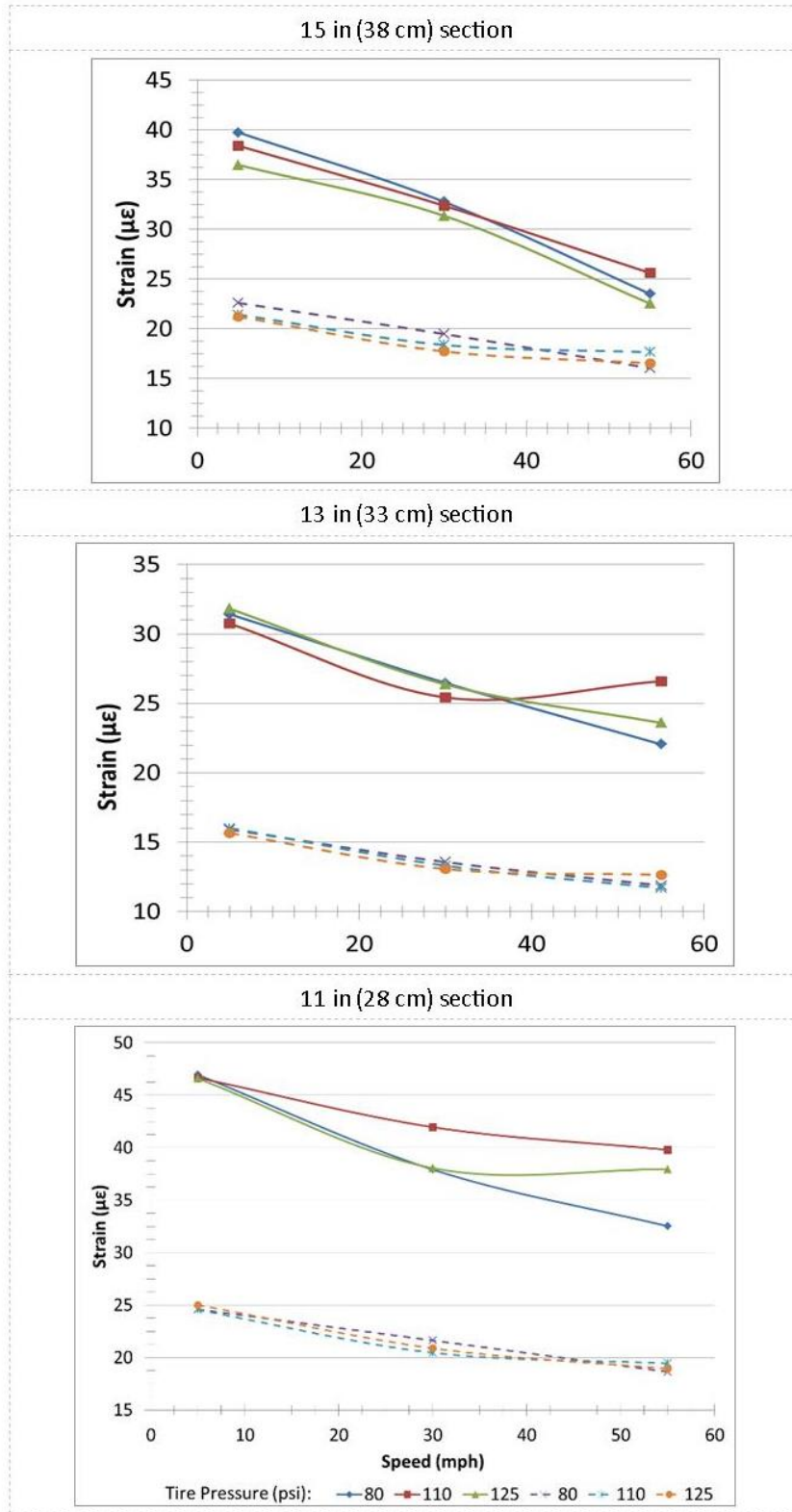


Figure 20. Maximum longitudinal strain in FRL versus speed (1 in = 2.54 cm, 1 mph = 1.6 km/h). Solid lines indicate single axle wide-based tire, and dashed lines indicate tandem axle.

### **6.2.2 Influence of Tire Pressure on Longitudinal Strain in the FRL**

Tire pressure seemed to have minimal effects on longitudinal strain located in the FRL. The effect of tire pressure is displayed in Figure 21. In order to reduce the effects of lateral tire offset, one run for each tire pressure and speed with less than 2 in (5 cm) of lateral tire offset was used to generate all sets of results. Additionally, only tandem axle generated strains were used in order to create an accurate comparison. Figure 21 plots strain against tire pressure for all three sections and all testing speeds. Tire pressure had little influence on the longitudinal strain in the FRL, especially at lower testing speeds, with virtually no influence occurring at a speed of 5 mph (8 km/h). Some inconsistencies were discovered for the single axle truck traveling at speeds of 30 mph (48 km/h) and 55 mph (89 km/h) but the differences were still fairly minimal. Tire pressure appeared to have the strongest influence on the 11 in (28 cm) section and its influence was reduced as pavement thickness increased.

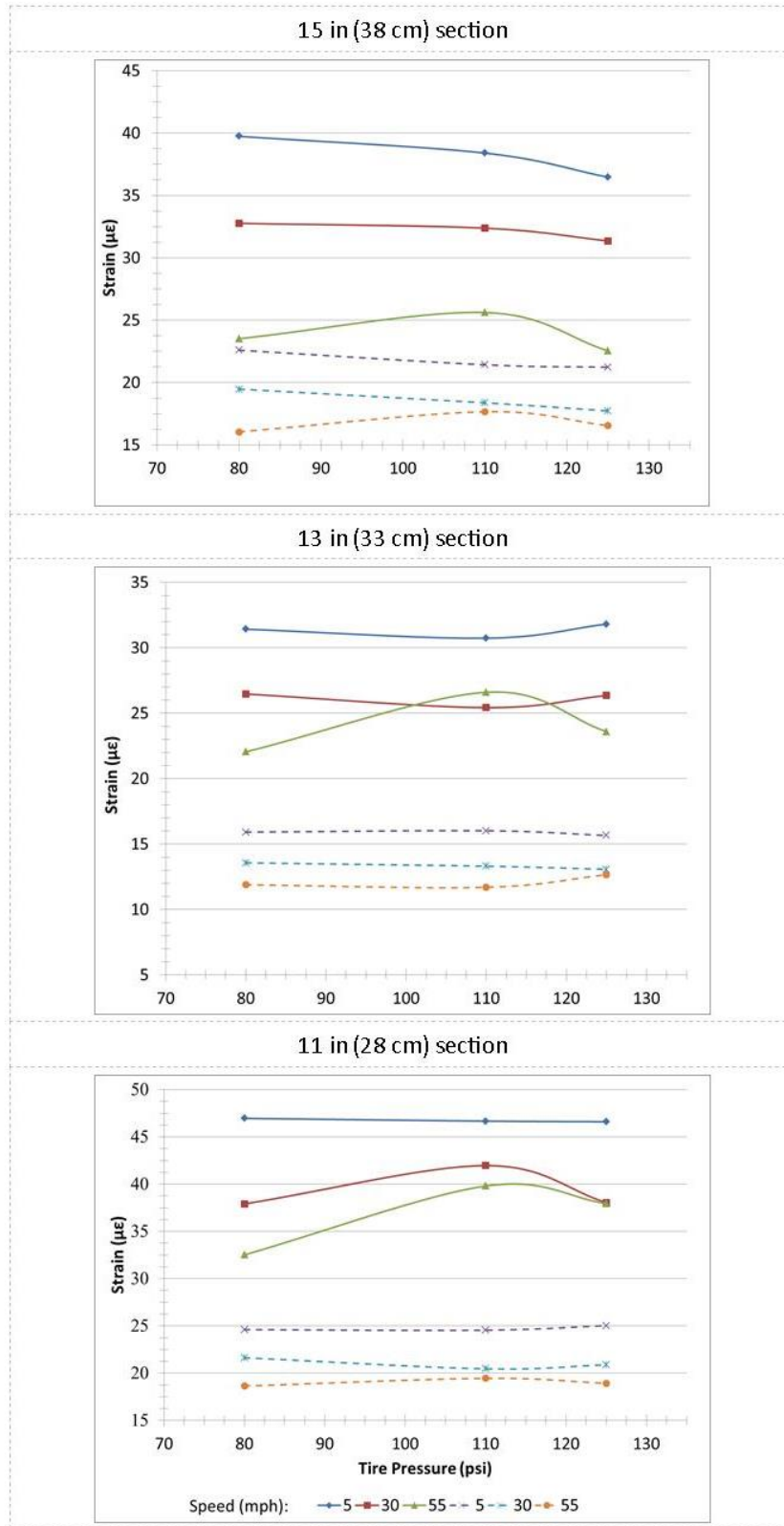


Figure 21. Maximum longitudinal strain in FRL versus tire pressure (1 in = 2.54 cm, 1 psi = 6.89 kPa). Solid lines indicate single axle wide-based tire, and dashed lines indicate tandem axle.



### 6.3 Longitudinal Strain in the Base Layer

Strains in the base layer were monitored during CVL testing for two reasons. One reason was to analyze the propagation of strain through the pavement and provide an indication of the pavement structure's strain distribution. The second reason was to monitor the base layer's potential for cracking.

Longitudinal strains found in the base layer, like longitudinal strain in the FRL, were greatest in the 11 in (28 cm) section. Table 6 shows the maximum and average maximum longitudinal strain measured in the base layer for the 11 in (28 cm) section. The maximum longitudinal strain recorded in the base layer for the 11 in (28 cm) section was 23.17  $\mu\epsilon$  during single axle truck testing at 5 mph (8 km/h) with a tire pressure of 125 psi (862 kPa). Table 6 displays the average base layer strain for the 11 in (28 cm) section ranged between 9  $\mu\epsilon$  and 19  $\mu\epsilon$  for the single axle truck and 6  $\mu\epsilon$  and 11  $\mu\epsilon$  for the tandem axle truck. Similar to the FRL, longitudinal strains were greater in the base layer when testing with the single axle truck, although, correlations between the tandem axle truck and single axle truck were avoided since maximum strains produced in the base layer by the tandem axle truck were occasionally the result of the steer axle. All maximum and average maximum longitudinal strains in the base layer of the 11 in (28 cm) section were discovered while testing at 5 mph (8 km/h) for each tire pressure. Additionally, strains provided in Table 6 typically increased with tire pressure.

**Table 6. Maximum longitudinal strain in the base layer for the 11 in (28 cm) section ( $\mu\epsilon$ ).**

Tire Pressure (psi)   (kPa)		Speed (mph (km/h))					
		5 (8)		30 (48)		55 (89)	
		<i>Average</i>	<i>Max</i>	<i>Average</i>	<i>Max</i>	<i>Average</i>	<i>Max</i>
Single Axle Wide-Base Tire (29 Kip (129 kN) Axle Load)							
80	552	14.50	18.64	12.07	15.13	9.65	11.87
110	758	16.40	21.06	14.38	19.22	11.85	15.02
125	862	18.46	23.71	14.05	18.20	12.05	17.73
Tandem Axle Dual Tire (37 Kip (165 kN) Axle Load)							
80	552	9.06	10.82	7.21	9.06	6.07	8.01
110	758	10.24	12.12	7.50	9.27	6.28	8.94
125	862	9.99	13.48	7.99	9.83	7.31	9.14

Similar to longitudinal strain measurements in the FRL, the 13 in (33 cm) section received the lowest longitudinal strains in the base layer. Table 7 provides a summary of longitudinal strain in the base layer for the 13 in (33 cm) section. The maximum strain discovered was 16.02  $\mu\epsilon$  as shown in Table 7. This maximum strain was discovered at 5 mph (8 km/h), 110 psi (758 kPa) tire pressure, and testing with the single axle truck. Furthermore, average longitudinal strains in the base layer ranged between 7  $\mu\epsilon$  and 14  $\mu\epsilon$  for the single axle truck and 4  $\mu\epsilon$  and 7  $\mu\epsilon$  for the tandem axle truck. Average maximum longitudinal strains in the base layer of the 13 in (33 cm) sections were greatest when testing at 5 mph (8 km/h) for each tire pressure. Additionally, average maximum longitudinal strains were maximized at 125 psi for each speed except for single axle truck testing at 55 mph where it was maximized at 110 psi.

**Table 7. Maximum longitudinal strain in the base layer for the 13 in (33 cm) section ( $\mu\epsilon$ ).**

Tire Pressure (psi)   (kPa)		Speed (mph (km/h))					
		5 (8)		30 (48)		55 (89)	
		<i>Average</i>	<i>Max</i>	<i>Average</i>	<i>Max</i>	<i>Average</i>	<i>Max</i>
Single Axle Wide-Base Tire (29 Kip (129 kN) Axle Load)							
80	552	12.14	15.01	9.68	11.76	7.78	9.29
110	758	12.94	16.02	10.37	13.48	9.32	11.13
125	862	13.12	15.89	10.66	13.68	8.85	11.15
Tandem Axle Dual Tire (37 Kip (165 kN) Axle Load)							
80	552	6.19	7.60	5.30	7.04	4.62	5.83
110	758	6.47	8.27	5.42	7.27	4.57	5.82
125	862	6.89	9.16	5.77	7.51	4.71	5.87

The 15 in (38 cm) section had longitudinal strains in the base layer that were slightly higher than those in the 13 in (33 cm) section, as seen in Table 8. The largest maximum longitudinal strain in the base layer was 18.23  $\mu\epsilon$ , obtained during single axle truck testing at 5 mph (8 km/h) with a tire pressure of 125 psi (862 kPa). Average strain measurements ranged between 9  $\mu\epsilon$  and 15  $\mu\epsilon$  for the single axle truck and 5  $\mu\epsilon$  and 8  $\mu\epsilon$  for the tandem axle truck. Slightly different from the 11 in (28 cm) and 13 in (33 cm) sections, Table 8 illustrates an increase in average maximum strain between tire pressures of 80 psi (552 kPa) and 110 psi (758 kPa) but then a slight decrease between 110 psi (758 kPa) and 125 psi (862 kPa). This trend occurred for each testing speed. When comparing each tire pressure, it was discovered that the maximum average longitudinal strain was found at a 5 mph (8 km/h) testing speed.

**Table 8. Maximum longitudinal strain in the base layer for the 15 in (38 cm) section ( $\mu\epsilon$ ).**

Tire Pressure (psi)   (kPa)		Speed (mph (km/h))					
		5 (8)		30 (48)		55 (89)	
		<i>Average</i>	<i>Max</i>	<i>Average</i>	<i>Max</i>	<i>Average</i>	<i>Max</i>
Single Axle Wide-Base Tire (29 Kip (129 kN) Axle Load)							
80	552	13.74	16.65	10.99	13.49	9.03	11.18
110	758	14.68	18.10	11.92	14.89	9.61	13.56
125	862	13.30	18.23	10.89	15.00	9.04	12.98
Tandem Axle Dual Tire (37 Kip (165 kN) Axle Load)							
80	552	7.32	9.16	6.64	9.47	5.35	6.22
110	758	7.50	9.45	6.75	8.77	6.82	9.82
125	862	7.47	9.96	6.42	9.33	6.34	9.58

### 6.3.1 Influence of Speed on Longitudinal Strain in the Base Layer

Like the longitudinal strain in the FRL, the longitudinal strain in the base layer decreased as speed increased. This is presented in Table 6, Table 7, Table 8, and Figure 22. Figure 22, for the 11 in (28 cm), 13 in (33 cm), and 15 in (38 cm) sections, relates longitudinal strain in the base layer to speed without the effects of lateral tire offset and is categorized by tire pressure and axle configuration. Another observation similar to that of the longitudinal strain in the FRL was longitudinal strain in the base layer tended to stabilize at higher speeds when testing at higher tire

pressures but only occurred in the 11 in (28 cm) and 13 in (33 cm) sections as shown in Figure 22. Although, as the section thickness was increased the correlation became more linear for all three tire pressures with a purely linear trend resulting in the 15 in (38 cm) section. This was especially true for testing with the single axle truck while testing with the tandem axle truck remained more consistent.

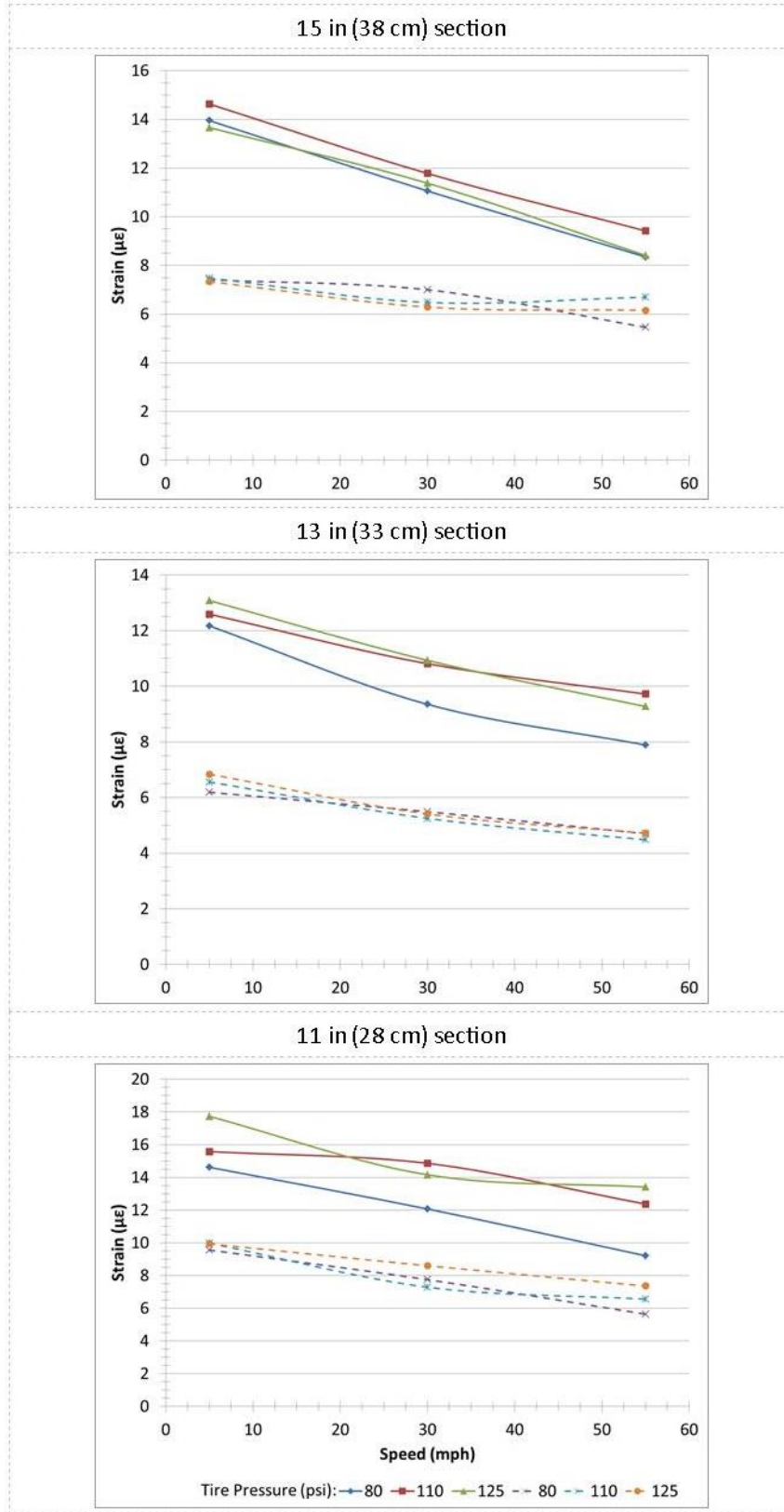


Figure 22. Maximum longitudinal strain in base layer versus speed (1 in = 2.54 cm, 1 mph = 1.6 km/h). Solid lines indicate single axle wide-based tire, and dashed lines indicate tandem axle.

### **6.3.2 Influence of Tire Pressure on Longitudinal Strain in the Base Layer**

Although tire pressure had minimal impacts on tandem axle truck testing, a clear increase in strain was witnessed as tire pressures were increased for the single axle truck. Figure 23 was created to relate longitudinal strain in the base layer and tire pressure for each test section and testing speed. Similar to earlier comparisons, the lateral tire offset factor was removed by analyzing runs with little wheel wander and tandem axle produced strains were used for tandem axle truck test runs. The chart showed an increase in strain with tire pressure for the single axle truck until the tire pressure reached its maximum of 125 psi (862 kPa). The truck tires were inflated to 125 psi (862 kPa) under cold conditions in the garage and tire pressures as high as 140 psi (965 kPa) were seen after the tires had warmed due to the trucks being driven during test runs. When the truck tires were inflated to tire pressure of 125 psi (862 kPa) or more, they were so highly inflated that a bouncing effect may have occurred when the trucks drove over the strain gages. Figure 23 shows the influence of tire pressure was reduced as pavement thickness was increased.

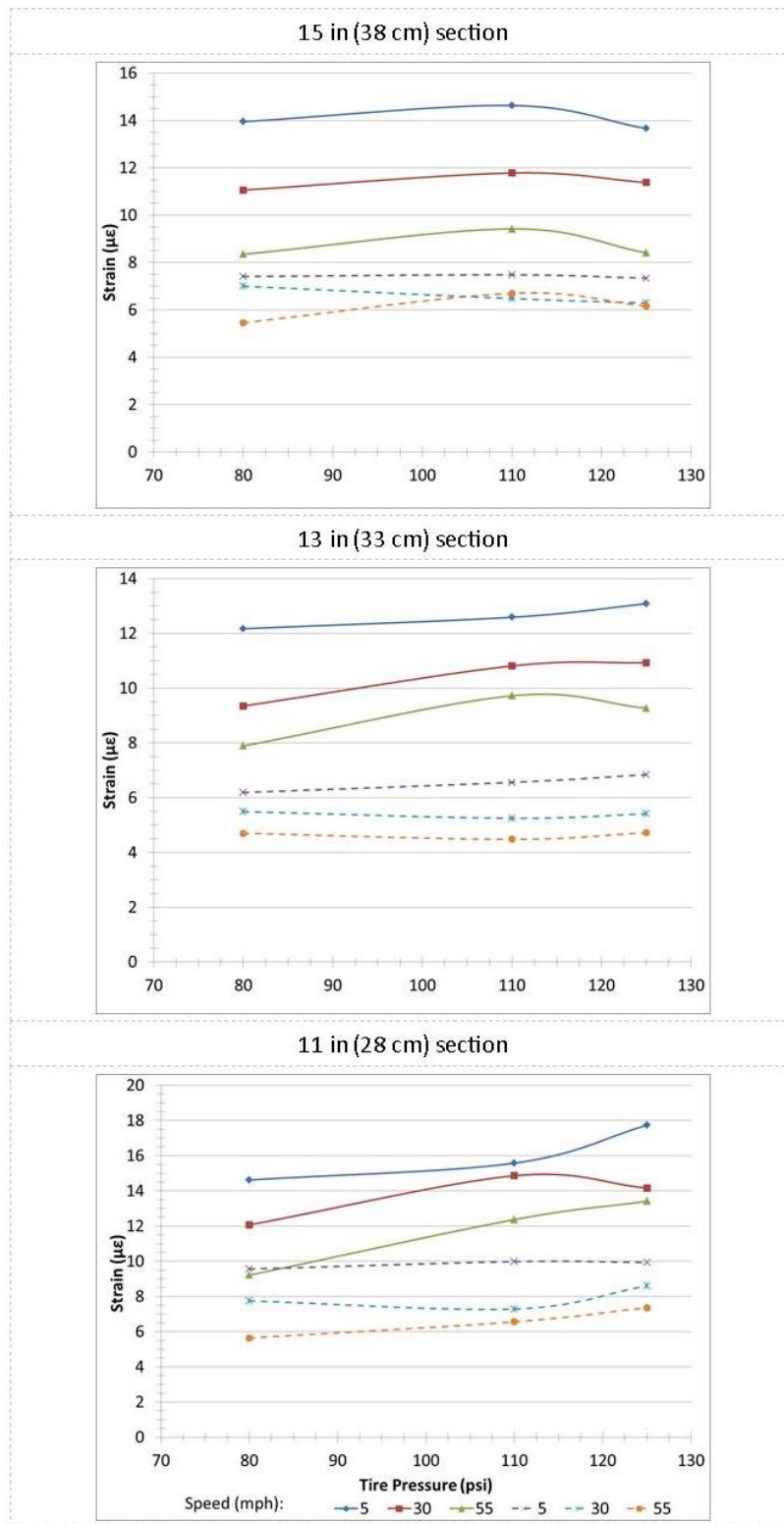


Figure 23. Maximum longitudinal strain in the base layer versus tire pressure (1 in = 2.54 cm, 1 psi = 6.89 kPa). Solid lines indicate single axle wide-based tire, and dashed lines indicate tandem axle.

### 6.4 Transverse Strain in the Base Layer

Transverse strain gages were installed in the base layer of DEL-23 test sections because the critical strain was not always in the longitudinal direction. Transverse strain results in the base layer were greatest in the 11 in (28 cm) section. A summary of the maximum and average maximum transverse strains found in the base layer is displayed in Table 9. The highest transverse strain measured in the base layer of the 11 in (28 cm) section was 12.74  $\mu\epsilon$  which was recorded during single axle truck testing with a tire pressure of 125 psi (862 kPa) at 5 mph (8 km/h). Transverse strains in the base layer for the 11 in (28 cm) section varied between 6  $\mu\epsilon$  and 13  $\mu\epsilon$  for testing conducted with the single axle truck and 3  $\mu\epsilon$  and 10  $\mu\epsilon$  for testing conducted with the tandem axle truck. For each tire pressure, the maximum and average maximum transverse strain was greatest at 5 mph (8 km/h). With respect to tire pressure, the maximum and average maximum transverse strain always occurred at 110 psi (758 kPa) or 125 psi (862 kPa) tire pressure for each testing speed.

**Table 9. Maximum transverse strain in the base layer for the 11 in (28 cm) section ( $\mu\epsilon$ ).**

Tire Pressure (psi)   (kPa)		Speed (mph (km/h))					
		5 (8)		30 (48)		55 (89)	
		<i>Average</i>	<i>Max</i>	<i>Average</i>	<i>Max</i>	<i>Average</i>	<i>Max</i>
Single Axle Wide-Base Tire (29 Kip (129 kN) Axle Load)							
80	552	9.80	10.51	8.07	9.63	6.93	7.95
110	758	11.11	12.32	8.75	10.61	9.21	12.68
125	862	12.15	12.74	9.20	10.86	7.55	9.82
Tandem Axle Dual Tire (37 Kip (165 kN) Axle Load)							
80	552	6.55	9.36	3.26	6.19	5.42	6.85
110	758	9.04	11.47	3.95	6.29	3.22	5.64
125	862	6.84	10.95	4.93	9.09	6.43	9.13

Although longitudinal strains in the 13 in (33 cm) section were found to be lower than the 11 in (28 cm) and 15 in (38 cm) sections, the transverse strains in the base layer were typically higher than the other two sections especially when testing with the single axle truck. A summary of transverse strain discovered in the base layer of the 13 in (33 cm) section is presented in Table 10. The maximum transverse strain occurred during single axle truck testing at 5 mph (8 km/h) with a tire pressure of 125 psi (862 kPa) and was 15.87  $\mu\epsilon$ . Single axle, average transverse strain ranged between 8  $\mu\epsilon$  and 15  $\mu\epsilon$  while transverse axle, average transverse strains ranged between 3  $\mu\epsilon$  and 12  $\mu\epsilon$ . For the 13 in (33 cm) section, as displayed in Table 10, average transverse strains were typically maximized at a tire pressure of 125 psi (862 kPa) with a one discrepancy where the average transverse strain while testing with the single axle truck at 55 mph (89 km/h) was maximized at 110 psi (758 kPa) tire pressure. Additionally, average maximum transverse strains in the base layer, for each tire pressure, occurred at 5 mph (8 km/h) except for the tandem axle truck implementing a tire pressure of 125 psi (862 kPa).

**Table 10. Maximum transverse strain in the base layer for the 13 in (33 cm) section ( $\mu\epsilon$ ).**

Tire Pressure (psi)   (kPa)		Speed (mph (km/h))					
		5 (8)		30 (48)		55 (89)	
		<i>Average</i>	<i>Max</i>	<i>Average</i>	<i>Max</i>	<i>Average</i>	<i>Max</i>
Single Axle Wide-Base Tire (29 Kip (129 kN) Axle Load)							
80	552	13.03	14.43	10.82	11.33	8.80	9.65
110	758	13.42	14.41	11.15	12.58	9.92	11.43
125	862	14.39	15.87	11.29	13.00	9.83	11.13
Tandem Axle Dual Tire (37 Kip (165 kN) Axle Load)							
80	552	4.95	6.32	4.94	6.31	4.43	5.94
110	758	6.23	7.72	4.87	7.10	3.93	4.64
125	862	7.20	9.06	11.29	13.00	9.83	11.13

Transverse strains in the base layer of the 15 in (38 cm) section were slightly reduced compared to those of the 13 in (33 cm) section. Table 11 provides the maximum and average maximum transverse strains in the base layer of the 15 in (38 cm) section. As seen in Table 11, the maximum strain obtained was 15.64  $\mu\epsilon$  during single axle truck testing at 5 mph (8 km/h) with its tires inflated to 110 psi (758 kPa). Average transverse strains in the base layer of the 15 in (38 cm) section fluctuated between 8  $\mu\epsilon$  and 14  $\mu\epsilon$  for single axle truck testing and 4  $\mu\epsilon$  and 8  $\mu\epsilon$  for tandem axle truck testing. Table 11 shows that strains were largest at a tire pressure of 125 psi (862 kPa) except for testing conducted with the single axle truck at 5 and 30 mph (48 km/h). Also, transverse strains in the base layer of the 15 in (38 cm) section were greatest at 5 mph (8 km/h) for each tire pressure.

**Table 11. Maximum transverse strain in the base layer for the 15 in (38 cm) section ( $\mu\epsilon$ ).**

Tire Pressure (psi)   (kPa)		Speed (mph (km/h))					
		5 (8)		30 (48)		55 (89)	
		<i>Average</i>	<i>Max</i>	<i>Average</i>	<i>Max</i>	<i>Average</i>	<i>Max</i>
Single Axle Wide-Base Tire (29 Kip (129 kN) Axle Load)							
80	552	12.48	15.23	9.95	12.23	8.05	9.62
110	758	13.28	15.64	10.85	12.58	8.29	10.05
125	862	13.17	15.44	9.61	12.53	8.65	10.08
Tandem Axle Dual Tire (37 Kip (165 kN) Axle Load)							
80	552	6.11	7.33	5.49	6.46	4.64	6.13
110	758	6.32	7.80	5.49	6.30	5.41	6.21
125	862	7.13	8.46	5.89	7.05	5.45	6.22

#### 6.4.1 Influence of Speed on Transverse Strain in the Base Layer

Similar to other strain responses previously discussed, transverse strain in the base layer decreased with increasing speeds. Figure 24 relates transverse strain found in the base layer to speed. Test runs used for the figure incorporated little or no lateral tire offset and only tandem axle produced strains were used. For the 11 in (28 cm) section the transverse strain in the base layer resulting from the single axle truck seemed to decrease with speed but became stable once a speed of 30 mph (48 km/h) was achieved. This was especially true for the higher tire pressures, 110 psi (758 kPa) and 125 psi (862 kPa). For the 13 in (33 cm) and 15 in (38 cm)



sections, as shown in Figure 24, transverse strains in the base layer typically linearly decreased with increasing testing speeds for the single axle truck and also for the tandem axle truck.

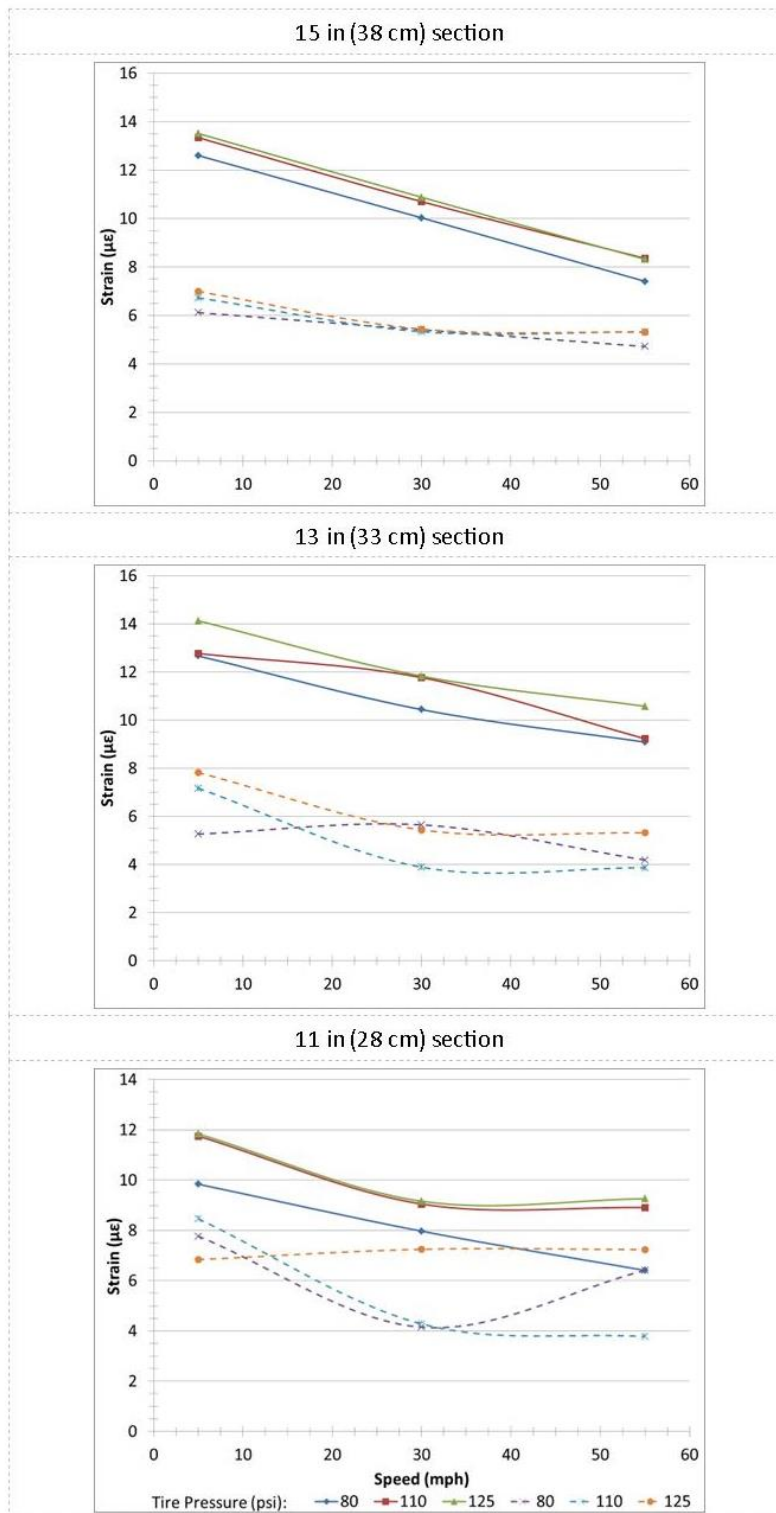


Figure 24. Maximum transverse strain in the base layer versus speed (1 in = 2.54 cm, 1 mph = 1.6 km/h). Solid lines indicate single axle wide-based tire, and dashed lines indicate tandem axle.

#### **6.4.2 Influence of Tire Pressure on Transverse Strain in the Base Layer**

Similar to the longitudinal strains in the base, transverse strains in the base layer tended to increase with increasing tire pressures. Figure 25 relates transverse strain in the base layer to tire pressure without the influence of wheel wander or the steer axle of the tandem axle truck. Figure 25, while observing the 11 in (28 cm) and 15 in (38 cm) sections, showed as tire pressure increased, transverse strains in the base layer increased but began to stabilize as the tire pressure reached upper limits. This was especially true for testing using the single axle truck. There tended to be minimal changes in strain measurements between tire pressure of 110 psi (758 kPa) and 125 psi (862 kPa). Unlike other sections, the 13 in (33 cm) section transverse strains in the base layer were fairly constant between 80 psi (552 kPa) and 110 psi (758 kPa) tire pressure but increased significantly between 110 psi (758 kPa) and 125 psi (862 kPa) tire pressure when conducting single axle truck testing. Overall, tire pressure had a minimal influence on transverse strain in the base layer especially during testing involving the tandem axle truck.

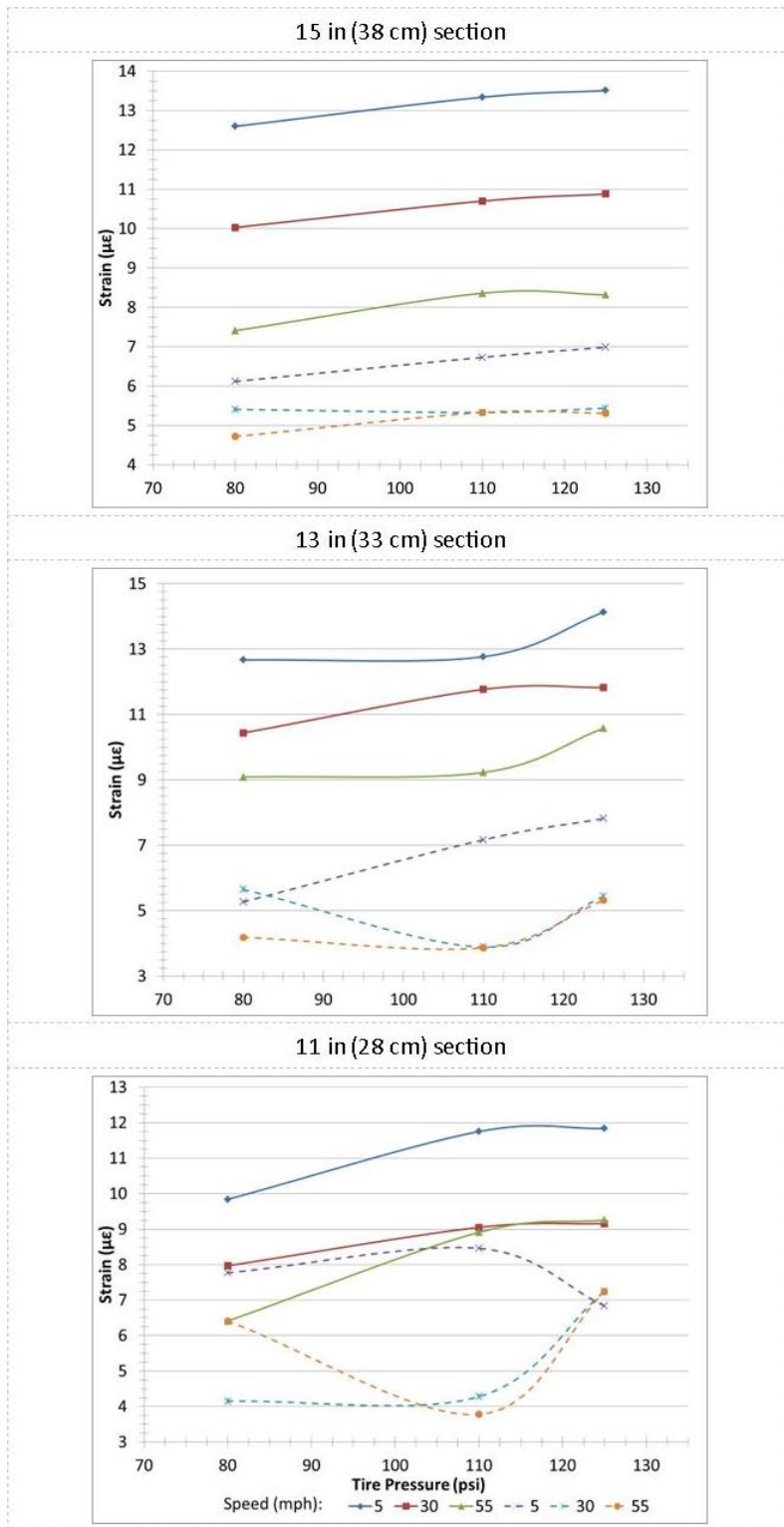


Figure 25. Maximum transverse strain in in the base layer vs. tire pressure (1 in = 2.54 cm, 1 psi = 6.89 kPa). Solid lines indicate single axle wide-based tire, and dashed lines indicate tandem axle.

## 6.5 Comparisons Between Strain Responses

Transverse strains in the base layer were typically discovered to be less than longitudinal strains in the base layer for the 11 in (28 cm) and 15 in (38 cm) sections, although, for the 13 in (33 cm) section transverse strains were typically found to be greater than longitudinal strains. Table 12, Table 13, and Table 14 compare longitudinal and transverse strains in the base layer of the 11 in (28 cm), 13 in (33 cm), and 15 in (38 cm) sections respectively. The tables do not incorporate influences of lateral wheel offset. Furthermore, due to the mixture of maximum strains produced by either the tandem axle or steer axle of the tandem axle truck, strains produced by the tandem axle were used for this comparison. For the 11 in (28 cm) section, as portrayed in Table 12, when testing both the single axle truck and tandem axle truck, longitudinal strains were greater in magnitude than transverse strains independent of tire pressure, speed, or axle configuration. A switch of critical strains from longitudinal to transverse was prevalent in the 13 in (33 cm) section when testing with the single axle truck as shown in Table 13. This was an important discovery because the critical strains for these tests in the base layer were the transverse strains. In the 15 in (38 cm) section, as displayed in Table 14, all of the longitudinal strains were greater than the transverse strains.

**Table 12. Longitudinal versus transverse strains in the base layer for the 11 in (28 cm) section ( $\mu\epsilon$ ).**

Tire Pressure (psi)   (kPa)		Speed (mph (km/h))					
		5 (8)		30 (48)		55 (89)	
		<i>Transverse</i>	<i>Longitudinal</i>	<i>Transverse</i>	<i>Longitudinal</i>	<i>Transverse</i>	<i>Longitudinal</i>
Single Axle Wide-Base Tire (29 Kip (129 kN) Axle Load)							
80	552	9.84	14.62	7.97	12.07	6.41	9.21
110	758	11.75	15.58	9.05	14.86	8.91	12.37
125	862	11.84	17.73	9.16	14.16	9.26	13.41
Tandem Axle Dual Tire (37 Kip (165 kN) Axle Load)							
80	552	2.50	8.42	1.77	7.09	1.86	5.02
110	758	2.63	8.71	2.00	6.65	1.80	5.81
125	862	2.71	8.98	2.82	7.32	3.65	6.02

**Table 13. Longitudinal versus transverse strains in the base layer for the 13 in (33 cm) section ( $\mu\epsilon$ ).**

Tire Pressure (psi)   (kPa)		Speed (mph (km/h))					
		5 (8)		30 (48)		55 (89)	
		<i>Transverse</i>	<i>Longitudinal</i>	<i>Transverse</i>	<i>Longitudinal</i>	<i>Transverse</i>	<i>Longitudinal</i>
Single Axle Wide-Base Tire (29 Kip (129 kN) Axle Load)							
80	552	12.67	12.17	10.44	9.35	9.09	7.89
110	758	12.77	12.59	11.77	10.81	9.23	9.72
125	862	14.13	13.08	11.83	10.93	10.58	9.27
Tandem Axle Dual Tire (37 Kip (165 kN) Axle Load)							
80	552	4.70	6.19	4.24	5.31	3.62	4.70
110	758	5.27	6.33	3.89	5.25	3.33	4.38
125	862	4.96	5.95	4.28	5.05	3.99	4.59

**Table 14. Longitudinal versus transverse strains in the base layer for the 15 in (38 cm) section ( $\mu\epsilon$ ).**

Tire Pressure (psi)   (kPa)		Speed (mph (km/h))					
		5 (8)		30 (48)		55 (89)	
		<i>Transverse</i>	<i>Longitudinal</i>	<i>Transverse</i>	<i>Longitudinal</i>	<i>Transverse</i>	<i>Longitudinal</i>
Single Axle Wide-Base Tire (29 Kip (129 kN) Axle Load)							
80	552	12.60	13.95	10.03	11.06	7.41	8.35
110	758	13.34	14.63	10.70	11.78	8.36	9.42
125	862	13.51	13.66	10.88	11.38	8.32	8.41
Tandem Axle Dual Tire (37 Kip (165 kN) Axle Load)							
80	552	6.00	7.41	5.05	7.00	4.43	5.46
110	758	5.98	7.48	5.33	6.48	5.33	6.70
125	862	6.86	7.52	5.44	6.38	5.31	7.14

The longitudinal strains measured in the base layer were significantly lower than longitudinal strains measured in the FRL in each of the three sections. This was due to strain gages located in the base layer being closer to the neutral axis and therefore experiencing less bending. Table 15, Table 16, and Table 17 compare longitudinal strain values obtained in the base and FRL for single axle truck testing in the 11 in (28 cm), 13 in (33 cm), and 15 in (38 cm) sections respectively. Wheel wander effects were removed for this comparison. Tandem axle truck testing was also removed from this analysis since, in the base layer, it was no longer consistently producing the strains with its tandem axle load.

**Table 15. Maximum longitudinal strain in FRL versus in base layer for single axle wide-base tire truck test with 29 kip (129 kN) axle load for the 11 in (28 cm) section ( $\mu\epsilon$ ).**

Single Axle Wide-Base Tire (29 Kip (129 kN) Axle Load)							
Tire Pressure (psi)   (kPa)		Speed (mph (km/h))					
		5 (8)		30 (48)		55 (89)	
		<i>FRL</i>	<i>Base Layer</i>	<i>FRL</i>	<i>Base Layer</i>	<i>FRL</i>	<i>Base Layer</i>
80	552	46.96	14.62	37.91	12.07	32.52	9.21
110	758	46.67	15.58	41.96	14.86	39.80	12.37
125	862	46.60	17.73	38.05	14.16	37.95	13.41

**Table 16. Maximum longitudinal strain in FRL versus in base layer for single axle wide-base tire truck test with 29 kip (129 kN) axle load for the 13 in (33 cm) section ( $\mu\epsilon$ ).**

Single Axle Wide-Base Tire (29 Kip (129 kN) Axle Load)							
Tire Pressure (psi)   (kPa)		Speed (mph (km/h))					
		5 (8)		30 (48)		55 (89)	
		<i>FRL</i>	<i>Base Layer</i>	<i>FRL</i>	<i>Base Layer</i>	<i>FRL</i>	<i>Base Layer</i>
80	552	31.42	12.17	26.47	9.35	22.05	7.89
110	758	30.74	12.59	25.43	10.81	26.60	9.72
125	862	31.81	13.08	26.36	10.93	23.60	9.27

**Table 17. Maximum longitudinal strain in FRL versus in base layer for single axle wide-base tire truck test with 29 kip (129 kN) axle load for the 15 in (38 cm) section ( $\mu\epsilon$ ).**

Tire Pressure		Speed (mph (km/h))					
		5 (8)		30 (48)		55 (89)	
(psi)	(kPa)	<i>FRL</i>	<i>Base Layer</i>	<i>FRL</i>	<i>Base Layer</i>	<i>FRL</i>	<i>Base Layer</i>
80	552	39.75	13.95	32.77	11.06	23.52	8.35
110	758	38.40	14.63	32.38	11.78	25.62	9.42
125	862	36.47	13.66	31.36	11.38	22.54	8.41

## 7 CVL Testing Pavement Response in Summer

Controlled vehicle load testing was conducted on the perpetual pavement test sections during July 1, 10, and 11, 2013 on the 15 in (38 cm), 11 in (28 cm), and 13 in (33 cm) sections, respectively, to determine pavement response under hot weather conditions. Each section was tested during the warmest period of the day, between 10:00 AM and 3:00 PM, with temperatures measured every 10 minutes. Although pavement temperatures remained fairly consistent during testing some variations were seen throughout the course of testing for each section and between testing days. The air temperature sensor was placed directly over the pavement at a low elevation, so that the temperature recorded includes ambient air temperature and heat radiated from the pavement surface, thus peak values for air temperature are higher than commonly reported ambient temperatures, and in this case may exceed 100°F (37.8°C). Temperatures recorded during the test days can be found in tabular form in Appendix F, starting with Table F.4. The test procedure was identical to the cold weather test procedure, using the same axle configurations, loads, speeds, and tire pressures.

Figure 26 displays the air and pavement temperatures recorded during testing of the 11 in (28 cm) section on July 10, 2013. Figure 27 illustrates the air and pavement temperatures measured during testing of the 13 in (33 cm) section on July 11, 2013. The 15 in (38 cm) section was tested on July 1, 2013. Figure 28 shows the air and pavement temperatures measured during testing of that section. Temperatures were recorded every 10 minutes in each graph.

Tables containing the full set of strain data are presented in Appendix G starting with Table G.19, and tables with the measurements collected from the LVDTs and pressure cells are given in Appendix H, starting with Table H.10. The subsequent discussion is based on maximum and average response values obtained.

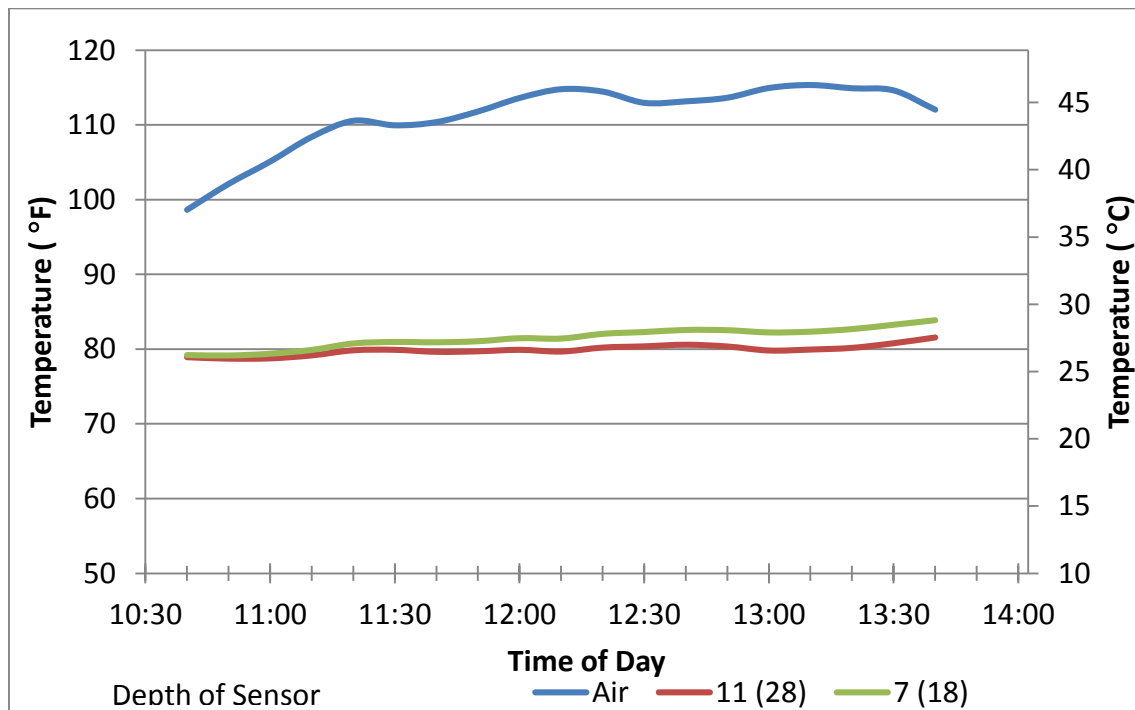


Figure 26. 11 in (28 cm) section temperature profile during CVL testing July 10, 2013.



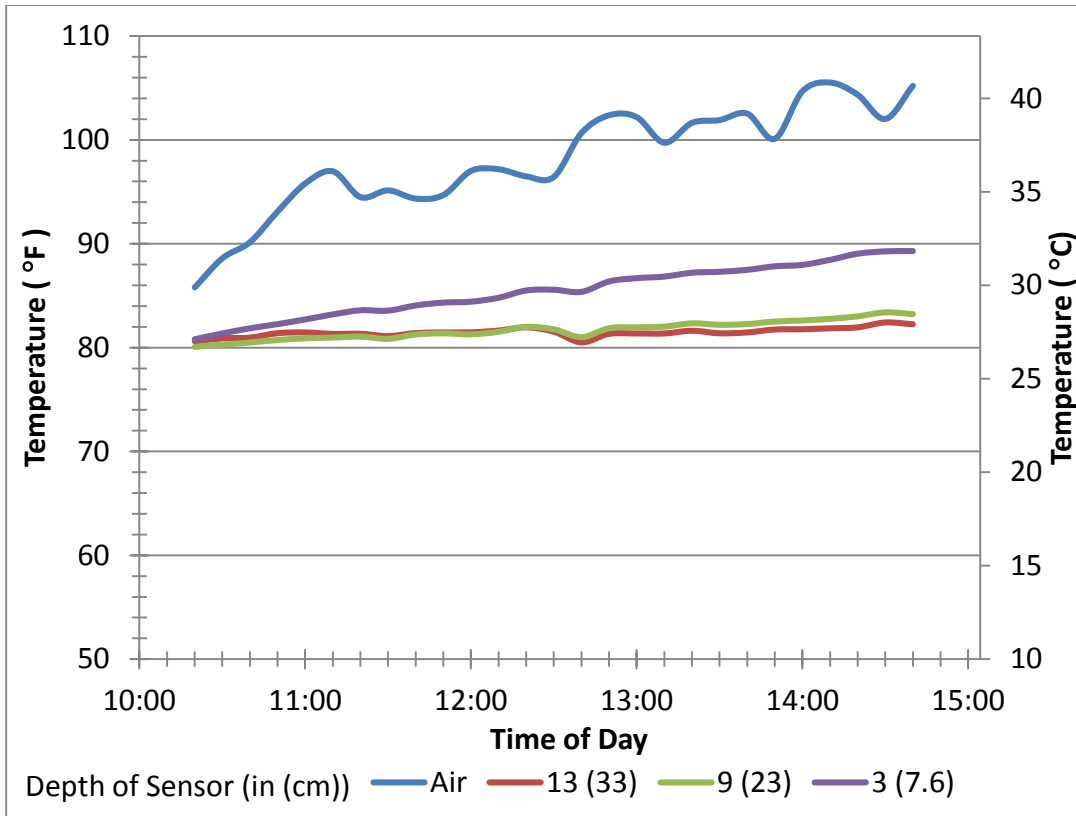


Figure 27. 13 in (33 cm) section temperature profile during CVL testing, July 11, 2013.

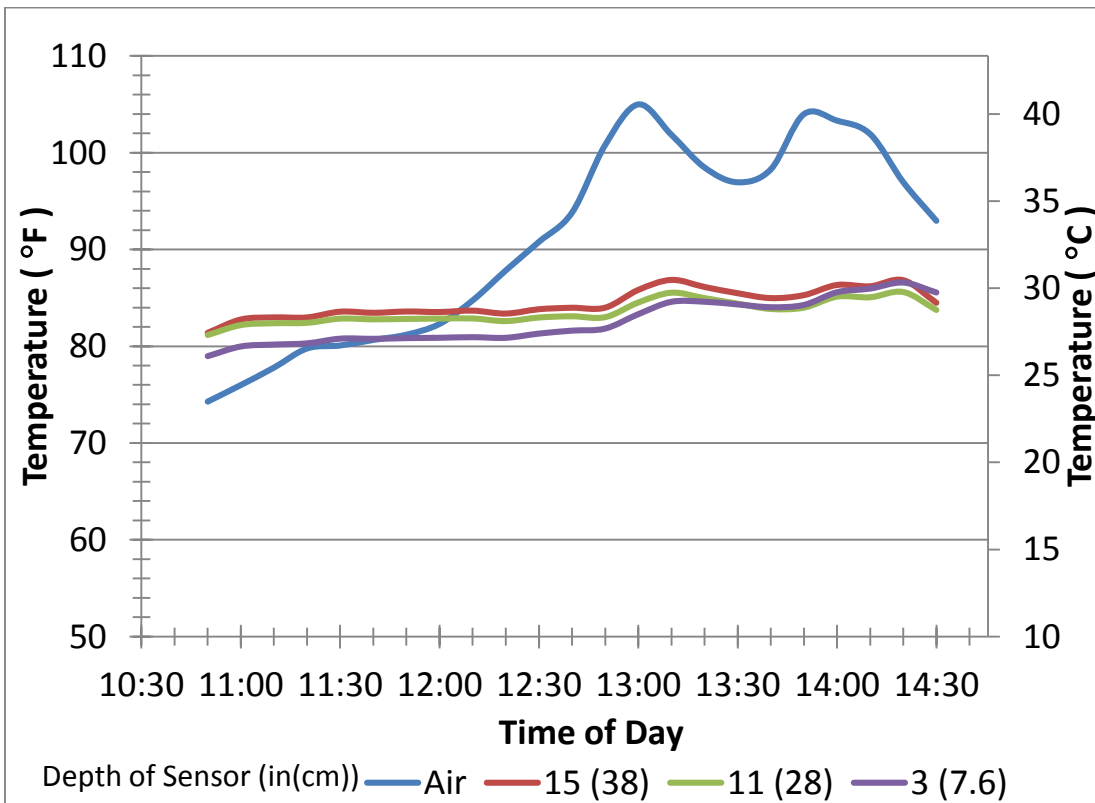


Figure 28. 15 in (38 cm) section temperature profile during CVL testing, July 1, 2013.

**7.1 Longitudinal Strain in the FRL**

The 11 in (28 cm) section received the highest longitudinal strains in the FRL in comparison with the 13 in (33 cm), and 15 in (38 cm) sections. Table 18 shows the average maximum longitudinal strain and maximum longitudinal strain measured in the FRL for testing conducted on the 11 in (28 cm) section. It compares strains found at various speeds and tire pressures for both the single axle wide-based tire and tandem axle dual tire trucks. As seen in Table 3 the maximum longitudinal strain recorded in the FRL for the 11 in (28 cm) section was 143.25  $\mu\epsilon$ . This value was captured during single axle truck testing at a truck speed of 5 mph (8 km/h) and a tire pressure of 110 psi (758 kPa). Table 3 presents average longitudinal strains in the FRL ranging between 56  $\mu\epsilon$  and 107  $\mu\epsilon$  for tests involving the single axle truck and 48  $\mu\epsilon$  and 78  $\mu\epsilon$  for tandem axle truck testing. The highest average and maximum values for the longitudinal strain in the FRL for the 11 in (28 cm) section were consistently seen during 5 mph (8 km/h) testing for each tire pressure.

**Table 18. Maximum longitudinal strain in the FRL for the 11 in (28 cm) section ( $\mu\epsilon$ ).**

Tire Pressure (psi)   (kPa)		Speed (mph (km/h))					
		5 (8)		30 (48)		55 (89)	
		<i>Average</i>	<i>Max</i>	<i>Average</i>	<i>Max</i>	<i>Average</i>	<i>Max</i>
Single Axle Wide-Base Tire (21 Kip (93 kN) Axle Load)							
80	552	95.95	137.69	73.09	102.83	72.65	92.12
110	758	106.50	143.25	73.86	100.34	64.23	89.41
125	862	101.45	138.56	73.11	99.57	56.41	71.43
Tandem Axle Dual Tire (37 Kip (165 kN) Axle Load)							
80	552	74.36	106.26	57.05	76.18	52.02	66.07
110	758	78.10	105.32	56.64	72.71	50.76	69.56
125	862	74.11	99.37	52.24	66.84	48.12	66.44

The 13 in (33 cm) section received significantly lower longitudinal strains in the FRL than the 11 in (28 cm) section. Table 19 presents a summary of longitudinal strains measured in the FRL during testing on the 13 in (33 cm) section. The maximum FRL longitudinal strain obtained in the 13 in (33 cm) section was 85.04  $\mu\epsilon$  which was considerably less than the 11 in (28 cm) section. The maximum longitudinal strain in the FRL for the 13 in (33 cm) section occurred when testing at 5 mph (8 km/h) with a tire pressure of 80 psi (552 kPa) and the single axle truck. Table 19 shows average longitudinal strain in the FRL for the 13 in (33 cm) section ranged between 35  $\mu\epsilon$  and 76  $\mu\epsilon$  for the single axle truck and 26  $\mu\epsilon$  and 53  $\mu\epsilon$  for the tandem axle truck. Similar to the 11 in (28 cm) section, Table 19 also shows strains produced by the single axle truck were consistently higher than strains produced by the tandem axle truck. Longitudinal strain in the FRL were also, once again, highest when testing at 5 mph (8 km/h) for each tire pressure, although, they were maximized between all three tire pressures for each speed.

**Table 19. Maximum longitudinal strain in the FRL for the 13 in (33 cm) section ( $\mu\epsilon$ ).**

Tire Pressure (psi)   (kPa)		Speed (mph (km/h))					
		5 (8)		30 (48)		55 (89)	
		<i>Average</i>	<i>Max</i>	<i>Average</i>	<i>Max</i>	<i>Average</i>	<i>Max</i>
Single Axle Wide-Base Tire (21 Kip (93 kN) Axle Load)							
80	552	75.04	85.04	44.20	50.92	39.88	42.15
110	758	68.51	77.14	45.59	49.62	37.62	41.26
125	862	66.00	73.99	40.13	43.63	35.98	40.23
Tandem Axle Dual Tire (37 Kip (165 kN) Axle Load)							
80	552	52.84	61.89	37.00	39.09	31.60	33.97
110	758	47.32	54.74	31.47	34.58	27.90	30.55
125	862	46.20	62.88	31.35	34.69	26.53	29.69

The 15 in (38 cm) sections received higher longitudinal strain in the FRL compared to the 13 in (33 cm) section, although, they were still substantially lower than measurements in the 11 in (28 cm) section. One possible explanation for higher resulting strains in the 15 in (38 cm) section compared to the 13 in (33 cm) section could be the difference in subgrade resilient modulus. The 13 in (33 cm) section was constructed on chemically stabilized subgrade which had a resilient modulus of 40 ksi (276 MPa) while the 15 in (38 cm) section was constructed on a subgrade which had a resilient modulus of 20 ksi (138 MPa). Table 20 displays the maximum and average maximum longitudinal strains recorded in the FRL for the 15 in (38 cm) section. The maximum strain was 102.18  $\mu\epsilon$ . The maximum strain was measured during 5 mph (8 km/h) testing using the single axle truck at a tire pressure of 80 psi (552 kPa). Average longitudinal strain in the FRL ranged between 42  $\mu\epsilon$  and 78  $\mu\epsilon$  for testing utilizing the single axle truck and 37  $\mu\epsilon$  and 53  $\mu\epsilon$  with the tandem axle truck. Once more, the highest strains were obtained during 5 mph (8 km/h) for each tire pressure.

**Table 20. Maximum longitudinal strain in the FRL for 15 in (38 cm) section ( $\mu\epsilon$ ).**

Tire Pressure (psi)   (kPa)		Speed (mph (km/h))					
		5 (8)		30 (48)		55 (89)	
		<i>Average</i>	<i>Max</i>	<i>Average</i>	<i>Max</i>	<i>Average</i>	<i>Max</i>
Single Axle Wide-Base Tire (21 Kip (93 kN) Axle Load)							
80	552	77.92	102.18	57.62	66.32	42.11	47.77
110	758	74.97	96.44	54.42	62.28	47.79	50.97
125	862	70.46	93.20	55.20	65.19	44.23	46.38
Tandem Axle Dual Tire (37 Kip (165 kN) Axle Load)							
80	552	52.42	66.85	43.71	51.69	41.69	46.81
110	758	52.45	70.16	44.17	50.98	39.63	47.49
125	862	47.78	62.28	41.66	48.88	37.80	43.56

### 7.1.1 Influence of Speed on Longitudinal Strain in the FRL

Figure 29 is a chart of strain versus speed for both axle configurations and all three tire pressures in the 11 in (28 cm), 13 in (33 cm), and 15 in (38 cm) sections. The figure clearly shows a decrease in longitudinal strain in the FRL as speed increased for all tire pressures, in each section, and for both axle configurations. The influence of speed on strain was most

prevalent in the 15 in (38 cm) section while its influence in the 13 in (33 cm) and 11 in (28 cm) sections was less. Longitudinal strain in the FRL decreased more with speed for testing conducted with the single axle truck, and strains for the single axle truck were always larger than for tandem axle.

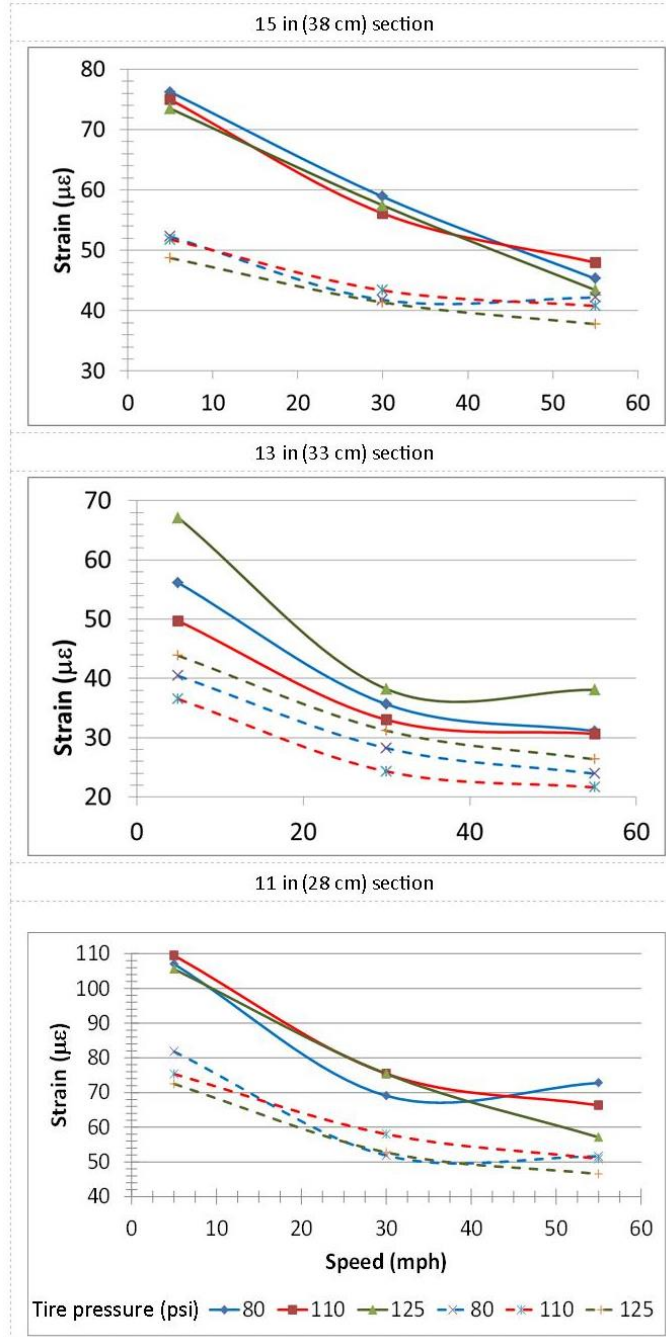


Figure 29. Maximum longitudinal strain in FRL versus speed (1 in = 2.54 cm, 1 mph = 1.6 km/h). Solid lines indicate single axle wide-based tire, and dashed lines indicate tandem axle.

### **7.1.2 Influence of Tire Pressure on Longitudinal Strain in the FRL**

Tire pressure seemed to have minimal effects on longitudinal strain located in the FRL. The effect of tire pressure is displayed in Figure 30. In order to reduce the effects of lateral tire offset, one run for each tire pressure and speed with less than 2 in (5 cm) of lateral tire offset was used to generate all sets of results. Additionally, only tandem axle generated strains were used in order to create an accurate comparison. Figure 30 plots strain against tire pressure for all three sections and all testing speeds. Tire pressure had little influence on the longitudinal strain in the FRL, especially at lower testing speeds, with virtually no influence occurring at a speed of 5 mph (8 km/h). Some inconsistencies were discovered for the single axle truck traveling at speeds of 30 mph (48 km/h) and 55 mph (89 km/h) but the differences were still fairly minimal.

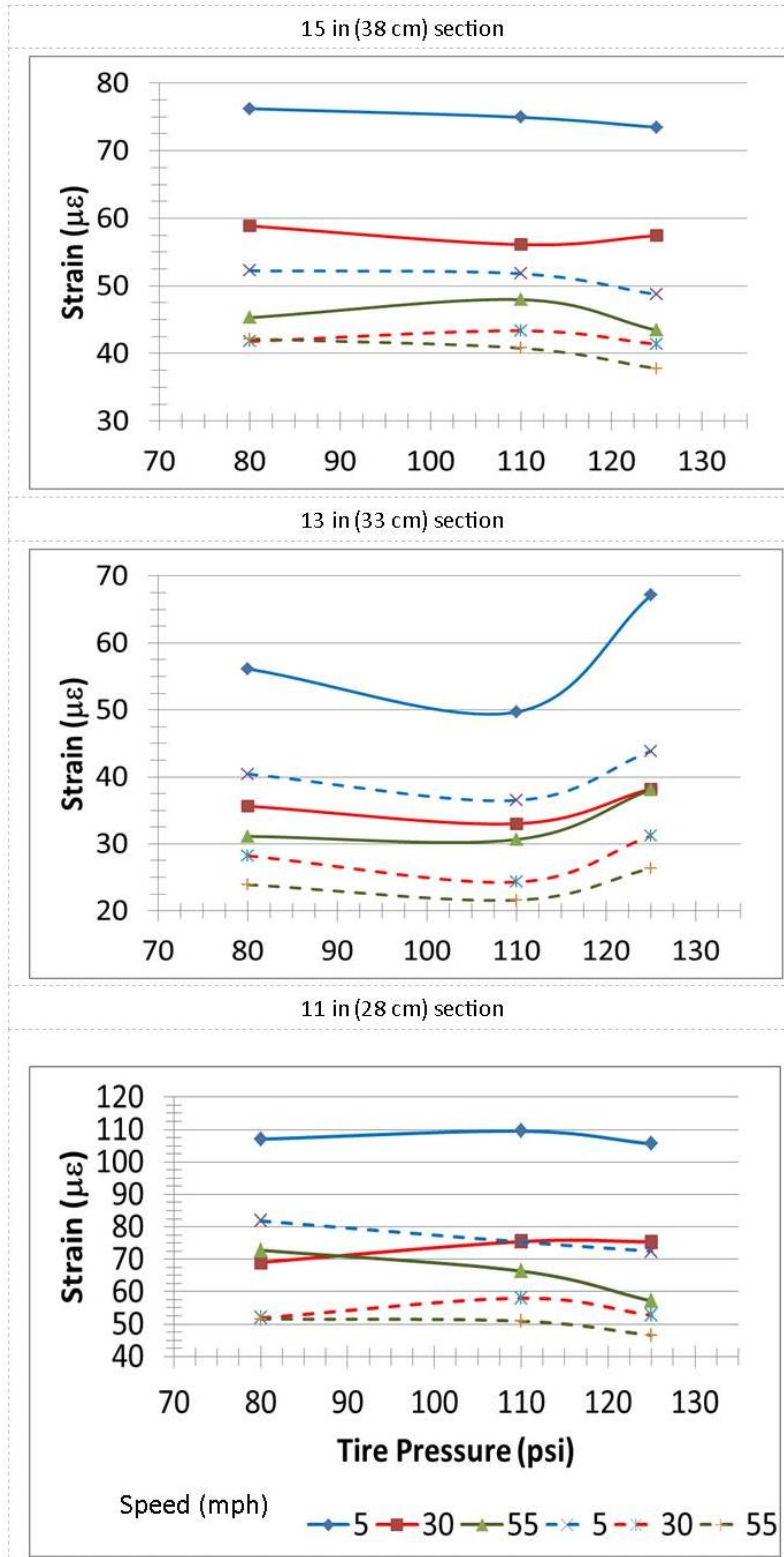


Figure 30. Maximum longitudinal strain in FRL versus tire pressure (1 in = 2.54 cm, 1 psi = 6.89 kPa). Solid lines indicate single axle wide-based tire, and dashed lines indicate tandem axle.

### 7.2 Longitudinal Strain in the Base Layer

Longitudinal strains found in the base layer, like longitudinal strain in the FRL, were greatest in the 11 in (28 cm) section. Table 21 shows the maximum and average maximum longitudinal strain measured in the base layer for the 11 in (28 cm) section. The maximum longitudinal strain recorded in the base layer for the 11 in (28 cm) section was 83.58  $\mu\epsilon$  during single axle truck testing at 5 mph (8 km/h) with a tire pressure of 125 psi (862 kPa). The average base layer strain for the 11 in (28 cm) section ranged between 21  $\mu\epsilon$  and 66  $\mu\epsilon$  for the single axle truck and between 12  $\mu\epsilon$  and 47  $\mu\epsilon$  for the tandem axle truck. Similar to the FRL, longitudinal strains were greater in the base layer when testing with the single axle truck. The strain values at 5 mph (8 km/h) were larger than those at higher speeds for each tire pressure.

**Table 21. Maximum longitudinal strain in the base layer for the 11 in (28 cm) section ( $\mu\epsilon$ ).**

Tire Pressure (psi)   (kPa)		Speed (mph (km/h))					
		5 (8)		30 (48)		55 (89)	
		<i>Average</i>	<i>Max</i>	<i>Average</i>	<i>Max</i>	<i>Average</i>	<i>Max</i>
Single Axle Wide-Base Tire (21 kip (93 kN) Axle Load)							
80	552	53.58	73.71	28.08	39.38	22.71	28.32
110	758	65.52	81.40	34.72	42.92	22.10	30.03
125	862	62.58	83.58	36.55	41.94	21.45	26.54
Tandem Axle Dual Tire (37 kip (165 kN) Axle Load)							
80	552	34.93	49.97	18.02	28.48	12.62	17.30
110	758	44.66	56.31	21.07	26.92	14.72	17.56
125	862	46.54	54.10	22.89	30.03	14.99	18.94

Similar to longitudinal strain measurements in the FRL, the 13 in (33 cm) section received the lowest longitudinal strains in the base layer. Table 22 provides a summary of longitudinal strain in the base layer for the 13 in (33 cm) section. The maximum strain discovered was 43.55  $\mu\epsilon$  as shown in Table 22, recorded at 5 mph (8 km/h), 125 psi (862 kPa) tire pressure, and testing with the single axle truck. Furthermore, average longitudinal strains in the base layer ranged between 14  $\mu\epsilon$  and 38  $\mu\epsilon$  for the single axle truck and 10  $\mu\epsilon$  and 25  $\mu\epsilon$  for the tandem axle truck. Average maximum longitudinal strains in the base layer of the 13 in (33 cm) sections were greatest when testing at 5 mph (8 km/h) for each tire pressure.

**Table 22. Maximum longitudinal strain in the base layer for the 13 in (33 cm) section ( $\mu\epsilon$ ).**

Tire Pressure (psi)   (kPa)		Speed (mph (km/h))					
		5 (8)		30 (48)		55 (89)	
		<i>Average</i>	<i>Max</i>	<i>Average</i>	<i>Max</i>	<i>Average</i>	<i>Max</i>
Single Axle Wide-Base Tire (21 kip (93 kN) Axle Load)							
80	552	35.94	41.46	18.70	23.85	14.92	19.61
110	758	35.49	40.97	21.99	27.97	15.71	20.49
125	862	37.97	43.55	19.69	25.83	15.49	20.42
Tandem Axle Dual Tire (37 kip (165 kN) Axle Load)							
80	552	22.34	26.97	14.19	20.12	10.53	12.77
110	758	24.11	29.91	13.35	19.69	10.49	12.49
125	862	22.71	27.99	13.43	17.56	10.61	13.16

The 15 in (38 cm) section received longitudinal strain results in the base layer slightly higher than the 13 in (33 cm) section. Table 23 offers maximum and average maximum longitudinal strain in the base layer for the 15 in (38 cm) section. The largest maximum longitudinal strain in the base layer for the 15 in (38 cm) section was 49.37  $\mu\epsilon$ , just less than 50  $\mu\epsilon$ , and it was obtained during single axle truck testing at 5 mph (8 km/h) with a tire pressure of 110 psi (758 kPa). Table 23 shows average strain measurements ranged between 16  $\mu\epsilon$  and 40  $\mu\epsilon$  for the single axle truck and 14  $\mu\epsilon$  and 26  $\mu\epsilon$  for the tandem axle truck. The maximum average longitudinal strain was found at a 5 mph (8 km/h) testing speed, regardless of tire pressure.

**Table 23. Maximum longitudinal strain in the base layer for the 15 in (38 cm) section ( $\mu\epsilon$ ).**

Tire Pressure (psi)   (kPa)		Speed (mph (km/h))					
		5 (8)		30 (48)		55 (89)	
		<i>Average</i>	<i>Max</i>	<i>Average</i>	<i>Max</i>	<i>Average</i>	<i>Max</i>
Single Axle Wide-Base Tire (21 kip (93 kN) Axle Load)							
80	552	37.64	47.92	24.14	32.11	16.29	23.97
110	758	39.12	49.37	24.78	34.88	19.45	26.50
125	862	38.23	47.16	25.95	37.92	18.78	25.63
Tandem Axle Dual Tire (37 kip (165 kN) Axle Load)							
80	552	24.37	30.73	16.99	21.50	14.21	17.20
110	758	25.30	34.52	17.95	22.92	14.73	22.37
125	862	24.31	32.20	17.29	21.38	14.72	21.63

### 7.2.1 Influence of Speed on Longitudinal Strain in the Base Layer

Like the longitudinal strain in the FRL, the longitudinal strain in the base layer decreased as speed increased, as can be seen in Table 21, Table 22, and Table 23. Figure 31, for the 11 in (28 cm), 13 in (33 cm), and 15 in (38 cm) sections, relates longitudinal strain in the base layer to speed without the effects of lateral tire offset and is categorized by tire pressure and axle configuration. Another observation similar to the longitudinal strain in the FRL was longitudinal strain in the base layer tended to stabilize at higher speeds when testing at higher tire pressures but only occurred in the 11 in (28 cm) and 13 in (33 cm) sections as shown in Figure 22. Although, as the section thickness was increased the correlation became more linear for all three tire pressures with a nearly linear trend in the 15 in (38 cm) section. This was especially true for testing with the single axle truck.



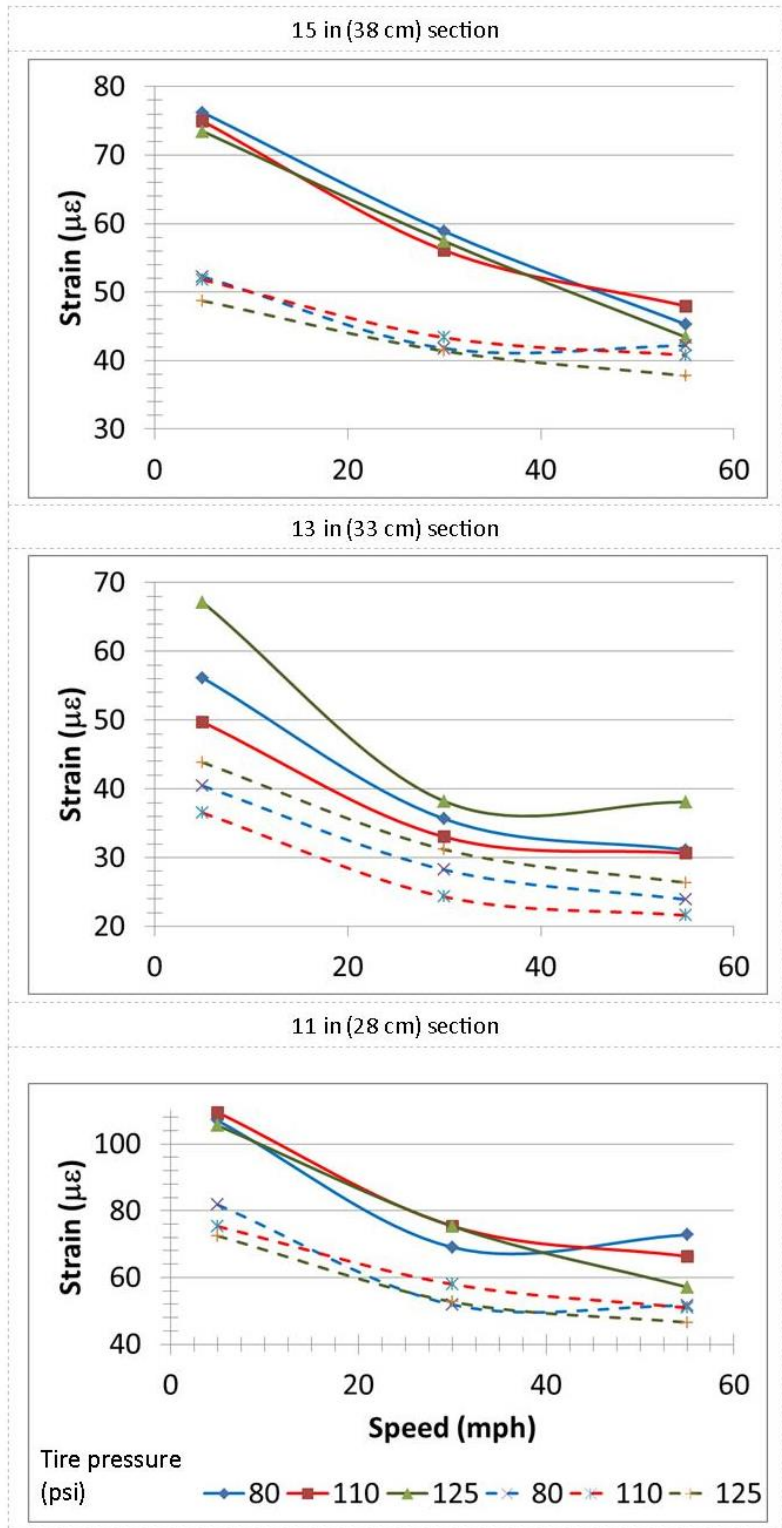


Figure 31. Maximum longitudinal strain in base layer versus speed (1 in = 2.54 cm, 1 mph = 1.6 km/h). Solid lines indicate single axle wide-based tire, and dashed lines indicate tandem axle.

### **7.2.2 Influence of Tire Pressure on Longitudinal Strain in the Base Layer**

Tire pressure had minimal impacts on tandem axle truck testing. Figure 32 plots longitudinal strain in the base layer and tire pressure for each test section and testing speed. Similar to earlier comparisons, the lateral tire offset factor was removed by analyzing runs with little wheel wander and tandem axle produced strains were used for tandem axle truck test runs. Figure 32 shows the influence of tire pressure was reduced as pavement thickness was increased.

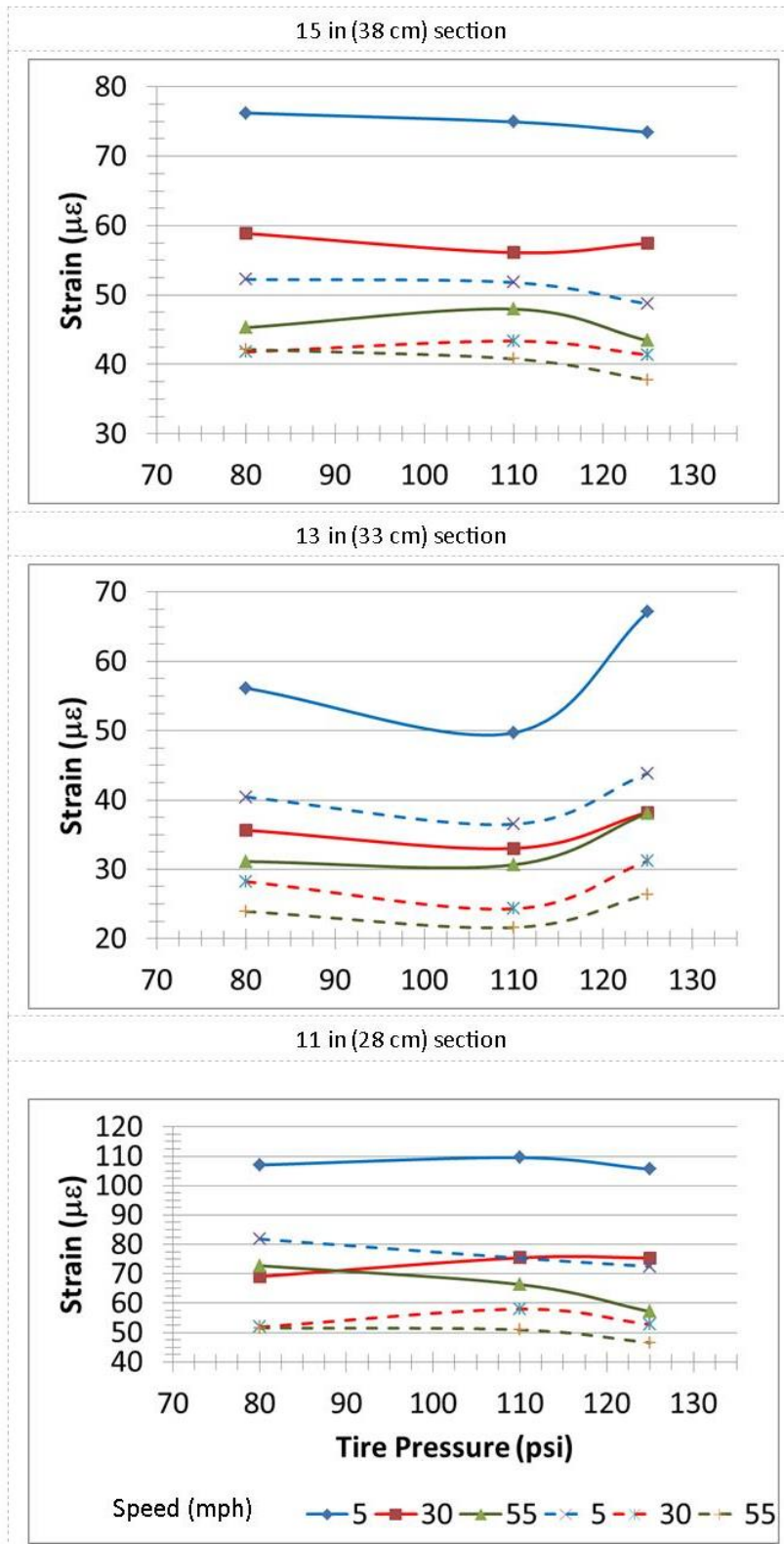


Figure 32. Maximum longitudinal strain in the base layer versus tire pressure (1 in = 2.54 cm, 1 psi = 6.89 kPa). Solid lines indicate single axle wide-based tire, and dashed lines indicate tandem axle.

### 7.3 Transverse Strain in the Base Layer

Transverse strain results in the base layer were greatest in the 11 in (28 cm) section. A summary of the maximum and average maximum transverse strains found in the base layer is displayed in Table 24. The highest transverse strain measured in the base layer of the 11 in (28 cm) section was 61.08  $\mu\epsilon$  which was recorded during tandem axle truck testing with a tire pressure of 125 psi (862 kPa) at 5 mph (8 km/h). Average transverse strains in the base layer for the 11 in (28 cm) section varied between 15  $\mu\epsilon$  and 47  $\mu\epsilon$  for testing conducted with the single axle truck and -18  $\mu\epsilon$  and 50  $\mu\epsilon$  for testing conducted with the tandem axle truck, where the negative number indicates a compressive strain. For each tire pressure, the maximum and average maximum transverse strain was greatest at 5 mph (8 km/h).

**Table 24. Maximum transverse strain in the base layer for the 11 in (28 cm) section ( $\mu\epsilon$ ).**

Tire Pressure (psi)   (kPa)		Speed (mph (km/h))					
		5 (8)		30 (48)		55 (89)	
		<i>Average</i>	<i>Max</i>	<i>Average</i>	<i>Max</i>	<i>Average</i>	<i>Max</i>
Single Axle Wide-Base Tire (21 kip (93 kN) Axle Load)							
80	552	32.38	42.69	17.86	22.70	16.05	16.55
110	758	46.34	54.67	20.44	23.67	15.41	17.86
125	862	44.50	53.44	23.50	25.02	16.44	18.68
Tandem Axle Dual Tire (37 kip (165 kN) Axle Load)							
80	552	27.85	52.62	-9.40	-15.40	-11.84	-14.27
110	758	49.89	58.81	-12.55	-17.85	14.51	16.03
125	862	44.87	61.08	20.65	25.71	12.78	16.94

Although longitudinal strains in the 13 in (33 cm) section were found to be lower than the 11 in (28 cm) and 15 in (38 cm) sections, the transverse strains in the base layer were typically higher than the other two sections especially when testing with the single axle truck. A summary of transverse strain discovered in the base layer of the 13 in (33 cm) section is presented in Table 25. The maximum transverse strain occurred during single axle truck testing at 5 mph (8 km/h) with a tire pressure of 80 psi (552 kPa) and was 70.19  $\mu\epsilon$ . Single axle, average transverse strain ranged between 23  $\mu\epsilon$  and 50  $\mu\epsilon$  while transverse axle, average transverse strains ranged between 15  $\mu\epsilon$  and 33  $\mu\epsilon$ . For the 13 in (33 cm) section, as displayed in Table 10, average transverse strains were typically maximized at a tire pressure of 80 psi (552 kPa) excepting the single axle truck at the higher speeds. Additionally, average maximum transverse strains in the base layer, for each tire pressure, occurred at 5 mph (8 km/h).

**Table 25. Maximum transverse strain in the base layer for the 13 in (33 cm) section ( $\mu\epsilon$ ).**

Tire Pressure (psi)   (kPa)		Speed (mph (km/h))					
		5 (8)		30 (48)		55 (89)	
		<i>Average</i>	<i>Max</i>	<i>Average</i>	<i>Max</i>	<i>Average</i>	<i>Max</i>
Single Axle Wide-Base Tire (21 Kip (93 kN) Axle Load)							
80	552	47.32	70.19	24.69	46.38	23.54	44.43
110	758	48.77	68.10	31.22	50.88	25.22	44.30
125	862	49.22	63.96	25.91	42.70	24.36	41.39
Tandem Axle Dual Tire (37 Kip (165 kN) Axle Load)							
80	552	30.16	51.16	21.91	39.92	15.45	29.62
110	758	32.66	49.55	18.63	36.25	15.01	28.24
125	862	28.15	43.06	17.60	32.33	15.14	24.76

Transverse strains in the base layer of the 15 in (38 cm) section were slightly reduced compared to those of the 13 in (33 cm) section. Table 26 provides the maximum and average maximum transverse strains in the base layer of the 15 in (38 cm) section. As seen in Table 26, the maximum strain obtained was 61.59  $\mu\epsilon$  during single axle truck testing at 5 mph (8 km/h) with its tires inflated to 110 psi (758 kPa). Average transverse strains in the base layer of the 15 in (38 cm) section fluctuated between 21  $\mu\epsilon$  and 53  $\mu\epsilon$  for single axle truck testing and 18  $\mu\epsilon$  and 33  $\mu\epsilon$  for tandem axle truck testing. Transverse strains in the base layer of the 15 in (38 cm) section were greatest at 5 mph (8 km/h) for each tire pressure.

**Table 26. Maximum transverse strain in the base layer for the 15 in (38 cm) section ( $\mu\epsilon$ ).**

Tire Pressure (psi)   (kPa)		Speed (mph (km/h))					
		5 (8)		30 (48)		55 (89)	
		<i>Average</i>	<i>Max</i>	<i>Average</i>	<i>Max</i>	<i>Average</i>	<i>Max</i>
Single Axle Wide-Base Tire (21 Kip (93 kN) Axle Load)							
80	552	49.07	58.37	31.30	37.49	21.25	25.69
110	758	52.13	61.59	31.86	37.67	24.30	29.23
125	862	50.35	60.78	25.96	36.43	24.75	29.25
Tandem Axle Dual Tire (37 Kip (165 kN) Axle Load)							
80	552	27.18	32.39	21.95	25.69	18.21	21.30
110	758	32.11	39.92	23.22	27.05	20.41	27.04
125	862	32.03	42.21	22.80	26.08	19.58	24.76

### 7.3.1 Influence of Speed on Transverse Strain in the Base Layer

Transverse strain in the base layer decreased with increasing speeds, as was the case with other strains. Figure 33 relates transverse strain found in the base layer to speed. Test runs used for the figure incorporated little or no lateral tire offset and only tandem axle produced strains were used. For the 15 in (38 cm) section the transverse strain in the base layer resulting from the single axle truck decreased sharply from 5 mph (8 km/h) to 30 mph (48 km/h), with a further, but less steep, decrease at a speed of 55 mph (89 km/h); the decrease much less steep with the tandem axle truck. For the 13 in (33 cm) and 15 in (38 cm) sections, the speed related decreases in the transverse strains were more pronounced for the tandem axle truck, particularly for the 11 in (28 cm) section, where there was a pronounced dip at 30 mph (48 km/h) at 80 psi (552 kPa)

and 110 psi (758 kPa). The single axle truck had a similar difference with speed in all three sections.

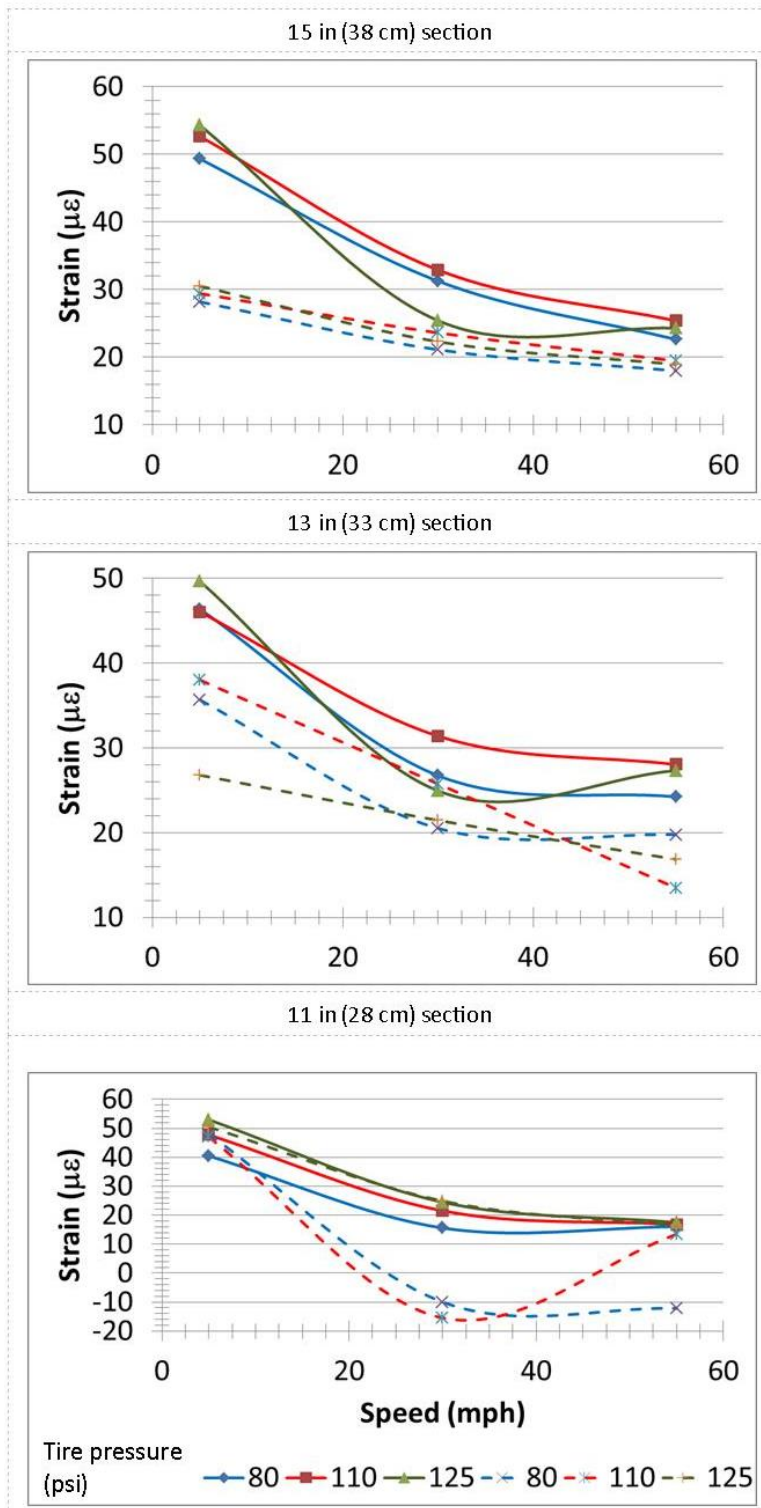


Figure 33. Maximum transverse strain in the base layer versus speed (1 in = 2.54 cm, 1 mph = 1.6 km/h). Solid lines indicate single axle wide-based tire, and dashed lines indicate tandem axle.

### **7.3.2 Influence of Tire Pressure on Transverse Strain in the Base Layer**

Figure 34 relates transverse strain in the base layer to tire pressure without the influence of wheel wander or the steer axle of the tandem axle truck. In the 15 in (38 cm) sections, showed as tire pressure increased, transverse strains in the base layer generally increased slightly, with the obvious exception of the single axle truck at 110 psi (758 kPa). For the 13 in (33 cm) section transverse strains in the base layer either peaked or dipped at 110 psi (758 kPa) tire pressure but increased significantly between 110 psi (758 kPa). The 11 in (28 cm) section had slight increases for single axle loads and a more pronounced increase with tandem axle loads.

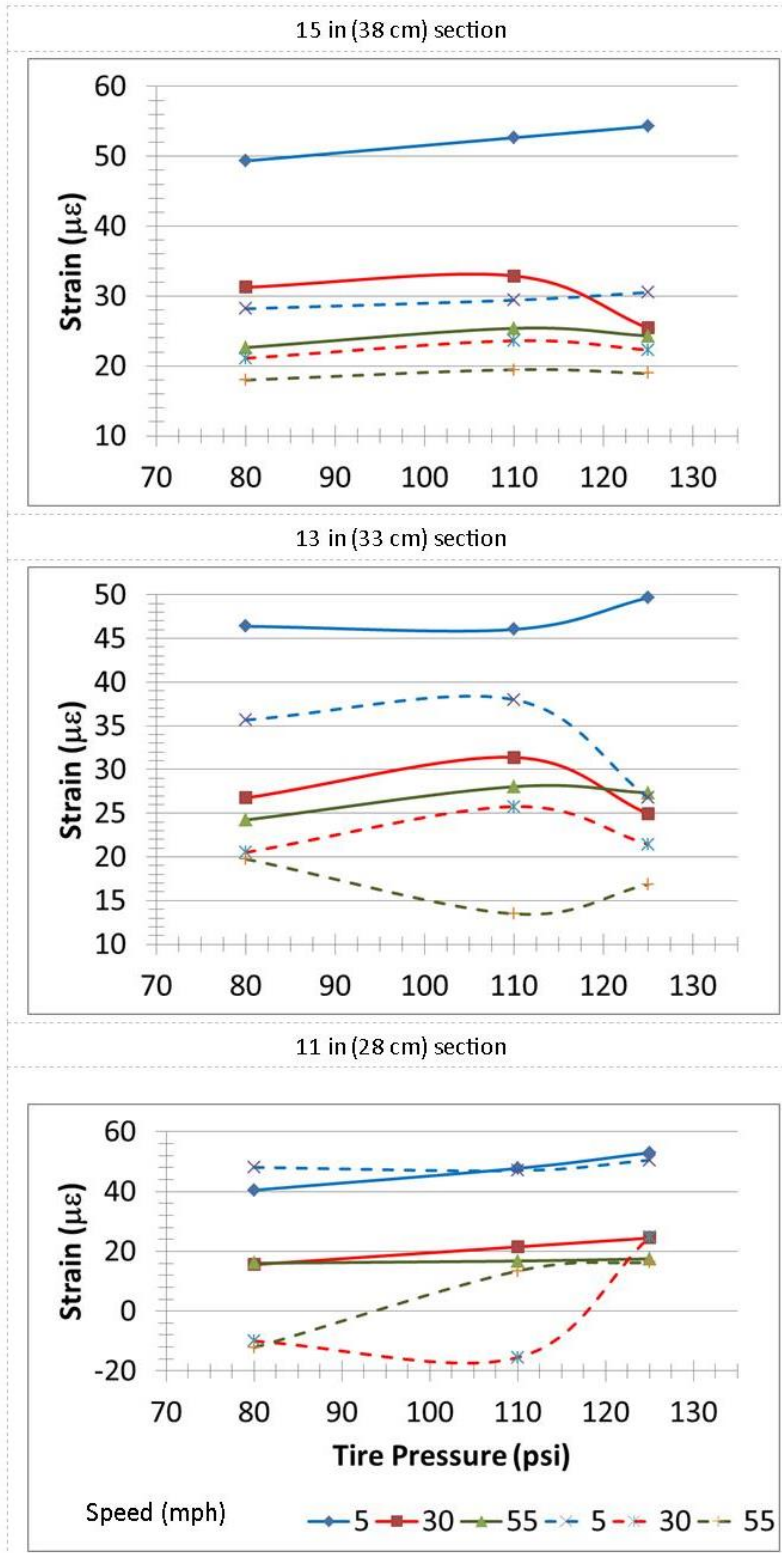


Figure 34. Maximum transverse strain in the base layer versus tire pressure (1 in = 2.54 cm, 1 psi = 6.89 kPa). Solid lines indicate single axle wide-based tire, and dashed lines indicate tandem axle.



## 7.4 Comparisons Between Strain Responses

Transverse strains in the base layer were typically discovered to be less than longitudinal strains in the base layer for the 11 in (28 cm) section, although, for the 13 in (33 cm) and 15 in (38 cm) sections transverse strains were typically found to be greater than longitudinal strains. Table 27, Table 28, and Table 29 compare longitudinal and transverse strains in the base layer of the 11 in (28 cm), 13 in (33 cm), and 15 in (38 cm) sections respectively. Once more, the tables do not incorporate influences of lateral wheel offset. Furthermore, due to the mixture of maximum strains produced by either the tandem axle or steer axle of the tandem axle truck, strains produced by the tandem axle were used for this comparison. For the 11 in (28 cm) section, as portrayed in Table 27, when testing both the single axle truck and tandem axle truck, longitudinal strains were greater in magnitude than transverse strains independent of tire pressure, speed, or axle configuration, except for the tandem axle configuration at 5 mph (8 km/h), and for the highest pressure at 55 mph (89 km/h). Also note a negative value for some transverse strains indicates compression. A switch of critical strains from longitudinal to transverse was prevalent in the 13 in (33 cm) section when testing with the single axle truck as shown in Table 28. This was an important discovery because the critical strains for these tests in the base layer were the transverse strains. In the 15 in (38 cm) section, as displayed in Table 29, all of the transverse strains were greater than the longitudinal strains.

**Table 27. Longitudinal versus transverse strains in the base layer for the 11 in (28 cm) section ( $\mu\epsilon$ ).**

Tire Pressure (psi)   (kPa)		Speed (mph (km/h))					
		5 (8)		30 (48)		55 (89)	
		<i>Transverse</i>	<i>Longitudinal</i>	<i>Transverse</i>	<i>Longitudinal</i>	<i>Transverse</i>	<i>Longitudinal</i>
Single Axle Wide-Base Tire (21 kip (93 kN) Axle Load)							
80	552	40.46	64.36	15.56	21.10	16.04	22.64
110	758	47.76	71.67	21.50	35.46	16.78	22.43
125	862	52.96	68.34	24.46	36.61	17.49	21.47
Tandem Axle Dual Tire (37 kip (165 kN) Axle Load)							
80	552	48.07	43.27	-10.00	13.92	-12.19	14.17
110	758	46.98	43.77	-15.51	21.11	13.43	14.55
125	862	50.49	47.63	24.87	25.24	16.37	15.41

**Table 28. Longitudinal versus transverse strains in the base layer for the 13 in (33 cm) section ( $\mu\epsilon$ ).**

Tire Pressure (psi)   (kPa)		Speed (mph (km/h))					
		5 (8)		30 (48)		55 (89)	
		<i>Transverse</i>	<i>Longitudinal</i>	<i>Transverse</i>	<i>Longitudinal</i>	<i>Transverse</i>	<i>Longitudinal</i>
Single Axle Wide-Base Tire (21 kip (93 kN) Axle Load)							
80	552	46.39	34.74	26.74	19.86	24.23	15.63
110	758	46.04	33.46	31.40	21.72	28.04	16.36
125	862	49.66	38.46	24.94	19.00	27.34	16.77
Tandem Axle Dual Tire (37 kip (165 kN) Axle Load)							
80	552	35.67	22.97	20.51	13.56	19.76	10.53
110	758	38.01	25.58	25.76	15.39	13.49	10.14
125	862	26.79	21.52	21.45	13.93	16.85	10.90

**Table 29. Longitudinal versus transverse strains in the base layer for the 15 in (38 cm) section ( $\mu\epsilon$ ).**

Tire Pressure (psi)   (kPa)		Speed (mph (km/h))					
		5 (8)		30 (48)		55 (89)	
		<i>Transverse</i>	<i>Longitudinal</i>	<i>Transverse</i>	<i>Longitudinal</i>	<i>Transverse</i>	<i>Longitudinal</i>
Single Axle Wide-Base Tire (21 kip (93 kN) Axle Load)							
80	552	49.34	37.39	31.26	24.72	22.64	17.39
110	758	52.66	39.08	32.90	25.05	25.39	19.46
125	862	54.29	39.23	25.42	26.05	24.31	18.26
Tandem Axle Dual Tire (37 kip (165 kN) Axle Load)							
80	552	28.19	23.91	21.11	16.85	17.99	14.20
110	758	29.42	25.17	23.61	16.93	19.47	15.00
125	862	30.52	25.80	22.30	17.14	18.93	14.79

The longitudinal strains measured in the base layer were significantly lower than the longitudinal strains measured in the FRL in each of the three sections. This was due to strain gages located in the base layer being closer to the neutral axis and therefore experiencing less bending. Table 30, Table 31, and Table 32 compare longitudinal strain values obtained in the base and FRL for single axle truck testing in the 11 in (28 cm), 13 in (33 cm), and 15 in (38 cm) sections respectively. Wheel wander effects were removed for this comparison. Tandem axle truck testing was also removed from this analysis since, in the base layer it was no longer consistently producing the strains with its tandem axle load.

**Table 30. Maximum longitudinal strain in FRL versus in base layer for single axle wide-base tire truck test with 29 kip (129 kN) axle load for the 11 in (28 cm) section ( $\mu\epsilon$ ).**

Tire Pressure (psi)   (kPa)		Speed (mph (km/h))					
		5 (8)		30 (48)		55 (89)	
		<i>FRL</i>	<i>Base Layer</i>	<i>FRL</i>	<i>Base Layer</i>	<i>FRL</i>	<i>Base Layer</i>
80	552	107.04	64.36	69.07	21.10	72.79	22.64
110	758	109.50	71.67	75.43	35.46	66.34	22.43
125	862	105.57	68.34	75.38	36.61	57.12	21.47

**Table 31. Maximum longitudinal strain in FRL versus in base layer for single axle wide-base tire truck test with 29 kip (129 kN) axle load for the 13 in (33 cm) section ( $\mu\epsilon$ ).**

Tire Pressure (psi)   (kPa)		Speed (mph (km/h))					
		5 (8)		30 (48)		55 (89)	
		<i>FRL</i>	<i>Base Layer</i>	<i>FRL</i>	<i>Base Layer</i>	<i>FRL</i>	<i>Base Layer</i>
80	552	56.13	34.74	35.64	19.86	31.12	15.63
110	758	49.69	33.46	33.02	21.72	30.65	16.36
125	862	67.11	38.46	38.21	19.00	38.09	16.77

**Table 32. Maximum longitudinal strain in FRL versus in base layer for single axle wide-base tire truck test with 29 kip (129 kN) axle load for the 15 in (38 cm) section ( $\mu\epsilon$ ).**

Tire Pressure (psi)   (kPa)		Speed (mph (km/h))					
		5 (8)		30 (48)		55 (89)	
		<i>FRL</i>	<i>Base Layer</i>	<i>FRL</i>	<i>Base Layer</i>	<i>FRL</i>	<i>Base Layer</i>
80	552	76.23	37.39	58.87	24.72	45.30	17.39
110	758	74.94	39.08	56.11	25.05	47.97	19.46
125	862	73.47	39.23	57.44	26.05	43.43	18.26

## 8 PerRoad Analysis

To evaluate the perpetual nature of the test sections constructed on DEL-23, an analysis of the test sections was performed using the mechanistic based software program, PerRoad. PerRoad was developed by NCAT for the Asphalt Pavement Alliance (APA). The software relies on layered elastic theory and Monte Carlo simulation. It integrates loading and seasonal data with flexible pavement's layer material properties and thicknesses (Romanello 2007). Additionally, the software incorporates endurance limits and strain-based transfer functions to predict damage accumulation and, therefore, the in-service life of the pavement structure being analyzed.

### 8.1 Loading Conditions

In order to accurately analyze the DEL-23 test sections, loading properties were entered into the PerRoad program through a vehicle classification distribution. The program requires the percent annual average daily truck traffic (%AADTT) for vehicle classifications 4 through 13. These percentages were determined for the test sections by Weigh-in-motion (WIM) scales installed on the northbound lanes of DEL-23. Although the traffic seen for the test sections on the northbound lanes of DEL-23 will be significantly different than for the test sections on North Waldo Road, the traffic on the northbound lanes of DEL-23 is considerably higher than that of North Waldo Road creating a conservative analysis for the test sections on North Waldo Road.

A Mettler-Toledo WIM system was installed in DEL-23 at the time of original construction in 1996. The scales are used to continuously monitor traffic in all four lanes. Each vehicle crossing the WIM load plates in the pavement generates data including gross weight, classification, date and hour of crossing, and the weight and spacing of individual vehicle axles. Figure 35 and Figure 36 are photographs of the sensors.



Figure 35. WIM Scales on DEL 23.



**Figure 36. WIM Scales on DEL 23.**



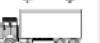
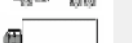



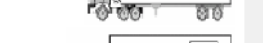


### **8.1.1 Vehicle Classification Distribution**

In order to obtain a vehicle classification distribution for the test sections on DEL-23, AADTTs for vehicle classifications 4 through 13 were generated by ODOT from data collected by the WIM scales for 2010, 2011, and 2012. These three years were then averaged, converted into percentages and entered into the PerRoad program. Table 33 provides the %AADTTs used and Figure 37 is a screen capture of the PerRoad Vehicle Type Distribution screen. Data used to calculate %AADTTs is provided in Appendix J.

**Table 33. Vehicle type distribution.**

<b>Class</b>	<b>%AADTT</b>
4	1.85%
5	14.41%
6	3.10%
7	3.08%
8	4.23%
9	69.74%
10	0.87%
11	2.17%
12	0.48%
13	0.07%

Roadway Functional Classification: Rural Principal Arterial

Vehicle Classification	% AADTT	Average Number of Axles Per Vehicle		
		Single	Tandem	Tridem
 4	1.85	1.62	0.39	0
 5	14.41	2	0	0
 6	3.1	1.02	0.99	0
 7	3.08	1	0.26	0.83
 8	4.23	2.38	0.67	0
 9	69.74	1.13	1.93	0
 10	0.87	1.19	1.09	0.89
 11	2.17	4.29	0.26	0.06
 12	0.48	3.52	1.14	0.06
 13	0.07	2.15	2.13	0.35
Total	100			

Buttons: Cancel Changes, Accept Changes

**Figure 37. Vehicle type distribution as entered into PerRoad.**

After the Vehicle Type Distribution data was entered into the PerRoad program, the program used standard values for the average number of axles per vehicle classification to generate a current axle load distribution, as shown in PerRoad's Loading Conditions screen, Figure 38. ODOT WIM scale measurements of general traffic data on DEL-23 were obtained from data collected in 2010, 2011, and 2012.

General Traffic Data

Two-Way AADT: 27530      % Trucks: 11.76      % Trucks in Design Lane: 90 %

Axles Groups / Day: 4179      % Truck Growth: 3.61      Directional Distribution: 50 %

Input Load Spectra by Vehicle Type

Loading Configurations (Check All That Apply)

Single 48.5 %       Tandem 50.28 %       Tridem 1.23 %       Steer 0 %

Current Configuration: Single

Current Axle Load Distribution

Axle Wt kip	% Axles	Axle Wt kip	% Axles	Axle Wt kip	% Axles	Axle Wt kip	% Axles	Axle Wt kip	% Axles
0-2	0	24-26	0.31	48-50	0	72-74	0	96-98	0
2-4	4.41	26-28	0.19	50-52	0	74-76	0	98-100	0
4-6	10.41	28-30	0.09	52-54	0	76-78	0	100-102	0
6-8	11.58	30-32	0.05	54-56	0	78-80	0	102-104	0
8-10	19.73	32-34	0.04	56-58	0	80-82	0	104-106	0
10-12	25.78	34-36	0.02	58-60	0	82-84	0	106-108	0
12-14	14.26	36-38	0.02	60-62	0	84-86	0	108-110	0
14-16	5.88	38-40	0.01	62-64	0	86-88	0	110+	0
16-18	3.36	40-42	0	64-66	0	88-90	0		
18-20	2.06	42-44	0	66-68	0	90-92	0	Total	100
20-22	1.18	44-46	0	68-70	0	92-94	0		
22-24	0.61	46-48	0	70-72	0	94-96	0		

Cancel Changes      Import Load Spectra      Save Load Spectra      Accept Changes

Figure 38. Loading conditions as entered into PerRoad.

## 8.2 Structural and Seasonal Information

In order for the PerRoad software to correlate modulus values for a variation of temperatures seen during different seasons, the duration and mean air temperature for each season were obtained using average monthly temperatures for Delaware, Ohio from The Weather Channel (2013). Table 34 displays the seasonal information used. Appendix J provides monthly average temperatures for Delaware, Ohio.

Table 34. Seasonal information for Ohio (The Weather Channel, 2013).

Season	Winter	Fall	Summer	Spring
Duration (weeks)	13	9	21	9
Average Temperature (°F)	31	50	70	48
Average Temperature (°C)	-0.4	9.7	20.9	8.6

Because the PerRoad program only allows a pavement structure of five layers or less, for the DEL-23 analysis, the surface and intermediate layers were combined. The layer thicknesses and specifications were provided in Table 1 and Table 2. Typical design values for the Modulus of Elasticity and Poisson's Ratio at 70°F (21°C) were provided by Sargand et al. (2008) and are shown in Table 35 along with the values chosen for the PerRoad analysis. Figure 39 displays the Structural and Seasonal Information screen.

**Table 35. Elastic modulus and Poison's ratio for pavement materials.**

Layer	Values from Sargand et al. (2008)			Input Values for PerRoad		
	Modulus of Elasticity, $E$		Poison's Ratio, $\nu$	Modulus of Elasticity, $E$		Poison's Ratio, $\nu$
	(ksi)	(MPa)		(ksi)	(MPa)	
Surface/Intermediate	1500	10342	0.35	1500	10342	0.35
Base	500-1500	3447 - 10342	0.35	1200	8274	0.35
Fatigue Resistant	500-1500	3447 - 10342	0.35	800	5516	0.35
DGAB	10	69	0.40	10	69	0.40
Subgrade (untreated / lime stabilized)	5	34	0.45	20/40*	138/276*	0.45

\*Since the modulus of the subgrade was previously obtained, it was used.

The screenshot shows the PerRoad software interface with the following settings:

- # of Layers:** 5 (selected)
- Seasonal Information:**
  - Season:  Summer,  Fall,  Winter,  Spring,  Spring2
  - Duration (weeks): Summer: 21, Fall: 9, Winter: 13, Spring: 9, Spring2: 0
  - Mean Air Temperature, F: Summer: 70, Fall: 50, Winter: 31, Spring: 48, Spring2: 70
  - Temperature Correction:
- Layer 1:** Material Type: AC, PG Grade: 64, -28, Min Modulus: 50000, Modulus: 1500000, Max Modulus: 4000000, Poisson's Ratio: 0.35, Min-Max: 0.15 - 0.4, Thickness: 3
- Layer 2:** Material Type: AC, PG Grade: 64, -22, Min Modulus: 50000, Modulus: 1200000, Max Modulus: 4000000, Poisson's Ratio: 0.35, Min-Max: 0.15 - 0.4, Thickness: 4
- Layer 3:** Material Type: AC, PG Grade: 64, -22, Min Modulus: 50000, Modulus: 800000, Max Modulus: 4000000, Poisson's Ratio: 0.35, Min-Max: 0.15 - 0.4, Thickness: 4
- Layer 4:** Material Type: Gran Base, PG Grade: 64, -22, Min Modulus: 5000, Modulus: 10000, Max Modulus: 50000, Poisson's Ratio: 0.4, Min-Max: 0.35 - 0.45, Thickness: 6
- Layer 5:** Material Type: Soil, PG Grade: 64, -22, Min Modulus: 3000, Modulus: 40000, Max Modulus: 40000, Poisson's Ratio: 0.45, Min-Max: 0.2 - 0.5, Thickness: Infinite

**Figure 39. Structural and seasonal information as entered into PerRoad.**

### 8.3 Performance Criteria

In order to evaluate the performance of the perpetual pavement test sections, performance criteria were assigned at four different locations in the PerRoad program. By assigning performance criteria, such as horizontal strain, vertical stress, or vertical deflection, and a corresponding threshold limit, the PerRoad program computed the percent of pavement responses that fell below the given threshold limit for a variety of loading and temperature conditions it developed. The program also returned a value for each condition and, therefore, a maximum value was obtained for each pavement response. A performance criterion was assigned to evaluate pavement deflection, horizontal strain in the base layer and FRL, and



pressure on the subgrade surface. Table 36 provides the location, performance criteria, and threshold limit used.

**Table 36. Perpetual pavement performance criteria used in PerRoad.**

Location		Performance Criteria	Threshold Limit
Layer	Position		
Base Layer	Bottom	Horizontal Strain	50 $\mu\epsilon$
FRL	Bottom	Horizontal Strain	70 $\mu\epsilon$
DGAB	Bottom	Vertical Deflection	20 mil (508 mm)
DGAB	Bottom	Vertical Pressure	8/4 psi (55/27 kPa)

The final PerRoad function utilized was fatigue transfer functions for strain performance criteria. The fatigue transfer functions within the PerRoad program calculated the fatigue life of the pavement, or the number of years until damage occurs ( $D=0.1$ ), for test sections which were analyzed to have strain responses greater than their respective threshold limits. The PerRoad software required the input of the empirical constants,  $k_1$  and  $k_2$ , in order to complete fatigue transfer functions. Priest and Timm (2006) conducted a study using the NCAT Test Track in order to develop these empirical constants. The empirical constants they generated were used for this analysis and are shown in Table 37.

**Table 37. Fatigue transfer function empirical constants (values from Timm & Priest 2006).**

Empirical Constant	Base Layer	FRL
$K_1$	0.4831	3.063
$K_2$	0.4814	3.007

## 8.4 Results

The following provides results obtained from the PerRoad analysis using the structures utilized in the DEL-23 test sections. The PerRoad program includes variability in the layer thicknesses and moduli that would realistically occur between different construction projects. The analysis should be used in consideration for future construction projects.

Table 38 displays the results obtained for the 11 in (28 cm) section. The table shows 97.72% of the strains generated in the FRL were less than 70  $\mu\epsilon$  resulting in a fatigue life of 324 years. The 11 in (28 cm) section had the shortest fatigue life compared to the 13 in (33 cm) and 15 in (38 cm) sections. The maximum horizontal strain calculated in the FRL during the analysis was 125.59  $\mu\epsilon$ . In the base layer, the maximum horizontal strain found was 72.51  $\mu\epsilon$  and 99.94% of the strains calculated were less than 50  $\mu\epsilon$ . The table also shows 99.40% of the vertical deflections calculated at the bottom of the DGAB were less than 20 mil (508  $\mu\text{m}$ ) and the maximum deflection found was 39.27 mil (997  $\mu\text{m}$ ). Additionally, the maximum subgrade pressure discovered during the analyses was 6.82 psi (47 kPa) and all subgrade pressures calculated were less than 8 psi (55 kPa). The 11 in (28 cm) section had the highest values of subgrade deflection and pressure compared to the 13 in (33 cm) and 15 in (38 cm) sections.

**Table 38. PerRoad results for 11 in (28 cm) section.**

Pavement Response	Maximum Pavement Response	Percent Below Threshold	Years to D = 0.1
Horizontal Strain in the Base Layer	72.51 $\mu\epsilon$	99.94	474.8
Horizontal Strain in the FRL	125.59 $\mu\epsilon$	97.72	324.85
Vertical Deflection of the Subgrade	39.27 mil (997 $\mu\text{m}$ )	99.4	NA
Subgrade Pressure	6.82 psi (47.0 kPa)	100	NA

Table 39 shows the results for the 13 in (33 cm) section obtained from the PerRoad analysis and indicates the maximum horizontal strain in the FRL found during the analysis was 111.78  $\mu\epsilon$  and 99.70% of the strains were less than 70  $\mu\epsilon$ . The fatigue life corresponding to fatigue cracking occurring in the FRL was calculated to be 385 years. All of the horizontal strains calculated for the base layer were less than 50  $\mu\epsilon$  and the maximum strain obtained was 48.11  $\mu\epsilon$ , as shown in Table 39. The 13 in (33 cm) section received a maximum subgrade vertical deflection of 31.72 mil (806  $\mu\text{m}$ ) during the analysis and 99.60% of the deflections were less than 20 mil (508  $\mu\text{m}$ ). Additionally, the 13 in (33 cm) section obtained a maximum subgrade pressure of 5.28 psi (36.4 kPa) which was less than the threshold limit of 8 psi (55 kPa).

**Table 39. PerRoad results for 13 in (33 cm) section.**

Pavement Response	Maximum Pavement Response	Percent Below Threshold	Years to D = 0.1
Horizontal Strain in the Base Layer	48.11 $\mu\epsilon$	100	Infinite
Horizontal Strain in the FRL	111.78 $\mu\epsilon$	99.7	385.5
Vertical Deflection of the Subgrade	31.72 mil (806 $\mu\text{m}$ )	99.6	NA
Subgrade Pressure	5.28 psi (36.4 kPa)	100	NA

The 15 in (38 cm) section was analyzed to have the longest fatigue life. Table 40 shows the PerRoad results for the 15 in (38 cm) section. The maximum horizontal strain calculated in the FRL was 110.66  $\mu\epsilon$  and 99.60% of the strains obtained from the analysis were less than 70  $\mu\epsilon$ . The fatigue life corresponding to horizontal strain in the FRL was 402 years. Table 40 also shows that the maximum horizontal strain discovered in the base layer during the analysis was 73.32  $\mu\epsilon$  and 99.96% of the strains generated were less than 50  $\mu\epsilon$ . The PerRoad program found that 99.66% of the vertical deflections produced at the bottom of the DGAB were less than 20 mil (508  $\mu\text{m}$ ) and the maximum deflection obtained was 29.65 mil (753  $\mu\text{m}$ ). Furthermore, the maximum subgrade pressure calculated by the software was 3.87 psi (26.7 kPa) which was less than the 15 in (38 cm) sections threshold limit of 4 psi (28 kPa). The 15 in (38 cm) section received the lowest values of subgrade deflection and pressure compared to the 11 in (28 cm) and 13 in (33 cm) sections.

**Table 40. PerRoad results for 15 in (38 cm) section.**

Pavement Response	Maximum Pavement Response	Percent Below Threshold	Years to D = 0.1
Horizontal Strain in the Base Layer	73.32 $\mu\epsilon$	99.96	474.55
Horizontal Strain in the FRL	110.66 $\mu\epsilon$	99.9	402.77
Vertical Deflection of the Subgrade	29.65 mil (753 $\mu\text{m}$ )	99.66	NA
Subgrade Pressure	3.87 psi (26.7 kPa)	100	NA

## 9 Material Properties

In this chapter, the material properties of all materials used in the test sections of this project are described, with emphasis on the asphalt concrete mix properties. On each test section of DEL-23, there are four layers of asphalt (surface, intermediate, base, and FRL) placed on a dense graded aggregate base, as shown in Table 41. These layers rest on A-6 subgrade, with the top 18 in (45.72 cm) stabilized for 13 in (33 cm) section (39BS803) and 11 in (28 cm) section (39BN803), but no stabilization on the 15 in (38 cm) section (39D168).

On each test section built in the APLF, there are three layers of asphalt (surface, intermediate, and base) placed on a dense graded aggregate base, as shown in Table 44. These layers rest on 18 in (46 cm) of cement stabilized subgrade.

The bulk of this chapter discusses the properties measured for the asphalt mixes, while the properties of the base and subgrade layers are discussed in references given in the last section of this chapter.

### 9.1 DEL-23 Asphalt Concrete Material Properties

The mix design properties for both the DEL-23 sections were provided by the Shelly Company on the day each was paved. The binder properties were provided by the Ohio Department of Transportation Division of Construction Management, Office of Materials Management, Asphalt Materials Section. The following tables show the thickness (Table 41), mix design properties (Table 42), and binder properties (Table 43) for the AC layers on the DEL-23 site.

**Table 41. DEL-23 layer thicknesses**

Layer	ODOT Item	Layer Thickness for Each Section							
		39D168		39P186		39BS803		39BN803	
		(in)	(cm)	(in)	(cm)	(in)	(cm)	(in)	(cm)
Surface	424	1.00	2.54	1.00	2.54	1.00	2.54	1.00	2.54
Intermediate	442	2.00	5.08	2.00	5.08	2.00	5.08	2.00	5.08
AC Base	302	8.00	20.32	6.00	15.24	6.00	15.24	4.00	10.16
FRL	302	4.00	10.16	4.00	10.16	4.00	10.16	4.00	10.16
<b>Total AC</b>	-	<b>15.00</b>	<b>38.10</b>	<b>13.00</b>	<b>33.02</b>	<b>13.00</b>	<b>33.02</b>	<b>11.00</b>	<b>27.94</b>
Aggregate Base	304	6.00	15.24	6.00	15.24	6.00	15.24	6.00	15.24
Lime stabilized subgrade	206	NA	NA	NA	NA	18	45.72	18	45.72
Subgrade (type)	-	A-6a		A-6a		A-6a		A-6a	

Note: Cores from 39P186 indicated total AC thickness of 16 in (41 cm).

**Table 42. AC mix design and volumetrics for DEL-23 sections.**

Layer	Surface	Intermediate	AC Base	FRL
Mix (ODOT No.)	424	442	302	302-FRL
Gradation (% passing)				
2" (50.8 mm)	100	100	100	100
1 1/2" (38 mm)	100	100	99	99
1" (25.4 mm)	100	100	84	84
3/4" (19 mm)	100	95	69	69
1/2" (12.5 mm)	100	84	60	60
3/8" (9.5 mm)	99	76	54	54
#4 (4.75 mm)	87	49	33	33
#8 (2.36 mm)	56	35	22	22
#16 (1.18 mm)	37	23	15	15
#30 (0.600 mm)	25	15	10	10
#50 (0.300 mm)	9	8	8	8
#100 (0.150 mm)	5	5	6	6
#200 (0.075 mm)	3.9	3.7	3.9	3.9
Agg. Blend $G_{sb}$	2.558	2.578	2.587	2.587
$G_{mm}$	2.343	2.454	2.459	2.443
% Binder Content	7.6	4.9	4.2	4.6
% Virgin Binder	7.6	4.9	3.2	3.6
Asphalt Binder	PG 76-22M	PG 64-28	PG 64-22	PG 64-22
Design, Air Voids (%)	4	4	4	3
F/A	0.5	0.8	-	-
RAP %	0	0	20	20

**Table 43. DEL-23 binder properties.**

PG Grade	Phase Angle	Test Temperature		$G^*$	
	(degrees)	(°F)	(°C)	(Pa)	(psi)
76-22	69.0	168.8	76	1102	0.16
64-28	83.0	147.2	64	1310	0.19
64-22	86.7	147.2	64	1408	0.20

## 9.2 APLF Asphalt Concrete Material Properties

The following tables show the thickness (Table 44) and mix design properties (Table 45) for the AC layers for the Highly Modified Asphalt (HiMA) and controlled pavement sections in the APLF, as provided by Shelly Company at the time of paving. The binder properties in Table 46 for the HiMA binder were provided from the NCAT report on High Polymer Mixtures (Timm, et al., 2012); along with control binder information from ODOT's Division of Construction Management, Office of Materials Management, Asphalt Materials Section.

**Table 44. APLF test section layer thicknesses.**

Layer	ODOT Item	Layer thickness for each section							
		Lane A (HiMA)		Lane B (HiMA)		Lane C (HiMA)		Lane D (Control)	
		(in)	(cm)	(in)	(cm)	(in)	(cm)	(in)	(cm)
Surface	424	1.50	3.81	1.50	3.81	1.50	3.81	1.50	3.81
Intermediate	442	1.75	4.45	1.75	4.45	1.75	4.45	1.75	4.45
AC Base	302	4.75	12.07	5.75	14.61	6.75	17.15	7.75	19.69
<b>Total AC</b>	-	<b>8.00</b>	<b>20.33</b>	<b>9.00</b>	<b>22.87</b>	<b>10.00</b>	<b>25.41</b>	<b>11.00</b>	<b>27.95</b>
Aggregate Base	304	6.00	15.24	6.00	15.24	6.00	15.24	6.00	15.24
Cement stabilized subgrade	206	18.00	45.72	18.00	45.72	18.00	45.72	18.00	45.72
Subgrade (type)	-	A-6/A-7		A-6/A-7		A-6/A-7		A-6/A-7	

**Table 45. AC Mix Design and Volumetrics for HiMA and control materials in APLF.**

Layer	Surface	Intermediate	AC Base-Kraton	AC Base-Control
Mix (ODOT No.)	442	442	302	302
Gradation (% passing)				
2" (50.8 mm)	100	100	100	100
1 1/2" (38 mm)	100	100	100	100
1" (25.4 mm)	100	100	87	87
3/4" (19 mm)	100	96	78	78
1/2" (12.5 mm)	100	80	68	68
3/8" (9.5 mm)	93	69	58	58
#4 (4.75 mm)	57	48	39	39
#8 (2.36 mm)	38	35	28	28
#16 (1.18 mm)	27	26	22	22
#30 (0.600 mm)	19	18	16	16
#50 (0.300 mm)	11	11	9	9
#100 (0.150 mm)	7	7	6	6
#200 (0.075 mm)	4.8	4.9	4.3	4.3
Agg. Blend $G_{sb}$	2.393	2.636	2.646	2.646
$G_{mm}$	2.440	2.496	2.480	2.485
% Binder Content	5.7	4.4	4.4	4.3
% Virgin Binder	5	3.2	2.7	2.5
Asphalt Binder	PG 88-22M	PG 88-22	PG 88-22	PG 64-22
Design, Air Voids (%)	3.5	4	4	4
F/A	0.8	1.1	-	-
RAP %	15	25	35	35

**Table 46. APLF test section binder properties.**

PG Grade	Phase Angle	Test Temperature		G*	
	(degrees)	(°F)	(°C)	(Pa)	(psi)
88-22 (HiMA) (Timm et al., 2012)	48.9	212.0	100	800	0.12
64-22 (Control)	86.7	147.2	64	1408	0.20

### 9.3 Dynamic Modulus of AC Materials

To determine the frequency and temperature dependent viscoelastic material properties of the asphalt concrete materials used in this project, master curves were computed using laboratory data. Dynamic modulus tests of AC specimens were performed in accordance to AASHTO TP 62. Specimens were compacted during paving at the asphalt plant using the Superpave Gyratory Compactor (SGC) in accordance with AASHTO T312. Specimens were compacted to a thickness of 165 mm (6.5 in) and a 150 mm (5.91 in) diameter with a 7% target air void. The specimens were then cut and cored to meet size requirements for AASHTO TP 62; specimens were 100 mm (3.94 in) diameter and 150 mm (5.91 in) thickness.

Each specimen was tested using the Asphalt Mixture Performance Tester (AMPT, also known as the simple performance test) for dynamic modulus at the following temperatures in order 4.4 °C (40 °F), 21.1 °C (70 °F), 37.8 °C (100 °F), and 54.4 °C (130 °F). For each test temperature, the dynamic modulus was calculated using various loading frequencies that included: 25 Hz, 10 Hz, 5 Hz, 1 Hz, 0.5 Hz, and 0.1 Hz in that order. The dynamic modulus can be determined by the following equation:

$$|E^*| = \sigma_0 / \varepsilon_0$$

Where:

$|E^*|$  = Dynamic modulus

$\sigma_0$  = Average peak stress over the last five periods

$\varepsilon_0$  = Average peak strain over the last five periods

The results of the dynamic modulus tests for the 424 surface mix, 442 intermediate mix, 302 Asphalt Concrete (AC) Base mix, and the 302 Fatigue Resistance Layer (FRL) mix of the DEL-23 pavements are shown in Table 47 through Table 50.

**Table 47. Average dynamic modulus of the 424 Surface Layer on DEL 23**

Temperature	Frequency	Dynamic Modulus	
	(Hz)	(ksi)	(MPa)
40 °F (4.4 °C)	25	1973	13602
	10	1810	12477
	5	1665	11481
	1	1347	9290
	0.5	1217	8389
	0.1	896	6178
70 °F (21.1 °C)	25	1101	7593
	10	927	6394
	5	798	5501
	1	540	3722
	0.5	451	3108
	0.1	284	1960
100 °F (37.8 °C)	25	405	2790
	10	305	2105
	5	248	1708
	1	149	1027
	0.5	125	859
	0.1	80	551
130 °F (54.4 °C)	25	179	1232
	10	132	909
	5	115	793
	1	83	572
	0.5	76	523
	0.1	63	436



**Table 48. Average dynamic modulus of the 442 intermediate layer on DEL 23.**

Temperature	Frequency	Dynamic Modulus	
	(Hz)	(ksi)	(MPa)
40 °F (4.4 °C)	25	2433	16778
	10	2363	16295
	5	2295	15822
	1	2069	14267
	0.5	1939	13367
	0.1	1556	10727
70 °F (21.1 °C)	25	1716	11830
	10	1475	10171
	5	1279	8817
	1	824	5683
	0.5	652	4492
	0.1	349	2403
100 °F (37.8 °C)	25	690	4758
	10	491	3388
	5	373	2569
	1	193	1330
	0.5	148	1017
	0.1	87	597
130 °F (54.4 °C)	25	248	1710
	10	172	1184
	5	132	913
	1	80	550
	0.5	67	463
	0.1	50	344

**Table 49. Average dynamic modulus of the 302 AC base layer on DEL 23.**

Temperature	Frequency	Dynamic Modulus	
	(Hz)	(ksi)	(MPa)
40 °F (4.4 °C)	25	2769	19089
	10	2621	18074
	5	2500	17234
	1	2184	15060
	0.5	2037	14042
	0.1	1676	11554
70 °F (21.1 °C)	25	1776	12242
	10	1566	10800
	5	1408	9711
	1	1057	7289
	0.5	918	6329
	0.1	635	4379
100 °F (37.8 °C)	25	889	6133
	10	724	4991
	5	612	4222
	1	401	2767
	0.5	331	2280
	0.1	208	1432
130 °F (54.4 °C)	25	422	2909
	10	327	2254
	5	268	1848
	1	168	1156
	0.5	137	945
	0.1	87	602

**Table 50. Average dynamic modulus of the 302 FRL on DEL 23.**

Temperature	Frequency	Dynamic Modulus	
	(Hz)	(ksi)	(MPa)
40 °F (4.4 °C)	25	2610	17995
	10	2495	17200
	5	2395	16511
	1	2119	14609
	0.5	1982	13662
	0.1	1628	11226
70 °F (21.1 °C)	25	1745	12030
	10	1534	10576
	5	1370	9448
	1	998	6878
	0.5	849	5850
	0.1	550	3794
100 °F (37.8 °C)	25	833	5744
	10	656	4521
	5	538	3711
	1	325	2243
	0.5	258	1781
	0.1	150	1032
130 °F (54.4 °C)	25	354	2438
	10	261	1801
	5	207	1424
	1	120	828
	0.5	96	661
	0.1	59	408

The results of the dynamic modulus tests for the 442 surface mix, 442 intermediate mix, 302 AC base mix (with Kraton binder), and the 302 AC base mix (control binder) used in the HiMA study in the APLF are shown in Table 51 through Table 54.

**Table 51. Average dynamic modulus of the 442 surface layer HiMA.**

Temperature	Frequency	Dynamic Modulus	
	(Hz)	(ksi)	(MPa)
40 °F (4.4 °C)	25	2079	14336
	10	1937	13358
	5	1816	12520
	1	1547	10669
	0.5	1424	9816
	0.1	1160	7998
70 °F (21.1 °C)	25	1116	7697
	10	976	6732
	5	872	6010
	1	653	4504
	0.5	576	3971
	0.1	411	2834
100 °F (37.8 °C)	25	535	3690
	10	440	3033
	5	377	2602
	1	252	1739
	0.5	218	1503
	0.1	142	980
130 °F (54.4 °C)	25	281	1935
	10	223	1537
	5	191	1318
	1	129	893
	0.5	113	780
	0.1	83	571

**Table 52. Average dynamic modulus of the 442 intermediate layer HiMA.**

Temperature	Frequency	Dynamic Modulus	
	(Hz)	(ksi)	(MPa)
40 °F (4.4 °C)	25	2216	15278
	10	2073	14291
	5	1953	13466
	1	1665	11478
	0.5	1534	10576
	0.1	1243	8570
70 °F (21.1 °C)	25	1304	8994
	10	1145	7897
	5	1022	7049
	1	765	5276
	0.5	668	4606
	0.1	468	3228
100 °F (37.8 °C)	25	624	4303
	10	507	3494
	5	428	2951
	1	278	1914
	0.5	233	1604
	0.1	151	1040
130 °F (54.4 °C)	25	257	1773
	10	193	1332
	5	161	1110
	1	105	721
	0.5	90	620
	0.1	66	453

**Table 53. Average dynamic modulus of the 302 AC base HiMA with Kraton polymer.**

Temperature	Frequency	Dynamic Modulus	
	(Hz)	(ksi)	(MPa)
40 °F (4.4 °C)	25	2925	20167
	10	2769	19089
	5	2627	18112
	1	2291	15796
	0.5	2132	14702
	0.1	1775	12239
70 °F (21.1 °C)	25	1737	11975
	10	1552	10702
	5	1400	9652
	1	1070	7379
	0.5	944	6507
	0.1	670	4622
100 °F (37.8 °C)	25	882	6078
	10	733	5056
	5	628	4327
	1	416	2870
	0.5	357	2462
	0.1	238	1639
130 °F (54.4 °C)	25	377	2596
	10	290	1997
	5	248	1706
	1	162	1119
	0.5	131	906
	0.1	103	708

**Table 54. Average dynamic modulus of the 302 AC base with no polymer for control section in APLF.**

Temperature	Frequency	Dynamic Modulus	
	(Hz)	(ksi)	(MPa)
40 °F (4.4 °C)	25	2879	19850
	10	2729	18816
	5	2581	17797
	1	2250	15514
	0.5	2089	14406
	0.1	1727	11906
70 °F (21.1 °C)	25	1710	11792
	10	1515	10445
	5	1364	9406
	1	1028	7087
	0.5	895	6170
	0.1	628	4330
100 °F (37.8 °C)	25	833	5746
	10	677	4669
	5	569	3921
	1	358	2465
	0.5	295	2031
	0.1	184	1271
130 °F (54.4 °C)	25	294	2024
	10	211	1453
	5	171	1176
	1	105	727
	0.5	88	606
	0.1	64	439

A shift factor must be determined in order to build a master curve. The shift factor  $a(T)$ , is calculated by finding the best-fit second-order polynomial when plotting the shift factor against the test temperature. The following equation describes this relationship:

$$\log a(T) = C_1 + C_2 * T + C_3 * T^2$$

Where:

$a(T)$  = Shift Factor  
 $T$  = Test Temperature  
 $C_i$  = regression coefficients

The dynamic modulus is determined at various temperatures and is plotted against frequency. The data is then shifted to a reference temperature (21.1°C (70°F)) to form the master curve for the mix. This parallel shift is performed by determining the reduced frequency for each test frequency and temperature based on the reference temperature. The following equation is used to determine the reduced frequency:

$$\log f_r = \log f + \log a(T)$$

Where:

$f_r$  = Reduced Frequency at the Reference Temperature (Hz)  
 $f$  = Actual Test Frequency at the Test Temperature (Hz)

The AASHTO Mechanistic Empirical Pavement Design Guide (MEPDG) uses the following sigmoidal model to estimate the dynamic modulus of an asphalt mix for curve fitting purposes:

$$\log |E^*| = \delta + \frac{\alpha}{1 + e^{\beta + \gamma(\log f_r)}}$$

Where

$|E^*|$  = Dynamic Modulus ( $10^6$  psi)  
 $\alpha, \beta, \gamma, \delta$  are fitting parameters:  
 $\delta$  is the minimum value of  $E^*$  ( $10^6$  psi);  
 $\alpha + \delta$  is the maximum value of  $E^*$  ( $10^6$  psi);  
and  $\beta$  and  $\gamma$  are dimensionless parameters describing the shape of the sigmoidal function

By using the Solver feature in Microsoft Excel, the laboratory-calculated dynamic modulus can be compared to the dynamic modulus estimated using the sigmoidal equation and minimizing the sum of the square of the Error, defined as follows:

$$Error^2 = \left[ \frac{E_{Lab}^* - E_{Sigmoidal}^*}{E_{Lab}^*} \right]^2$$

The Error is calculated for each frequency and temperature and then summed for the entire data set ( $\Sigma Error^2$ ). In Solver, the objective cell is the  $\Sigma Error^2$ ; it is set to become as low as possible (min) by changing  $\delta, \alpha, \beta, \gamma, C_1, C_2,$  and  $C_3$  using an iteration method. The following

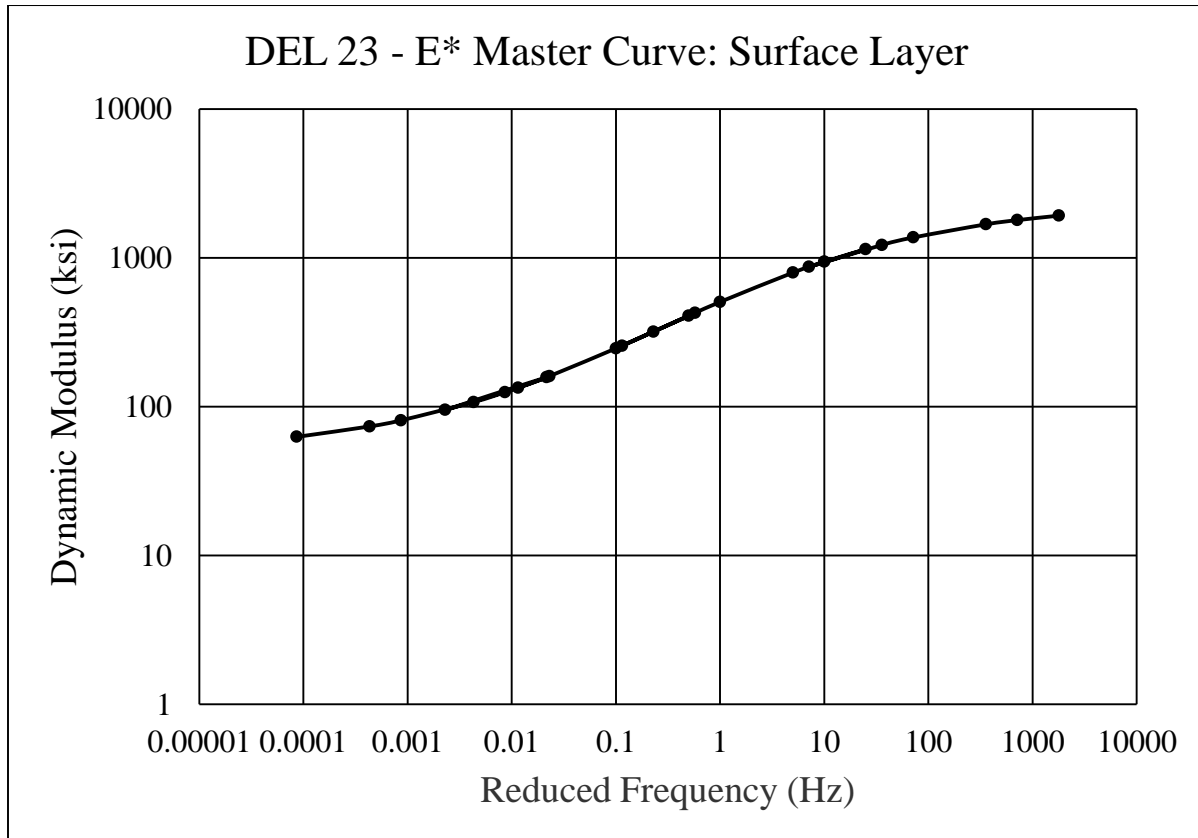


table is a summary of the curve fitting parameters and regression coefficients solved in Solver for each layer and site.

**Table 55. Curve fitting parameters and regression coefficients for each AC layer.**

Site	Layer	$\delta$	$\alpha$	$\beta$	$\gamma$	$C_1$	$C_2$	$C_3$
DEL 23	Surface	0.376	-1.694	0.418	0.747	4.662	-0.075	0.00012
	Intermediate	0.634	-2.049	0.603	0.626	4.171	-0.060	0.00001
	AC Base	0.626	-6.030	2.211	0.296	7.363	-0.131	0.00037
	FRL	0.546	-2.054	1.036	0.555	4.788	-0.074	0.00008
HiMA APLF	Surface	0.485	-2.250	0.859	0.421	6.712	-0.120	0.00034
	Intermediate	0.495	-2.341	1.049	0.452	5.451	-0.089	0.00016
	AB Base (Kraton)	0.631	-2.431	1.131	0.411	5.700	-0.093	0.00017
	AB Base (Control)	0.605	-2.648	1.269	0.438	5.315	-0.083	0.00011

The dynamic modulus master curves as a function of reduced frequency and shift factors as a function of temperature are given below for the 424 surface mix, 442 intermediate mix, 302 Asphalt Concrete (AC) base mix, and the 302 Fatigue Resistant Layer (FRL) mix of the Delaware 23 sections in Figure 40 through Figure 47.



**Figure 40. Dynamic modulus master curve for 424 surface layer on DEL 23.**

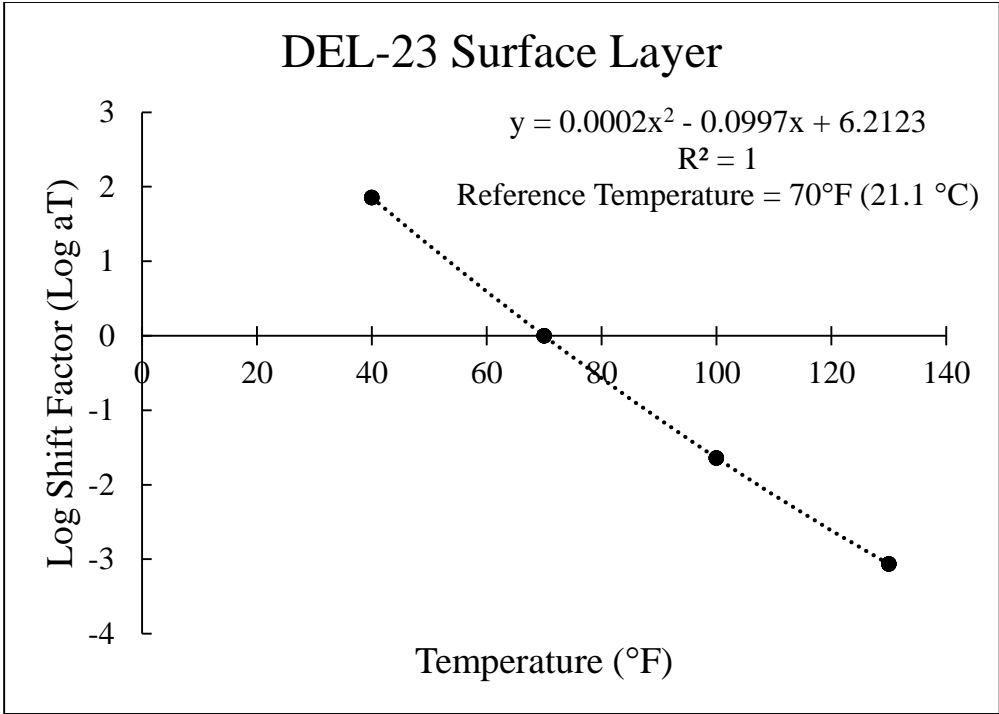


Figure 41. Shift factor vs. temperature for 424 surface layer on DEL 23.

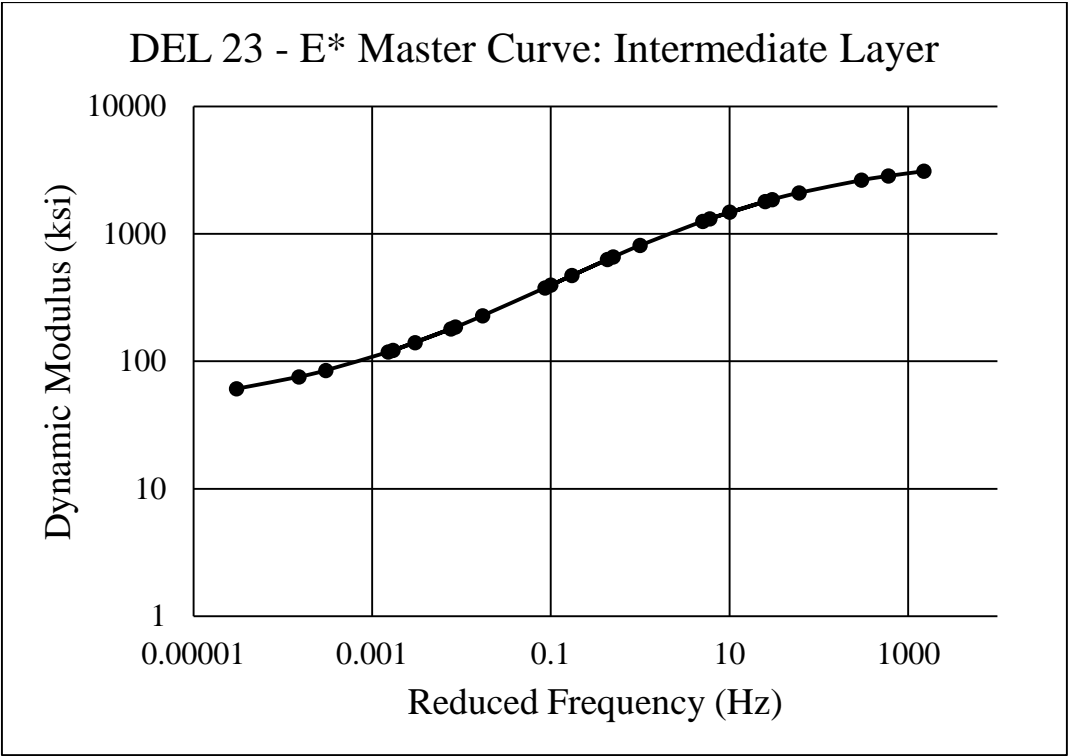
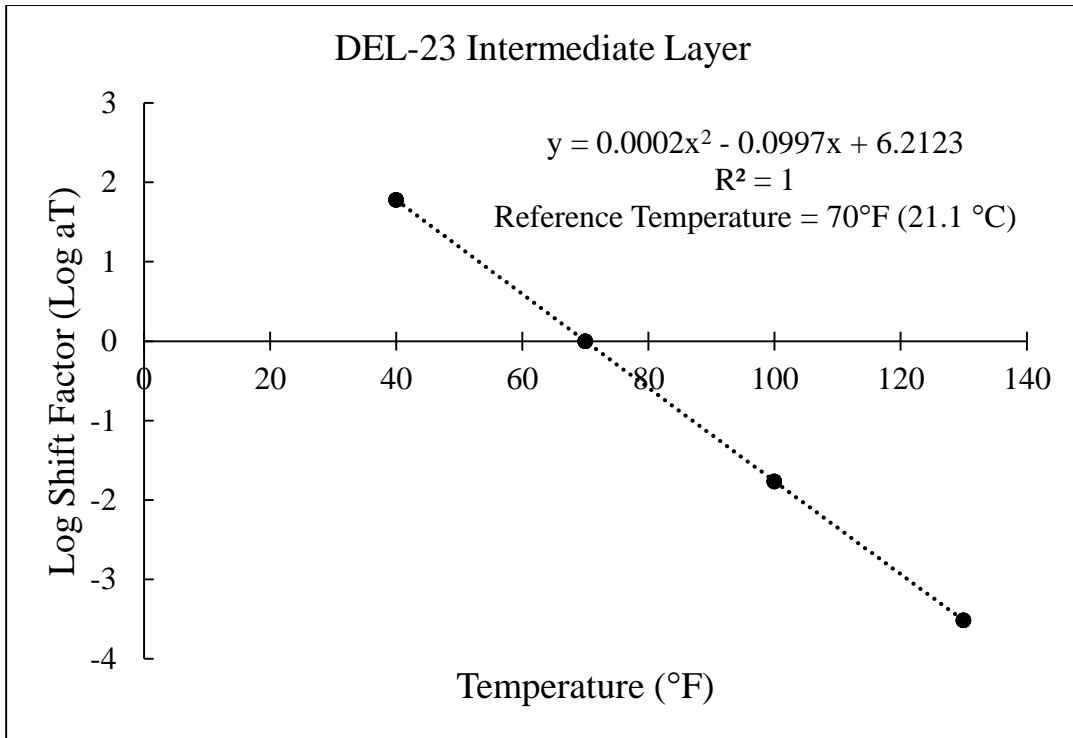
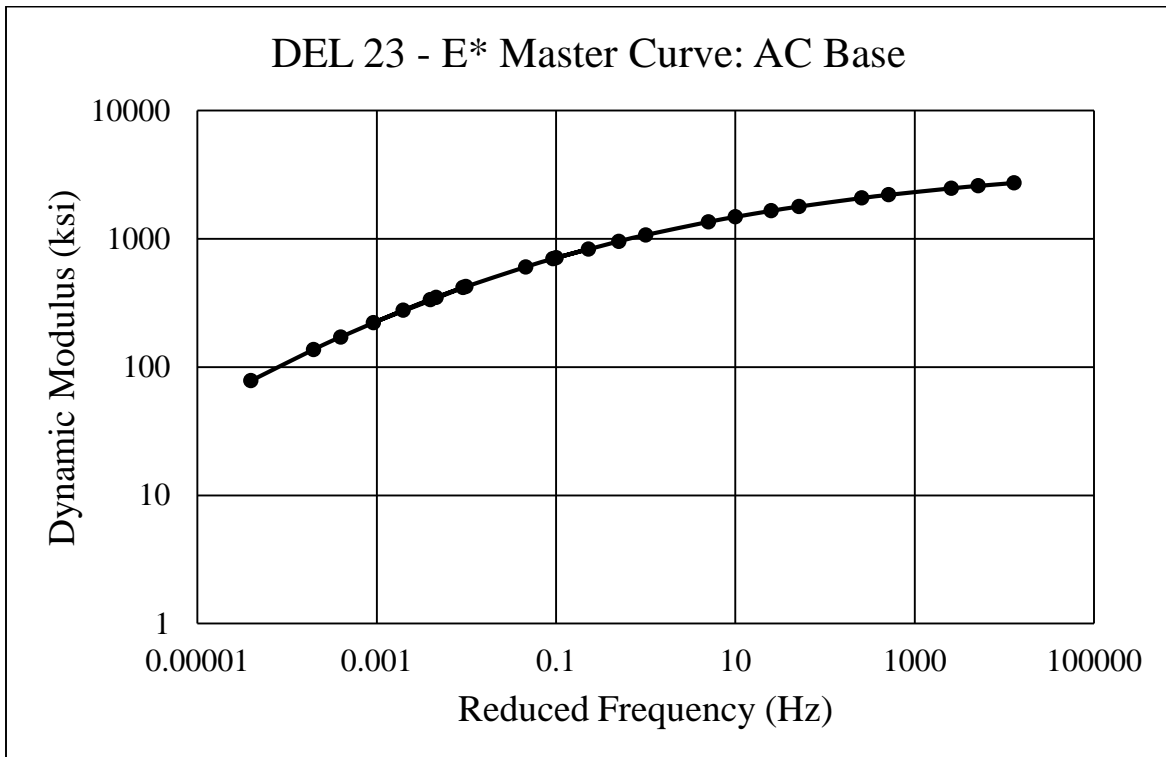


Figure 42. Dynamic modulus master curve for 442 intermediate layer on DEL 23.



**Figure 43. Shift factor vs. temperature for 442 intermediate layer on DEL 23.**



**Figure 44. Dynamic modulus master curve for 302 AC base layer on DEL 23.**

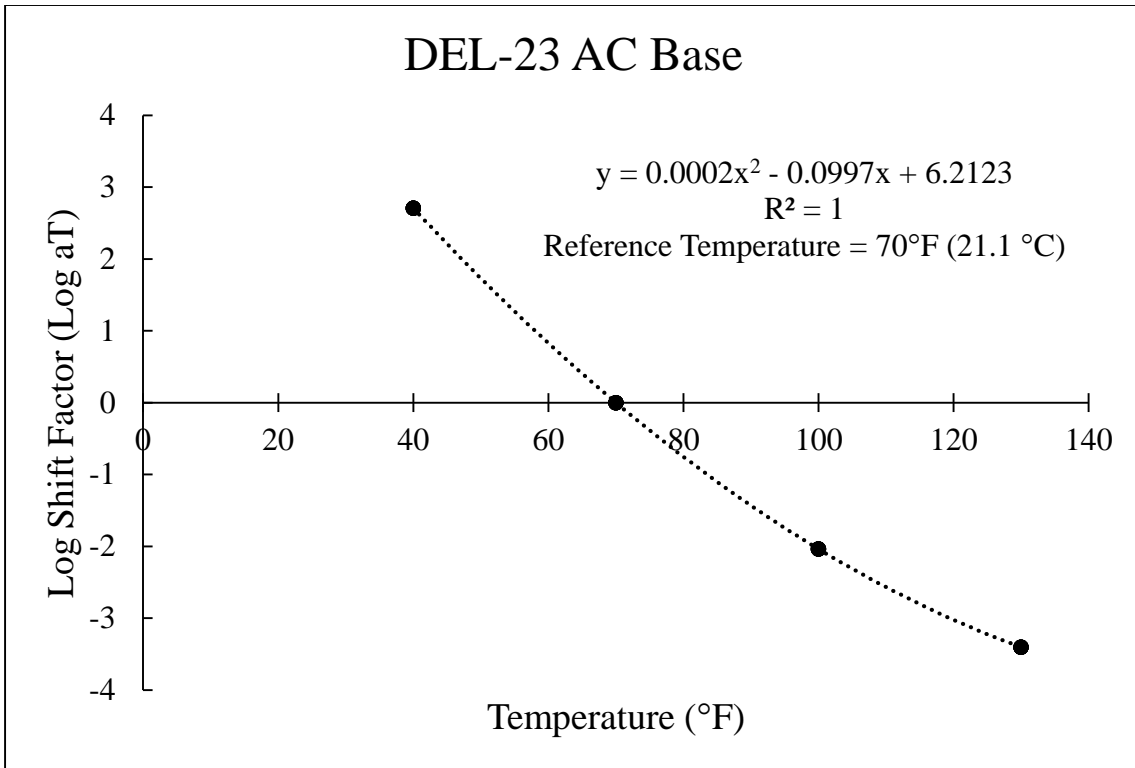


Figure 45. Shift factor vs. temperature for 302 AC base layer on DEL 23.

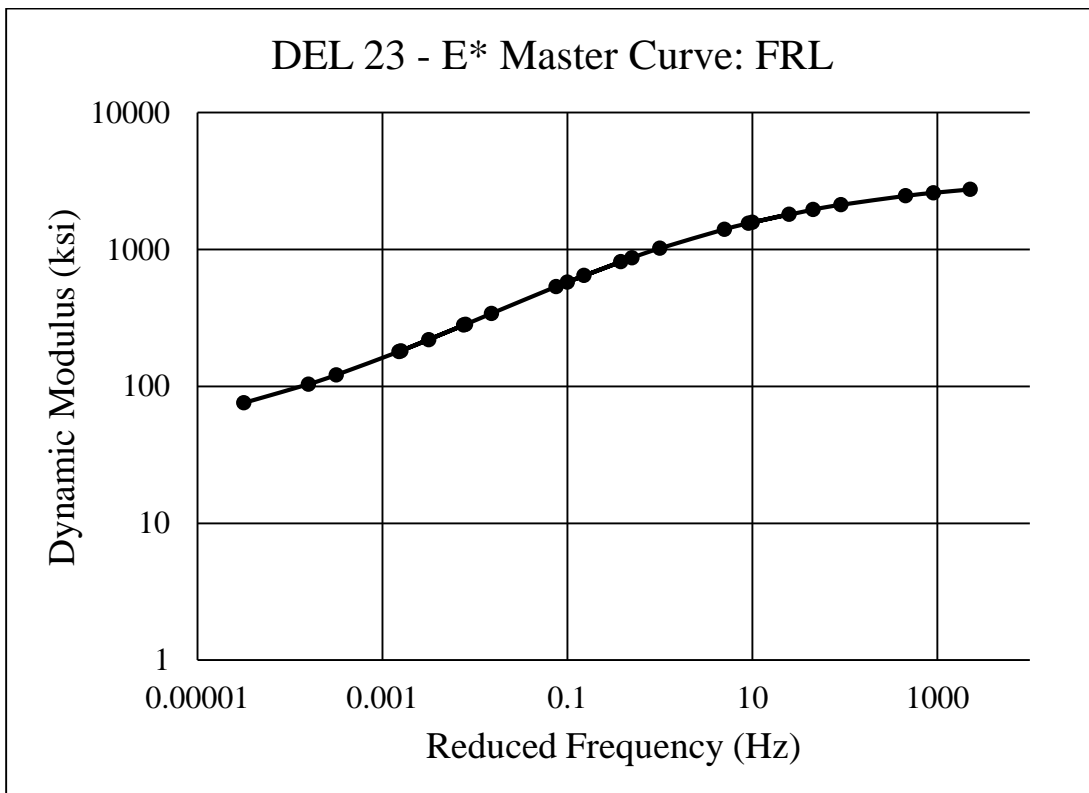
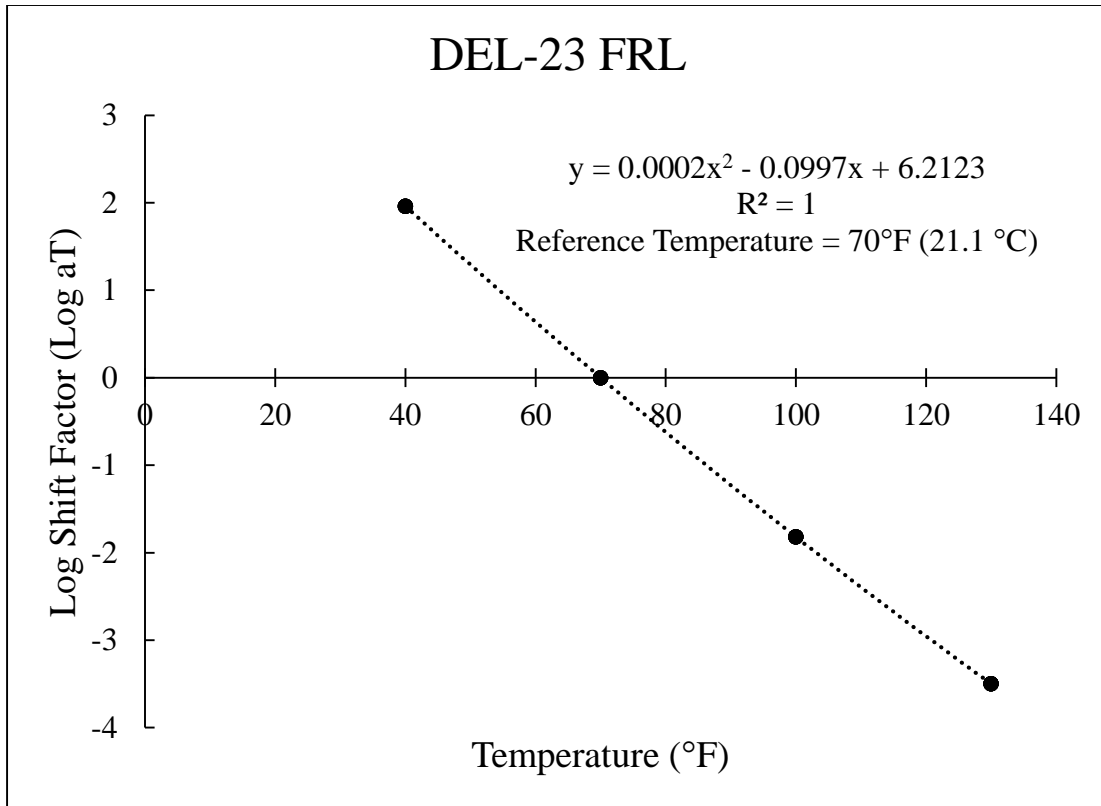


Figure 46. Dynamic modulus master curve for 302 FRL on DEL 23.



**Figure 47. Shift factor vs. temperature for 302 FRL on DEL 23.**

The dynamic modulus master curves as a function of reduced frequency and shift factors as a function of temperature are given below for the 442 surface mix, 442 intermediate mix, 302 AC base mix (with Kraton binder), and the 302 AC base mix (control binder) for the HiMA study in the APLF in Figure 48 through Figure 55.

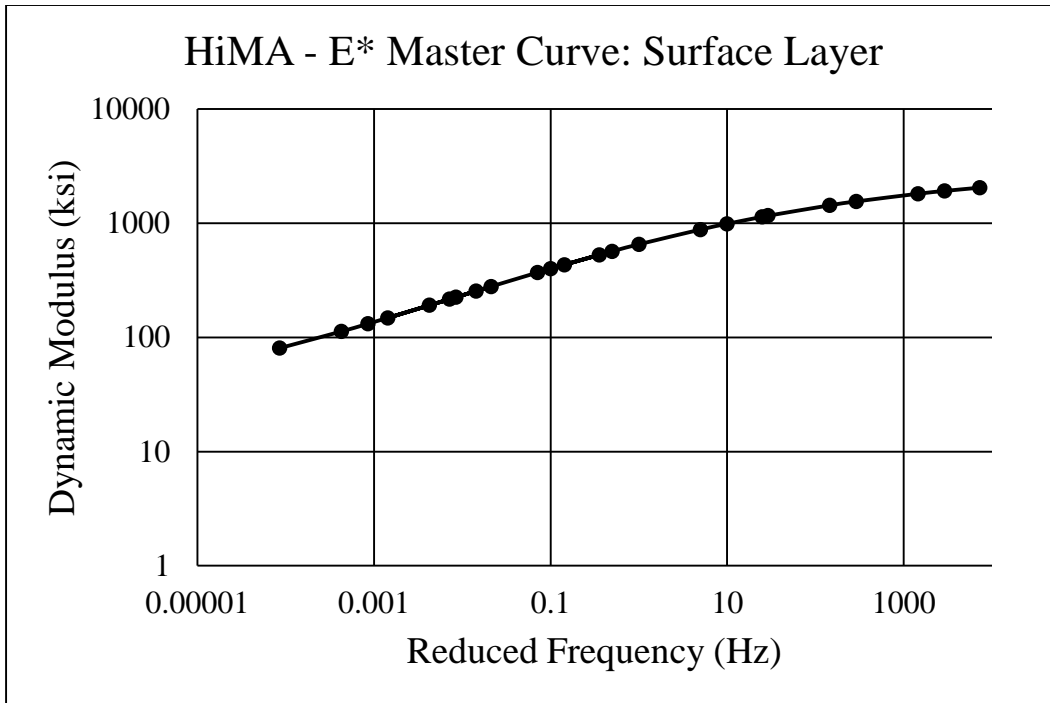


Figure 48. Dynamic modulus master curve for 442 HiMA surface layer in APLF.

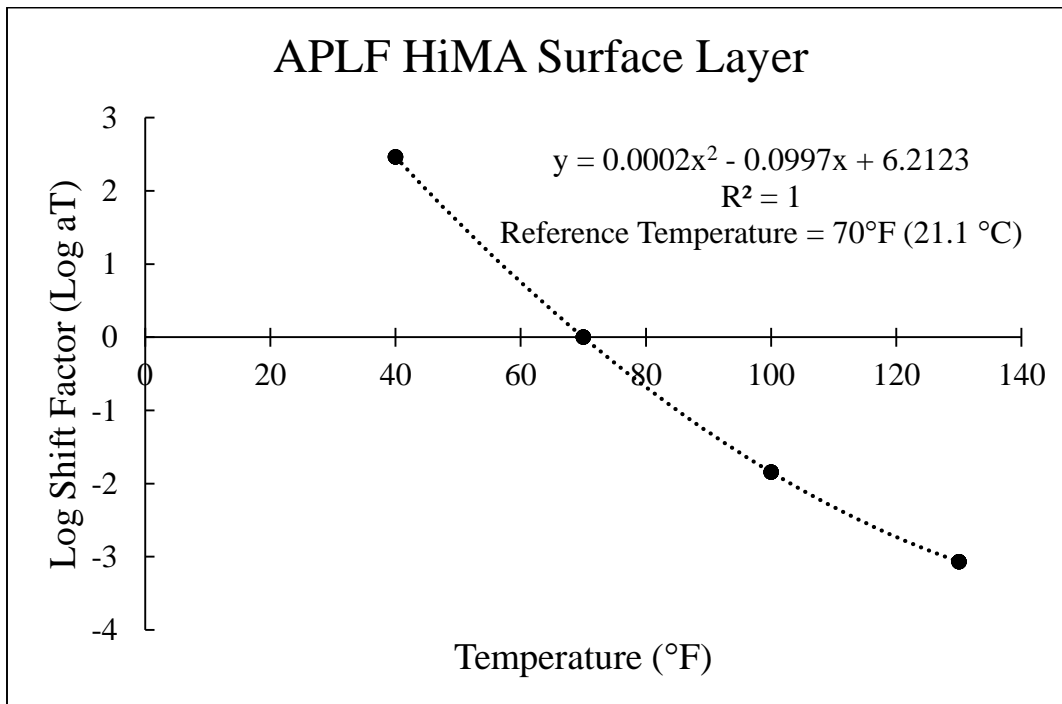


Figure 49. Shift factor vs. temperature for 442 HiMA surface layer in APLF.

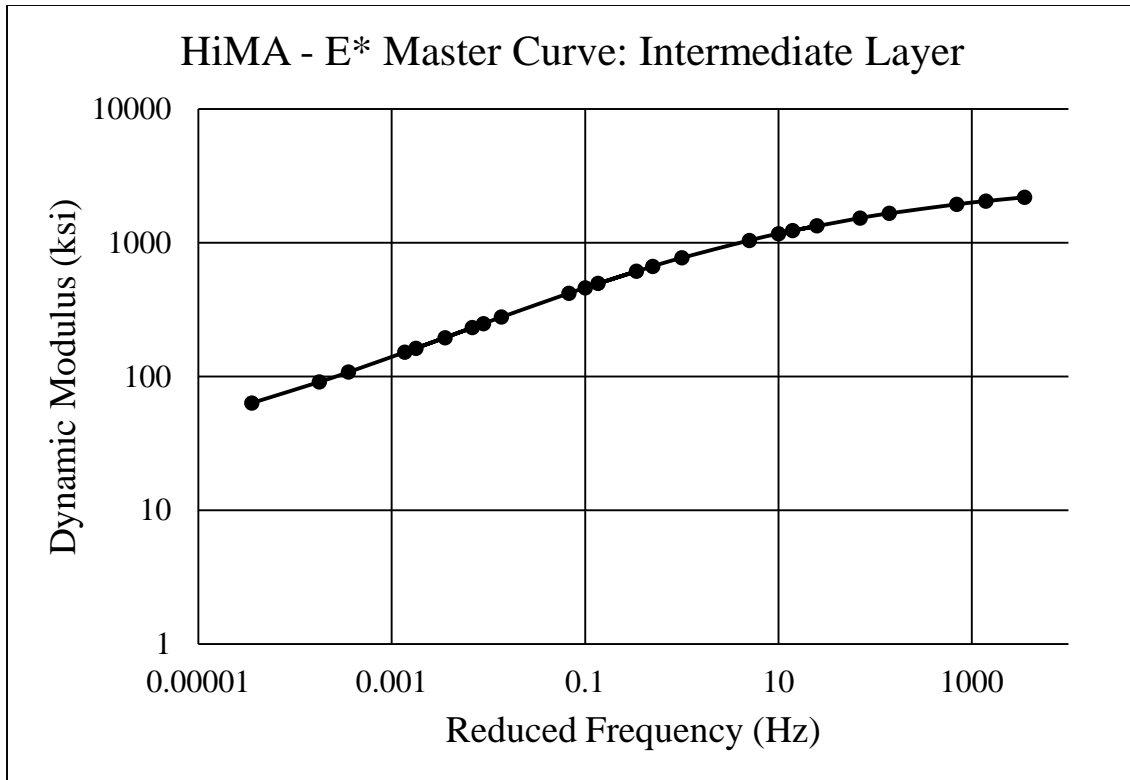


Figure 50. Dynamic modulus master curve for 442 HiMA intermediate layer in APLF.

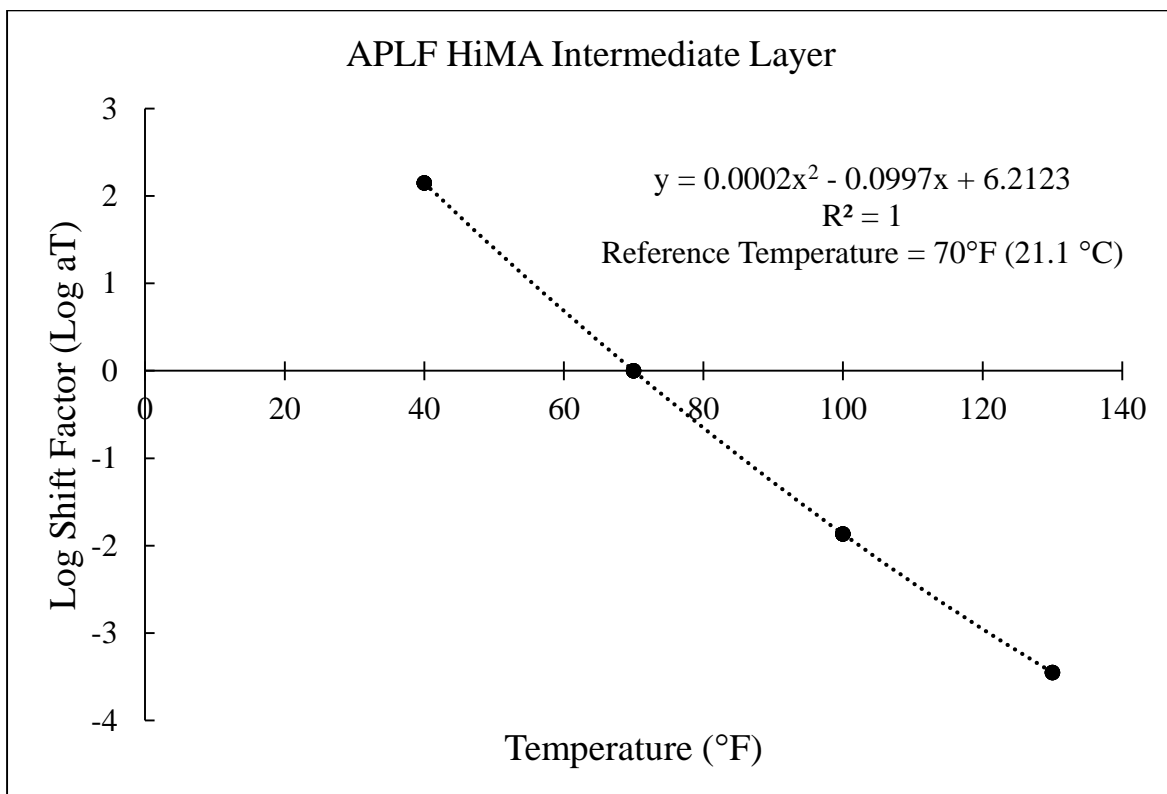


Figure 51. Shift factor vs. temperature for 442 HiMA intermediate layer in APLF.

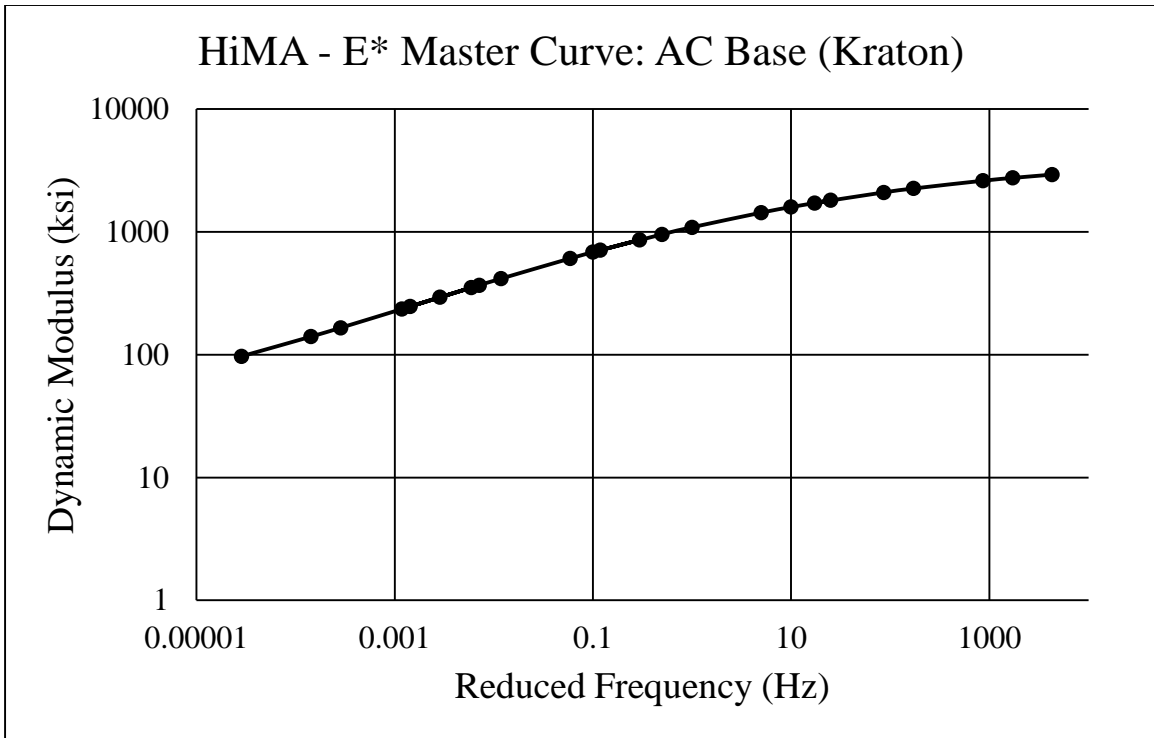


Figure 52. Dynamic modulus master curve for 302 HiMA AC base with Kraton polymer in APLF.

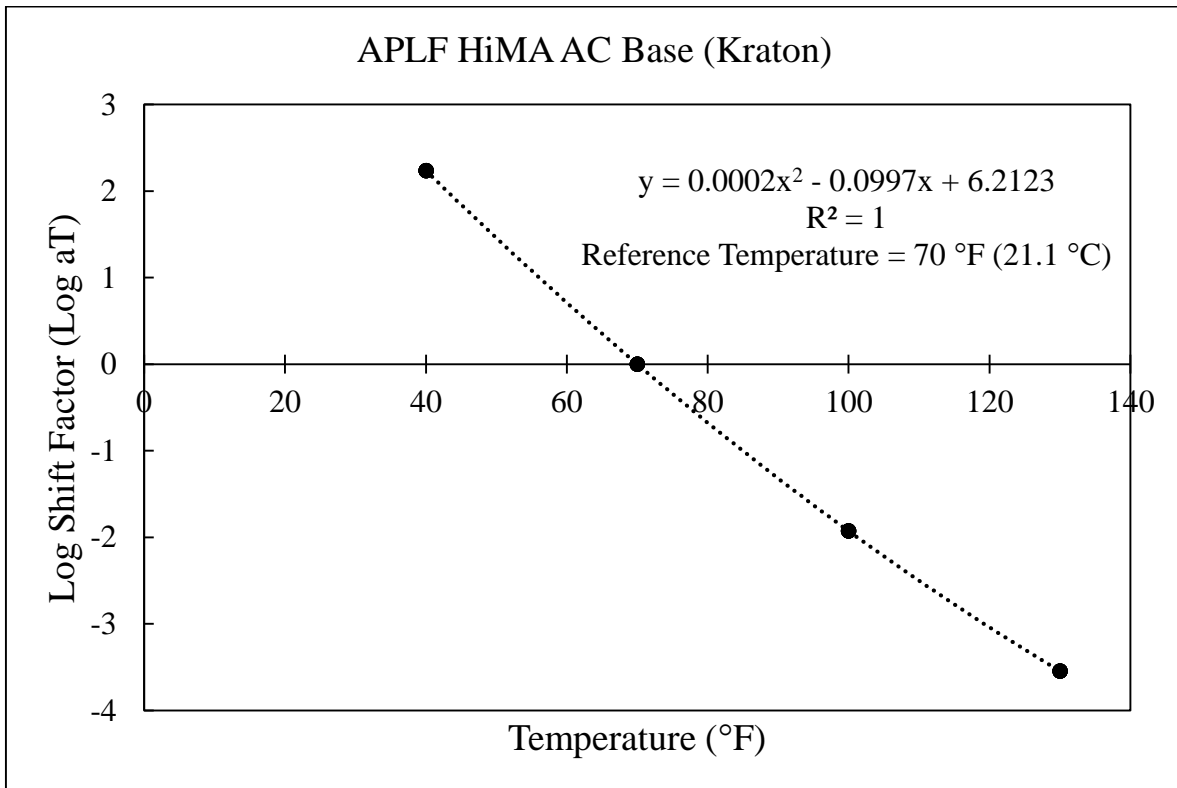


Figure 53. Shift factor vs. temperature for 302 HiMA AC base with Kraton polymer in APLF.



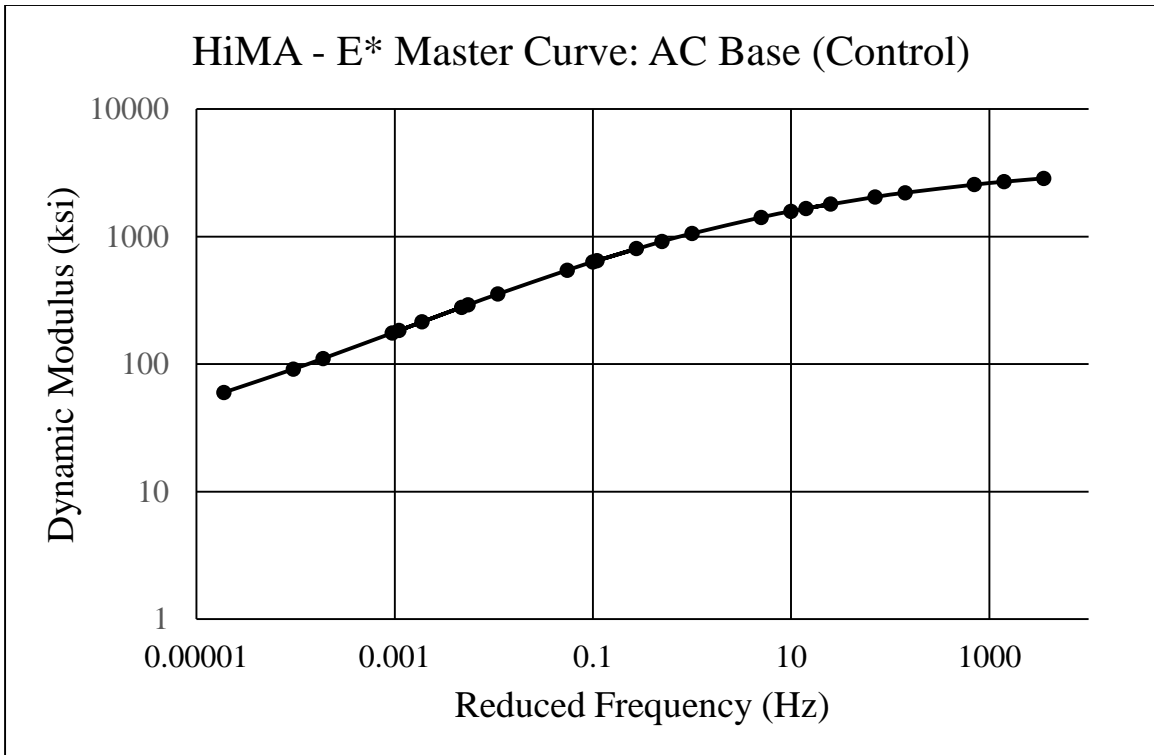


Figure 54. Dynamic modulus master curve for 302 AC base with control binder in APLF.

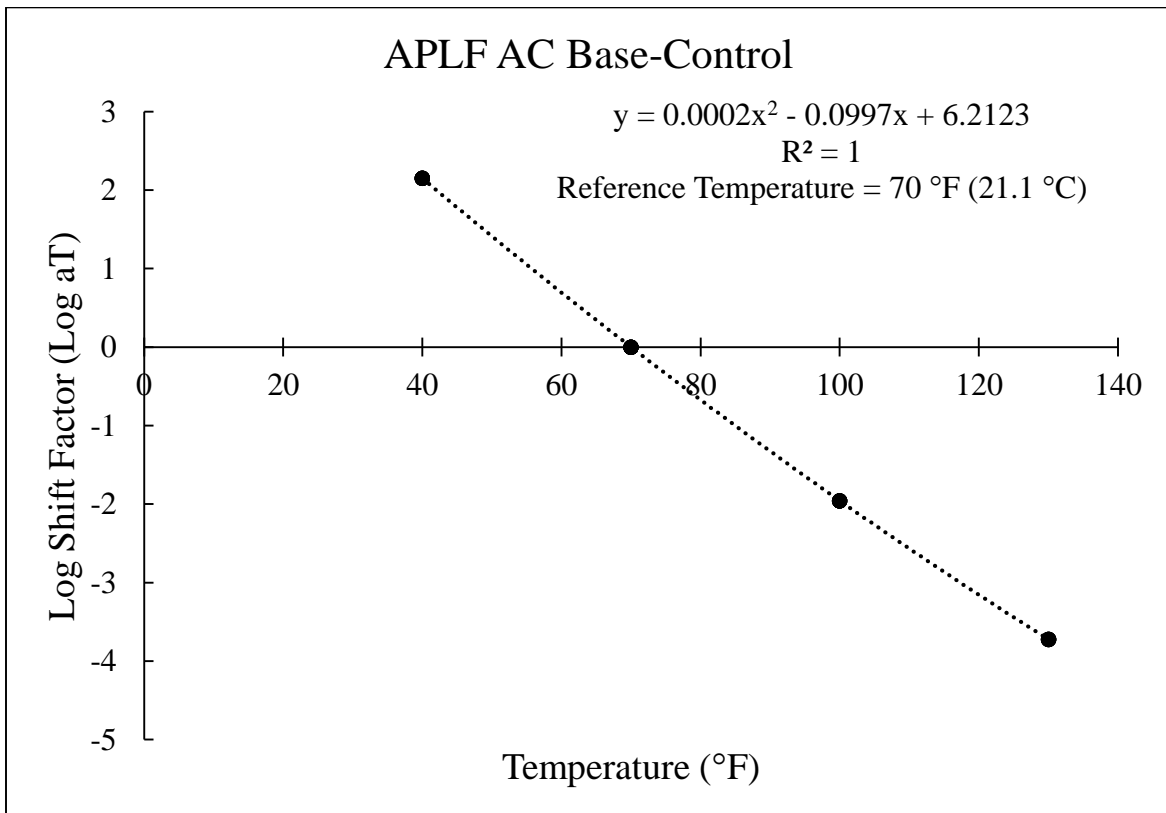


Figure 55. Shift factor vs. temperature for 302 AC base with control binder in APLF.

#### **9.4 Aggregate Base and Subgrade Properties**

The base and subgrade material properties for the DEL-23 and APLF sections were listed in previous reports to ODOT. Further information pertaining to the material properties of the compacted subgrade and ODOT 304 material properties, please refer to the report by Teruhisa Masada, Shad M. Sargand, Basel Abdalla and J. Ludwig Figueroa, *Materials Properties for Implementation of Mechanistic-Empirical (M-E) Pavement Design Procedures*, (Masada, et al., 2004), and in Shad M. Sargand and J. Ludwig Figueroa, *Monitoring And Modeling Of Pavement Response And Performance Task A: Ohio*, (Sargand and Figueroa, 2010).

Material properties for stabilized subgrade and ODOT 304 material above it, are discussed in the following report by Shad Sargand, Issam Khoury, Jayson Gray, and Anwer Al-Jhayyish: *Incorporating Chemical Stabilization of the Subgrade in Pavement Design and Construction Practices* (Sargand et al, 2014).

## 10 Evaluation of Highly Modified Asphalt

Highly Modified Asphalt (HiMA) utilizes a new modified binder created by Kraton Polymers that contains a 7.5% styrene butadiene styrene (SBS) polymer to improve stiffness at high temperatures. HiMA mixture has also been investigated at the National Center for Asphalt Technology (NCAT) test track near Auburn, Alabama. Based on the promise shown in the NCAT evaluations, an experiment was proposed at the Accelerated Pavement Load Facility (APLF) to determine if HiMA's improved stiffness would allow for a thinner perpetual pavement design. The four test sections at the APLF range in thicknesses between 8 in (20 cm) to 11 in (28 cm) in 1 in (2.54 cm) increments to determine where the pavement transitions from standard to perpetual response, with the 11 in (28 cm) pavement built as a control to match the depth of the thinnest DEL-23 section. The build-ups for each lane are given in Table 44 above.

### 10.1 The Accelerated Pavement Load Facility

The Accelerated Pavement Loading Facility (APLF), located in Lancaster Ohio, consists of a concrete lined rectangular pit 45 feet (13.7 m) long by 38 feet (11.6 m) wide by 8 feet (2.5 m) deep. The facility has two large sliding doors on the north and south end of the facility which allow large construction vehicles to enter and exit freely, a feature which makes the APLF unique. As an indoor facility, tests may be performed at any time in the year. The facility also houses industrial grade heating and cooling units to test and maintain pavements at desired temperatures, which can be anywhere in the range of 10°F (-12.2°C) to 130°F (54.4°C). Dynamic and static wheel testing can be accomplished by either a dual or single wide-based tires. The wheel is mounted onto a track system that is supported by two I-beams. The mounted wheel support feature allows for the ability to maintain a desired wheel load and pressure on a precise location for repeated loadings on a test pavement. The APLF is capable of a wheel load of up to 30,000 lb (133 kN) with the option of wheel offsetting to measure wander effects. A dynamic loading test inside the APLF can be seen below in Figure 56.



Figure 56. Load wheel passing over test pavement in the APLF.

## 10.2 Instrumentation of pavements in the APLF

In an agreement with the Ohio Department of Transportation (ODOT), it was decided to use an instrumentation plan similar to those employed in prior perpetual pavement studies (e.g. Sargand, Figueroa, Edwards, and Al-Rawashdeh, 2009); therefore, strain gages, thermocouples, and linear variable differential transformers (LVDT) were chosen to measure the dynamic load responses of the highly modified asphalt pavement and the subgrade within the APLF. Strain gages were installed to measure the horizontal strains at the base of the fatigue and the intermediate layers. Thermocouples were installed throughout the entire depth of the pavement in each test sections to monitor the internal temperatures during testing. The LVDTs were used to observe the vertical deflections of the subgrade and the asphalt pavement structure while dynamic wheel loading occurred. Upon completing gage selection, an AutoCAD document was created for use as a reference during construction. An example of the instrumentation for test lane A can be seen below in Figure 57.

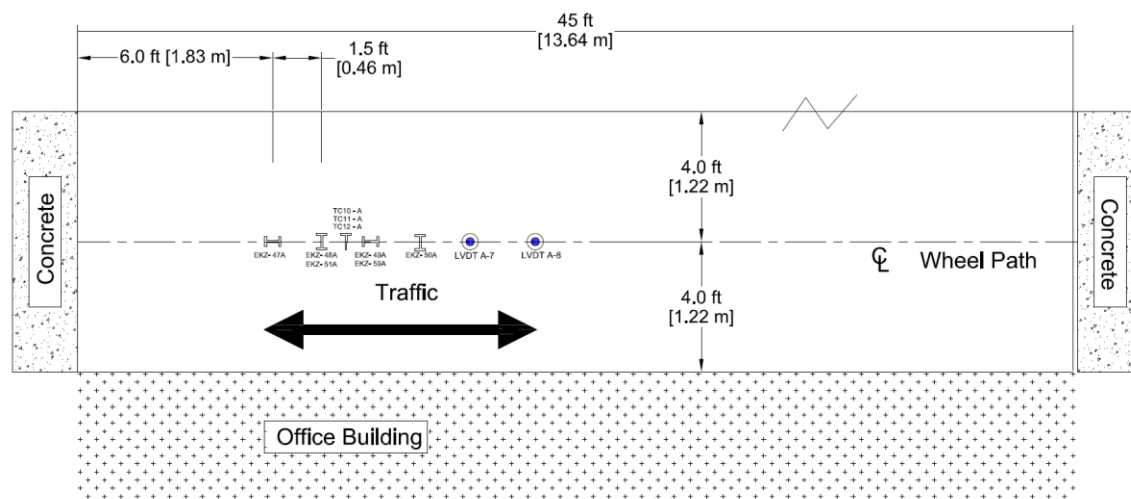


Figure 57. Gage layout in APLF test lane A, which is similar to the other lanes.

Before gages were installed in the APLF, a 6 in (15.2 cm) layer of crushed 304 aggregate base was placed, leveled, and compacted on top of the existing subgrade, which was stabilized with cement to a depth of 18 in (46 cm). Following compaction, the grid layout designed using AutoCAD was implemented inside the APLF.

Four test lanes were measured to size and the centerlines were marked with spray paint. From previous research studies performed in the APLF, it was decided the first strain gage in the bottom of the fatigue layer would be placed along the centerline of each test section 6 ft (1.8 m) from the concrete platform on the south end of the facility. At this distance the initial balancing of the loads prior to the motion of the wheel would have dissipated enough to eliminate the possibility of false readings from the initial load of the wheel.

### 10.2.1 Strain Gage Installation

A total of 24 KM-100HAS strain gages (6 per lane) were selected to measure horizontal pavement strains. The KM-100HAS strain gage, designed by Tokyo Sokki Kenkyujo, has two reinforcing bars that allow the asphalt to securely adhere the gage to the pavement. Each gage

had a resistance of 350  $\Omega$  and was used in a full bridge configuration connected to terminal boards using lead wires.

Using the KM-100HAS, the pavement strains were measured in the longitudinal and transverse directions at the bottom of the AC Base and intermediate layers of each test section. The bottom of the AC Base, where bottom-up cracking commonly occurs in asphalt pavements, was chosen to have a total of 4 gages (2 in the longitudinal, 2 in transverse) to accurately monitor responses. As previously stated, the first strain gage was placed along the centerline of the lane at a distance of 6 feet (1.8 m) from the concrete platform in a longitudinal direction. To allow for substantial areal coverage each gage was offset 1.5 feet (0.46 m) down the length of the test section along the centerline. In addition, ensuing strain gages would be placed in alternating longitudinal and transverse directions. The remaining two strain gages would be placed at the bottom of the intermediate layer. The first gage of the intermediate layer would be measured 7.5 feet (2.3 m) from the concrete platform along the same centerline used for the base layer gages. This gage would be placed in the same direction as the gage in the AC Base layer in order to properly compare the strain reading between these two layers. The sixth strain gage was offset 1.5 feet (0.46 m) from the prior gage and installed such that comparisons could be made to the third strain gage in the AC Base layer. Each subsequent test section follows this layout.

In order to ensure accurate readings from any gage, proper installation procedures must be followed. The placement and orientation of the strain gages were selected to provide substantial information at the bottom of the AC base and intermediate layers in each test section. To safeguard the strain gages from unintentional damages and movement that may occur as a result of the asphalt paver, hand installation was necessary. Asphalt was taken directly from the paver and used during installation. The asphalt was spread under and around the gage in a thin layer less than 1 in (2.54 cm) thick. The strain gage was then placed on top of the asphalt in the correct direction that was previously decided for that position of the gage. Once in place, the gage was buried with more asphalt from the paver and lightly compacted to further ensure no damages or movement of the gage from the paver.

### **10.2.2 Thermocouple Installation**

A total of twelve T-22N-.75E(T)9A192 thermocouples (three per lane) were used to measure temperatures within the test section pavements, because this model is known to effectively work over the target range of temperatures in the APLF. The thermocouples were connected to a data logger to record results.

One of the twelve thermocouples was designated to measure the air temperature within the facility during dynamic testing. The temperature was monitored throughout the entire depth of the pavement by having one thermocouple in the bottom of each layer of the test section. The installation process of the thermocouples was the same as previously discussed in the strain gage section of this report; however, the location was chosen to be 8.25 feet (2.5 m) from the concrete platform along the centerline of the test section.

### **10.2.3 Linear Variable Differential Transformer (LVDT) Installation**

Two Linear Variable Differential Transformers (LVDTs) at a total of eight locations (two per lane) were selected to be used to measure vertical pavement deflection and subgrade deflection in the APLF. The two LVDT's used were GHSD-750-250 gages purchased from AST Macro Sensors.

The LVDT installation used a process similar to the strain gage instrumentation. The LVDT installation began before any asphalt was placed inside the facility. Using the corner of the south concrete platform closest to the office as a reference point, the centerlines of each test section were determined. Once the centerlines for each test section were marked on each side of the concrete platform, a chalk line was used to form a straight line on the dense graded aggregate base (DGAB). From the south concrete platform two LVDT markers were sprayed on the DGAB at 12 ft (3.6 m) and 13.5 ft (4.1 m) for each test lane. At the 12 ft (3.6 m) mark, holes were excavated down to the subgrade where a shallow LVDT steel plate was placed. Holes were bored at the 13.5 ft (4.1 m) marker to a depth of 3 ft (0.91 m) into the subgrade to install deep rods to measure subgrade deflections. To ensure the hole would not collapse during construction a PVC pipe was installed into the hole.

After placing the asphalt, the LVDT holes were located and marked again using the reference point. The pavement marks were then cored to the depth of the LVDT steel plate and the PVC piping. A rod extension was attached to the plate and deep rods grouted into the drilled hole. Next, LVDT cases were screwed and epoxied into place; such that, the cases would sit flush with the surface layer of the test sections.

#### 10.2.4 Profilometer Measurements

For the APLF project, a rolling wheel profilometer was used to measure surface rutting across the 4 test sections. Rutting, next to cracking, is one of the most common distresses an asphalt pavement will endure over its entire lifespan. For this purpose, surface profiles were taken of each test section to analyze the rutting of each lane. This profiler, developed by ORITE, consists of a 10 foot (3 m) track that allows a wheel to measure elevations to 5 mil (127  $\mu\text{m}$  or 1%) accuracy at 0.5 in (1.27 cm) intervals (WMA, 2009). The rolling wheel profilometer can be seen below in Figure 58.



Figure 58. Rolling wheel profilometer in use at the APLF.

From previous research performed in the APLF with the profilometer, it was suggested the profilometer be rotated to minimize the effects of rutting in adjacent test lanes on the elevation of the profiler supports as well as to allow more data points to be collected. The rolling distance of the wheel was measured to be 9.33 feet (2.84 m); therefore, since the lanes were 8 feet (2.5 m) wide, an optimum angle of  $31^\circ$  was chosen. To ensure rut measurements were taken from the same locations, metal washers were epoxied to the surface of each test pavement at the location where each support contacted the asphalt. The total distance between each leg was measured and an optimum layout was created using AutoCAD such that four profiles were taken at equally spaced intervals along each test section. In order to compensate for the starting location of the profiler wheel, which is in front of the legs, profiler positions on Lane C and Lane D were a mirror image of those on Lane A and Lane B. The profilometer layout on the pavement can be seen in Figure 59.

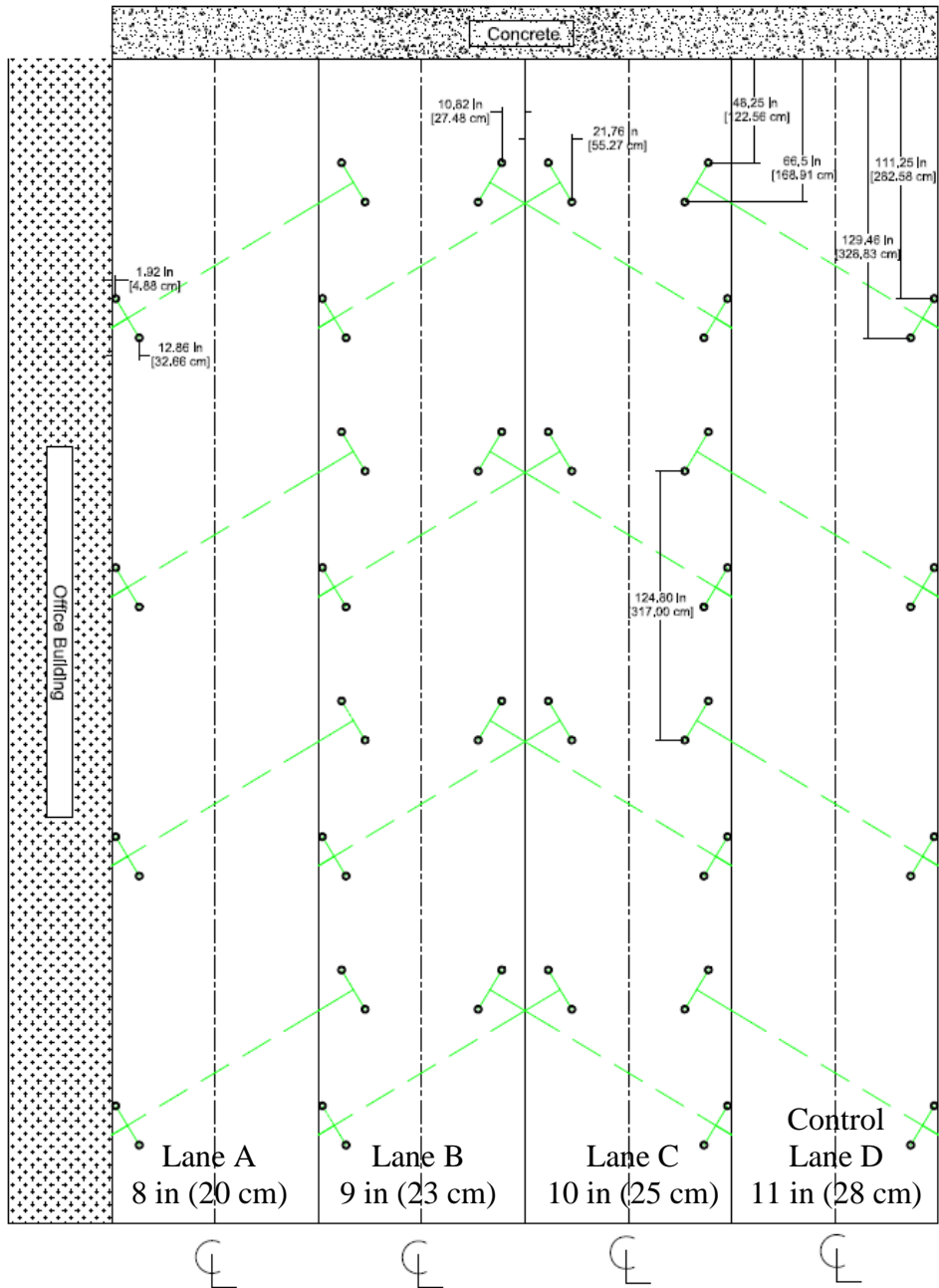


Figure 59. Overhead view of test pavements in APLF showing placement of profilometer.

As agreed upon between ODOT and ORITE, the strains and displacement of the test pavements caused by the dynamic wheel loadings would be analyzed as well as the susceptibility of pavement rutting. Rutting was measured initially and again after 100, 300, 1000, 3000, and 10,000 wheel passes per test section respectively. The pavement profiles were recorded using a Windows DOS program created by ORITE.

### 10.3 APLF Testing Pavement Responses

Dynamic load testing was conducted in the APLF on the highly modified asphalt mix designed by Kraton Polymers containing 7.5% polymer content during the months of May



through September 2014. Testing was performed at two temperatures (70°F (21.1°C) and 100°F (37.8°C)). Upon completion of 10000 passes on all lanes at 70°F (21.1°C), the temperature was increased to 100°F (37.8°C), the temperature allowed to stabilize through the pavement thickness, and 10000 passes were then applied to all lanes at the higher temperature. Profiles were taken to measure rutting of each test section prior to loading and upon completion of 100, 300, 1000, 3000, and 10,000 passes of a 9000 lb (40 kN) load. After completion of 100, 3000, and 10000 passes, the lead wires were attached to the LVDTs and twelve passes of three wheel loads (6000 lb (27 kN), 9000 lb (40 kN) and 12000 lb (53 kN)), at various offsets to the centerline of the lane, were applied to analyze the test section’s pavement response. The tire travelled at an approximate speed of 5 mph (8 km/h). Longitudinal strains in the base layer of each test section were compared to calculated endurance limits to determine which sections met the perpetual pavement design criteria. Deflections were measured at the bottom of the 304 aggregate base and 36 in (91 cm) into the subgrade.

### 10.3.1 Strain Responses in the HiMA Pavement

During testing, strain responses were measured in the same direction as traffic (the rolling load wheel), called the longitudinal direction, and in the perpendicular or “transverse” direction. Strains found in the longitudinal direction initially produced compressive strains as the wheel approached the gage as well as after the wheel passed over the gage. However, while the wheel was over the gage the strains in the pavement switched from compressive to tensile strains. Figure 60 shows the longitudinal strains recorded for 8 in (20 cm) pavement (Lane A) during a 12 kip (53 kN) load while the entire pavement was kept at 70°F (21°C).

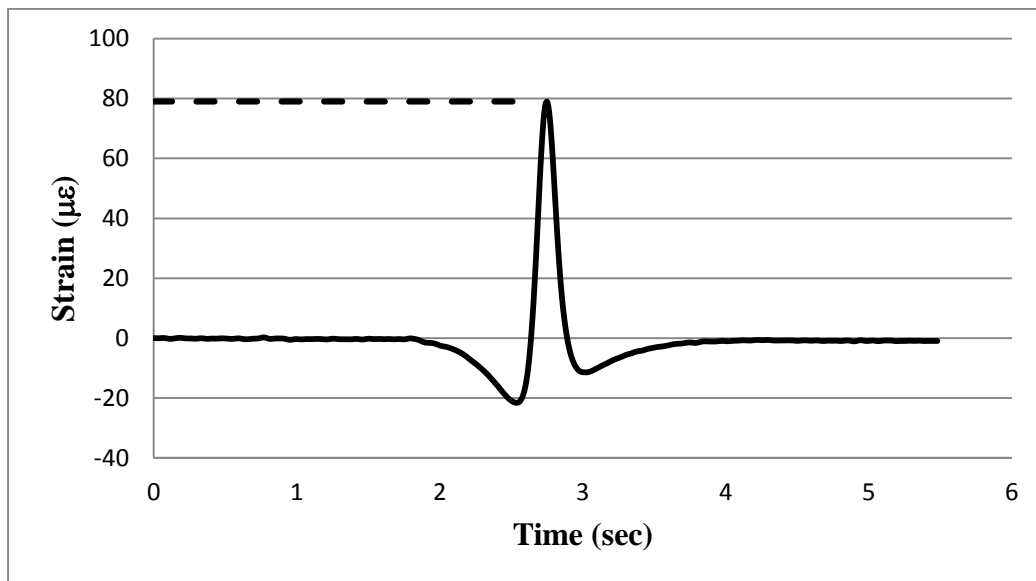


Figure 60. Longitudinal strain at bottom of AC base in Lane A, 70°F (21°C), 12 kip (53 kN) load.

As seen in the Figure, the maximum longitudinal strain produced for the 8 inch lane was found to be 79 µε and is represented by the dashed line. The compressive strains in the pavement are represented by the negative values in the figure, whereas the positive values are representative of the tensile strains. The figure shows that as the wheel approaches the

longitudinal strain gage, the pavement initially starts to go into compression but as the wheel continues over the gage the pavement changes to tension briefly before returning to compression.

Strains measured in the transverse direction caused the pavement to act in both compression and tension depending on the depth in the pavement. Transverse strains measured at the bottom of the AC base produced tensile strains, while strains measured at the bottom of the intermediate layer produced compressive strains. Figure 61 shows the transverse strains recorded for the 10 in (25 cm) pavement (Lane C) during a 12 kip (53 kN) load while the full depth of the pavement structure was maintained at 70°F (21°C).

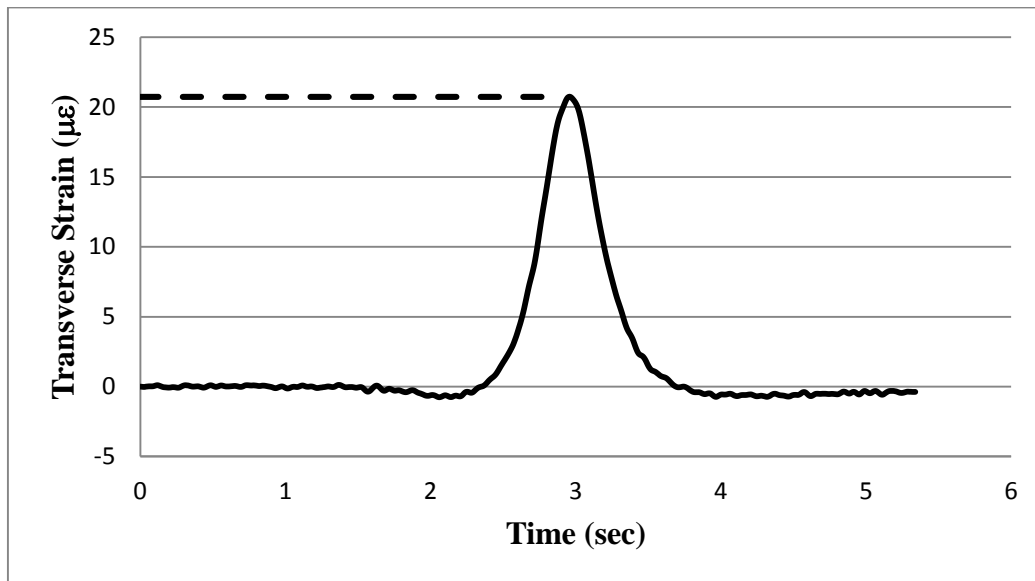


Figure 61. Transverse strain at bottom of AC base in Lane C, 70°F (21°C), 12 kip (53 kN) load.

### 10.3.2 Longitudinal Strain in HiMA Base Caused by Adjusted Load

The 8 in (20 cm) test section, Lane A, produced the highest longitudinal strains in the AC base during dynamic testing in the APLF. The following table shows the average and maximum longitudinal strains found in Lane A (8 in (20 cm)), Lane B (9 in (23 cm)), Lane C (10 in (25 cm)), and the control Lane D (11 in (28 cm)) produced during testing in the 70° F (21.1°C) and the 100°F (37.8°C) temperatures under three wheel loads of 6000 lb (27 kN), 9000 lb (40 kN), and 12000 lb (53 kN). Table 56 shows the highest maximum strains of 79 µε and 113 µε were produced under the 12,000 lb (53 kN) wheel loads for both temperatures on the thinnest (8 in (20 cm)) test section. The results show the 10 in (25 cm) section (Lane C) using the HiMA, produced strains lower than the 11 in (28 cm) control (Lane D) for testing at 70° F (21.1°C) and yielded similar longitudinal strains at 100°F (37.8°C).

**Table 56. Average and maximum longitudinal strains in base layer ( $\mu\epsilon$ ).**

Lane	AC thickness		Load ( lb (kN))					
			6000 (27)		9000 (40)		12000 (53)	
	(in)	(cm)	<i>Avg</i>	<i>Max</i>	<i>Avg</i>	<i>Max</i>	<i>Avg</i>	<i>Max</i>
70° F (21.1° C)								
A	8	20	35	43	54	61	70	79
B	9	23	31	36	48	54	62	69
C	10	25	21	24	35	39	46	51
D	11	28	27	43	40	55	52	67
100° F (37.8° C)								
A	8	20	62	66	89	93	106	113
B	9	23	41	46	63	73	79	83
C	10	25	34	44	50	56	61	67
D	11	28	27	34	43	56	56	73

Figure 62 is a plot of average maximum longitudinal strains versus the three wheel loads applied during testing at 70° F (21.1°C), and the results of testing done at 100°F (37.8°C) can be seen in Figure 63. As seen in the table as well as the following Figure 62 and Figure 63, typically the 11 in (28 cm) control lane (Lane D) produced the lowest average maximum longitudinal strains in the AC base layer at 100°F (37.8°C) under all three loads, while at 70° F (21.1°C), the 10 in (25 cm) HiMA lane (Lane C) produced the lowest average maximum longitudinal strains.

As seen in Figure 62, longitudinal strains in the 10 in (25 cm) section (Lane C) were less than those in the 11 in (28 cm) control section (Lane D) during testing conducted at 70°F (21.1°C). However, the 8 in (20 cm) and 9 in (23 cm) sections both produced average maximum longitudinal strains higher than strains in the AC base of the 11 in (28 cm) control lane.

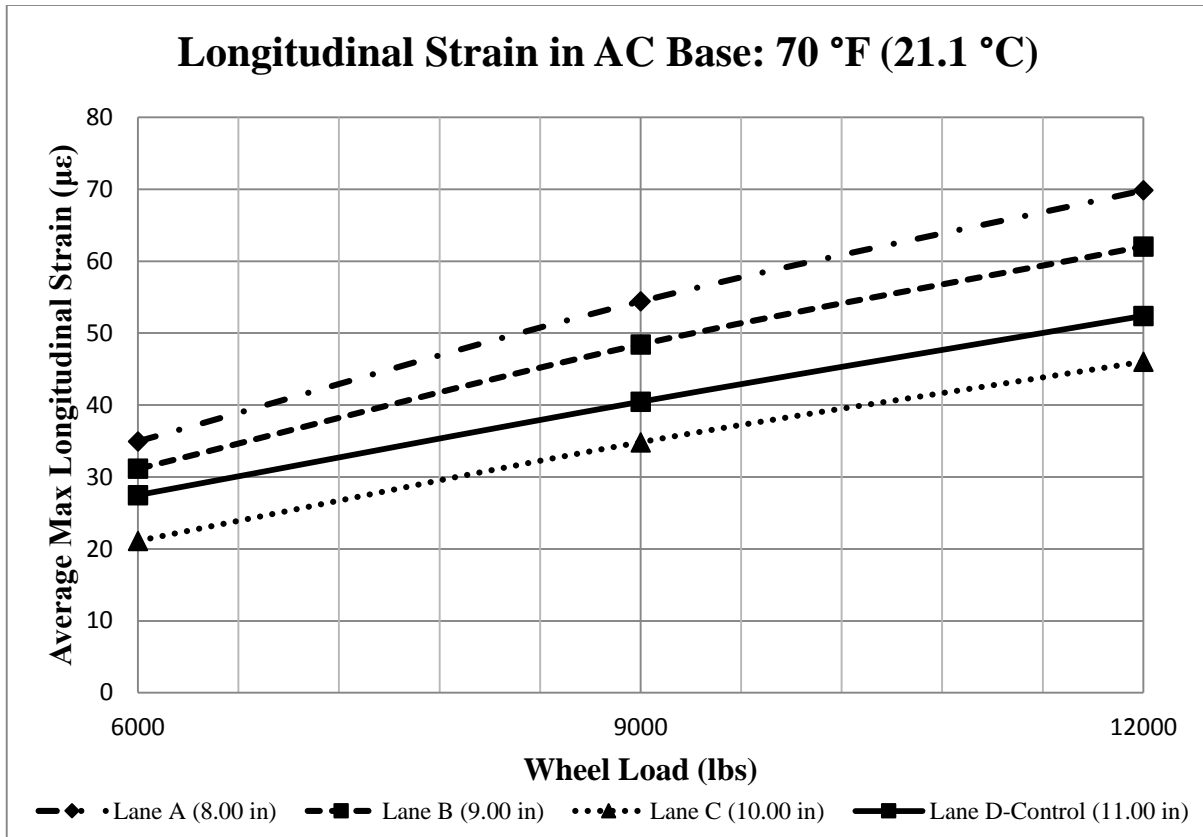


Figure 62. Average max longitudinal strains for APLF test sections at 70°F (21.1°C) (6000 lb = 27 kN, 9000 lb = 40 kN, 12,000 lb = 53 kN) (8 in = 20 cm, 9 in = 23 cm, 10 in = 25 cm, 11 in = 28 cm).

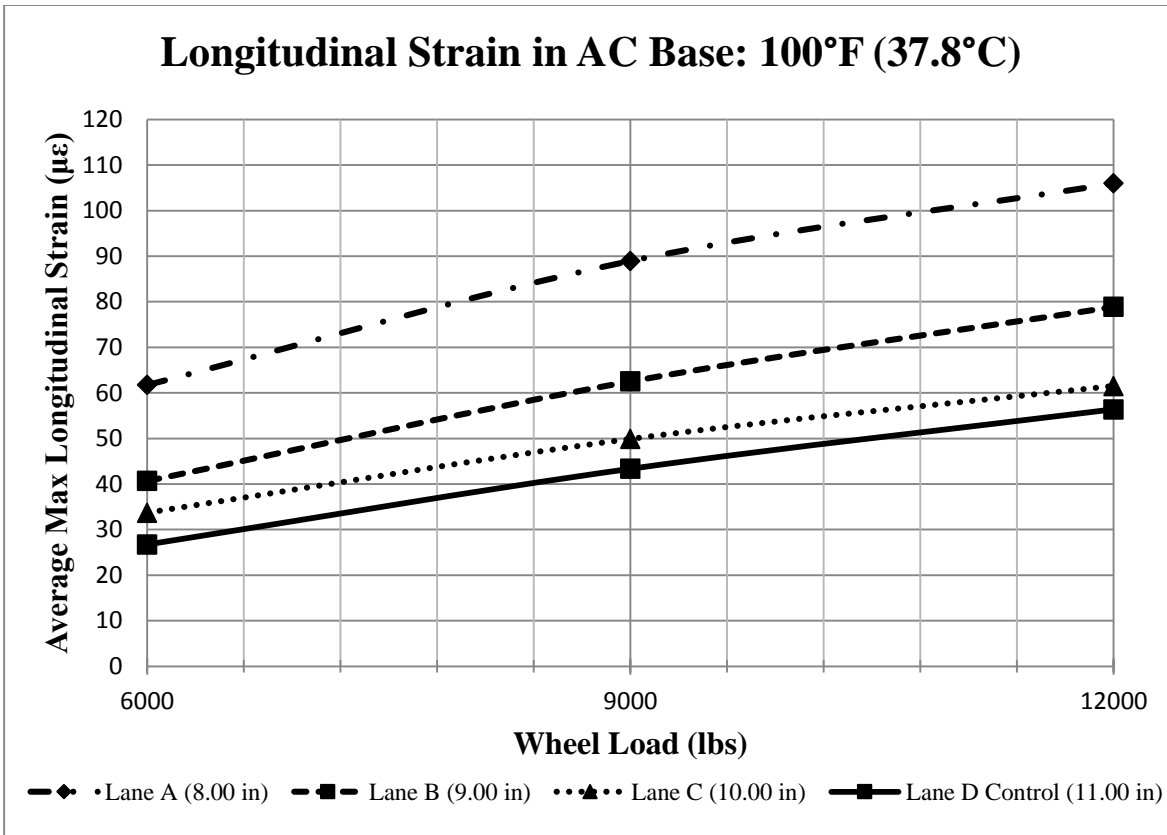


Figure 63. Average max longitudinal strains for APLF test sections at 100°F (37.8°C) (6000 lb = 27 kN, 9000 lb = 40 kN, 12,000 lb = 53 kN) (8 in = 20 cm, 9 in = 23 cm, 10 in = 25 cm, 11 in = 28 cm).

At 100°F (37.8°C), once again Lane A and Lane B produced higher longitudinal strains than the other two test sections. As seen in Figure 63, the effects of temperature on the 8 in (20 cm) section caused much higher strains to be produced when being compared to the 9 in (23 cm) and 10 in (25 cm) HiMA sections and the 11 in (28 cm) control section.

### 10.3.3 Influence of Temperature on Strain in HiMA Base

It was expected that the increase in temperature from 70°F (21.1°C) to 100°F (37.8°C), would cause an increase in the amount of strains generated in the HiMA Base. Table 57 shows the average longitudinal strain increase that occurred within each test section in the AC base layers under the 6000 lb (27 kN), 9000 lb (40 kN), and 12,000 lb (53 kN) wheel loads.

Table 57. Percent increase in longitudinal strains due to temperature increase.

Lane	AC thickness		Load (lb (kN))		
	(in)	(cm)	6000 (27)	9000 (40)	12000 (53)
A	8	20	177%	164%	152%
B	9	23	131%	129%	127%
C	10	25	160%	143%	134%
D	11	28	97%	107%	108%

### 10.3.4 Rutting in APLF

The asphalt mixes tested in the APLF appear to be very resistant to rutting. Amongst all test sections the 8 in (20 cm) test section, which exhibited the highest peak strains for both temperatures, was analyzed as an example to show the minimal amounts of rutting measured in the test pavements. Rutting was measured to be 0.012 in. (0.303 mm) in the 8 in (20 cm) test section (Lane A) after 10,000 wheel passes conducted at 70°F (21.1°C). Additionally, the accumulated rutting was measured after 10,000 wheel passes conducted at 100°F (37.8°C) and was found to be 0.046 in. (1.168 mm). Figure 64 shows the profile history in the 8 in (20 cm) section from profiles taken after 100, 300, 1000, 3000, and 10,000 wheel passes with the wheel loaded to 9000 lb (40 kN), whereas Figure 65 shows the profile history with testing conducted at 100°F (37.8°C). Both figures show the initial profiles of the 8 in (20 cm) section as a bolded line and indicated by the number “0” and the 10,000 passes indicated by the dotted line.

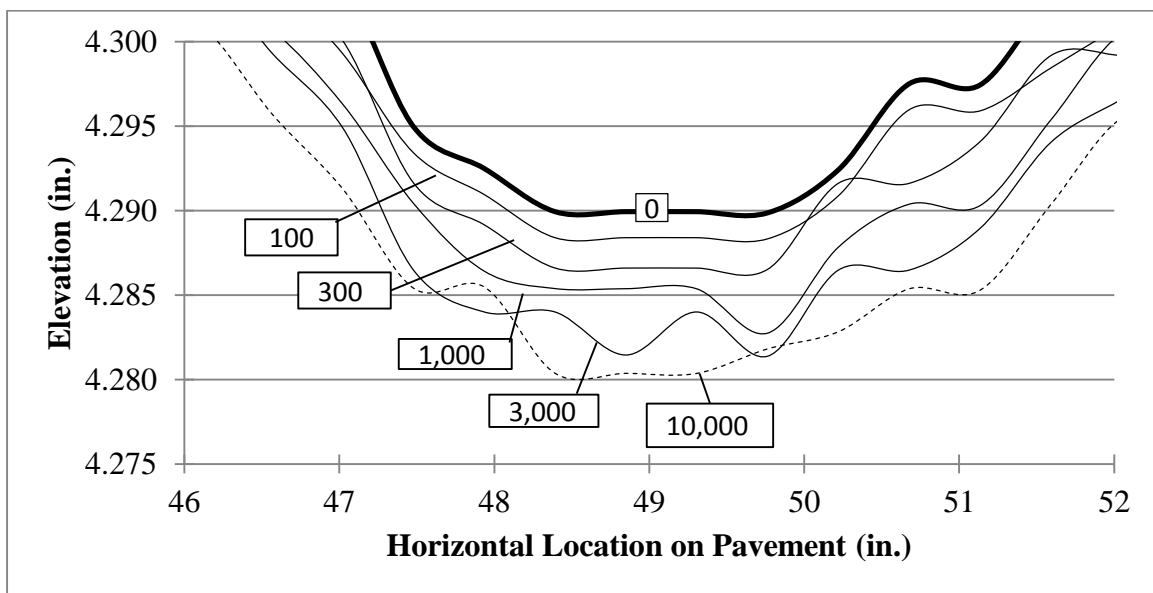


Figure 64. Profile history of 8 in (20 cm) section (Lane A) in APLF at 70°F (21.1°C) (1 in = 2.54 cm).

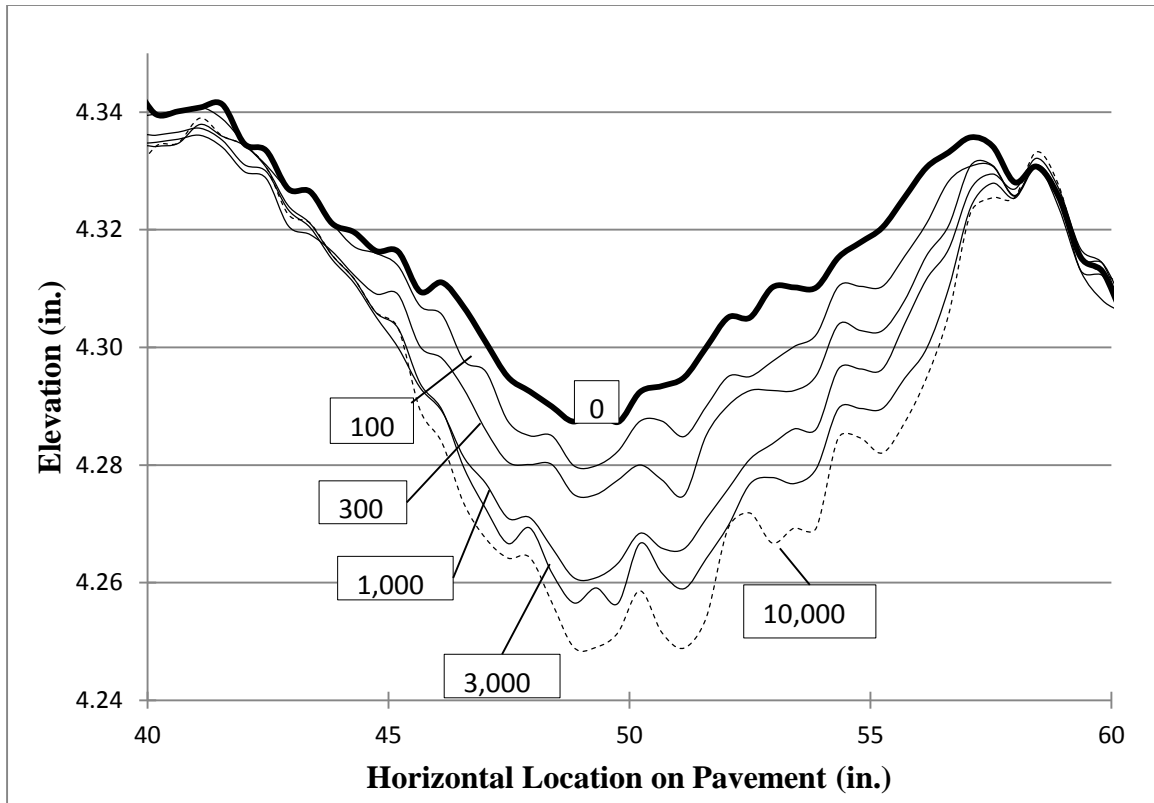


Figure 65. Profile history of 8 in (20 cm) section (Lane A) in APLF at 100°F (37.8°C) (1 in = 2.54 cm).

Further evaluation was performed at locations that showed the largest rutting in each test section. Maximum rut depths were calculated by taking the original profile elevation and subtracting successive profile section elevations. The maximum difference in elevations in each test section occurred along the wheel path when the sections were kept at a temperature of 100°F (37.8°C). Table 58 shows the maximum rut depths for the APLF test sections.

Table 58. Maximum rut depth for APLF lanes at 100°F (37.8°C).

Number of Passes	Lane A		Lane B		Lane C		Lane D	
	(in)	(cm)	(in)	(cm)	(in)	(cm)	(in)	(cm)
<b>100</b>	0.013	0.032	0.009	0.023	0.013	0.034	0.012	0.030
<b>300</b>	0.020	0.051	0.016	0.041	0.022	0.055	0.025	0.065
<b>1,000</b>	0.029	0.074	0.026	0.066	0.037	0.093	0.038	0.096
<b>3,000</b>	0.036	0.091	0.036	0.091	0.038	0.095	0.054	0.137
<b>10,000</b>	0.046	0.117	0.050	0.128	0.054	0.138	0.069	0.174
<b>Pavement thickness</b>	8	20	9	23	10	25	11	28

The maximum values from the previous table were plotted against the number of passes at 9000 lb (40 kN) load and can be seen in Figure 66.

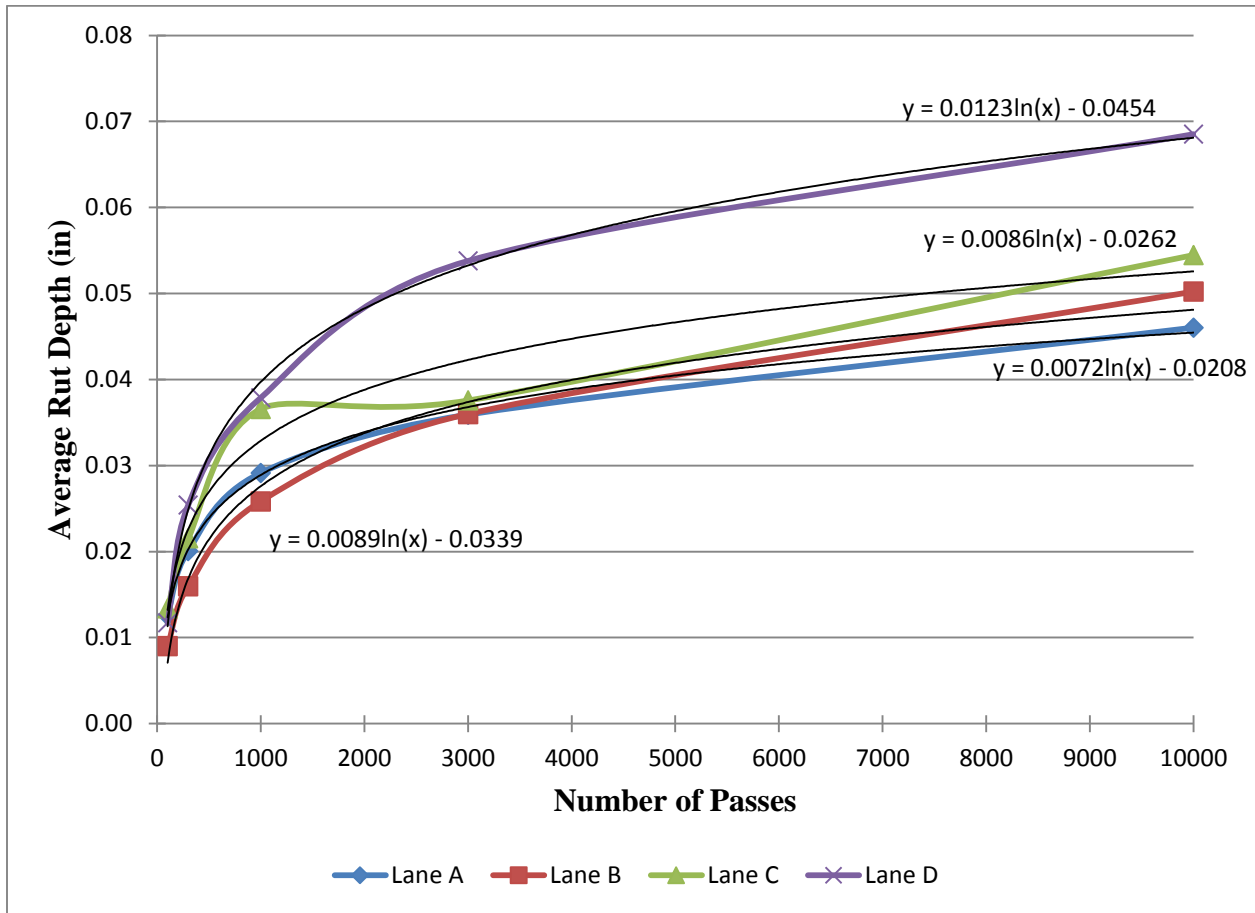


Figure 66. Rut depth vs. number of passes for HiMA at 100°F (37.8°C) (1 in =2.54 cm).

Using the trend lines produced in Figure 66, logarithmic equations were used to model the rutting behavior of each test section for the HiMA study. Table 59 shows the trend line parameters that are based on the equation  $y = A \cdot \ln(x) + B$ .

Table 59. Trendline parameters for HiMA lanes.

Pavement Section	Trend line parameters at 100°F (37.8°C)			
	A (in)	A (cm)	B	R <sup>2</sup>
Lane A	0.0072	0.0183	-0.0208	0.9982
Lane B	0.0089	0.0226	-0.0339	0.9868
Lane C	0.0086	0.0218	-0.0262	0.9598
Lane D	0.0123	0.0312	-0.0454	0.9979

ODOT has four classifications for rutting: high, medium, low, and none. High rutting consists of any rut depth that exceeds 0.75 in. (1.91 cm), medium rutting falls between 0.75 in. – 0.375 in. (1.91 cm – 0.95 cm), low rutting falls between 0.375 in. – 0.125 in. (0.95 cm – 0.32 cm), and any rutting below 0.125 in. (0.32 cm) is considered “No Rutting” (Sargand et al., 2009).

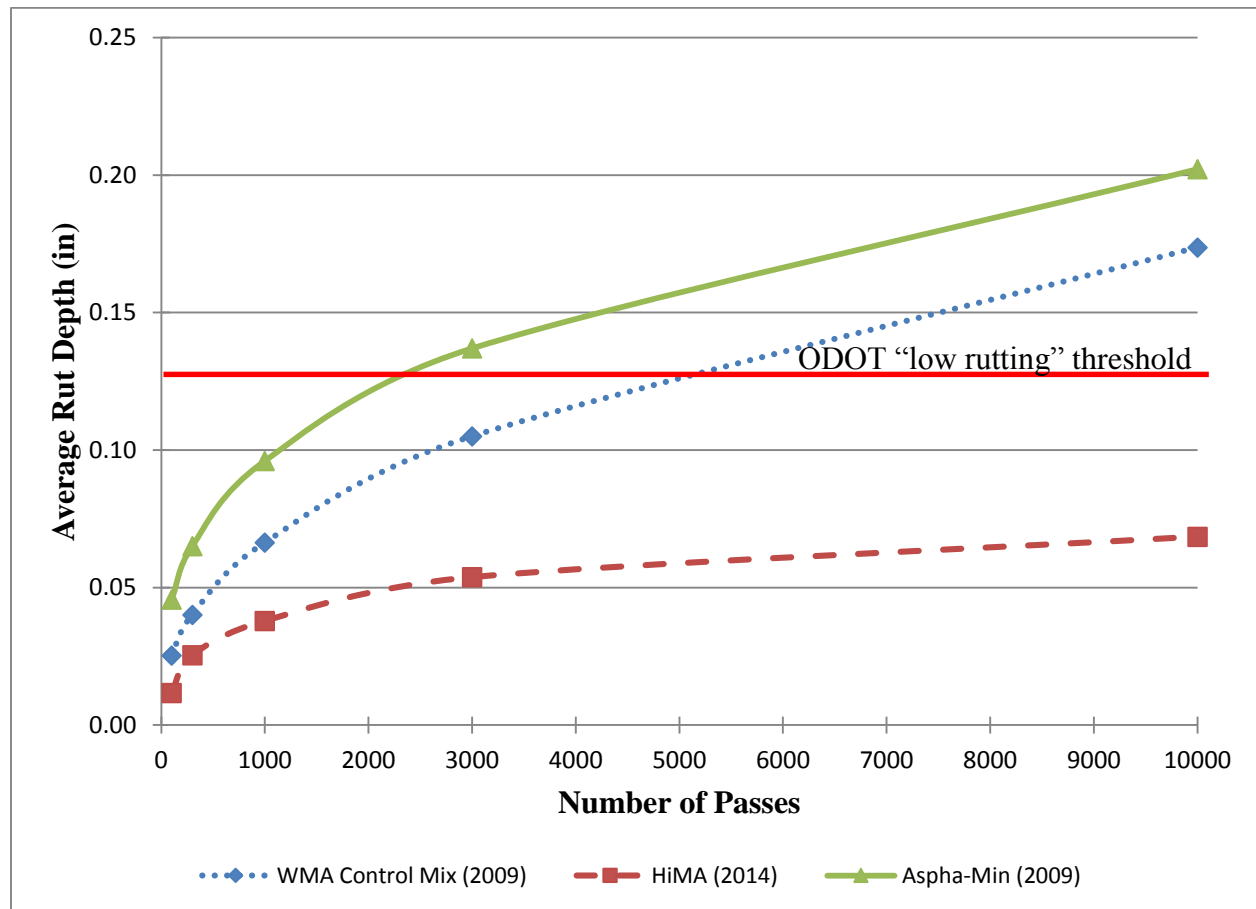


For this project no rut values were found to exceed the “Low Rut” threshold of 0.125 in (0.32 cm), as can be seen in Table 58.

Since only one type of surface mix was used in the HiMA project, rutting data from the WMA project in 2009 was used to compare against the HiMA surface mix, which had been subjected to a similar experimental protocol (Sargand et al., 2009). Table 60 and Figure 67 compare the maximum rut depths found in the HiMA and WMA projects while the test sections were maintained at high temperatures of approximately 100°F (37.8°C). The Aspha-min and Control surface mixes were chosen to compare against the HiMA surface mix.

**Table 60. Maximum rut depth for APLF and WMA surface mixes under high temperature. WMA data from Sargand et al. (2009).**

Number of Passes	HiMA Lane D		WMA 3N Aspha-min		WMA 4N Control	
	(in)	(cm)	(in)	(cm)	(in)	(cm)
100	0.012	0.030	0.046	0.116	0.025	0.064
300	0.025	0.065	0.065	0.165	0.040	0.102
1,000	0.038	0.096	0.096	0.244	0.066	0.169
3,000	0.054	0.137	0.137	0.348	0.105	0.267
10,000	0.069	0.174	0.202	0.513	0.174	0.441



**Figure 67. Comparison of average rut depths between HiMA and WMA mixes at high temperature in APLF (1 in = 2.54 cm).**

As shown in Figure 67, the HiMA surface produced much lower rutting over the same number of loading passes. To determine how much more rut resistant the HiMA was compared to the WMA mixes, further numerical analysis was completed. Using the ODOT classification for “Low Rut” and arranging the trend line parameter equation discussed previously for the HiMA and the trend line parameter equation from the WMA report, the number of passes could be solved for by setting the rut depth equal to 0.125 in. (0.32 cm) and solving for the number of passes. Table 61 shows the results to using this technique. The HiMA surface would need over 1 million passes at 9000 lb (40 kN) to reach low rutting. This value is significantly greater than those for Aspha-Min (2260 passes) and the control (4551 passes).

**Table 61. Number of passes of 9000 lb (40kN) load to reach low rutting classification (0.125 in = 0.32 cm).**

<b>Mix</b>	<b>Number of passes to reach low rutting threshold</b>
HiMA	1,038,885
Aspha-Min	2260
Control	4551

In 2013, NCAT created Report 13-03 (Timm et al., 2013), in which the researchers compared rut resistance of a 5.75 in (14.6 cm) HiMA Kraton mix section to a control section consisting of 7 in (17.8 cm) of AC. The NCAT report concluded there was a significantly lower rate of rutting in the HiMA compared to the control mix (Timm et al., 2013). Based on the findings between the APLF and the WMA projects, this report agrees with that claim. HiMA binder appears to resist rutting in the surface and intermediate layers better than standard HMA and WMA mixes.

## 11 Estimating the Fatigue Endurance Limit

The key to designing a perpetual pavement is eliminating bottom-up fatigue cracking. The perpetual pavement design includes a top layer designed to resist rutting and tire wear, an intermediate layer that also resists rutting, and a rich bottom layer designed to resist fatigue cracking, known as the fatigue resistance layer (FRL). The thicknesses of the layers are increased so that the strain at the bottom of the FRL, where it contacts the dense graded aggregate base (DGAB) never exceeds a specified value of the longitudinal tensile strain, called the “fatigue endurance limit”, in regular use.

The fatigue endurance limit can be estimated using the results of the dynamic modulus test to estimate the initial flexural stiffness ( $E_0$ ). The NCHRP project 9-44A included a vigorous laboratory testing program and development of a model which estimates the fatigue endurance limit based on results of the beam fatigue test (Witczak et al, 2013). This model calculated the Stiffness Ratio ( $SR$ ) based on applied tensile strain, rest period, number of loading cycles, and the initial flexural stiffness for the beam fatigue test. The endurance limit of an asphalt mix can be determined by setting the Stiffness Ratio equal to one and solving for the tensile strain. The following equation is shown again to reiterate the various terms that affect the Stiffness Ratio:

$$SR = 2.0844 - 0.1386 \cdot \log(E_0) - 0.4846 \cdot \log(\varepsilon) - 0.2012 \cdot \log(N) + 1.4103 \cdot \tanh(0.8471 \cdot RP) + 0.0320 \cdot \log(E_0) \cdot \log(\varepsilon) - 0.0954 \cdot \log(E_0) \cdot \tanh(0.7154 \cdot RP) - 0.4746 \cdot \log(\varepsilon) \cdot \tanh(0.6574 \cdot RP) + 0.0041 \cdot \log(N) \cdot \log(E_0) + 0.0557 \cdot \log(N) \cdot \log(\varepsilon) + 0.0689 \cdot \log(N) \cdot \tanh(0.259 \cdot RP)$$

Where:

$SR$  = stiffness ratio = stiffness measured at any load cycle during beam fatigue testing to the initial stiffness of the specimen

$E_0$  = initial flexural stiffness (ksi)

$\varepsilon$  = applied tensile strain ( $\mu\varepsilon$ )

$RP$  = rest period (sec)

$N$  = number of load cycles

The NCHRP project 9-44A report included a sensitivity study which concluded  $N$  has little to no effect on the Stiffness Ratio. Since there is no effect,  $N$  is set to 200,000 cycles for this analysis, as recommended by the NCHRP 9-44 A researchers (Witczak et al, 2013). On the other hand, the Rest Period ( $RP$ ) had a major effect on the endurance limit. However, once the rest period reached or exceeded 5 seconds, the endurance limits became very similar. Since this occurs, rest periods were plotted for different pavement mixes to show the variation. For experimental analysis of the DEL-23 pavement and the HiMA pavement inside the APLF, a common rest period of five seconds was used. Figure 68 is an example of how the rest period and flexural stiffness can affect the fatigue endurance limit.

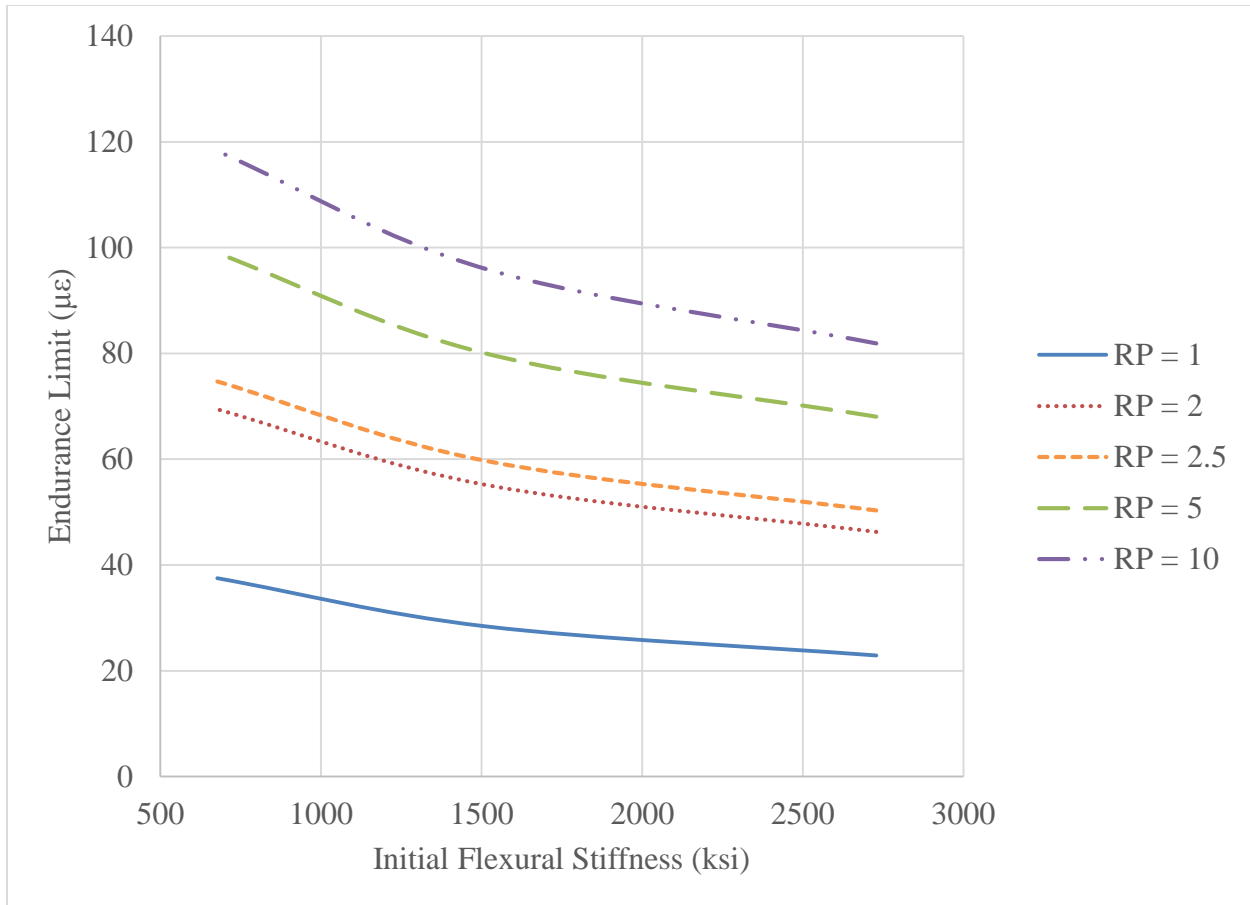


Figure 68. AC base endurance limit vs. flexural stiffness at various Rest Periods (RP) in seconds for APLF control mix.

### 11.1 Effect of the Initial Flexural Stiffness

The flexural stiffness of the mix has an effect on the endurance limit. In general, as the stiffness decreases, the endurance limit increases due to the material becoming more flexible and ductile. Consequently, as the stiffness increases, the endurance limit decreases due to the mix becoming more brittle. The value of the dynamic modulus and flexural stiffness for a mix is dependent on the temperature and frequency. The dynamic modulus is lower at the higher temperature and higher at the lower temperature. Relationships between the dynamic modulus and temperature for each base layer mix will be determined to estimate the value of the dynamic modulus at a particular test temperature.

Since the flexural stiffness is so crucial, estimating flexural stiffness based on the dynamic modulus is somewhat controversial. The NCHRP Design Guide assumes the dynamic modulus is equal to the initial flexural stiffness, whereas Kansas researchers found the dynamic modulus is about two times the value of the initial flexural stiffness (Romanoschi, et al, 2006). Romanoschi, et al., also states the frequency of the dynamic modulus used for comparison was 10 Hz. Both assumptions will be used to compare the various endurance limits for this analysis ( $E_0 = E^*$  and  $E_0 = E^*/2$ ) at a loading frequency of 10 Hz for the dynamic modulus.

## 11.2 Endurance Limits Based on Laboratory Tested Temperatures

Table 62 is a summary of endurance limits for each site and AC base mixes when using the NCHRP assumption that dynamic modulus is equal to initial flexural stiffness ( $E_0 = E^*$ ):

**Table 62. Estimation of endurance limit when  $E_0 = E^*$ , RP = 5 seconds, f = 10 Hz, N = 200,000, SR = 1.**

Site	Mix	Test Temp $T$		Dynamic Modulus $E^*$		Initial Flexural Stiffness $E_0$		Endurance Limit $\epsilon_t$
		(°F)	(°C)	(ksi)	(GPa)	(ksi)	(GPa)	( $\mu\epsilon$ )
DEL-23	FRL	40	4.4	2495	17.20	2495	17.20	70
		70	21.1	1534	10.58	1534	10.58	80
		100	37.8	656	4.52	656	4.52	100
HiMA APLF	AC Base: Control	40	4.4	2729	18.82	2729	18.82	68
		70	21.1	1515	10.45	1515	10.45	80
		100	37.8	677	4.67	677	4.67	99
	AC Base: Kraton	40	4.4	2622	18.08	2622	18.08	69
		70	21.1	1591	10.97	1591	10.97	79
		100	37.8	653	4.50	653	4.50	100

Table 63 is a summary of endurance limits for each site and AC base mixes when using the Kansas testing results that state the dynamic modulus is two times larger than initial flexural stiffness ( $E_0 = E^*/2$ ). As expected, the estimated endurance limits are larger when  $E_0 = E^*/2$ .

**Table 63. Estimation of endurance limit when  $E_0 = E^*/2$ , RP = 5 seconds, f = 10 Hz, N = 200000, SR = 1.**

Site	Mix	Test Temp $T$		Dynamic Modulus $E^*$		Initial Flexural Stiffness $E_0$		Endurance Limit $\epsilon_t$
		(°F)	(°C)	(ksi)	(GPa)	(ksi)	(GPa)	( $\mu\epsilon$ )
DEL-23	FRL	40	4.4	2495	17.20	1247	8.60	84
		70	21.1	1534	10.58	767	5.29	96
		100	37.8	656	4.52	328	2.26	119
HiMA APLF	AC Base: Control	40	4.4	2729	18.82	1365	9.41	82
		70	21.1	1515	10.45	757	5.22	96
		100	37.8	677	4.67	339	2.34	118
	AC Base: Kraton	40	4.4	2622	18.08	1311	9.04	83
		70	21.1	1591	10.97	795	5.48	95
		100	37.8	653	4.50	326	2.25	119

## 11.3 Comparison of Endurance Limits and Strain Results from Field Testing

Since temperatures of the laboratory testing are not always equal to temperatures measured in the field in the asphalt base layers, relationships must be developed to better estimate the endurance limits of the pavement structures. These relationships are based on a second-order polynomial regression curve for each mix that is based on the dynamic modulus at 10 Hz versus test temperature. The following equation was used to describe this relationship:

$$E^*(T) = aT^2 + bT + c$$

Where:

$T$  = Test Temperature (°F)

$a, b, c$  = Regression Coefficients

Table 64 and Table 65 are a summary of the dynamic modulus results versus temperature at a frequency of 10 Hz and the resulting regression coefficients respectively. The equation for  $E^*(T)$  can also be solved for metric units (GPa) by substituting  $T_F = T_C * (9/5) + 32$  and expanding the polynomials and multiplying by a conversion factor from ksi to GPa to find new coefficients for an equation of the same form quadratic in Celsius temperature, shown in bottom part of Table 65.

**Table 64. Dynamic modulus results at 10 Hz.**

Temperature		Dynamic Modulus at 10 Hz					
		DEL-23 FRL		HiMA-AC Base-Kraton		APLF-AC Base-Control	
(°F)	(°C)	(ksi)	(GPa)	(ksi)	(GPa)	(ksi)	(GPa)
40	4.4	2495	17.20	2769	19.09	2729	18.82
70	21.1	1534	10.58	1552	10.70	1515	10.45
100	37.8	656	4.52	733	5.05	677	4.67
130	54.4	261	1.80	290	2.00	211	1.45

**Table 65. Second order regression coefficients for each mix. English units at top, metric units at bottom.**

AC Base Mix	Regression Coefficients			
	$a$ (ksi/°F <sup>2</sup> )	$b$ (ksi/°F)	$c$ (ksi)	R <sup>2</sup>
DEL-23 FRL	0.1573	-51.998	4343	0.9973
HiMA-AC Base-Kraton	0.2147	-64.015	4984	1
HiMA-AC Base-Control	0.2077	-63.286	4927.9	1
	$a_c$ (GPa/°C <sup>2</sup> )	$b_c$ (GPa/°C)	$c_c$ (GPa)	R <sup>2</sup>
DEL-23 FRL	0.00351	-0.5204	19.5821	0.9973
HiMA-AC Base-Kraton	0.00480	-0.6239	21.7555	1
HiMA-AC Base-Control	0.00464	-0.6204	21.4802	1

To determine whether a pavement structure is perpetual, the stiffness ratio must be greater than or equal to one when the strain is entered into the model. From both DEL-23 and HiMA testing, the average maximum strains were determined during field testing. By inserting the strain values measured in the field and solving for Stiffness Ratio, perpetual pavement status can be determined. The dynamic modulus used is based on the temperature measured in the field, the second-order polynomial equations for each mix will ensure the dynamic modulus selected for the analysis is representative of the temperature conditions in the AC base layer for each site and day tested.

It is important to note the strains measured for the DEL-23 testing is based on a single axle, single wide based tire load of 14 kip (62 kN) whereas the APLF average maximum strains recorded were based on a tandem axle, dual tire load of 12 kip (53 kN). The loads are similar but the single tire configuration is expected to result in higher strain readings. As before, the initial flexural stiffness will be estimated using both  $E_0 = E^*$  and  $E_0 = E^*/2$ . Table 66 and Table 67 show the FEL of the DEL-23 test temperatures and the results of the stiffness ratio when the average maximum strains measured are put into the endurance limit prediction model.

**Table 66. DEL-23 fatigue endurance limit at test temperatures  $E_0 = E^*$ ,  $RP = 5$  seconds,  $f = 10$  Hz,  $N = 200000$ ,  $SR = 1$ .**

Date	Lane	Pavement Depth		Avg. Temp $T$		Dynamic Modulus $E^*$		Initial Flexural Stiffness $E_0$		FEL $\epsilon_t$
		(in)	(cm)	(°F)	(°C)	(ksi)	(GPa)	(ksi)	(GPa)	( $\mu\epsilon$ )
11/29/2012	39D168	15	38	41	5.0	2460	16.96	2460	16.96	70
12/18/2012	39BN803	11	28	44	6.7	2364	16.30	2364	16.30	71
12/19/2012	39BS803	13	33	44	6.7	2352	16.22	2352	16.22	71
7/1/2013	39D168	15	38	84	28.9	1075	7.41	1075	7.41	88
7/10/2013	39BN803	11	28	80	26.7	1192	8.22	1192	8.22	85
7/11/2013	39BS803	13	33	81	27.2	1151	7.94	1151	7.94	86

**Table 67. DEL-23 stiffness ratio based on the average peak strain measured during the controlled vehicle load tests ( $E_0 = E^*$ ),  $RP = 5$  seconds,  $f = 10$  Hz,  $N = 200000$ .**

Date	Lane	Pavement Depth		Avg. Temp $T$		Initial Flexural Stiffness $E_0$		Stiffness Ratio $SR$	Avg. Peak Strain	FEL $\epsilon_t$
		(in)	(cm)	(°F)	(°C)	(ksi)	(GPa)		( $\mu\epsilon$ )	( $\mu\epsilon$ )
11/29/2012	39D168	15	38	41	5.0	2460	16.96	1.15	38	70
12/18/2012	39BN803	11	28	44	6.7	2364	16.30	1.1	47	71
12/19/2012	39BS803	13	33	44	6.7	2352	16.22	1.2	31	71
7/1/2013	39D168	15	38	84	28.9	1075	7.41	1.04	74	88
7/10/2013	39BN803	11	28	80	26.7	1192	8.22	<b>0.96</b>	101	85
7/11/2013	39BS803	13	33	81	27.2	1151	7.94	1.05	70	86

Based on the testing results from DEL-23, the summer testing showed the 11 in (28 cm) section (39BN803) had a stiffness ratio less than one when the initial flexural stiffness was set equal to the dynamic modulus at the respective test temperature. All other test sections for summer and winter showed the stiffness ratio greater than or equal to one; they could be classified as perpetual pavement sections based on the model prediction. Table 68 and Table 69 show the results of the model prediction when the initial flexural stiffness is equal to one half of the dynamic modulus.

**Table 68. DEL-23 Fatigue endurance limits at test temperatures ( $E_0 = E^*/2$ ),  $RP = 5$  seconds,  $f = 10$  Hz,  $N = 200000$ ,  $SR = 1$ .**

Date	Lane	Pavement Depth		Avg. Temp $T$		Dynamic Modulus $E^*$		Initial Flexural Stiffness $E_0$		FEL $\epsilon_t$
		(in)	(cm)	(°F)	(°C)	(ksi)	(GPa)	(ksi)	(GPa)	( $\mu\epsilon$ )
11/29/2012	39D168	15	38	41	5.0	2460	16.96	1230	8.48	85
12/18/2012	39BN803	11	28	44	6.7	2364	16.30	1182	8.15	85
12/19/2012	39BS803	13	33	44	6.7	2352	16.22	1176	8.11	86
7/1/2013	39D168	15	38	84	28.9	1075	7.41	537	3.70	105
7/10/2013	39BN803	11	28	80	26.7	1192	8.22	596	4.11	102
7/11/2013	39BS803	13	33	81	27.2	1151	7.94	575	3.96	103

**Table 69. DEL-23 stiffness ratio based on the average peak strain measured during the controlled vehicle load tests ( $E_0 = E^*/2$ ),  $RP = 5$  seconds,  $f = 10$  Hz,  $N = 200000$ .**

Date	Lane	Pavement Depth		Avg. Temp $T$		Initial Flexural Stiffness $E_0$		Stiffness Ratio $SR$	Avg. Peak Strain	FEL $\epsilon_t$
		(in)	(cm)	(°F)	(°C)	(ksi)	(GPa)		( $\mu\epsilon$ )	( $\mu\epsilon$ )
11/29/2012	39D168	15	38	41	5.0	1230	8.48	1.20	38	85
12/18/2012	39BN803	11	28	44	6.7	1182	8.15	1.15	47	86
12/19/2012	39BS803	13	33	44	6.7	1176	8.11	1.25	31	86
7/1/2013	39D168	15	38	84	28.9	537	3.70	1.09	74	105
7/10/2013	39BN803	11	28	80	26.7	596	4.11	1.00	101	102
7/11/2013	39BS803	13	33	81	27.2	575	3.96	1.10	70	103

When using the assumption the initial flexural stiffness is half of the dynamic modulus, all of the pavement sections on DEL-23 have a stiffness ratio greater than or equal to one. Using this assumption, all the pavement sections can be classified as perpetual based on the beam fatigue model. The temperatures inside the APLF were controlled for testing purposes. Two temperatures were selected for testing 70 °F (21.1°C) and 100 °F (37.8°C). Also, the strains used for perpetual pavement analysis were based on a tandem axle, dual tire configuration with a 12,000 lb (53 kN) load applied to the pavement. Table 70 and Table 71 show the FEL of the HiMA test temperatures and the results of the stiffness ratio when the average maximum strains measured are inputted into the endurance limit prediction model.

**Table 70. APLF fatigue endurance limits at test temperatures ( $E_0 = E^*$ ),  $RP = 5$  seconds,  $f = 10$  Hz,  $N = 200000$ ,  $SR = 1$ .**

Mix	Test Temp $T$		Dynamic Modulus $E^*$		Initial Flexural Stiffness $E_0$		FEL $\epsilon_t$
	(°F)	(°C)	(ksi)	(GPa)	(ksi)	(GPa)	( $\mu\epsilon$ )
AC Base: Control	70	21	1515	10.45	1515	10.45	80
	100	38	677	4.67	677	4.67	99
AC Base: Kraton	70	21	1552	10.70	1552	10.70	79
	100	38	733	5.05	733	5.05	97



**Table 71. APLF stiffness ratio based on the average peak strain measured during the controlled load tests ( $E_0 = E^*$ ),  $RP = 5$  seconds,  $f = 10$  Hz,  $N = 200000$ .**

Lane	Mix	Pavement Thickness		Test Temp $T$		Dynamic Modulus $E^*$		Initial Flexural Stiffness $E_0$		Stiffness Ratio $SR$	Avg. Peak Strain ( $\mu\epsilon$ )	FEL $\epsilon_t$ ( $\mu\epsilon$ )
		(in)	(cm)	(°F)	(°C)	(ksi)	(GPa)	(ksi)	(GPa)			
D	AC Base: Control	11	28	70	21	1515	10.45	1515	10.45	1.1	52	80
				100	38	677	4.67	677	4.67	1.14	56	99
C	AC Base: Kraton	10	25	70	21	1552	10.70	1552	10.70	1.13	46	79
				100	38	733	5.05	733	5.05	1.11	61	97
B	AC Base: Kraton	9	23	70	21	1552	10.70	1552	10.70	1.06	62	79
				100	38	733	5.05	733	5.05	1.05	79	97
A	AC Base: Kraton	8	20	70	21	1552	10.70	1552	10.70	1.03	70	79
				100	38	733	5.05	733	5.05	<b>0.98</b>	106	97

Based on the results of the HiMA testing, Lane A did not meet the criteria from perpetual pavement when the initial flexural stiffness was set equal to the dynamic modulus. Table 72 and Table 73 show the results of the endurance limit estimation when the initial flexural stiffness is half of the dynamic modulus.

**Table 72. APLF fatigue endurance limit at test temperatures ( $E_0 = E^*/2$ ),  $RP = 5$  seconds,  $f = 10$  Hz,  $N = 200000$ ,  $SR = 1$ .**

Mix	Test Temp $T$		Dynamic Modulus $E^*$		Initial Flexural Stiffness $E_0$		FEL $\epsilon_t$
	(°F)	(°C)	(ksi)	(GPa)	(ksi)	(GPa)	( $\mu\epsilon$ )
AC Base: Control	70	21	1515	10.45	757	5.22	96
	100	38	677	4.67	339	2.34	118
AC Base: Kraton	70	21	1552	10.70	776	5.35	95
	100	38	733	5.05	367	2.53	116

**Table 73. APLF stiffness ratio based on the average peak strain measured during the controlled load tests ( $E_0 = E^*/2$ ),  $RP = 5$  seconds,  $f = 10$  Hz,  $N = 200000$ .**

Lane	Mix	Pavement Thickness		Test Temp $T$		Dynamic Modulus $E^*$		Initial Flexural Stiffness $E_0$		Stiffness Ratio $SR$	Avg. Peak Strain ( $\mu\epsilon$ )	FEL $\epsilon_t$ ( $\mu\epsilon$ )
		(in)	(cm)	(°F)	(°C)	(ksi)	(GPa)	(ksi)	(GPa)			
D	AC Base: Control	11	28	70	21	1515	10.45	757	5.22	1.15	52	96
				100	38	677	4.67	339	2.34	1.19	56	118
C	AC Base: Kraton	10	25	70	21	1552	10.70	776	5.35	1.18	46	95
				100	38	733	5.05	367	2.53	1.16	61	116
B	AC Base: Kraton	9	23	70	21	1552	10.70	776	5.35	1.11	62	95
				100	38	733	5.05	367	2.53	1.1	79	116
A	AC Base: Kraton	8	20	70	21	1552	10.70	776	5.35	1.03	70	95
				100	38	733	5.05	367	2.53	1.02	106	116

When the dynamic modulus was set equal to the initial flexural stiffness, Lane A did not have a stiffness ratio greater than or equal to one. Unlike the previous analysis, when  $E_0 = E^*/2$ ,

Lane A met the criteria for perpetual pavement status. When using the assumption from the Kansas report, all of the lanes in the APLF are considered perpetual based on the model from the NCHRP project 9-44A report.

In Section 4.2 the literature behind the concept of the endurance limit was discussed. The endurance limit is the key element in the perpetual pavement design, namely that by building the pavement thick enough and using the appropriate materials to ensure the tensile stress at the bottom of the asphalt fatigue resistance layer never exceeds the endurance limit, you can prevent the bottom-up damage that typically leads to the need for a full-depth reconstruction. Instead the pavement will perform for 50 years or more provided with periodic surface course milling and replacement.

Early studies, such as those discussed in Romanello (2007) and Sargand, Figueroa, and Romanello (2008), arrived at a fixed endurance limit criterion of  $70 \mu\epsilon$  used in the construction of the WAY30 perpetual pavement. Since then the endurance limit has been adjusted, usually upward, depending on the material properties of the asphalt and/or aggregate being used. It is also possible to derive an endurance limit from the NCHRP 9-44A equation using the approach with  $E_0=E^*$  or  $E_0= E^*/2$ .

For the three pavements constructed and studied on DEL-23, they all meet even the original conservative  $70\mu\epsilon$  criterion for perpetual pavement except the thinnest pavement with 11 in (28 cm) thickness, as seen in Table 67. We can thus conclude that using a similar design and mix, a thickness of 13 in (33 cm) will be sufficient to create a perpetual pavement, when constructed on a stabilized subgrade. The only section included in the study on compacted subgrade consisted of 15 in (38 cm) of asphalt. Therefore, we can conclude that, using a similar design and mix, a thickness of 15 in (38 cm) will be sufficient to create a perpetual pavement on compacted subgrade.

## 12 Mechanistic-Empirical Pavement Design

Pavement design concepts and practices change as technologies advance. The Mechanistic-Empirical Pavement Design Guide (MEPDG) reflects the current consensus on pavement design, as developed and released under NCHRP Projects 1-37A and 1-40D. The MEPDG includes methods for analyzing and designing most types of new and rehabilitated flexible, rigid, and composite pavements. It emphasizes the use of sound principles of engineering mechanics as well as existing models and databases. With the high percentage of pavement projects in the US that involve the rehabilitation of existing pavements, the MEPDG specifically emphasizes rehabilitation design.

The AASHTOWare Pavement ME Design software package is a Microsoft Windows software package used to expedite the determination of suitable prescribed alternatives. The consistency between the rigid and flexible pavement modules allows for the same inputs and interfaces, whenever possible, giving the user the ability to examine either rigid or flexible pavement alternatives. The software is easily interfaced with any open database connectivity (ODBC)-compliant database. There are provisions to enable the use of other advanced database management systems.

The MEPDG performance was calibrated based on Long Term Pavement Performance (LTPP) database field pavement performance data. The LTPP database compiles measurements from thousands of flexible and rigid pavement projects nationwide, including data on design, material properties, climate, traffic, and performance data. Despite its nationwide orientation, the LTPP does not include extensive results from all states; some states did not participate, and others submitted data for only limited sites. The LTPP database does not yet include all materials used in highway construction. Also, when the MEPDG software was previously used to predict performance of pavements on local projects, the results did not correlate well with actual performance data. This shows the importance of local calibration.

The Ohio Department of Transportation (ODOT) attempted local calibration of the MEPDG software for pavements in Ohio, yet the conclusions state “The model may be valid only for the limited conditions under which they were evaluated” and “A more comprehensive evaluation effort is needed...” (Applied Research Associates, Inc, 2009, Vol. 4). Since 2009, NCHRP 1-40D and the implementation of new software has seen the asphalt models change, and the calibration factors created for the earlier MEPDG software are no longer usable, even within the original limitations. Since the M-E software is being used in this report to compare the performance of these sections and not to actually predict the field performance, the global calibration factors will be used. These runs will provide the necessary data for comparing the thickness designs.

### 12.1 MEPDG Inputs

Guidelines and software for generating input traffic data for Ohio for use with the M-E software were developed under State Job 134557 by A. Abbas and A. Frankhouser, in 2012 (Abbas and Frankhouser, 2012). In this report, their Table 66 “MEPDG Traffic Inputs Recommendations” is shown below as Table 74 and lists the MEPDG inputs recommended and will be used in our current analysis. Traffic data and growth factors were supplied by ODOT for the projects analyzed.

**Table 74. MEPDG traffic input recommendations (Abbas and Frankhouser, 2012).**

<b>Traffic Input</b>	<b>Recommendation</b>
AADTT	This traffic input shall be obtained from ODOT Traffic Monitoring Section.
D(%)	Use 50% (current ODOT value) for all roadways.
LF(%)	Level 2 (statewide average). Recommended values: 100% for 2-lane roadways, 95% for 4-lane roadways, 80% for 6-lane roadways, and 70% for 8 or more lane roadways.
Operational Speed	This traffic input shall be obtained from ODOT Traffic Monitoring Section.
MAF	Level 3 (MEPDG default).
VCD	This traffic input shall be estimated from a combination of site-specific short-term counts (Level 1) and seasonal adjustment factors for each truck class. The short-term counts shall be obtained from ODOT Traffic Monitoring Section. Level 2 (statewide average based on functional classification) analysis can be used for locations where site-specific data is not available.
HDF	Level 3 (MEPDG default) for flexible pavements and Level 2 (statewide average based on functional classification) for rigid pavements.
Growth Rate	This traffic input shall be obtained from ODOT Modeling and Forecasting Section (Certified Traffic).
ALS (Single, Tandem, Tridem, and Quad)	Level 2 (statewide average based on information from all sites)
No. of Axles per Truck	Level 2 (statewide average based on information from all sites)
Lateral Wander	Level 3 (MEPDG default)
Axle Configuration	Level 3 (MEPDG default)
Wheelbase Distribution	Level 3 (MEPDG default)

Material inputs for the M-E software used in this study are listed in Chapter 9. The material properties in Chapter 9 are used in the M-E software for Level 3 input. In this study, Level 1 input was used whenever possible, but in most cases Level 3 input was used to simplify the analysis. And since the M-E software results will be used for comparison between the various sites, as long as the input level is consistent, then the comparison will be valid.


## **12.2 MEPDG Results**

MEPDG results from Test Sections 39BN803, 39BS803, 39D168, and 39P168 on the US23 project and results from the test sections on I77 and US30 are presented in the order listed. Table 75, Table 76, Table 77, Table 78, Table 79, and Table 80 show the design inputs including the design structure for each of the test sections. Even though the software shows the subgrade as A-6, the performance parameters collected from on-site tests with DCP, FWD were used as input data to provide an accurate representation of the actual materials. Weather stations closest to the actual test sections were used in the analysis, and the AADT values were set to the same number for all sections to remove traffic as a variable in the comparisons. Table 81, Table 82, Table 83, Table 84, Table 85, and Table 86 show the distress summary for each section, and Figure 69 through Figure 80 show the M-E software results for each section.

**Table 75. Design inputs for Section 39BN803 on DEL-23 (1 in = 25.4 mm).**

Design Inputs					
Design Life:	50 years	Base construction:	May, 2015	Climate Data	40.078, -83.078
Design Type:	Flexible Pavement	Pavement construction:	June, 2016	Sources	
		Traffic opening:	September, 2016		

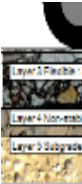
  

Design Structure			Volumetric at Construction:		Traffic		
	Layer type	Material Type	Thickness (in.):	Effective binder content (%)	7.6	Age (year)	Heavy Trucks (cumulative)
	Flexible	Default asphalt concrete	1.0	Air voids (%)	3.5	2016 (initial)	4,000
	Flexible	Default asphalt concrete	2.0			2041 (25 years)	24,837,000
	Flexible	Default asphalt concrete	8.0			2066 (50 years)	63,370,900
	NonStabilized	DGAB	6.0				
Subgrade	A-6	Semi-infinite					

**Table 76. Design inputs for Section 39BS803 on DEL-23 (1 in = 25.4 mm).**

Design Inputs					
Design Life:	50 years	Base construction:	May, 2015	Climate Data	40.078, -83.078
Design Type:	Flexible Pavement	Pavement construction:	June, 2016	Sources	
		Traffic opening:	September, 2016		

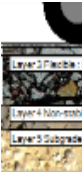
  

Design Structure			Volumetric at Construction:		Traffic		
	Layer type	Material Type	Thickness (in.):	Effective binder content (%)	7.6	Age (year)	Heavy Trucks (cumulative)
	Flexible	Default asphalt concrete	1.0	Air voids (%)	3.5	2016 (initial)	4,000
	Flexible	Default asphalt concrete	2.0			2041 (25 years)	24,837,000
	Flexible	Default asphalt concrete	10.0			2066 (50 years)	63,370,900
	NonStabilized	DGAB	6.0				
Subgrade	A6	Semi-infinite					

**Table 77. Design inputs for Section 39D168 on DEL-23 (1 in = 25.4 mm).**

Design Inputs					
Design Life:	50 years	Base construction:	May, 2015	Climate Data	40.078, -83.078
Design Type:	Flexible Pavement	Pavement construction:	June, 2016	Sources	
		Traffic opening:	September, 2016		

Design Structure			Volumetric at Construction:		Traffic		
	Layer type	Material Type	Thickness (in.):	Effective binder content (%)	7.6	Age (year)	Heavy Trucks (cumulative)
	Flexible	Default asphalt concrete	1.0	Air voids (%)	3.5	2016 (initial)	4,000
	Flexible	Default asphalt concrete	2.0			2041 (25 years)	24,837,000
	Flexible	Default asphalt concrete	12.0			2066 (50 years)	63,370,900
	NonStabilized	DGAB	6.0				
Subgrade	A-6	Semi-infinite					

**Table 78. Design inputs for Section 39P168 on DEL-23 (1 in = 25.4 mm).**

Design Inputs					
Design Life:	50 years	Base construction:	May, 2015	Climate Data	40.078, -83.078
Design Type:	Flexible Pavement	Pavement construction:	June, 2016	Sources	
		Traffic opening:	September, 2016		

Design Structure			Volumetric at Construction:		Traffic	
	Layer type	Material Type	Thickness (in.):	Effective binder content (%)	Age (year)	Heavy Trucks (cumulative)
	Flexible	Default asphalt concrete	1.0	7.6	2016 (initial)	4,000
	Flexible	Default asphalt concrete	2.0	Air voids (%)	2041 (25 years)	24,837,000
	Flexible	Default asphalt concrete	10.0	3.5	2066 (50 years)	63,370,900
	NonStabilized	DGAB	6.0			
Subgrade	A-6	Semi-infinite				

**Table 79. Design inputs for I77 test section (1 in = 25.4 mm).**

Design Inputs					
Design Life:	50 years	Base construction:	May, 2015	Climate Data	40.918, -81.443
Design Type:	Flexible Pavement	Pavement construction:	June, 2016	Sources	
		Traffic opening:	September, 2016		

Design Structure			Volumetric at Construction:		Traffic	
	Layer type	Material Type	Thickness (in.):	Effective binder content (%)	Age (year)	Heavy Trucks (cumulative)
	Flexible	Default asphalt concrete	1.5	5.7	2016 (initial)	4,000
	Flexible	Default asphalt concrete	1.8	Air voids (%)	2041 (25 years)	23,595,200
	Flexible	Default asphalt concrete	13.0	3.5	2066 (50 years)	60,202,300
	NonStabilized	DGAB	6.0			
Subgrade	A-6	Semi-infinite				

**Table 80. Design inputs for US30 test section (1 in = 25.4 mm).**

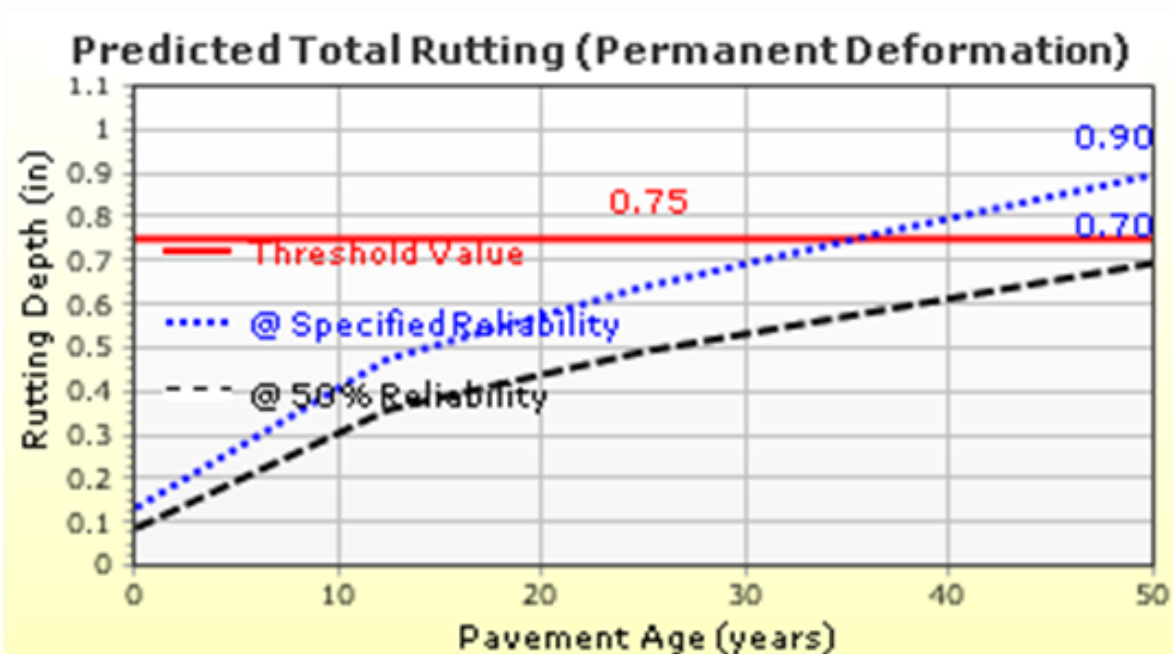
Design Inputs					
Design Life:	50 years	Base construction:	May, 2015	Climate Data	40.875, -81.887
Design Type:	Flexible Pavement	Pavement construction:	June, 2016	Sources	
		Traffic opening:	September, 2016		

Design Structure			Volumetric at Construction:		Traffic	
	Layer type	Material Type	Thickness (in.):	Effective binder content (%)	Age (year)	Heavy Trucks (cumulative)
	Flexible	Default asphalt concrete	1.5	6.6	2016 (initial)	4,000
	Flexible	Default asphalt concrete	1.8	Air voids (%)	2041 (25 years)	24,837,000
	Flexible	Default asphalt concrete	13.0	3.5	2066 (50 years)	63,370,900
	NonStabilized	DGAB	6.0			
Subgrade	A-6	Semi-infinite				

**Table 81. Distress prediction summary for Section 39BN803 on DEL-23 (1 in/mile = 15.78 mm/km =  $1.578 \times 10^{-5}$ ; 1 in = 25.4 mm; 1ft/mile = 18.94 cm/km =  $1.894 \times 10^{-4}$ ).**

Distress Prediction Summary					
Distress Type	Distress @ Specified Reliability		Reliability (%)		Criterion Satisfied?
	Target	Predicted	Target	Achieved	
Terminal IRI (in./mile)	172.00	256.05	90.00	28.21	Fail
Permanent deformation - total pavement (in.)	0.75	0.90	90.00	62.13	Fail
AC bottom-up fatigue cracking (percent)	25.00	2.37	90.00	100.00	Pass
AC thermal cracking (ft/mile)	1000.00	26.29	90.00	100.00	Pass
AC top-down fatigue cracking (ft/mile)	2000.00	1360.18	90.00	97.09	Pass
Permanent deformation - AC only (in.)	0.25	0.74	90.00	2.21	Fail



**Figure 69. Predicted total rutting for Section 39BN803 on DEL-23 (1in = 25.4 mm).**

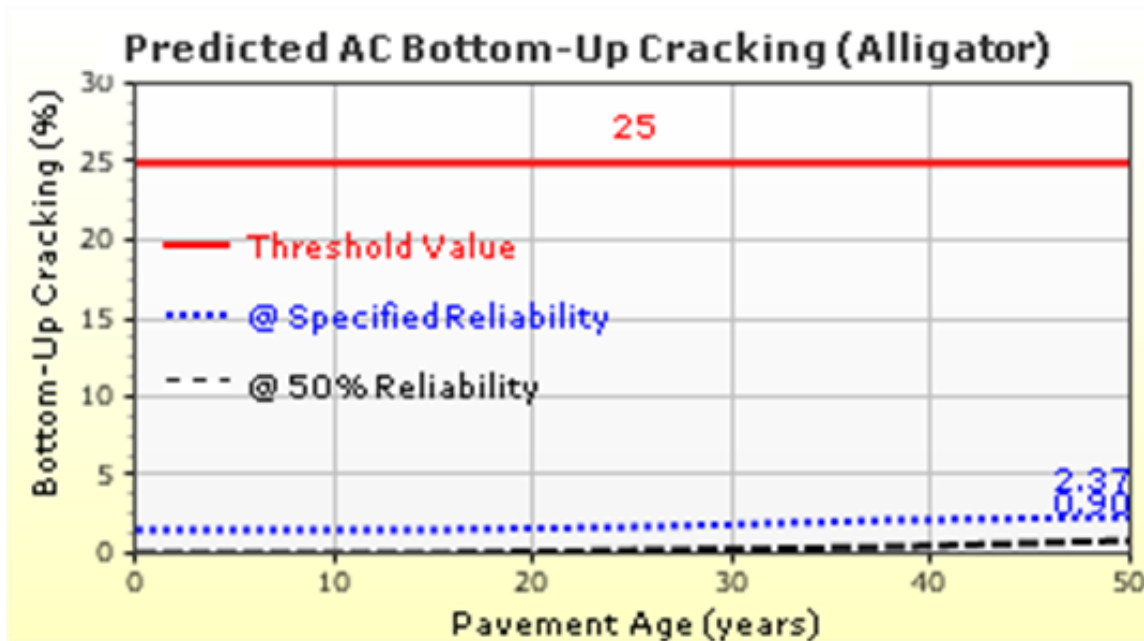


Figure 70. Predicted AC bottom-up cracking for Section 39BN803 on DEL-23.

Table 82. Distress summary for Section 39BS803 on DEL-23 (1 in/mile = 15.78 mm/km=1.578×10<sup>-5</sup>; 1 in = 25.4 mm; 1ft/mile = 18.94 cm/km = 1.894×10<sup>-4</sup>).

Distress Prediction Summary

Distress Type	Distress @ Specified Reliability		Reliability (%)		Criterion Satisfied?
	Target	Predicted	Target	Achieved	
Terminal IRI (in./mile)	172.00	247.28	90.00	33.70	Fail
Permanent deformation - total pavement (in.)	0.75	0.68	90.00	97.02	Pass
AC bottom-up fatigue cracking (percent)	25.00	1.76	90.00	100.00	Pass
AC thermal cracking (ft/mile)	1000.00	26.26	90.00	100.00	Pass
AC top-down fatigue cracking (ft/mile)	2000.00	1336.72	90.00	97.31	Pass
Permanent deformation - AC only (in.)	0.25	0.54	90.00	10.86	Fail



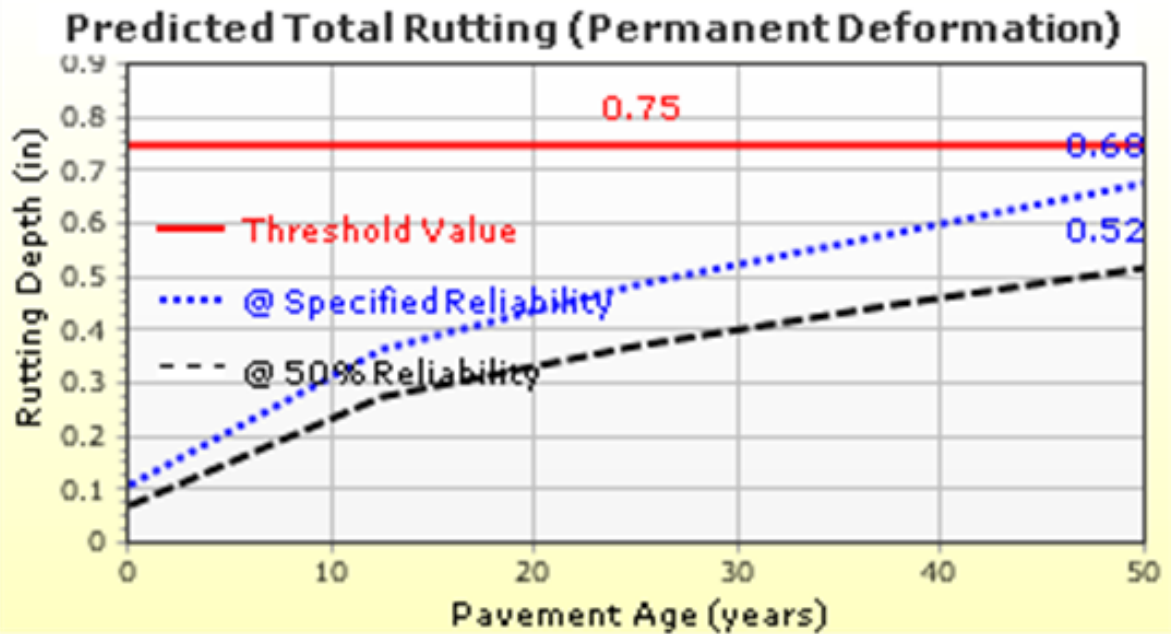


Figure 71. Predicted total rutting for Section 39BS803 on DEL-23 (1in = 25.4 mm).

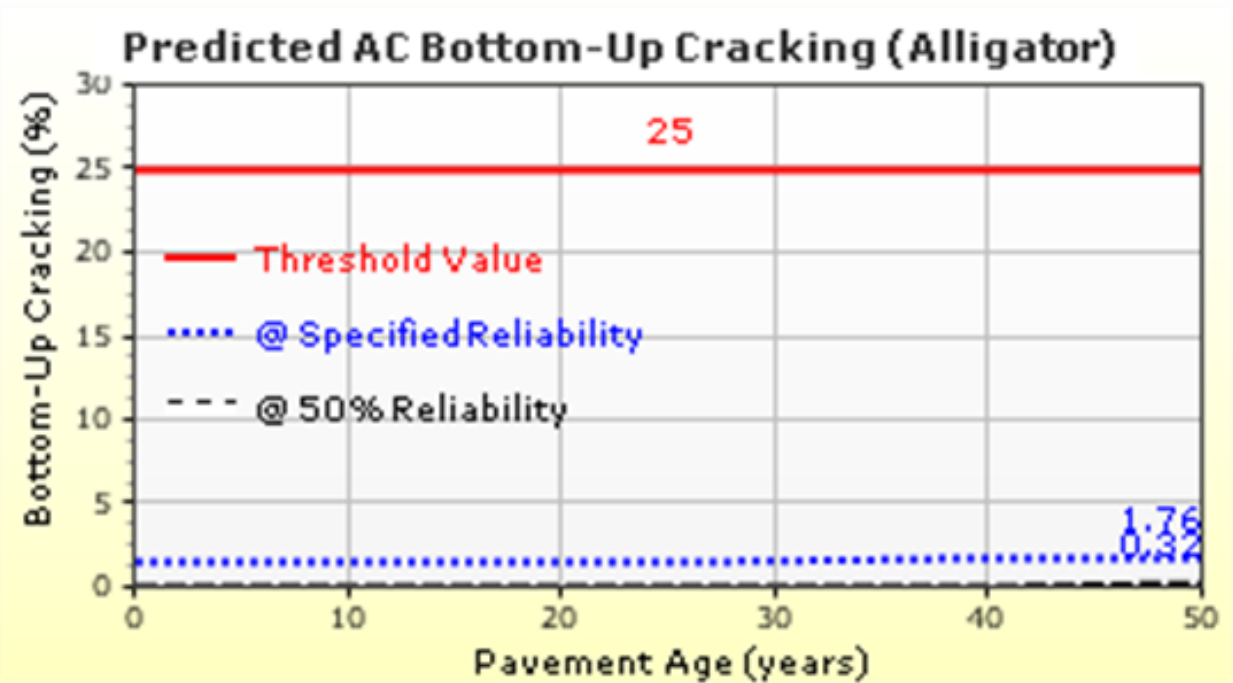
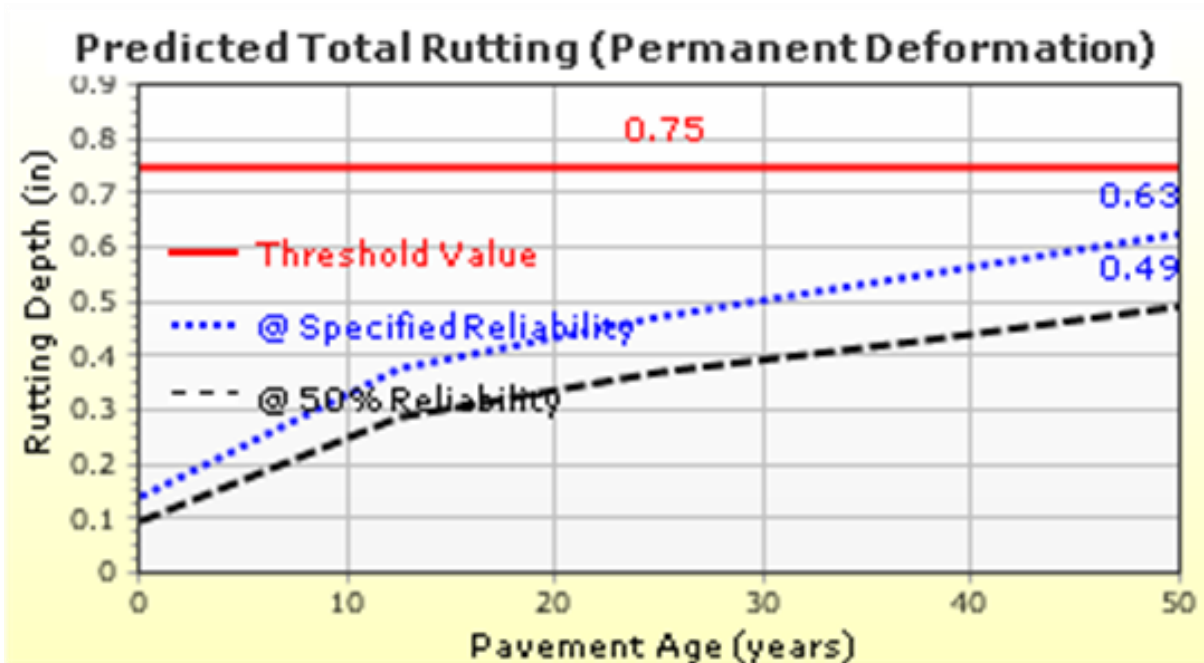


Figure 72. Predicted AC bottom-up cracking for Section 39BS803 on DEL-23.

**Table 83. Distress summary for Section 39D168 on DEL-23 (1 in/mile = 15.78 mm/km = 1.578×10<sup>-5</sup>; 1 in = 25.4 mm; 1ft/mile = 18.94 cm/km = 1.894×10<sup>-4</sup>).**

Distress Prediction Summary					
Distress Type	Distress @ Specified Reliability		Reliability (%)		Criterion Satisfied?
	Target	Predicted	Target	Achieved	
Terminal IRI (in./mile)	172.00	245.94	90.00	34.56	Fail
Permanent deformation - total pavement (in.)	0.75	0.63	90.00	99.20	Pass
AC bottom-up fatigue cracking (percent)	25.00	1.74	90.00	100.00	Pass
AC thermal cracking (ft/mile)	1000.00	26.23	90.00	100.00	Pass
AC top-down fatigue cracking (ft/mile)	2000.00	288.94	90.00	100.00	Pass
Permanent deformation - AC only (in.)	0.25	0.42	90.00	30.12	Fail



**Figure 73. Predicted total rutting for Section 39D168 on DEL-23 (1in = 25.4 mm).**

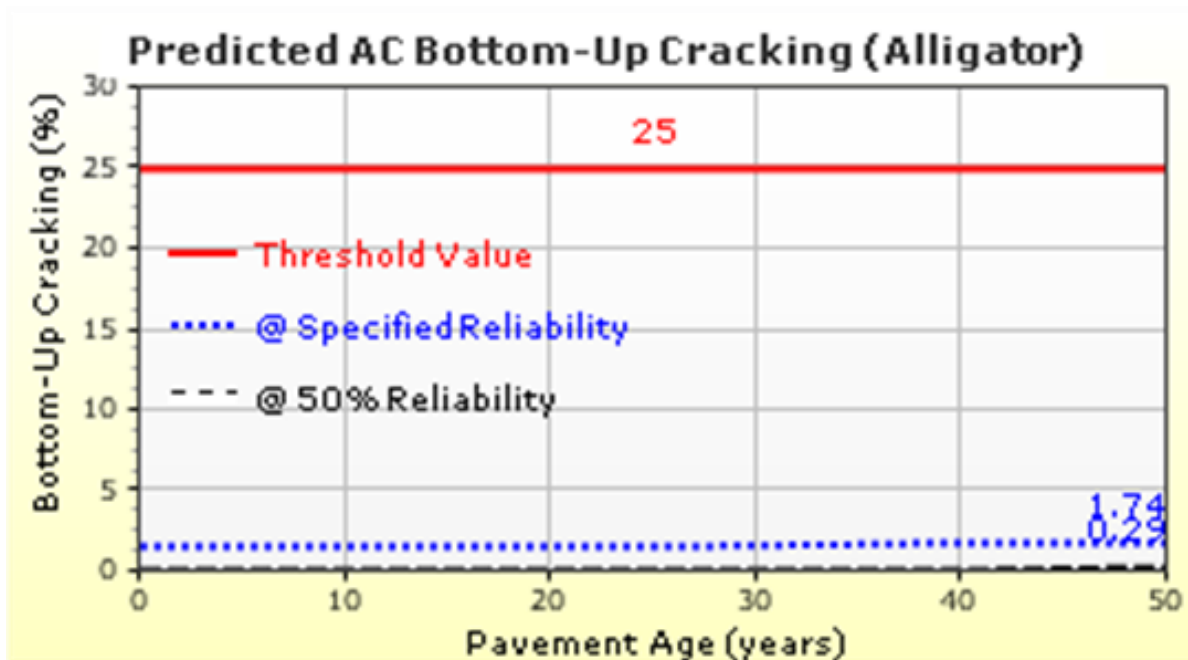


Figure 74. Predicted AC bottom-up cracking for Section 39D168 on DEL-23.

Table 84. Distress summary for Section 39P168 on DEL-23 (1 in/mile = 15.78 mm/km = 1.578×10<sup>-5</sup>; 1 in = 25.4 mm; 1ft/mile = 18.94 cm/km = 1.894×10<sup>-4</sup>).

Distress Prediction Summary					
Distress Type	Distress @ Specified Reliability		Reliability (%)		Criterion Satisfied?
	Target	Predicted	Target	Achieved	
Terminal IRI (in./mile)	172.00	251.31	90.00	31.03	Fail
Permanent deformation - total pavement (in.)	0.75	0.77	90.00	87.40	Fail
AC bottom-up fatigue cracking (percent)	25.00	2.08	90.00	100.00	Pass
AC thermal cracking (ft/mile)	1000.00	26.26	90.00	100.00	Pass
AC top-down fatigue cracking (ft/mile)	2000.00	547.49	90.00	100.00	Pass
Permanent deformation - AC only (in.)	0.25	0.53	90.00	11.15	Fail

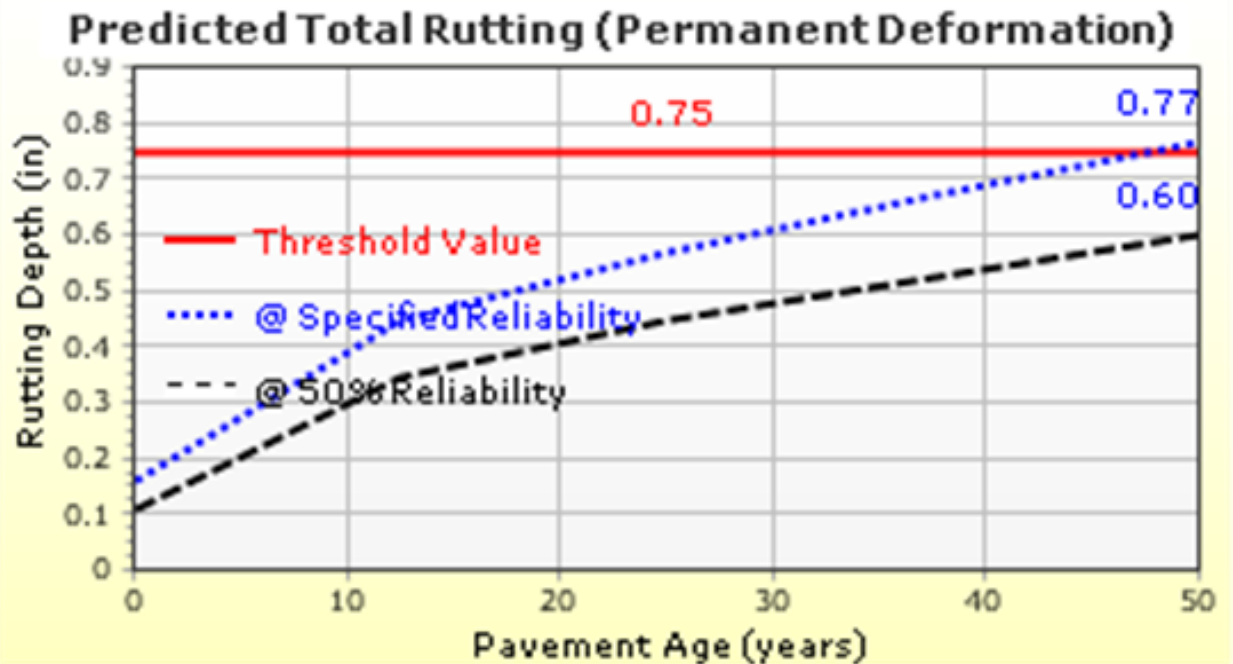


Figure 75. Predicted total rutting for Section 39P168 on DEL-23 (1in = 25.4 mm).

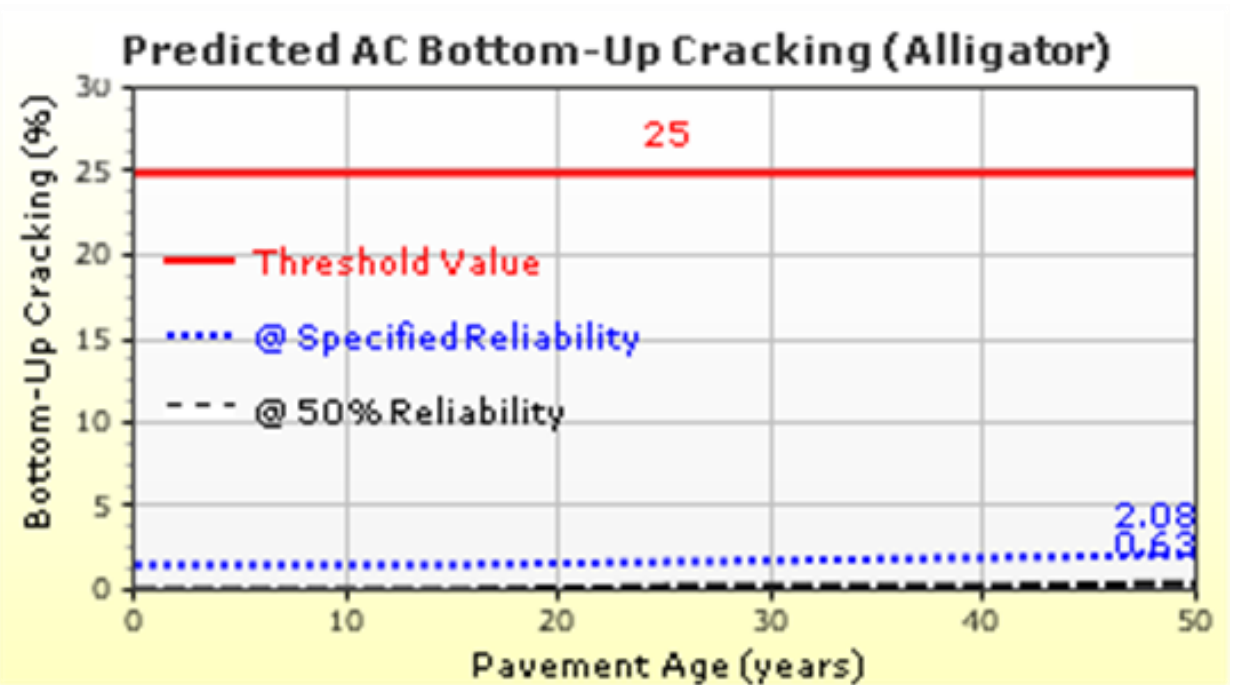
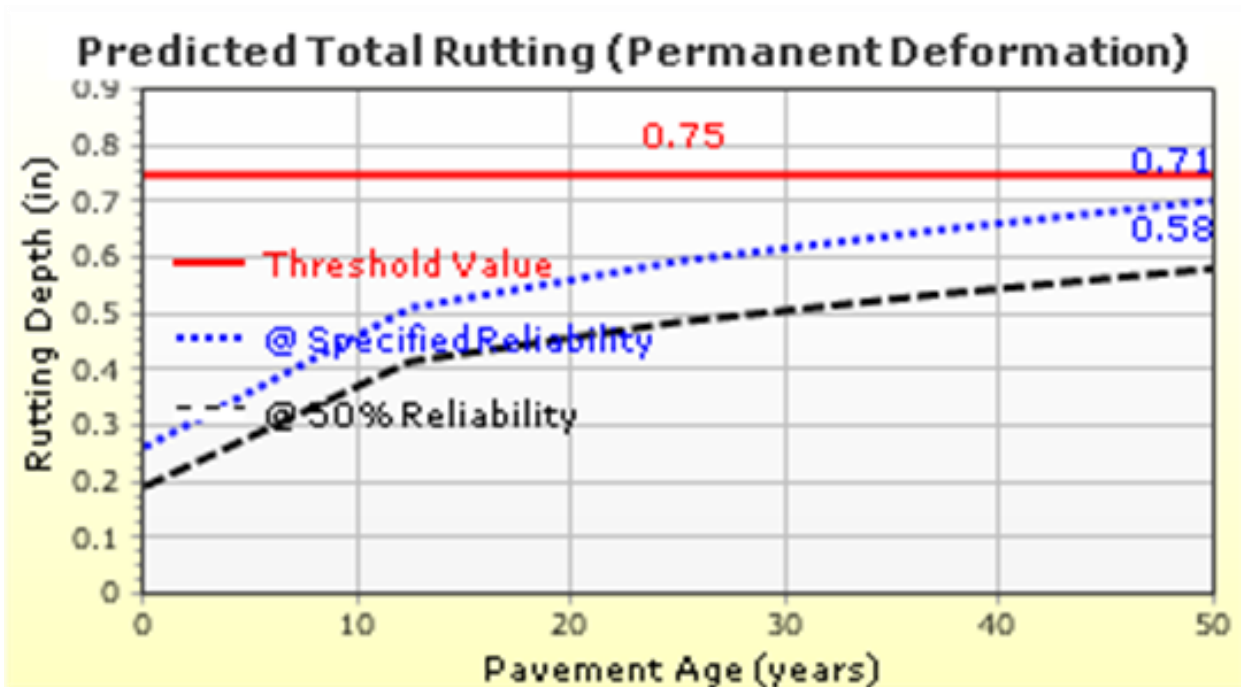


Figure 76. Predicted AC bottom-up cracking for Section 39P168 on DEL-23.

**Table 85. Distress summary for STA-77 test section (1 in/mile = 15.78 mm/km = 1.578×10<sup>-5</sup>; 1 in = 25.4 mm; 1ft/mile = 18.94 cm/km = 1.894×10<sup>-4</sup>).**

Distress Prediction Summary					
Distress Type	Distress @ Specified Reliability		Reliability (%)		Criterion Satisfied?
	Target	Predicted	Target	Achieved	
Terminal IRI (in./mile)	172.00	258.71	90.00	26.44	Fail
Permanent deformation - total pavement (in.)	0.75	0.71	90.00	95.82	Pass
AC bottom-up fatigue cracking (percent)	25.00	2.22	90.00	100.00	Pass
AC thermal cracking (ft/mile)	1000.00	27.82	90.00	100.00	Pass
AC top-down fatigue cracking (ft/mile)	2000.00	257.84	90.00	100.00	Pass
Permanent deformation - AC only (in.)	0.25	0.23	90.00	95.52	Pass



**Figure 77. Predicted total rutting for STA-77 test section (1in = 25.4 mm).**

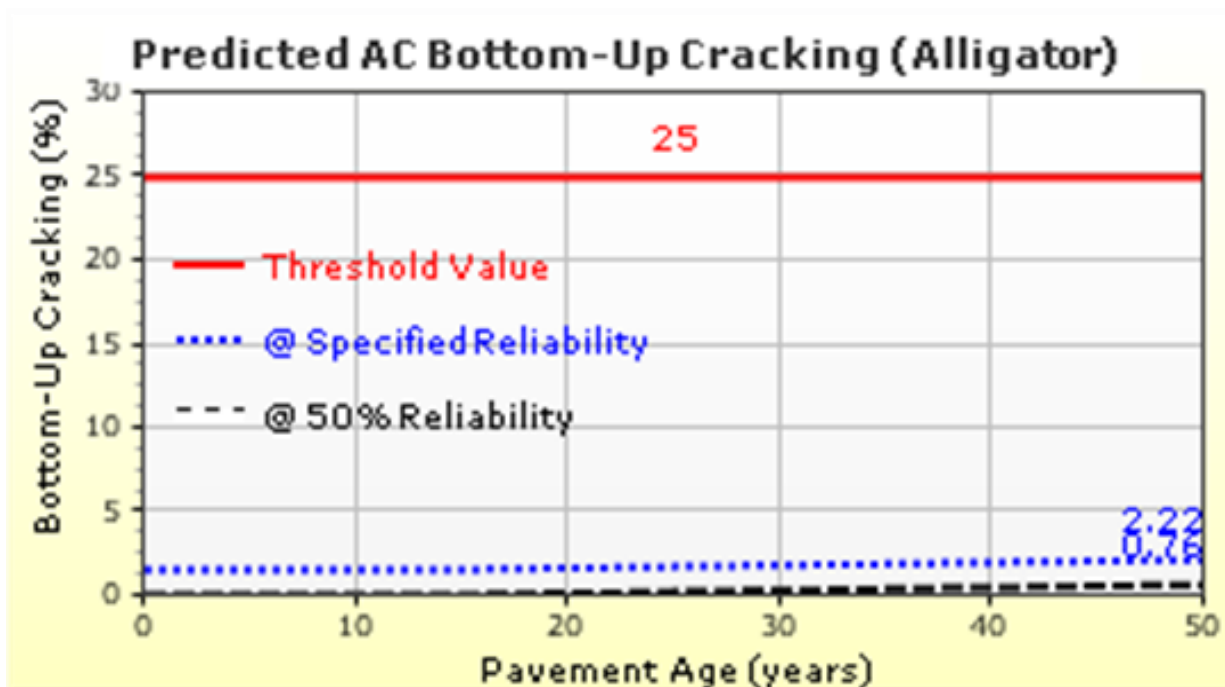


Figure 78. Predicted AC bottom-up cracking for STA-77 test section.

Table 86. Distress summary for WAY-30 test section (1 in/mile = 15.78 mm/km = 1.578×10<sup>-5</sup>; 1 in = 25.4 mm; 1ft/mile = 18.94 cm/km = 1.894×10<sup>-4</sup>).

Distress Prediction Summary					
Distress Type	Distress @ Specified Reliability		Reliability (%)		Criterion Satisfied?
	Target	Predicted	Target	Achieved	
Terminal IRI (in./mile)	172.00	262.45	90.00	24.33	Fail
Permanent deformation - total pavement (in.)	0.75	0.84	90.00	69.77	Fail
AC bottom-up fatigue cracking (percent)	25.00	2.73	90.00	100.00	Pass
AC thermal cracking (ft/mile)	1000.00	43.33	90.00	100.00	Pass
AC top-down fatigue cracking (ft/mile)	2000.00	258.02	90.00	100.00	Pass
Permanent deformation - AC only (in.)	0.25	0.32	90.00	62.31	Fail

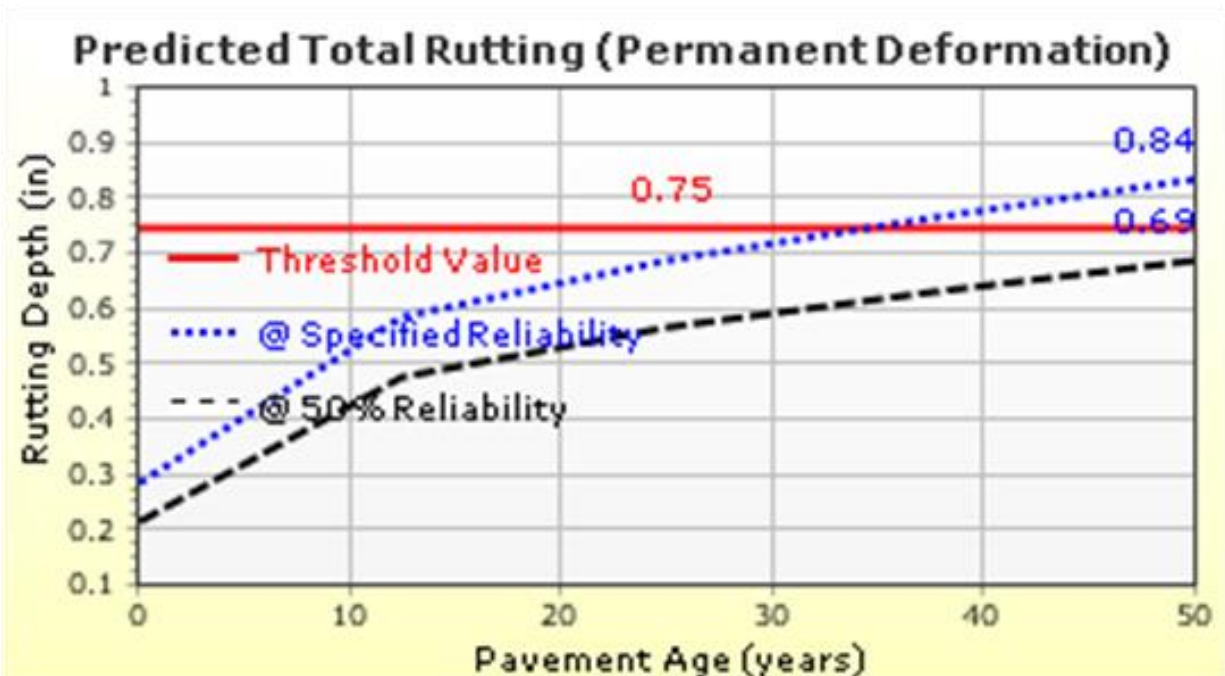


Figure 79. Predicted total rutting for WAY-30 test section (1in = 25.4 mm).

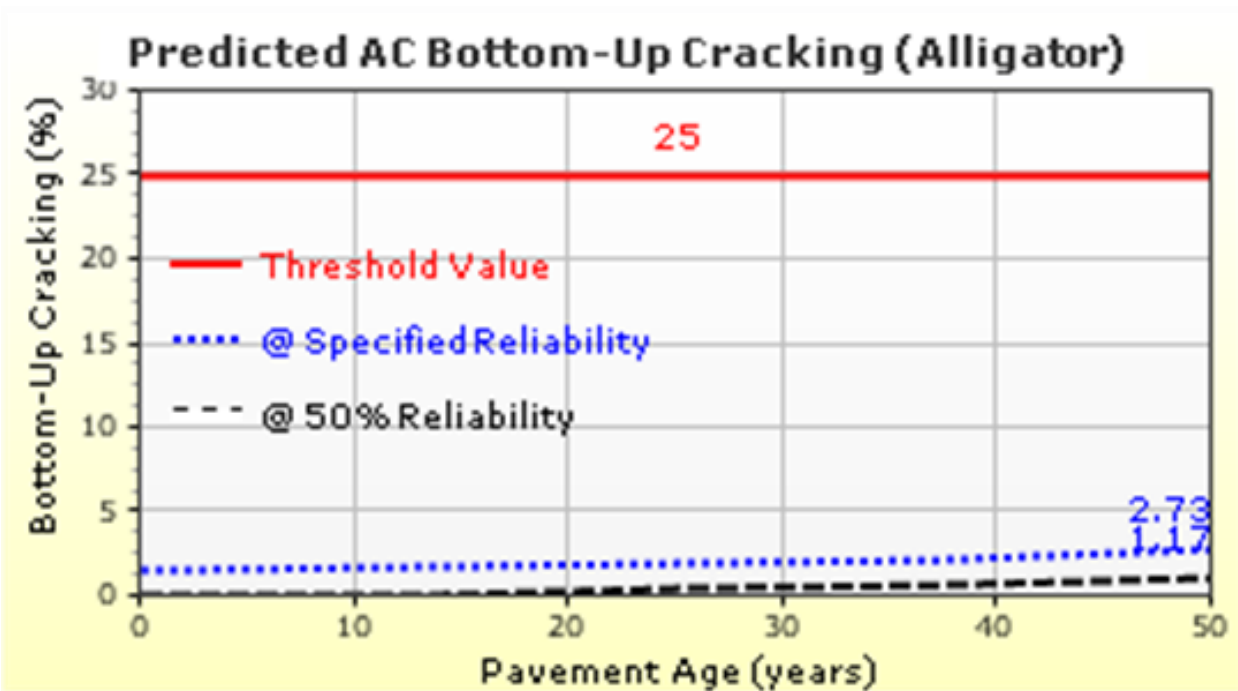


Figure 80. Predicted AC bottom-up cracking for WAY-30 test section.

### 12.3 Summary

The AASHTOWare Pavement ME Design software used in the preceding analysis was not calibrated for Ohio, instead the national or global calibration factors were used in this analysis. Material properties, traffic and weather data were those of the actual projects analyzed.

The ME software was used to compare the performance of the sections against each other and not necessarily to verify actual field performance. In this analysis, as presented by the data above, section 39BN803 (11 in (28 cm) thick pavement) performed poorly compared to the other thicker sections, but could still be considered a perpetual section according to the program. When the actual field strain data was analyzed it showed the 11 in (28 cm) section could not be considered a perpetual pavement section. More importantly, the predicted performance ranking of the test sections was similar to the results observed in the field.



## 13 Asphalt Perpetual Pavement Design: Utilizing Existing Pavement Systems

Sargand and Edwards (2010) conducted a forensic study on flexible and rigid pavements in Ohio. Specifically, pavements classified as “Excellent” and “Average” by the Ohio Department of Transportation (ODOT) were thoroughly investigated. The goal of the research was to determine what factors made the pavements perform well. Twenty asphalt sections were chosen for analysis, as listed in Table 87. Ten of these were rated “Excellent”, as listed in Table 88, and were built from materials listed in Table 89. These sections were distributed across Ohio, as shown in Figure 81, and varied in asphalt and aggregate base thickness, as listed in Table 88. Pavement cores were drilled out of each site to measure the layer thicknesses and test the strength properties in the laboratory. FWD tests were performed but no thorough analyses were conducted on the FWD results. Dynamic Cone Penetrometer (DCP) was used to test the stiffness of the base and subgrade materials. This project did not include determining whether or not the asphalt pavements were perpetual. By revisiting some of the same sites, verifying previous results, and analyzing new results from the forensic study, conclusions could be made regarding a pavement’s perpetual status. This forensic investigation was very useful in identifying excellent performing asphalt pavements and collecting valuable data, but much more in-depth analyses needs to be performed in order to make a better determination on an asphalt pavement’s performance. In 2012, five of those sites were revisited to perform additional tests, collect more samples, and verify test results. The following field and laboratory tests were used to analyze and interpret pavement performance:

- Falling Weight Deflectometer (FWD)
- Dynamic Cone Penetrometer (DCP)
- Portable Seismic Property Analyzer (PSPA)
- Indirect Tensile Strength Test (IDT)
- Resilient Modulus (E) Test

### ***13.1 Pavements selected for further analysis as perpetual pavement candidates***

The five pavements selected for follow-up visits were chosen based on a ranking system that took into account average daily traffic (ADT) from Class B&C commercial vehicles (“trucks”), subgrade modulus ( $M_R$ ), Falling Weight Deflectometer (FWD), rutting, Indirect Tensile Strength (ITS), Poisson’s Ratio, and Resilient Modulus. Each site was ranked for each test/property then averaged at the end to determine the best performing sites based on the original forensic investigation. Specifically, the IDT test was used to compare previous results to the present results found after the site selection. Table 90 and Table 91 show the results of the tests performed in 2010, the ranks of each test and the overall ranking of the sites in Table 92 and Table 93, respectively.

**Table 87. Flexible pavements selected for forensic investigation (Edwards & Sargand, 2010).**

County-Route	Straight Line Length (mi (km))	Direction	Age (years)	Condition
BUT 129	22 (35)	W	14	Average
BUT 129	25 (40)	W	14	Average
BUT 129	22 (35)	E	14	Excellent
CHP 68	2.5 (4.0)	N	14	Average
CHP 68	2 (3.2)	N	14	Excellent
CLA 41	4 (6.4)	N	17	Average
CLA 41	3 (4.8)	N	17	Excellent
DEL 23	18 (29)	S	18	Average
DEL 23	17 (27)	S	18	Excellent
GRE 35	21 (34)	E	14	Excellent
HAM 126	11 (18)	E	18	Excellent
HAM 747	1 (1.6)	S	27	Average
LAW 7	2 (3.2)	N	27	Average
LUC 2	22 (35)	E	13	Average
LUC 25	10 (16)	S	15	Excellent
PIK 32	19 (31)	W	17	Average
PIK 32	15 (24)	W	18	Excellent
PIK 32	19 (31)	E	17	Excellent
ROS 35	1 (1.6)	W	16	Excellent
VAN 30	18 (29)	E	15	Average

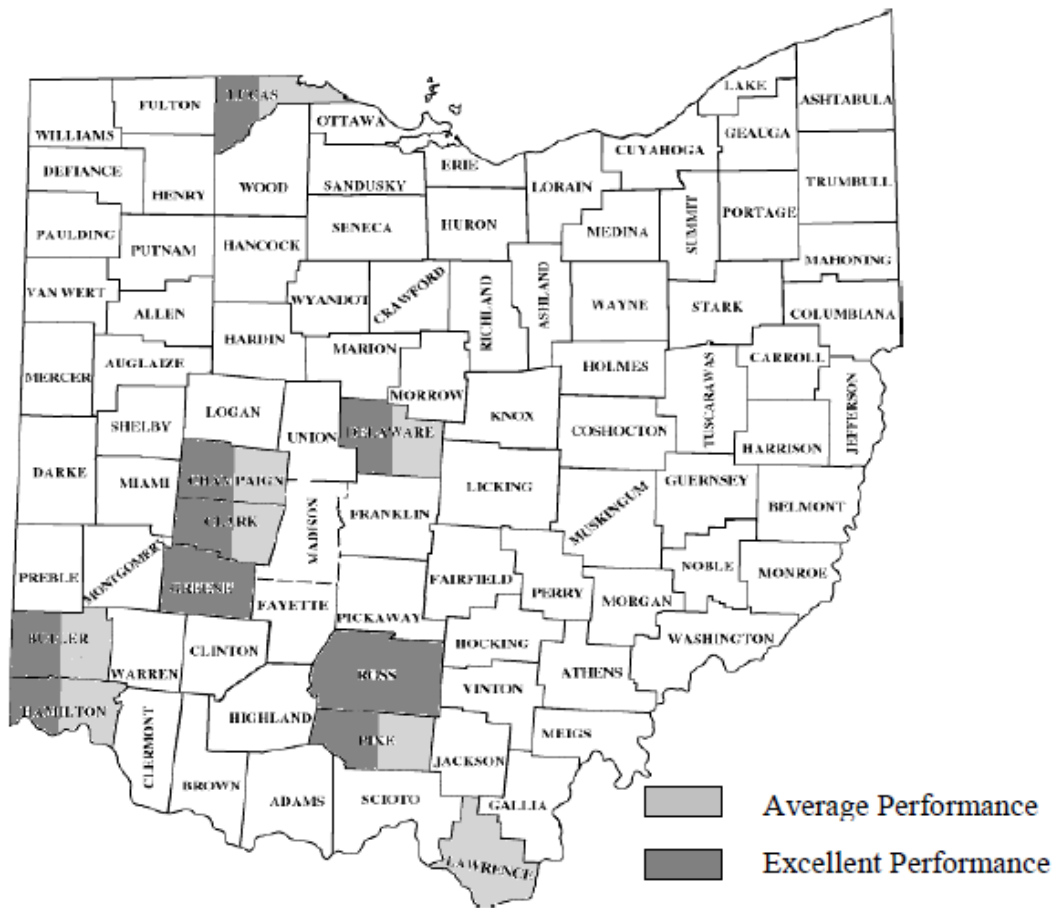
**Table 88. Layer characterization of “Excellent” rated sites (Edwards & Sargand, 2010). For each layer, thickness is given in in (cm) followed by ODOT item number, listed in Table 89.**

Site	Layers					
	Surface	Interm.	Base	Agg. Base 1	Agg. Base 2	Subgrade
	1	2	3	4	5	6
BUT-129-22E	1.25 in (3.18 cm) 446 T1	1.75 in (4.44 cm) 446 T2	10.00 in (25.40 cm) 302	4.00 in (10.16 cm) ATB	- -	- -
CHP-68-2N	1.50 in (3.81 cm) 448 T1H	1.75 in (4.44 cm) 448 T2	6.00 in (40.64 cm) 301	4.00 in (10.16 cm) 304	- -	- -
CLA-41-3N	1.25 in (3.18 cm) 404	1.75 in (4.44 cm) 402	7.00 in (17.78 cm) 301	5.00 in (12.70 cm) 304	- -	- -
DEL-23-17S	1.75 in (4.44 cm) 446 T1 PG 58-30	2.25 in (5.72 cm) 446 T2 PG 58-30	12.00 in (30.48 cm) 302 -	4.00 in (10.16 cm) ATB -	6.00 in (40.64 cm) 304 -	- - -
GRE-35-21E	1.50 in (3.81 cm) 448 T1H	1.75 in (4.44 cm) 448 T2	7.50 in (19.05 cm) 301	6.00 in (40.64 cm) 304	- -	- -
HAM-126-11E	1.50 in (3.81 cm) 446 T1	1.75 in (4.44 cm) 446 T2	7.50 in (19.05 cm) 301	6.00 in (40.64 cm) 304	6.00 in (40.64 cm) 310	6.00 in (40.64 cm) 206
LUC-25-10S	1.25 in (3.18 cm) 446 T1	1.75 in (4.44 cm) 446 T2	7.00 in (17.78 cm) 301	8.00 in (20.32 cm) 304	6.00 in (40.64 cm) 310	- -
PIK-32-15W	1.25 in (3.18 cm) 446 T1	1.75 in (4.44 cm) 446 T2	9.00 in (22.86 cm) 301	4.00 in (10.16 cm) ATB	6.00 in (40.64 cm) 304	- -
PIKE-32-19E	1.25 in (3.18 cm) 446 T1	1.75 in (4.44 cm) 446 T2	12.00 in (30.48 cm) 301	4.00 in (10.16 cm) ATB	4.00 in (10.16 cm) 310	- -
ROS-35-1W	1.25 in (3.18 cm) 446 T1	1.75 in (4.44 cm) 446 T2	10.00 in (25.40 cm) 301	4.00 in (10.16 cm) 307 NJ	8.00 in (20.32 cm) 304	8.00 in (20.32 cm) 206

(1 inch = 2.54 cm)

**Table 89. ODOT classifications for AC pavement materials (Edwards & Sargand, 2010).**

ODOT Item Number	Title
206	Chemically Stabilized Subgrade
301	Asphalt Concrete Base
302	Asphalt Concrete Base
304	Aggregate Base
307 NJ	Non-Stabilized Drainage Base
310	Aggregate Sub-Base
ATB	Asphalt Treated Base
402	Asphalt Concrete Mixing Plants
404	Asphalt Concrete Mixing Plants
446 T1	Surface Asphalt Concrete
446 T2	Intermediate Asphalt Concrete
448 T1H	Surface Asphalt Concrete
448 T2	Intermediate Asphalt Concrete



**Figure 81. Geographical distribution of selected asphalt pavements (Edwards & Sargand, 2010).**

**Table 90. Test results from forensic investigation (Edwards & Sargand, 2010), English units.**

Location	B&C ADT	M <sub>R</sub>	FWD	Rutting	ITS (TSR %)			Poisson's Ratio			E (ksi)		
		(ksi)	(in/kip)	(in)	Surface	Intermediate	AC Base	41 °F	77 °F	104 °F	41 °F	77 °F	104 °F
BUT 129-22E	2375	349	0.25	0.03	88.5	68.2	76.1	0	0.25	0.27	1416	1124	536
CHP 68-2N	1210	187	0.75	0.09	73.5	94.2	59.2	0.08	0.4	0.5	1210	480	422
CLA 41-3N	425	37.5	-	0.09	80.1	69.7	78.6	0.03	0.25	0.28	1209	830	359
DEL 23-17S	2460	41	0.42	0.06	70.9	69.6	62.6	0.11	0.25	0.34	2162	987	555
GRE 35-21E	2760	115	0.94	0.02	89.6	63.8	72.1	0.06	0.36	0.5	1190	676	262
HAM 126-11E	1750	193	0.58	0.13	54.6	59.7	81.6	N/A	N/A	N/A	N/A	N/A	N/A
LUC 25-10S	290	449	0.46	0.06	99.2	96.4	76.9	0.04	0.45	0.5	1198	577	311
PIK 32-15W	1210	151	0.37	0.03	70.5	75.6	77.2	0.02	0.25	0.44	1160	544	352
PIK 32-19E	1120	65	0.45	0.09	92.3	77.5	75.3	N/A	N/A	N/A	N/A	N/A	N/A
ROS 35-1W	2520	75.7	0.76	0.08	58.9	50.7	61.9	0.04	0.25	0.3	1308	947	511

**Table 91. Test results from forensic investigation (Edwards & Sargand, 2010), metric units.**

Location	B&C ADT	M <sub>R</sub>	FWD	Rutting	ITS (TSR %)			Poisson's Ratio			E (MPa)		
		(MPa)	(mm/kN)	(cm)	Surface	Intermediate	AC Base	5 °C	25 °C	40 °C	5 °C	25 °C	40 °C
BUT 129-22E	2375	2406	1.43	0.08	88.5	68.2	76.1	0	0.25	0.27	9763	7750	3696
CHP 68-2N	1210	1289	4.28	0.23	73.5	94.2	59.2	0.08	0.4	0.5	8343	3309	2910
CLA 41-3N	425	259	-	0.23	80.1	69.7	78.6	0.03	0.25	0.28	8336	5723	2475
DEL 23-17S	2460	283	2.40	0.15	70.9	69.6	62.6	0.11	0.25	0.34	14906	6805	3827
GRE 35-21E	2760	793	5.37	0.05	89.6	63.8	72.1	0.06	0.36	0.5	8205	4661	1806
HAM 126-11E	1750	1331	3.31	0.33	54.6	59.7	81.6	N/A	N/A	N/A	N/A	N/A	N/A
LUC 25-10S	290	3096	2.63	0.15	99.2	96.4	76.9	0.04	0.45	0.5	8260	3978	2144
PIK 32-15W	1210	1041	2.11	0.08	70.5	75.6	77.2	0.02	0.25	0.44	7998	3751	2427
PIK 32-19E	1120	448	2.57	0.23	92.3	77.5	75.3	N/A	N/A	N/A	N/A	N/A	N/A
ROS 35-1W	2520	522	4.34	0.20	58.9	50.7	61.9	0.04	0.25	0.3	9018	6529	3523

**Table 92. Ranking (1-10) of each test for each site in 2010.**

Location	B&C ADT	M <sub>R</sub>	FWD	Rut	ITS (TSR %)			Poisson's Ratio			E			Avg. Rank
					Surface	IM	AC Base	T <sub>low</sub>	T <sub>med</sub>	T <sub>high</sub>	T <sub>low</sub>	T <sub>med</sub>	T <sub>high</sub>	
BUT 129-22E	4	2	1	2	4	7	5	1	1	1	2	1	2	2.42
CHP 68-2N	6	4	7	7	6	2	10	7	7	6	4	8	4	6.00
CLA 41-3N	9	10	#N/A	7	5	5	2	3	1	2	5	4	5	4.83
DEL 23-17S	3	9	3	4	7	6	8	8	1	4	1	2	1	4.50
GRE 35-21E	1	6	9	1	3	8	7	6	6	6	7	5	8	6.00
HAM 126-11E	5	3	6	10	10	9	1	#N/A	#N/A	#N/A	#N/A	#N/A	#N/A	6.29
LUC 25-10S	10	1	5	4	1	1	4	4	8	6	6	6	7	4.42
PIK 32-15W	6	5	2	2	8	4	3	2	1	5	8	7	6	4.42
PIK 32-19E	8	8	4	7	2	3	6	#N/A	#N/A	#N/A	#N/A	#N/A	#N/A	5.00
ROS 35-1W	2	7	8	6	9	10	9	4	1	3	3	3	3	5.50

**Table 93. Overall rankings of sites from forensic investigation in 2010.**

Rank	Location	Revisited 2012
1	<b>BUT 129-22E</b>	Yes
2	<b>PIK 32-15W</b>	Yes
3	<b>LUC 25-10S</b>	Yes
4	DEL 23-17S	No
5	<b>CLA 41-3N</b>	Yes
6	PIK 32-19E	No
7	ROS 35-1W	No
8	<b>GRE 35-21E</b>	Yes
9	CHP 68-2N	No
10	HAM 126-11E	No

The bold sites within Table 93 were chosen to perform another set of forensic investigations. These particular sites were chosen to get a good mixture of performance expectations. The falling weight deflectometer, portable seismic property analyzer, rut depth measurements, pavement distress survey mapping, and the Indirect Tensile Strength (ITS) would be performed to confirm that the pavement structure had not changed since the Forensic Investigation in 2010.

IDT testing was used to compare results from the previous ITS data from the forensic investigation in 2010 to the ITS results found in this study. If the two tests had similar results, then the previous data found in the 2010 forensic investigation would be valid and could be used for this analysis. Wet samples were conditioned by vacuum saturation followed by an extensive freeze-thaw process, then tested at 25° C (77°F). Dry samples were not conditioned and were tested at 25° C (77°F). Tensile Strength Ratio (TSR) is the ratio of the wet tensile strength to the dry tensile strength in percent. A statistical analysis was performed comparing the results of the ITS from 2010 and 2012. In short, the ITS correlated very well between the two tests. Since there was a strong correlation between the two tests, further investigation of these sites that were rated “excellent” can be performed using the data from the Ohio Forensic Investigation of AC Pavements in 2010 (Sargand and Edwards, 2010).

### **13.2 Site Investigations**

The five sites that were selected from the Forensic Investigation in 2010 were revisited and similar forensic activities were performed on each, including coring, rut depth measurements, and FWD measurements, but not sub-base and subgrade sampling, since those materials likely did not change over the course of two years. On the same note, Dynamic Cone Penetrometer (DCP) testing was not carried out on the five selected sites for the same reason. However, the Portable Seismic Property Analyzer (PSPA), which measures a material’s ability to resist change in length due to seismic loading, was included in these site investigations. The site investigations included the following procedures:

- Find and locate sections based on county and mile markings alongside roadway.
- Perform cracking survey.
- Locate sampling points (typically 10 to 11 locations).
- FWD testing performed by ODOT at sample points.

- Perform PSPA test at sampling point.
- Drill cores at sampling points for visual investigation and further laboratory testing.

The following sites were revisited:

- Pike County, State Route 32, Mile Marker 15, Westbound (PIK 32-15W)
- Greene County, U.S. 35, Mile Marker 21, Eastbound (GRE 35-21E)
- Lucas County, State Route 25, Mile Marker 10, Southbound (LUC 25-10S)
- Clark County, State Route 41, Mile Marker 3, Northbound (CLA 41-3N)
- Butler County, State Route 129, Mile Marker 22, Eastbound (BUT 129-22E)

The following is a brief description of each site and assessment of its condition at the time it was revisited.

### 13.2.1 PIK 32-15W

This section of State Route 32 in Pike County is located in the South Central portion of Ohio, just west of U.S. 23. The road is known for its deep strength asphalt pavement. The current pavement structure on State Route 32 was constructed in 1994, making it 18 years old during the time of testing. A photograph of the site is given in Figure 82. Traffic studies show that the site was receiving an Average Daily Traffic (ADT) count of 1210 Class B & C vehicles (“trucks”) per day (Edwards and Sargand, 2010). The pavement appeared to be in decent condition, showing a few, minor cracks; these minor cracks, such as those shown in Figure 83, did not show any signs of full depth failure.



Figure 82. General view of PIK 32-15W.





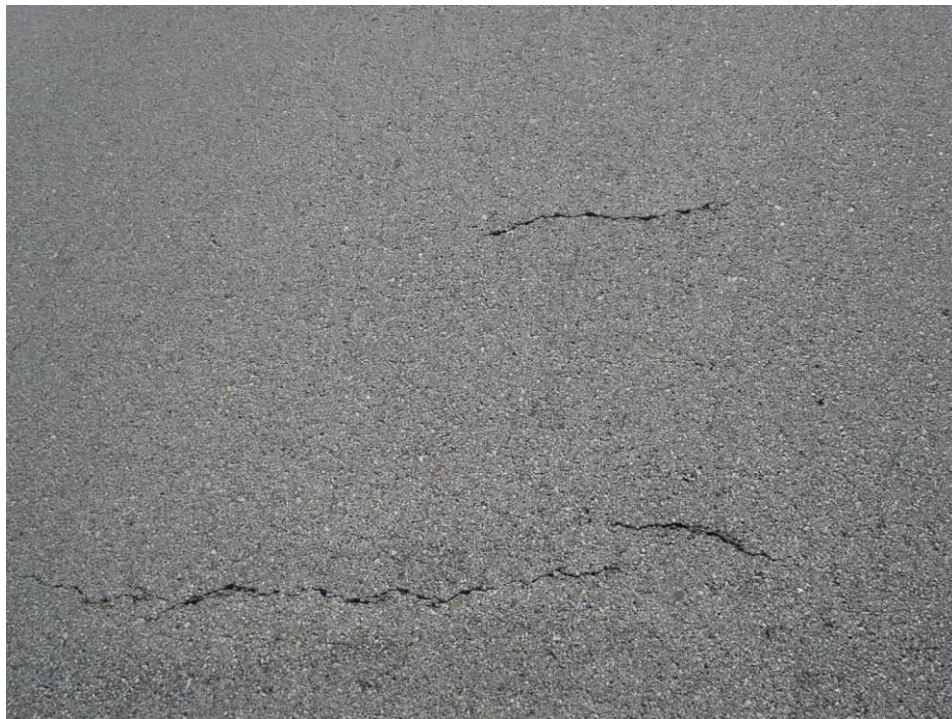
**Figure 83. Cracking on PIK 32-15W.**

### **13.2.2 GRE 35-21E**

This section along U.S. 35 in Greene County is in a rural area but still well-traveled by vehicles. The site is shown in Figure 84. Traffic studies show that the site received an ADT of 2760 Class B & C vehicles per day which was the most of all the sites investigated. The pavement structure was constructed in 1998, making it 14 years old at the time of the investigation. The section had been overlaid since 2010; so layer buildups were slightly different from those recorded in 2010 (Sargand and Edwards, 2010). Even with the recent overlay, small surface cracks were visible; giving evidence that bottom-up cracking occurred and propagated through the overlay. An example is shown in Figure 85.



**Figure 84. General view of GRE 35-21E site.**



**Figure 85. Cracking through recent overlay on GRE 35-21E.**

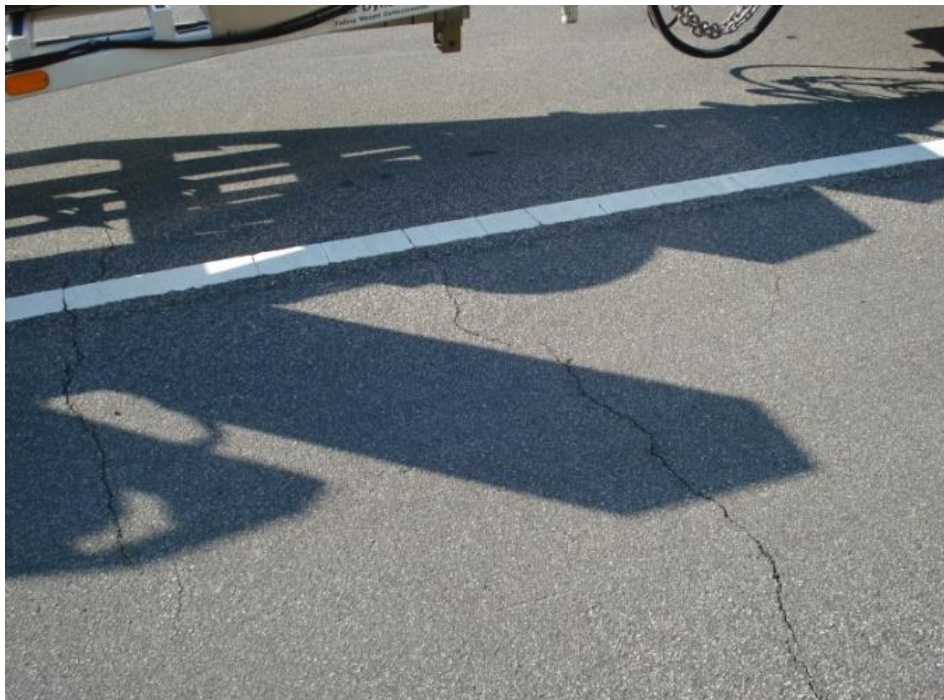
### **13.2.3 LUC 25-10S**

This section on State Route 25 was located on the outer belt of Toledo, Ohio. This had also been recently overlaid, shown in Figure 86. The current pavement structure was constructed in 1997 making it 15 years old during the investigation. Traffic studies show that the pavement

received only 290 Class B & C vehicles per day, which is the least amount of truck traffic of all the sites investigated (Edwards and Sargand, 2010). The original forensic study showed this site to have been almost entirely covered with sealant over the numerous cracks formed. Even after the new overlay, many cracks were present giving possible evidence of bottom up cracking, shown in Figure 87.



**Figure 86. General view of LUC 25-10S.**



**Figure 87. Cracking on LUC 25-10S.**

### **13.2.4 CLA 41-3N**

This section of State Route 41 is located in the middle of the small town of South Charleston, Ohio, near the city of Springfield and located in Clark County in West-Central Ohio. The site is shown in Figure 88. This pavement structure was constructed in 1995 making it 17 years old during the time of the investigation. Traffic studies show that the pavement received an ADT of only 425 Class B & C vehicles per day (Edwards and Sargand, 2010). The site was located right next to a large mill where heavy trucks traveled at low speeds in and out of the mill. This pavement did not pass the “eyeball” test, for it had many surface distresses. However, later tests show that considering the heavy truck abuse, the pavement structure was not in terrible condition and coring showed that bottom up cracking had not occurred. Figure 89 shows some of the distresses that were found.



**Figure 88. General view of CLA 41-3N.**



**Figure 89. Cracking on CLA 41-3N.**

### **13.2.5 BUT 129-22E**

This site on State Route 129 acted as a high-speed bypass in Butler County, near the Cincinnati, Ohio area. There were very few distresses in the pavement and most cracks had been sealed. This site, shown in Figure 90, was heavily traveled yet seemed to be the best pavement structure found in the site investigation. Traffic studies show that the pavement received an ADT of 2375 Class B & C vehicles per day. The pavement structure was constructed in 1998 making it 14 years old during the time of the investigation (Edwards and Sargand, 2010). The asphalt structure was very deep compared to the other sites. Figure 91 shows some of the distresses that were found.



**Figure 90. General view of BUT 129-22E.**



**Figure 91. Cracking on BUT 129-22E.**

### 13.3 Coring

In order to perform some of the laboratory experiments, core samples were removed from the pavements. Also, coring is another way to physically see and measure the various layers in an asphalt pavement structure. Figure 92 shows the core drill trailer in operation collecting a core, Figure 93 shows an example of a core sample and the various layers (surface layer starting on the left).



Figure 92. Using a core drill to obtain a sample core of AC pavement.



Figure 93. Core sample obtained from an AC pavement. The surface is at the left.

### 13.4 Field Testing

This section describes the various field tests performed for this research. Each section briefly describes the test setup as well as some of the theories involved in the data analysis, and displays the results of the tests.

#### 13.4.1 Falling Weight Deflectometer (FWD)

The FWD is a non-destructive testing device used to evaluate a pavement's condition. The ODOT FWD is a truck-trailer setup, where the operator controls the mechanism on the trailer from the truck. The trailer consists of a stack of weights which are lifted and dropped on a circular plate; the plate has a radius of 5.9 in (15 cm). The free-falling weight applies a dynamic load to the pavement structure which simulates a single heavy wheel load. Three different loads typically near 6000 lbs. (27 kN), 9000 lbs. (40 kN), and 12000 lbs. (53 kN), are applied at one location. A series of deflection sensors detect displacements along the pavement based on the applied loads at various radial distances from the applied load typically 0, 12, 24, 36, 48, and 60 inches (0, 30.5, 61, 91.4, 121.9, 152.4 cm). The data is collected by a system processor inside the truck then saved to a laptop (Texas Department of Transportation, 2008). Along with loads and deflections, the software managing the FWD system also records the air temperature.

The Washington State Department of Transportation (2005) has developed some innovative methods in quantifying the condition of pavement. Their program FWD-AREA calculates a deflection basin caused by the dynamic load of the FWD. A deflection basin is a trapezoidal area that develops in the pavement structure due to an applied load. They have also determined that the Modulus of Subgrade Reaction ( $M_R$ ) can be calculated using FWD data. The value of  $M_R$  is directly correlated to the deflection  $D_{24}$  of the sensor located 24 in (61 cm) from the center of the load (WSDOT, 2005).

$$M_R = 9000 * 0.2892 / (D_{24} / 1000)$$

Where:

$D_{24}$  = Measured Deflection from sensor 24 in (61 cm) from the center of the plate (mil)

$M_R$  = Modulus of Subgrade Reaction (psi)

In order to evaluate each layer of the asphalt pavement structure (surface, intermediate, AC base, aggregate base, and subgrade) using FWD data, back-calculation techniques can be applied. Back-calculation techniques are based on a mechanistic evaluation of the FWD results. The basic concept is layer thickness and Poisson's ratio are known and measured deflection basins and calculated deflection basins are matched. This is an iterative process applied until the desired convergence is met. The desired convergence is typically less than 1% and is quantified by Root Mean Square (*RMS*), which is calculated as follows:

$$RMS (\%) = \sqrt{\frac{1}{n_d} * \sum_{i=1}^n \left( \frac{d_{ci} - d_{mi}}{d_{mi}} \right)^2} * 100$$

Where:



$RMS$  = Root Mean Square error (%)  
 $d_{ci}$  = Calculated deflection  
 $d_{mi}$  = Measured deflection  
 $n_d$  = Number of deflection sensors

### 13.4.2 FWD Results

The following tables show the results of the FWD testing. All deflections were normalized to 9000 pounds (40 kN) and averaged for each deflection sensor, as shown in Table 94. Each sensor has a subscript which represents the distance from the center of the load. Table 95 shows the results of  $M_R$  for the subgrade at each site using the procedure described above.

**Table 94. Average FWD deflections Normalized to 9000 lb (40 kN). English units at top, metric units below. Metric subscripts for D indicate distance from center of load plate in mm.**

Site	$D_0$	$D_{12}$	$D_{24}$	$D_{36}$	$D_{48}$	$D_{60}$
	(mil)	(mil)	(mil)	(mil)	(mil)	(mil)
BUT-129-22E	2.21	1.47	1.18	0.98	0.79	0.66
CHP-68-2N	7.08	4.4	3.42	2.68	1.74	0.95
CLA-41-3N	6.43	4.86	3.36	2.22	1.42	0.98
DEL-23-17S	2.5	1.95	1.79	1.65	1.36	0.9
GRE-35-21E	8.05	5.51	3.63	2.35	1.54	1.1
HAM-126-11E	5.04	1.26	1.11	0.98	0.78	0.5
LUC-25-10S	4.4	2.53	1.6	1.12	0.84	0.69
PIK-32-15W	3.42	2.5	1.89	1.43	1.06	0.81
PIK-32-19E	4.07	2.92	2.66	2.38	1.94	1.19
ROS-35-1W	6.1	4.05	3.26	2.62	1.73	0.78

Site	$D_0$	$D_{305}$	$D_{610}$	$D_{914}$	$D_{1219}$	$D_{1524}$
	( $\mu\text{m}$ )	( $\mu\text{m}$ )	( $\mu\text{m}$ )	( $\mu\text{m}$ )	( $\mu\text{m}$ )	( $\mu\text{m}$ )
BUT-129-22E	56.1	37.3	30.0	24.9	20.1	16.8
CHP-68-2N	179.8	111.8	86.9	68.1	44.2	24.1
CLA-41-3N	163.3	123.4	85.3	56.4	36.1	24.9
DEL-23-17S	63.5	49.5	45.5	41.9	34.5	22.9
GRE-35-21E	204.5	140.0	92.2	59.7	39.1	27.9
HAM-126-11E	128.0	32.0	28.2	24.9	19.8	12.7
LUC-25-10S	111.8	64.3	40.6	28.4	21.3	17.5
PIK-32-15W	86.9	63.5	48.0	36.3	26.9	20.6
PIK-32-19E	103.4	74.2	67.6	60.5	49.3	30.2
ROS-35-1W	154.9	102.9	82.8	66.5	43.9	19.8

**Table 95. Average modulus of subgrade reaction for each site.**

Site	Modulus of Subgrade Reaction ( $M_R$ )	
	(ksi)	(MPa)
BUT-129-22E	92	634
CHP-68-2N	32	221
CLA-41-3N	32	221
DEL-23-17S	61	421
GRE-35-21E	30	207
HAM-126-11E	98	676
LUC-25-10S	68	469
PIK-32-15W	57	393
PIKE-32-19E	41	283
ROS-35-1W	33	228

### 13.4.3 Dynamic Cone Penetrometer (DCP)

The Dynamic Cone Penetrometer (DCP) is an in-situ field test used to determine the stiffness of subsurface (aggregate base and subgrade) materials underneath a pavement structure. For this research, the automated DCP was used. The automated DCP is mounted on a trailer and is pulled by a truck. The machine consists of a 5/8 in (1.59 cm) diameter rod that has a cone screwed into the bottom; the cone has a 60 degree angle from base to tip. The DCP has a 17.6 lb (8 kg) weight which is lifted by machine to a height of 22.6 inches (57.4 cm) and dropped in a free fall manner. The weight drives the rod and cone into the subsurface. Small sensors detect and record the distance the cone and rod traveled with each drop, known as the Penetration Rate (PR). (Wu and Sargand, 2007). The following figure displays the described DCP setup.



**Figure 94. Automated DCP in operation.**

The PR values measure the overall stiffness of the subsurface layers and can identify boundaries between layers. Wu and Sargand (2007) proposed the following equation to estimate the California Bearing Ratio (*CBR*):

$$CBR = 435/(PR)^{1.08}$$

Wu and Sargand (2007) also suggested using the *CBR* to determine the resilient modulus  $M_R$  for subsurface layers. The following equation was suggested to estimate  $M_R$  in psi:

$$M_R = 1500 * CBR$$

Wu and Sargand (2007) suggest using a mathematical method for interpreting where the layers are located using DCP data. First, the cumulative area  $A(x)$  under the response curve can be calculated by integrating the response  $R$ :

$$A(x) = \int_0^x R dx$$

The average response  $R_a$  is calculated by:

$$R_a = \frac{1}{a} \int_0^a R dx$$

The cumulative average area  $A_a(x)$  is found using:

$$A_a(x) = R_a * x$$

The difference between the cumulative area and the average cumulative area ( $Z(x)$ ) can be represented by:

$$Z(x) = A(x) - A_a(x)$$

Where:

$PR$  = Penetration Rate (in/blow)

$CBR$  = California Bearing Ratio

$A(x)$  = Cumulative Area

$R$  = Response

$x$  = Distance

$R_a$  = Average Response

$a$  = Maximum Depth Reached

The layers can be interoperated by the change in sign of the  $Z(x)$  function. Therefore, when  $Z(x)$  changes from positive to negative or vice versa along the vertical distance of the study, a change in layer material has occurred. Knowing the locations of the layers can assist in producing average  $M_R$  values for each layer of the subsurface. The results of the DCP field tests are shown in Table 96.

**Table 96. Summary of resilient moduli obtained from DCP data analysis.**

Site	Aggregate Base $M_R$		Subgrade $M_R$	
	(ksi)	(MPa)	(ksi)	(MPa)
BUT-129-22E	N/A	-	65	448
CHP-68-2N	90	621	66	455
CLA-41-3N	48	331	17	117
DEL-23-17S	53	365	20	138
GRE-35-21E	86	593	49	338
HAM-126-11E	71	490	37	255
LUC-25-10S	19	131	N/A	N/A
PIK-32-15W	128	883	89	614
PIKE-32-19E	57	393	25	172
ROS-35-1W	59	407	27	186

#### 13.4.4 Portable Seismic Property Analyzer (PSPA)

The Portable Seismic Property Analyzer (PSPA) test is an in-situ, non-destructive test easily operated in the field. This device consists of a source, two receivers, data acquisition

system, and a laptop connected to the PSPA by a USB cable. The PSPA measures sonic, ultrasonic, and resonant waves. It is capable of testing concrete pavement, asphalt pavement, base, and subgrade materials. Figure 95 displays the PSPA equipment.



**Figure 95. PSPA equipment (Geomeia Research & Development, 2007).**

The source taps the ground surface creating vibrations. These vibrations create waves which travel away from the source through the pavement layer. The PSPA picks up vibrations in the form of P-waves, S-waves, and R-waves. The signal recorded and stored by the data acquisition system. Figure 96 shows the PSPA in operation.



**Figure 96. Field operation of the PSPA on asphalt pavement.**

#### **13.4.4.1 Seismic Modulus**

The seismic modulus is a quantitative measurement of a material's ability to resist change in length. Larger values of seismic modulus indicate stiffer materials. It is calculated by time records of the near and far receivers. The difference in time of the S-wave arrival between the two receivers is measured, along with a known distance between the receivers. These measurements make it possible to calculate the seismic modulus ( $E$ ).

$$E = cV^2 = c \left( \frac{x}{t} \right)^2$$

Where:

$E$  = Seismic modulus

$c$  = Material constant

$V$  = Wave speed

$x$  = Distance between receivers

$t$  = Time difference between arrivals of S-Waves

Seismic modulus and resilient modulus are two different material properties that characterize strength. However, researchers have investigated relationships between the two. Williams and Nazarian (2007) conducted resilient modulus and seismic modulus tests on 30 different specimens. The results showed the seismic modulus was roughly two times the amount of the resilient modulus. They had tested this for different kinds of pavement materials such as aggregate, subgrade, and asphalt. The relationship found (resilient modulus versus seismic modulus) was independent to material type.

PSPA test was performed at various locations along the sites. The test was performed at each location until there were three values of the seismic modulus moderately close to each other; those values were then averaged. Table 97 shows the seismic modulus results of the PSPA tests.

**Table 97. PSPA seismic modulus test results.**

Site	AC seismic modulus	
	(ksi)	(MPa)
BUT-129-22E	2466	17002
CLA-41-3N	1162	8012
GRE-35-21E	748	5157
LUC-25-10S	1337	9218
PIK-32-15W	1936	13348

## 13.5 Laboratory Testing

### 13.5.1 Indirect Tensile Strength (ITS)

The ITS test is a destructive test which examines a pavement material's ability to resist indirect loading. For this research, testing was conducted in accordance to AASHTO 283 "Resistance of Compacted Asphalt Mixtures to Moisture-Induced Damage" (2007). Indirect loads are applied at a constant rate to cylindrical asphalt specimens. The maximum load the specimen receives is recorded and used to calculate ITS. Two characteristics of the ITS test are desired; the Tensile Strength ( $S_t$ ) and the Tensile Strength Ratio ( $TSR$ ). The following equations are used to calculate those two characteristics:

$$S_t = 2P/(\pi tD)$$

$$TSR = S_2/S_1$$

Where:

$S_t$  = Tensile Strength (psi)

$P$  = Maximum Load Recorded (lb)

$t$  = Thickness of Specimen (in)

$D$  = Diameter of Specimen (in)

$TSR$  = Tensile Strength Ratio

$S_1$  = Average Tensile Strength of Dry Specimens (psi)

$S_2$  = Average Tensile Strength of Conditioned Specimens (psi)

The results of the ITS test can be seen in Table 98 and Table 99. Both wet and dry tests are recorded;  $TSR$  values are also calculated.

**Table 98. ITS test results-English units.**

Site	Surface			Intermediate			Base		
	Wet (psi)	Dry (psi)	TSR (%)	Wet (psi)	Dry (psi)	TSR (%)	Wet (psi)	Dry (psi)	TSR (%)
BUT-129-22E	119	161	74%	77	162	48%	139	224	62%
CHP-68-2N	85	116	73%	57	60	95%	38	64	59%
CLA-41-3N	69	163	42%	112	192	58%	104	155	67%
DEL-23-17S	105	149	70%	99	142	70%	82	131	63%
GRE-35-21E	92	123	75%	76	127	60%	126	131	96%
HAM-126-11E	85	155	55%	79	133	59%	98	120	82%
LUC-25-10S	124	153	81%	89	131	68%	100	131	76%
PIK-32-15W	197	251	78%	148	241	61%	124	166	75%
PIKE-32-19E	141	153	92%	137	177	77%	90	120	75%
ROS-35-1W	98	167	59%	78	153	51%	71	115	62%

**Table 99. ITS test results-metric units.**

Site	Surface			Intermediate			Base		
	Wet (kPa)	Dry (kPa)	TSR (%)	Wet (kPa)	Dry (kPa)	TSR (%)	Wet (kPa)	Dry (kPa)	TSR (%)
BUT-129-22E	820	1110	74%	531	1117	48%	958	1544	62%
CHP-68-2N	586	800	73%	393	414	95%	262	441	59%
CLA-41-3N	476	1124	42%	772	1324	58%	717	1069	67%
DEL-23-17S	724	1027	70%	683	979	70%	565	903	63%
GRE-35-21E	634	848	75%	524	876	60%	869	903	96%
HAM-126-11E	586	1069	55%	545	917	59%	676	827	82%
LUC-25-10S	855	1055	81%	614	903	68%	689	903	76%
PIK-32-15W	1358	1731	78%	1020	1662	61%	855	1145	75%
PIKE-32-19E	972	1055	92%	945	1220	77%	621	827	75%
ROS-35-1W	676	1151	59%	538	1055	51%	490	793	62%

### 13.5.2 Laboratory Resilient Modulus Testing

For this study, the lab-based resilient modulus test was not performed. However, the data from Edwards and Sargand (2010) was found to be useful in this study; therefore the resilient modulus data were used for analysis.

Only the base layers were tested for resilient modulus since the surface and intermediate layers were not thick enough to test. The test is fairly simple; a direct load is applied to a known area. The load and strain are measured; stress and strain curves are plotted for each specimen. The resilient modulus is calculated by simply dividing the applied stress by the strain. This is a non-destructive test that is performed at three different temperatures: 41° F (5°C), 77° F (25°C),



and 104° F (40°C). Table 100 and Table 101 show the results of the resilient modulus test of the AC base layers in English units and metric units, respectively.

**Table 100. AC base layer resilient modulus test results-English units.**

Site	Resilient Modulus (ksi)		
	41° F	77° F	104° F
BUT-129-22E	1416	1124	536
CHP-68-2N	1210	480	422
CLA-41-3N	1209	830	359
DEL-23-17S	2162	987	555
GRE-35-21E	1190	676	262
HAM-126-11E	N/A	N/A	N/A
LUC-25-10S	1198	577	311
PIK-32-15W	1160	544	352
PIKE-32-19E	N/A	N/A	N/A
ROS-35-1W	1308	947	511

**Table 101. AC base layer resilient modulus test results-metric units.**

Site	Resilient Modulus (kPa)		
	5 °C	25 °C	40 °C
BUT-129-22E	9763	7750	3696
CHP-68-2N	8343	3309	2910
CLA-41-3N	8336	5723	2475
DEL-23-17S	14906	6805	3827
GRE-35-21E	8205	4661	1806
HAM-126-11E	N/A	N/A	N/A
LUC-25-10S	8260	3978	2144
PIK-32-15W	7998	3751	2427
PIKE-32-19E	N/A	N/A	N/A
ROS-35-1W	9018	6529	3523

### 13.6 Modeling Asphalt Pavement Response

Evercalc 5.0, developed by the Washington State Department of Transportation (2005), uses FWD deflection measurements to back-calculate the elastic modulus of each specified layer in an asphalt pavement system, using the iterative process shown in Figure 97. After finding the layer moduli, stresses and strains can be determined at various locations in the pavement system. For this study, the tensile strain at the bottom of the AC base layer, the critical response for a perpetual pavement, was the main focus.

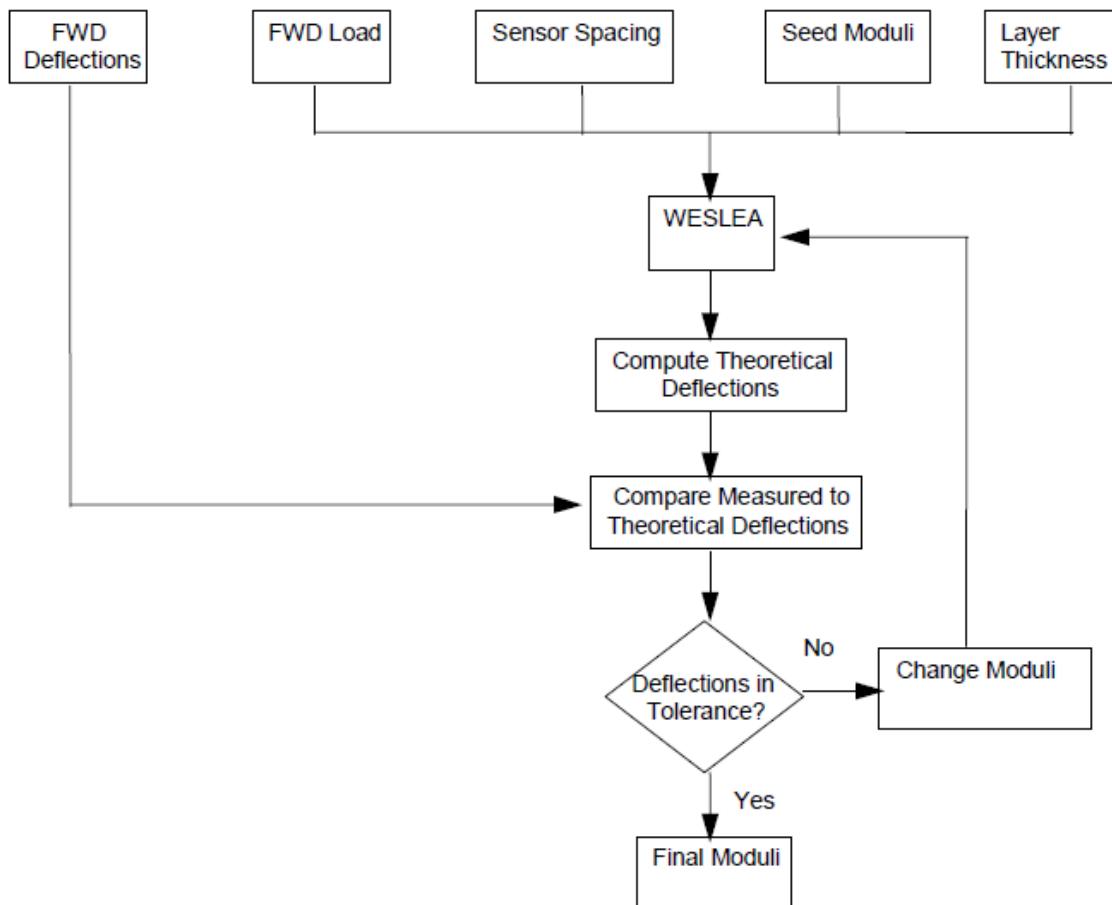


Figure 97. Simplified flowchart for Evercalc (WSDOT, 2005).

As shown in the flowchart, Evercalc uses the Waterways Engineering Station Layer Elastic Analysis (WESLEA), a layer elastic solution, to calculate theoretical deflections and a “modified augmented Gauss-Newton algorithm” for optimization (WSDOT, 2005). The following assumptions are made to simplify solutions:

- There is infinite horizontal length in the pavement
- Uniform thickness in layers
- The bottom layer (subgrade) is semi-infinite
- All layers are homogenous, isotropic, linear elastic, materials that can be distinguished by an elastic modulus and Poisson’s Ratio (assumed to be 0.35 for all layers in this study).

By use of an inverse solution, the elastic modulus of each layer is determined based on FWD deflections. Evercalc has the ability to evaluate up to 10 deflection sensors as well as up to 5 layers in an AC pavement system. A seed modulus is entered into the program along with an upper and lower boundary for modulus in each layer. Qin (2010) suggests using the limits shown in Table 102 for an asphalt pavement structure.

**Table 102. Typical ranges for elastic modulus (Qin, 2010).**

Layer Type	Material Type	Thickness		Poisson's Ratio	Modulus Range	
		(in)	(cm)		(ksi)	(MPa)
Surface	Asphalt	1.5	3.8	0.35	200 2500	1380 - 17200
Intermediate	Asphalt	1.75	4.4	0.35	200 2500	1381 - 17200
AC Base	Asphalt	13	33.0	0.35	200 2500	1382 - 17200
Sub-Base	Aggregate	6	15.2	0.35	10 100	70 - 690
Subgrade	Soil	-	-	0.4	3 30	21 - 207

The program iterates the layer moduli to match theoretical and measured deflections until final moduli are found. The final moduli are determined when the *RMS* reaches its desired amount (1%) or the lowest possible value is determined. Once the final moduli are found, stresses and strains at various locations in the pavement structure are computed by the program using a finite element algorithm. Table 103 shows the results of the Evercalc back-calculations for each site when subjected to a 9000 lb (40 kN) normalized load.

**Table 103. Evercalc 5.0 results.**

Site	$E_{\text{surface}}$		$E_{\text{intermediate}}$		$E_{\text{AC-base}}$		$E_{\text{agg-base}}$		$E_{\text{subgrade}}$		$\epsilon_{\text{AC}}^*$ ( $\mu\epsilon$ )
	(ksi)	(MPa)	(ksi)	(MPa)	(ksi)	(MPa)	(ksi)	(MPa)	(ksi)	(MPa)	
BUT-129-22E	3267	22525	2263	15603	1537	10597	1144	7888	65	448	7
CHP-68-2N	404	2785	353	2434	274	1889	51	352	36	248	105
CLA-41-3N	273	1882	402	2772	610	4206	48	331	17	117	69
DEL-23-17S	4374	30158	1641	11314	628	4330	411	2834	44	303	16
GRE-35-21E	373	2572	260	1793	222	1531	41	283	49	338	107
HAM-126-11E	3127	21560	1986	13693	407	2806	81	558	76	524	37
LUC-25-10S	1938	13362	566	3902	504	3475	71	490	66	455	57
PIK-32-15W	2974	20505	1652	11390	733	5054	56	386	55	379	39
PIKE-32-19E	3241	22346	911	6281	683	4709	51	352	62	427	36
ROS-35-1W	225	1551	331	2282	326	2248	59	407	27	186	77

\* $\epsilon_{\text{AC}}$  = Estimated strain at the bottom of the AC base layer using back-calculated moduli

## 13.7 Other FWD Techniques for Estimating Pavement Response

### 13.7.1 Liao Model

Liao (2007) developed a model used to evaluate the strain in the fatigue resisting layer. He based the model on actual strain measurements from strain gauges installed at the AC base layer in U.S. 30 perpetual pavement. The factors used in the model consisted of pavement temperature, modulus of subgrade reaction, thickness of the fatigue resisting layer, and the thickness of the aggregate base layer. The pavement temperature ( $T_{pav}$ ) is based on the study performed by Figueroa (2004) where pavement temperatures were studied all over Ohio. The temperatures are based on what region of Ohio the pavement is in. The following equation governs the relationship of pavement temperature to air temperature. The constants for the equation for various locations and regions in the state are provided in Table 104 .

$$T_{pav} = C_1 + C_2 T_{air} + C_3 T_{air}^2$$

Where:

$C_1, C_2, C_3$  = Regression Constants

$T_{pav}$  = Average Pavement Temperature ( $^{\circ}\text{C}$ )

$T_{air}$  = Air Temperature ( $^{\circ}\text{C}$ )

**Table 104. Average AC temperature vs. air temperature coefficients (Figueroa, 2004).**

Location	No. Points	$C_1$	$C_2$	$C_3$	$R^2$
North	75414	4.1409	0.9423	0.0027	0.8640
Central	118290	4.8118	0.8860	0.0052	0.8418
South	61152	5.2834	0.9113	0.0055	0.8431
All Sites	254856	4.7055	0.9107	0.0045	0.8475
Ohio Test Road	24133	5.0952	0.8889	0.0114	0.9117

Liao's model uses load multipliers to convert loads and deflections to 9000 pounds (40 kN). This is similar to what was executed in the Evercalc results. Liao (2007) analyzed 81 different cases to develop the model and used the field data to calibrate the model. The equation below was used by Liao (2007) to estimate the horizontal strain at the bottom of the AC base layer.

$$\varepsilon_{11} = 38.5924 - 2.6625 H_{ac} + 0.3925 T_{pav} + 3.3406 D_1$$

Where:

$\varepsilon_{11}$  = Tensile strain at the bottom of the AC base layer ( $\mu\varepsilon$ ) under a 9000 lb (40 kN) load

$H_{ac}$  = Thickness of AC base layer (in)

$T_{pav}$  = Temperature at mid-depth of AC base layer ( $^{\circ}\text{C}$ )

$D_1$  = FWD deflection at center of load (mil)

Table 105 shows the results of the FWD data using Liao's approach. The deflection data are those used in the Evercalc analysis.

**Table 105. FWD results using Liao model.**

Site	$\epsilon_{11}$ ( $\mu\epsilon$ )
BUT 129-22E	33
CHP 68-3N	57
CLA 41-3N	49
DEL 23-17S	25
GRE 35-21E	57
HAM 126-11E	49
LUC 25-10S	45
PIK 32-15W	36
PIK 32-19E	30
ROS 35-1W	46

### 13.7.2 N.C. State University FWD Model

Kim and Park (2002) developed a model using FWD data to predict tensile strain in the FRL. Deflection basin parameters were used to evaluate AC pavement performance. Specifically, the Base Damage Index (*BDI*) and the Area Under Pavement Profile (*AUPP*) were found to have a very strong correlation to tensile strain in the AC base layer. The following equations are used to calculate these deflection basin parameters.

$$BDI = D_{12} - D_{24}$$

$$AUPP = (5D_0 - 2D_{12} - 2D_{24} - D_{36})/2$$

Where:

$D_0$  = FWD deflection measured at location of applied load (mil)

$D_{12}$  = FWD deflection measured 12 in (305 mm) from location of applied load (mil)

$D_{24}$  = FWD deflection measured 24 in (610 mm) from location of applied load (mil)

$D_{36}$  = FWD deflection measured 36 in (914 mm) from location of applied load (mil)

Kim and Park (2002) used a statistical regression method to relate horizontal strain at the bottom of the AC base layer ( $\epsilon_{ac}$ ) to *BDI* and *AUPP* parameters;  $\epsilon_{ac}$  is based on the 9000 lb (40 kN) load used in the Evercalc analysis and Liao's model. Kim and Park (2002) developed their models for full depth asphalt and asphalt pavements with aggregate bases. For this study, the models designed for aggregate bases were used. Factors for Kim and Park's (2002) model consisted of *BDI*, thickness of the asphalt ( $H_{ac}$ ), and *AUPP*. The equations below were used to predict tensile strain at the bottom of the AC base layer ( $\epsilon_{ac}$ ) for aggregate base pavements.

$$\log(\epsilon_{ac}) = 1.082 \log(BDI) + 0.259 \log(H_{ac}) + 1.409$$

$$\log(\epsilon_{ac}) = 1.034 \log(AUPP) + 0.932$$

Where:

$\epsilon_{ac}$  = strain at the bottom of the AC base layer when subjected to a 9000 lb load ( $\mu\epsilon$ )

$BDI$  = Base Damage Index  
 $H_{ac}$  = total thickness of asphalt layer  
 $AUPP$  = Area Under Pavement Profile

Table 106 displays the results of the FWD model, showing the strain at the bottom of the AC base layer  $\epsilon_{ac}$  by use of the  $BDI$  and  $AUPP$  deflection basin indexes.

**Table 106. Kim and Park FWD model results.**

Site	BDI	AUPP
	$\epsilon_{ac}$ ( $\mu\epsilon$ )	$\epsilon_{ac}$ ( $\mu\epsilon$ )
BUT-129-22E	13	21
CHP-68-2N	82	90
CLA-41-3N	70	62
DEL-23-17S	15	17
GRE-35-21E	91	91
HAM-126-11E	50	53
LUC-25-10S	41	57
PIK-32-15W	32	33
PIK-32-19E	28	35
ROS-35-1W	73	71

Table 107 shows the overall averaged results of strain at the bottom of the AC base layer for each site at a 9000 lb (40 kN) FWD load for the various methods.

**Table 107. Average tensile strain at the bottom of the AC base layer from 9000 lb (40 kN) load.**

Site	$\epsilon_{ac}$ ( $\mu\epsilon$ )			
	BDI	AUPP	Liao	Evercalc
BUT-129-22E	13	21	19	7
CHP-68-2N	82	90	57	105
CLA-41-3N	70	62	52	69
DEL-23-17S	15	17	15	16
GRE-35-21E	91	91	59	107
HAM-126-11E	50	53	34	37
LUC-25-10S	41	57	45	57
PIK-32-15W	32	33	37	39
PIK-32-19E	28	35	30	36
ROS-35-1W	73	71	42	77

Back-calculation can be a difficult and time-consuming process. A quick, forward calculation method to estimate the strain at the bottom of the AC base layer is desirable. In general, the forward calculation results were lower (less conservative) than the Evercalc results. However, relationships between the forward and backward calculation methods were formed to give pavement designers an easy method to estimate back-calculated strain results using forward calculated equations. These models were graphically compared to the results found using the Evercalc, back-calculation method in the following figures. The strain results of the models

(BDI, AUPP, and Liao) were plotted on the X-axis while the Evercalc strain results were plotted on the Y-axis. Trend lines were formed so relationships between the models and back-calculated results could be determined, as shown in the following three figures.

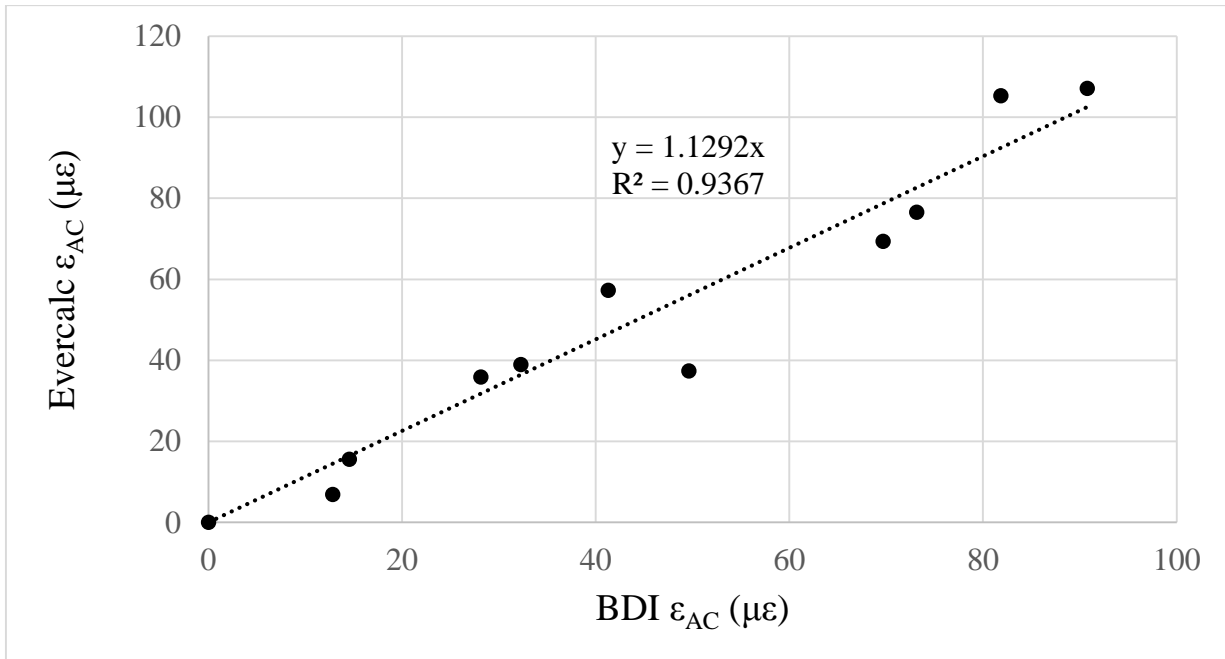


Figure 110. Evercalc vs. BDI strain results.

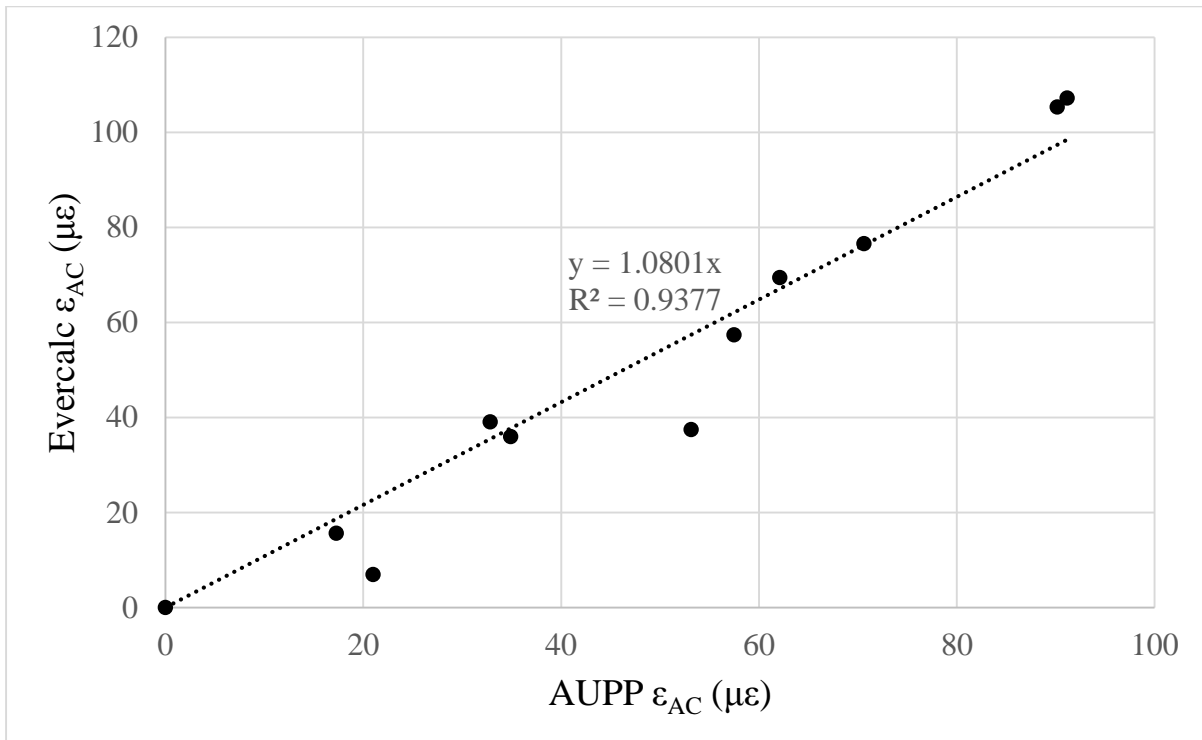
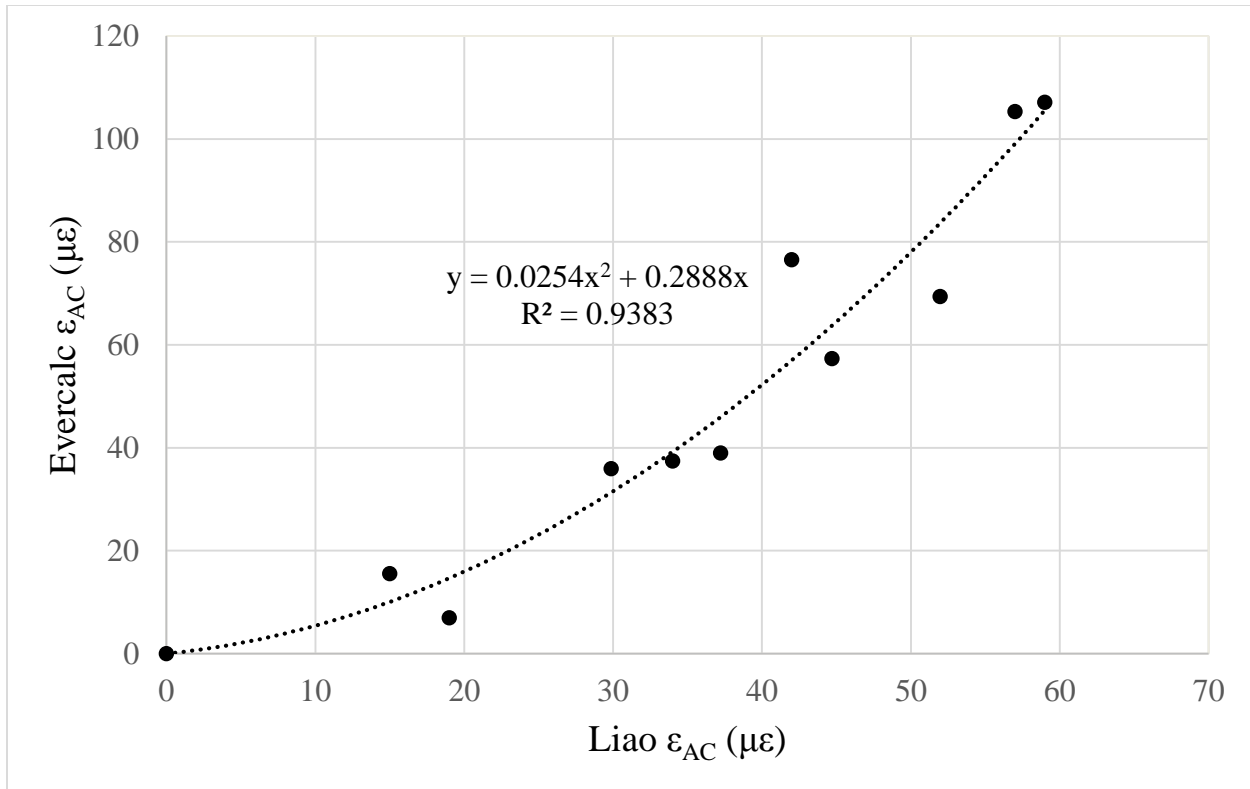


Figure 111. Evercalc vs. AUPP strain results.





**Figure 112. Evercalc vs. Liao strain results.**

The plots show there is an excellent relationship between the various models used and the back-calculated strain results; all of the  $R^2$  values were above 0.9. Based on this evaluation, the strain at the bottom of the AC base layer based on a 9000 lb (40 kN) FWD load can be estimated using any of the models along with the relationships between the model and the back-calculated values. Kim and Parks AUPP model would be the easiest and most accurate since it has a linear relationship with the Evercalc results. In the region near the perpetual pavement strain criterion  $\epsilon = 30\text{-}90 \mu\epsilon$ , the Evercalc value can be estimated by taking the Kim and Parks AUPP model value and adding  $10 \mu\epsilon$ .

### 13.8 Finite Element Modeling of Asphalt Pavement

Abaqus 6.9 (2009) was used to further evaluate the tensile strain in the AC base layer. Abaqus is a comprehensive finite element software package capable of evaluating nearly any simulations of various materials and parts. The evaluations include detailed information about stress, strain, and displacement nearly anywhere on a given part when subjected to a loading sequence. Parts are defined by their geometry and are portioned appropriately where there are interfaces. Material properties are defined; material behavior (linear elastic, viscoelastic ...), Young's Modulus, and Poisson's Ratio are defined for all pieces of the part. Meshing of the part is applied to the geometry; this creates locations for loads to be placed and results to be analyzed. Loads are then defined and placed at desired locations. Various loading simulations can be executed and the results are displayed at desired nodes on the part.

Confirming the back-calculated strain results from the Evercalc program would be valid if similar results could be achieved using a finite element analysis. The FWD loading is circular, whereas a truck tire load area is square. The modulus values found from the Evercalc program were used to define the various layers in the pavement structure in the finite element analysis. A 12 ft by 12 ft (3.66 m by 3.66 m) pavement section was created in the "parts" tab of Abaqus. The layer thickness was entered; each site had unique thicknesses. The subgrade layer was assumed to have an infinite thickness for analysis purpose. A mesh was created; medium sized meshing was applied to the top three layers while large meshing was applied to the bottom two layers. Figure 98 shows the geometry of the pavement section and the mesh applied.

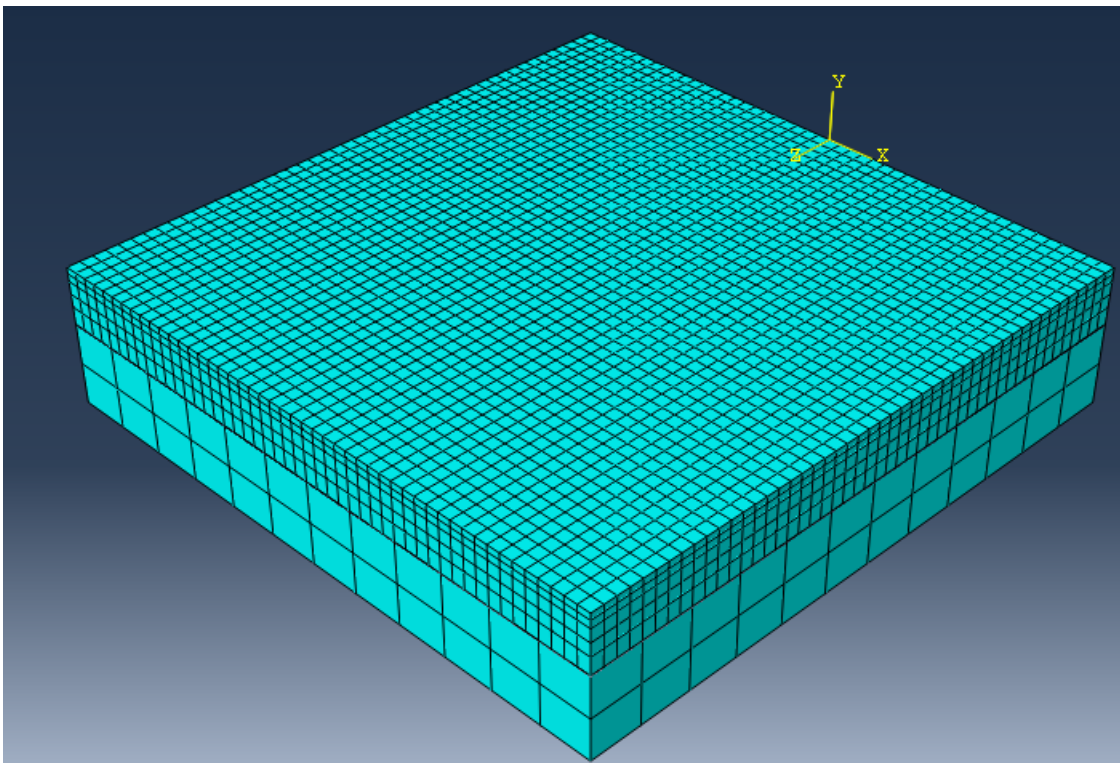
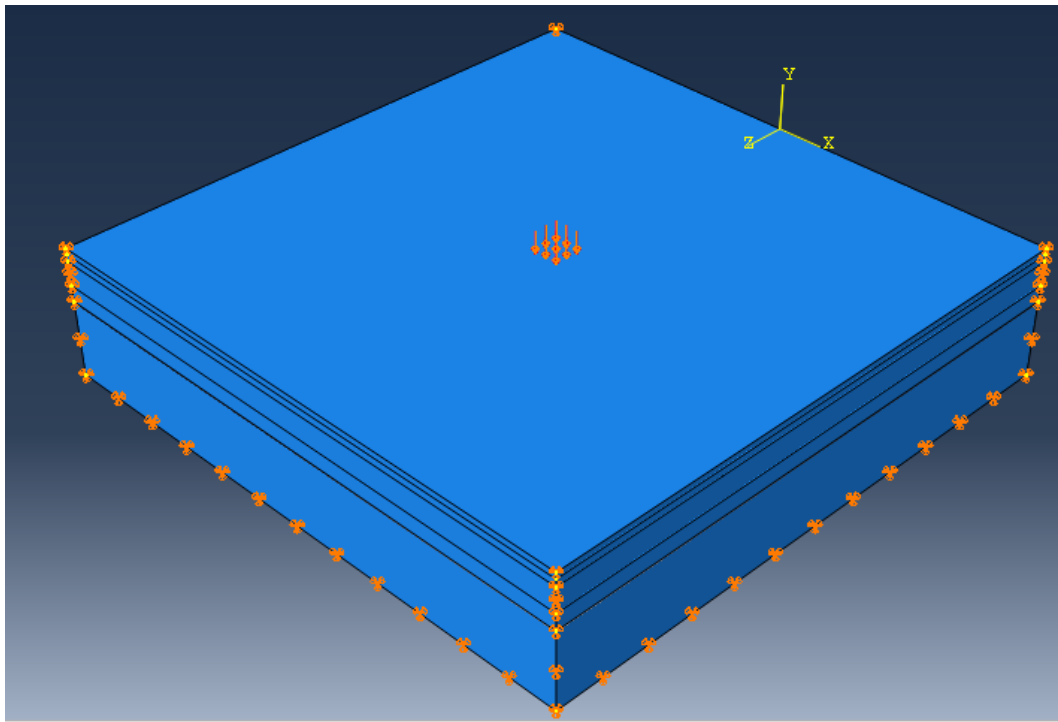


Figure 98. Pavement section mesh.

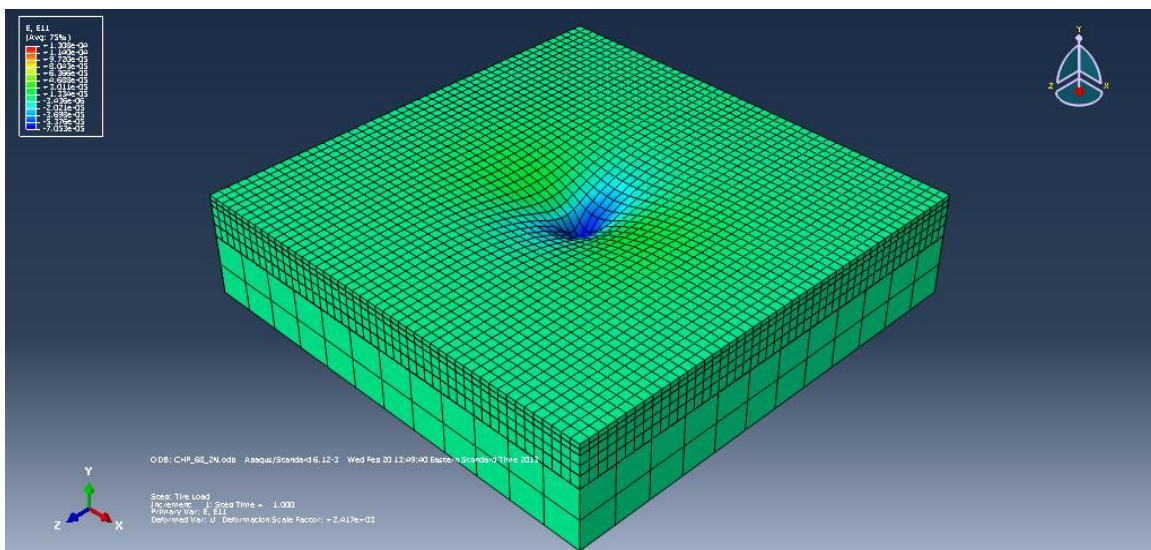
There were two different tire loadings applied to the pavement. The first tire orientation was a super-single tire that was applied to the center of the pavement; the tire occupied a 9 in by 9 in (22.9 cm by 22.9 cm) area. The other tire orientation was a dual tire setup where both tires

occupied a 9 in by 3 in (22.9 cm by 7.6 cm) area with 3 in (7.6 cm) spacing. Both of the tire orientations were loaded with 9000 lb (40 kN) which was similar to the FWD test. Figure 99 shows a typical pavement section with the tire load.



**Figure 99. Pavement section with tire load.**

The loading simulation was run with a 9000 lb (40 kN) traffic load on all of the pavement sections. Many node responses of stresses, strains, and displacements could have been analyzed. For this study, the X-Z strain (tensile strain) at the bottom of the AC base layer was used for analysis. Figure 100 shows a snapshot of the pavement response to the loading.



**Figure 100. Computed pavement response to load.**

The results of the finite element analysis are shown in Table 108 where  $\epsilon_{AC}$  is the strain at the bottom of the AC base layer when subjected to a 9000 lb (40 kN) tire load. The results of the Evercalc, back-calculation analysis are also shown in Table 108 for comparison.

**Table 108. Finite element model results.**

Site	Evercalc	Abaqus	
		Single Tire	Dual Tires
	$\epsilon_{AC}$ ( $\mu\epsilon$ )	$\epsilon_{AC}$ ( $\mu\epsilon$ )	$\epsilon_{AC}$ ( $\mu\epsilon$ )
BUT-129-22E	7	7	7
CHP-68-2N	105	101	91
CLA-41-3N	69	62	58
DEL-23-17S	16	11	10
GRE-35-21E	107	110	93
HAM-126-11E	37	45	38
LUC-25-10S	57	51	49
PIK-32-15W	39	32	27
PIK-32-19E	36	28	25
ROS-35-1W	77	75	61

The Abaqus results of the tensile strain at the bottom of the AC base layer were extremely close to the results found using the back-calculation technique for the single tire; the difference in strain was no more than 8  $\mu\epsilon$  among all the sites. The dual tire load showed the tensile strain measuring slightly less than that of the single tire load due to the load being distributed over a larger area. The single tire setup was used to compare the strain when DCP modulus values were used in the analysis.

For more confirmation on the back-calculation technique, the modulus of the subgrade found using the DCP was entered into Abaqus. The strain at the bottom of the AC base layer using subgrade modulus values from back-calculation and DCP were compared under a single tire load; the comparison is displayed in the Table 109.

**Table 109. Finite element model results using DCP subgrade modulus.**

Site	Abaqus		Evercalc
	DCP Subgrade Modulus		
	$\epsilon_{AC}$ ( $\mu\epsilon$ )		$\epsilon_{AC}$ ( $\mu\epsilon$ )
BUT-129-22E	7		7
CHP-68-2N	95		105
CLA-41-3N	66		69
DEL-23-17S	11		16
GRE-35-21E	109		107
HAM-126-11E	45		37
LUC-25-10S	51		57
PIK-32-15W	31		39
PIK-32-19E	29		36
ROS-35-1W	76		77

The results show the difference in the back-calculation and DCP subgrade modulus had little effect on the strain at the bottom of the AC base layer. These findings confirm the results found using the back-calculation techniques are valid and can be used for further analysis.

### 13.9 AC Pavement Testing Relationships

For this analysis, a conservative value of  $70 \mu\epsilon$  was used to define whether an AC pavement system was perpetual. Since the tensile strain at the bottom of the AC base layer ( $\epsilon_{AC}$ ) was based on only a 9000 lb (40 kN) tire load, a conservative value for the fatigue endurance limit had to be used since it would be realistic for a pavement to see loads higher than 9000 lb (40 kN) in a lifetime. Therefore, pavement systems with an estimated tensile strain at the bottom of the AC base layer less than  $70 \mu\epsilon$  can be considered perpetual if it is based on a 9000 lb (40 kN) FWD load.

DCP results show similar values of aggregate base and subgrade modulus to the FWD data. Table 110 and Table 111 compare moduli computed using the DCP and FWD data for the aggregate base modulus and the subgrade modulus, respectively.

**Table 110. Comparison of DCP vs. FWD based modulus of aggregate base.**

Site	Modulus of Aggregate Base			
	DCP		FWD	
	(ksi)	(MPa)	(ksi)	(MPa)
BUT-129-22E	N/A	N/A	N/A	N/A
CHP-68-2N	90	621	51	352
CLA-41-3N	48	331	48	331
DEL-23-17S	53	365	N/A	N/A
GRE-35-21E	86	593	41	283
HAM-126-11E	71	490	81	558
LUC-25-10S	19	131	71	490
PIK-32-15W	128	883	56	386
PIK-32-19E	57	393	51	352
ROS-35-1W	59	407	59	407

**Table 111. Comparison of DCP vs. FWD based modulus of subgrade.**

Site	Modulus of Subgrade			
	DCP		FWD	
	(ksi)	(MPa)	(ksi)	(MPa)
BUT-129-22E	65	448	65	448
CHP-68-2N	66	455	36	248
CLA-41-3N	17	117	17	117
DEL-23-17S	20	138	44	303
GRE-35-21E	49	338	49	338
HAM-126-11E	37	255	76	524
LUC-25-10S	N/A	N/A	66	455
PIK-32-15W	89	614	55	379
PIK-32-19E	25	172	62	427
ROS-35-1W	27	186	27	186

The results show some of the DCP moduli were very similar to the FWD moduli. The subgrade was definitely the most consistent between the two tests. The aggregate base can sometimes be difficult to examine due to the inconsistency of the material. Also, some of the sites had ATB and could not be tested with DCP.

The results of the SPA testing were compared to the calculated strain at the bottom of the AC base layer. Also, the seismic modulus was compared to the resilient modulus found from FWD back-calculation of the asphalt pavement. The layer moduli were averaged using a weighted average, which is based on the layer modulus and the thickness. The resilient modulus was multiplied by two, and then compared to the seismic modulus to see if Williams and Nazarian's (2007) correlation can be used. Figure 101 shows the relationship between the seismic modulus and tensile strain at the bottom of the AC base layer and Table 112 shows the resilient modulus and seismic modulus comparison.

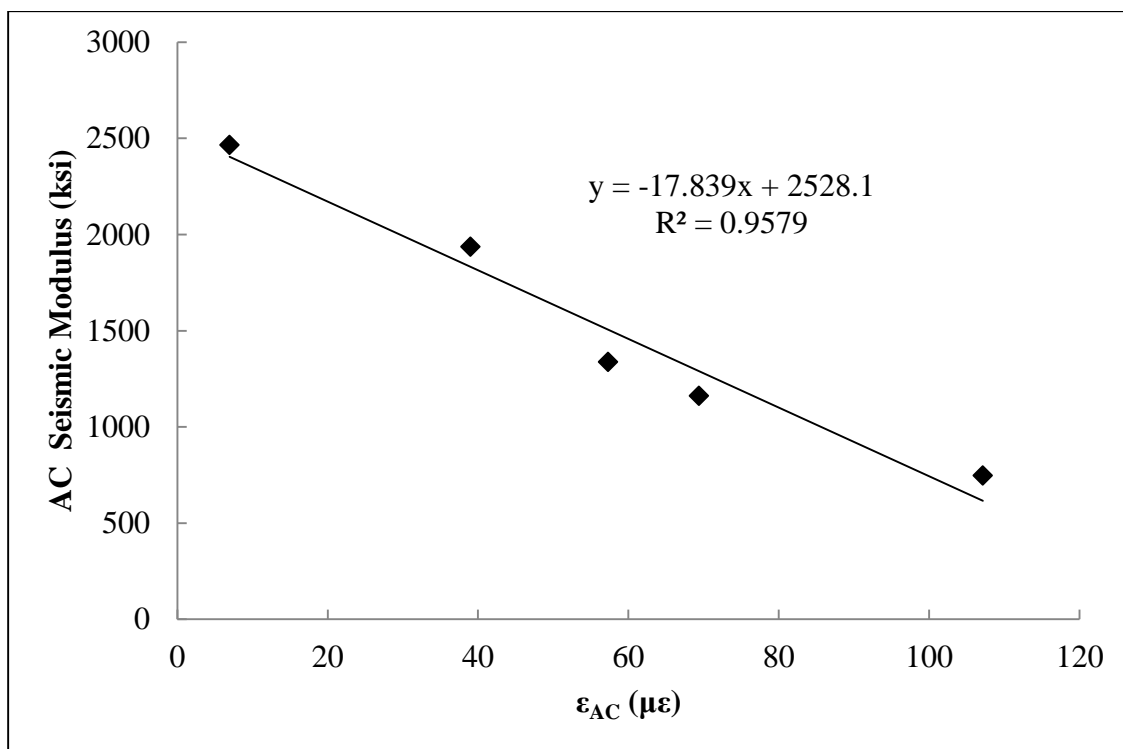


Figure 101. AC seismic modulus vs. strain at the bottom of the AC base layer.

Table 112. Comparison of seismic modulus and resilient modulus.

Site	$2 \times E_{AC}$		AC Seismic Modulus		% Difference
	(ksi)	(MPa)	(ksi)	(MPa)	
BUT-129-22E	2740	18892	2466	17002	11%
CLA-41-3N	1064	7336	1162	8012	9%
GRE-35-21E	688	4744	748	5157	8%
LUC-25-10S	1392	9597	1337	9218	4%
PIK-32-15W	2196	15141	1936	13348	13%

The results show a very strong correlation exists between seismic modulus and pavement performance. They suggest a pavement's performance can be analyzed by using the portable seismic property analyzer. The comparison between the resilient modulus found through back-calculation and the seismic modulus agree very well with Williams and Nazarian's (2007) research; the highest percent difference was 13%, while the average percent difference was 9%. These are exciting results, considering that the SPA is one of the easiest, least time-consuming field tests that can be performed. Also, the results suggest that resilient modulus of the AC pavement can be quickly estimated in the field using SPA.

The results of the IDT testing were compared to IDT testing from WAY-30 perpetual pavement. Kim et al. (2010) conducted various laboratory tests on asphalt samples that were designed for perpetual pavement. These asphalt layers, especially the fatigue resisting layer (FRL), had more asphalt content than the traditional AC base layer. Also, the binder used in the WAY-30 design included polymer treatment which usually adds to the strength of the pavement (PG 64-22), whereas the older pavements in this research were constructed before PG grading was popular. If the results of the IDT tests from WAY-30 fatigue resisting layer (FRL) are similar to the results of IDT tests found from the older pavements, then the quality of the older pavements have maintained their structural integrity. Table 113 shows the results of the IDT tests of the AC base layer for this research and Table 114 shows the IDT test results of the WAY-30 FRL.

**Table 113. ITS of AC base layers.**

Site	ITS Average	
	(psi)	(MPa)
BUT-129-22E	224	1.54
CHP-68-2N	64	0.44
CLA-41-3N	155	1.07
DEL-23-17S	131	0.90
GRE-35-21E	131	0.90
HAM-126-11E	120	0.83
LUC-25-10S	131	0.90
PIK-32-15W	166	1.14
PIKE-32-19E	120	0.83
ROS-35-1W	115	0.79

**Table 114. ITS of WAY-30 FRL (Kim et al., 2010).**

Date	AV	Indirect Tensile Strength (ITS)		ITS Average	
		(%)	(psi)	(MPa)	(psi)
7/13/2005	2.68	193.6	1.335	200.1	1.380
	3.29	196.1	1.352		
	2.84	210.7	1.453		
8/10/2005	3.57	178.5	1.231	209.7	1.446
	3.77	237.1	1.635		
	3.05	213.6	1.473		
8/15/2005	3.30	201.9	1.392	185.8	1.282
	3.61	180.0	1.241		
	3.73	175.6	1.211		
8/21/2005	3.15	161.5	1.114	156.8	1.081
	4.10	155.6	1.073		
	3.20	153.3	1.057		
9/11/2005	3.07	133.2	0.919	140.3	0.968
	2.79	146.3	1.009		
	3.28	141.5	0.976		
9/15/2005	3.11	124.5	0.859	135.5	0.935
	3.36	135.8	0.937		
	2.50	146.3	1.009		
9/22/2005	3.95	124.7	0.860	146.8	1.013
	3.66	134.4	0.927		
	3.25	181.4	1.251		
10/6/2005	3.44	159.1	1.097	152.1	1.049
	3.59	151.2	1.043		
	3.62	145.9	1.006		
10/13/2005	2.98	197.0	1.359	173.3	1.195
	3.36	147.8	1.019		
	3.50	175.0	1.207		
10/18/2005	3.50	191.0	1.317	164.0	1.131
	3.66	155.2	1.070		
	3.47	145.9	1.006		

The results from WAY-30 show ITS that range from 210 psi (1448 kPa) to 136 psi (938 kPa), average 166.5 psi (1148 kPa), where the results from the Forensic Investigation show ITS ranging from 224 psi (1544 kPa) to 64 psi (441 kPa). These results show some of the sites had ITS strengths as good if not better than the average strength of a rich AC base layer used in WAY-30. The sites that were below average typically did not show a low strain at the bottom of the AC base layer.

The ITS tests were compared to the calculated strain at the bottom of the AC base layer. Also, the ITS strength for the AC base layer was compared to the modulus found using FWD. For simplicity, only the dry specimens were analyzed and compared. Figure 102, Figure 103,



and Figure 104 show results of the ITS analysis for the surface layer, intermediate layer, and the base layer, respectively.

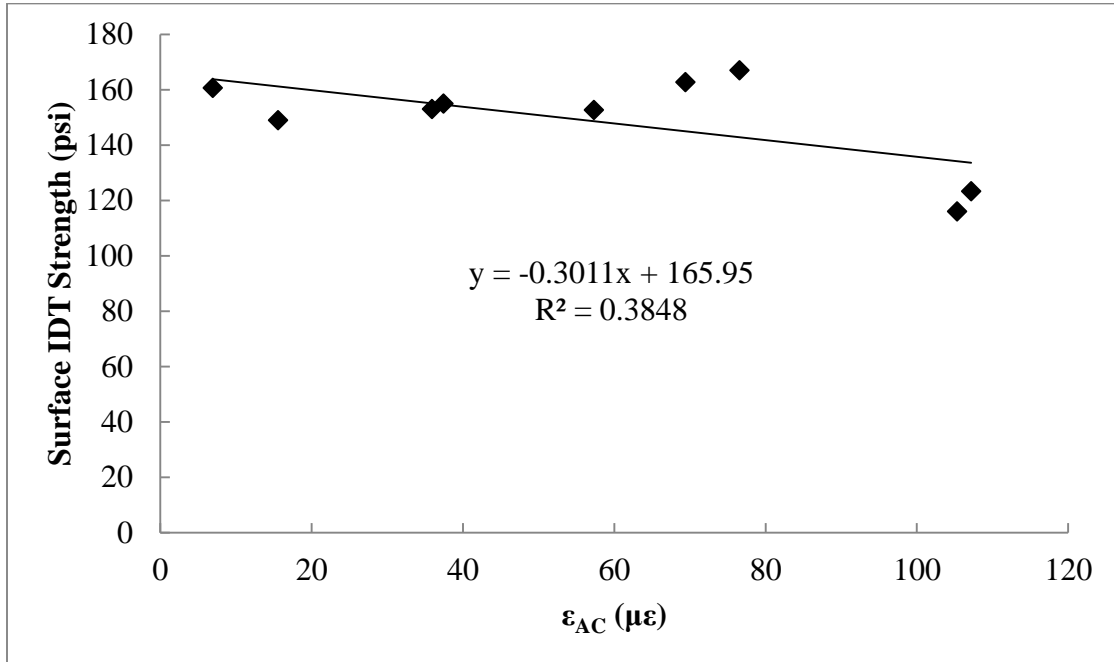


Figure 102. Surface layer ITS vs. strain at the bottom of the AC base layer.

The surface layer ITS results show that there is a slight correlation to the surface layer ITS strength and pavement performance. It is difficult to test ITS strength for surface layers because the layers are often very thin, so they are difficult to accurately test using ITS.

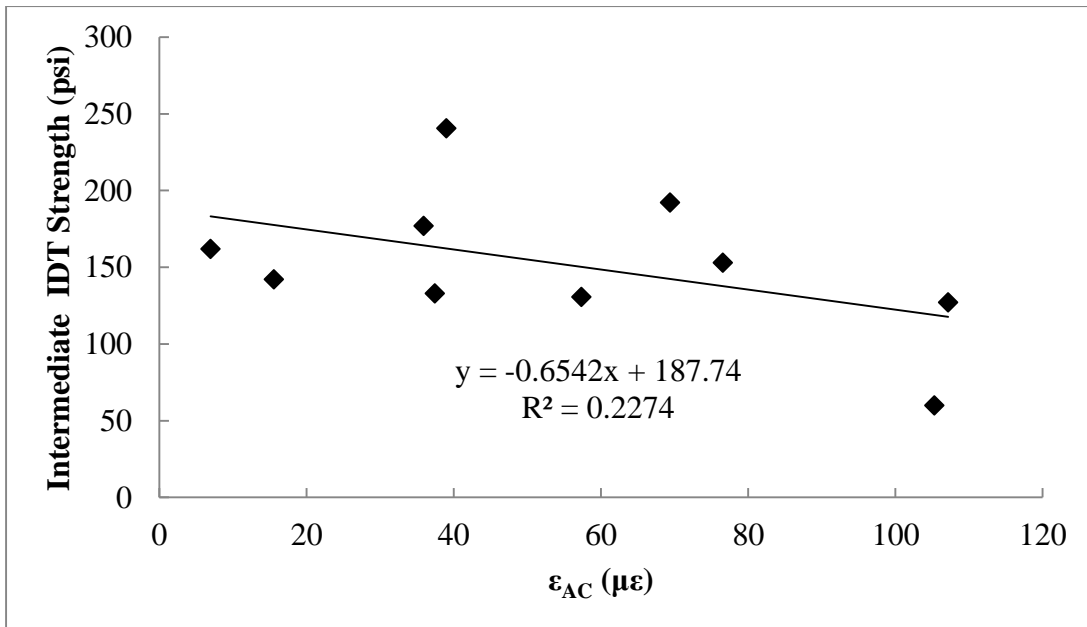


Figure 103. Intermediate layer ITS vs. strain at the bottom of the AC base layer.

Like the surface layer ITS test, the intermediate layer is often thin and difficult to accurately test. The figure shows a weak linear relationship between intermediate layer ITS and pavement performance. The results suggest that the intermediate ITS strength may not be the best option in determining whether an AC pavement is perpetual.

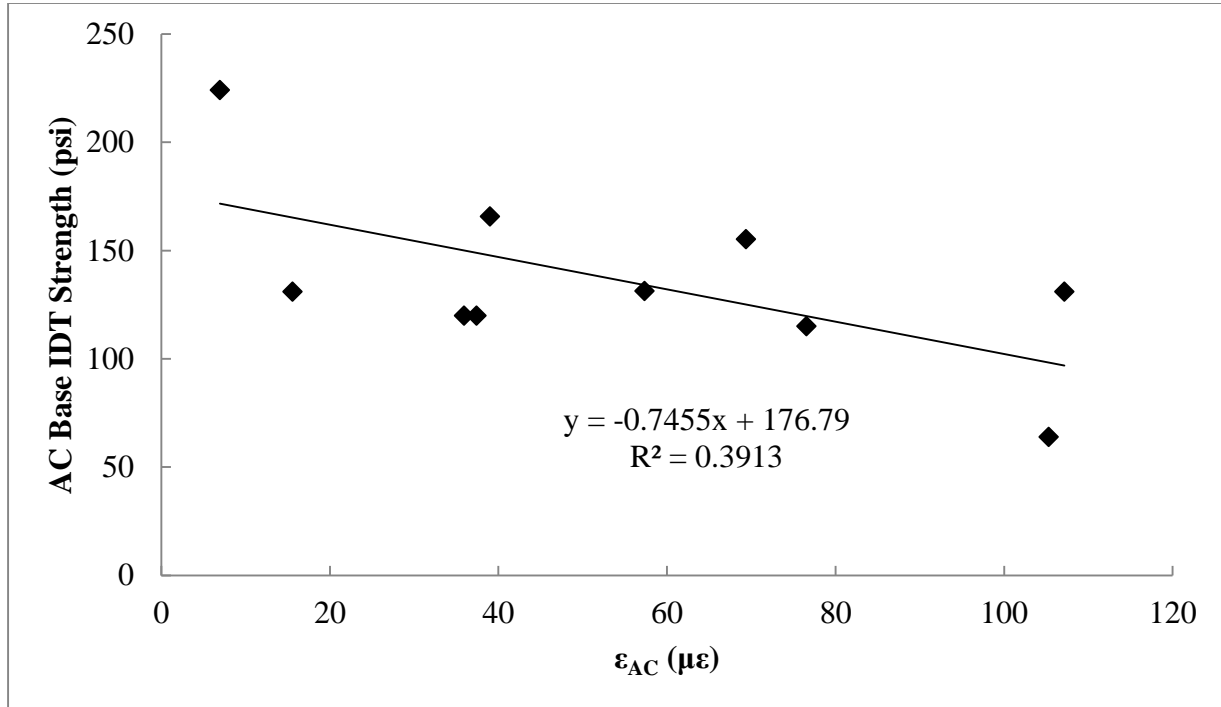


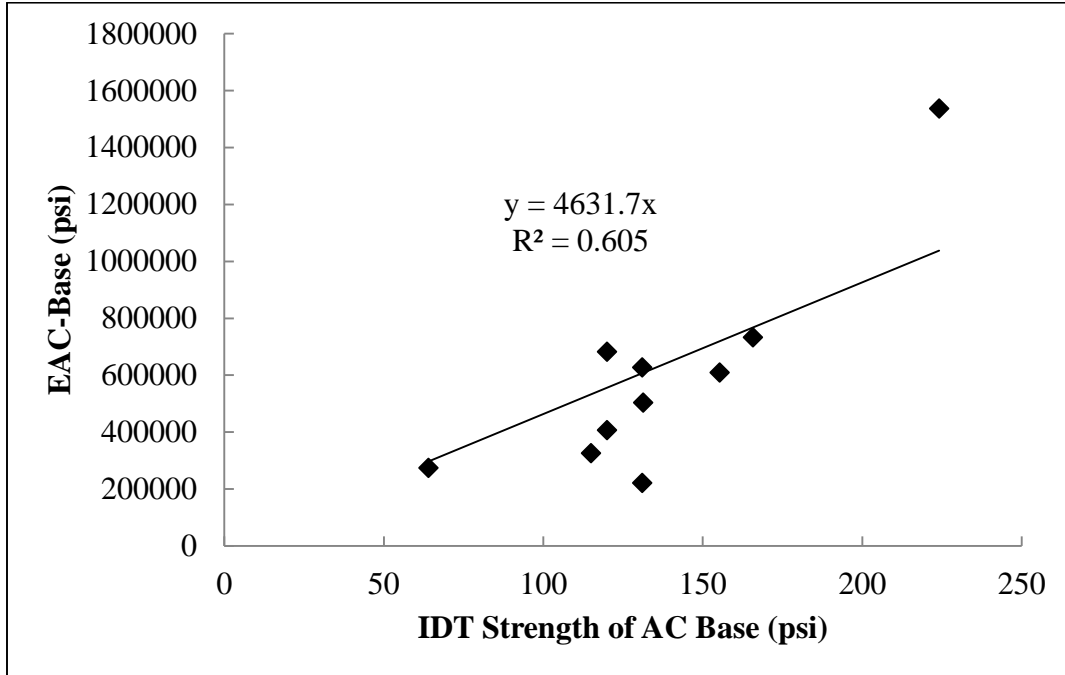
Figure 104. AC base layer ITS vs. strain at the bottom of the AC base layer.

The results show a slight linear relationship between the AC base layer ITS and pavement performance. Since the AC base layer is often the thickest layer of the asphalt structure, it is the easiest to test for ITS. The results show that testing the ITS of the surface layer and AC base layer may show that a pavement structure is perpetual but it probably is not the best option.

Table 115 compares the ITS strength of the AC base layer to the modulus of AC base layer found through back-calculation techniques, which is graphed in Figure 105.

Table 115. Comparison of the ITS and FWD modulus of the AC base layer.

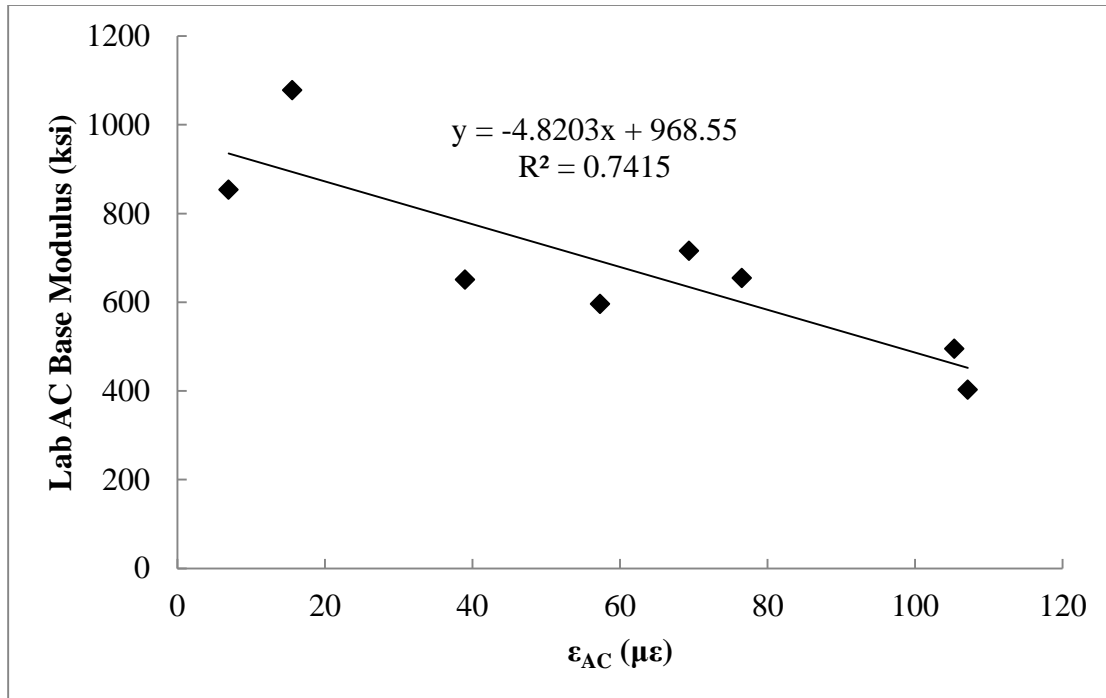
Site	ITS		FWD modulus	
	(psi)	(MPa)	(psi)	(MPa)
BUT-129-22E	224	1.54	1537000	10597
CHP-68-2N	64	0.44	274000	1889
CLA-41-3N	155	1.07	610000	4206
DEL-23-17S	131	0.90	628000	4330
GRE-35-21E	131	0.90	222000	1531
HAM-126-11E	120	0.83	407000	2806
LUC-25-10S	131	0.90	504000	3475
PIK-32-15W	166	1.14	733000	5054
PIK-32-19E	120	0.83	683000	4709
ROS-35-1W	115	0.79	326000	2248



**Figure 105. AC base ITS vs. strain at the bottom of the AC base layer.**

The results show the ITS strength can be roughly determined through FWD back-calculation techniques. The ITS values found in the AC base layer were common among typical asphalt specimens that were mixed with higher percent asphalt binder. These values, in general, make a good argument that these older asphalt concrete pavements have maintained the same quality of strength as new asphalt concrete pavements or those with higher asphalt content.

All the laboratory resilient modulus testing of the AC base layers was completed in the 2010 Forensic Study. As stated before, the surface and intermediate layers were too thin to test for the resilient modulus, therefore only the AC base layers were tested. Figure 106 compares the laboratory resilient modulus of the AC base layer to the strain in the AC base layer. The results were analyzed at the same temperature as the FWD results for each site.



**Figure 106. AC base laboratory resilient modulus vs. strain at the bottom of the AC base layer.**

The results show there is a strong correlation between the laboratory resilient modulus test of the AC base layer modulus and pavement performance. The laboratory resilient modulus test is often difficult and time consuming to perform; if FWD testing can produce similar results to the laboratory test, analysis of a pavement structure would be quicker and easier to accomplish.

The AC base layer modulus found in the laboratory was compared to the AC base layer modulus found using the Evercalc program. Table 116 shows the results of the comparison. It should be noted that the modulus found using the Evercalc program was at different temperatures from the moduli found in the lab; to be consistent, the lab resilient modulus results were linearly interpolated at the same temperature recorded during the FWD analysis. The results were similar for some sites; 56% difference was the largest calculated between the two tests while an average of 36% difference was found among all the sites. These findings show back calculation of the FWD data can roughly predict the same results as the laboratory resilient modulus test on AC base pavement except the results can be determined much easier and faster using the FWD.

**Table 116. AC base layer modulus comparison (Lab vs. FWD).**

Site	FWD				Laboratory						Interpolated E		% Diff.
	Temperature		Resilient Modulus		Resilient Modulus at Test Temperature								
	(°C)	(°F)	(ksi)	(MPa)	5°C (41°F)		25°C (77°F)		40°C (104°F)		(ksi)	(MPa)	
BUT 129-22E	32.9	91.2	1537	10597	1416	9763	1124	7750	536	3696	910	6274	51%
CHP 68-2N	26.8	80.2	274	1889	1210	8343	480	3309	422	2910	458	3158	50%
CLA 41-3N	26.8	80.2	610	4206	1209	8336	830	5723	359	2475	716	4937	16%
DEL 23-17S	26.7	80.1	628	4330	2162	14906	987	6805	555	3827	923	6364	38%
GRE 35-21E	34.9	94.8	222	1531	1190	8205	676	4661	262	1806	374	2579	51%
HAM 126-11E	33.5	92.3	407	2806	N/A	N/A	N/A	N/A	N/A	N/A	N/A	N/A	N/A
LUC 25-10S	27.2	81.0	504	3475	1198	8260	577	3978	311	2144	575	3964	13%
PIK 32-15W	24.8	76.6	733	5054	1160	7998	544	3751	352	2427	651	4488	12%
PIK 32-19E	24.6	76.3	683	4709	N/A	N/A	N/A	N/A	N/A	N/A	N/A	N/A	N/A
ROS 35-1W	35.2	95.4	326	2248	1308	9018	947	6529	511	3523	581	4006	56%

### **13.10 Summary and Observations on Existing Pavements**

Field testing, especially FWD testing, can be used to determine the quality of the AC pavement system. Back calculated moduli values and strain prediction models can be used to estimate the strain at the bottom of an asphalt pavement. For this study, a conservative value of 70  $\mu\epsilon$  at the bottom of the AC base layer was used as the qualification value for an AC pavement system to be considered perpetual. Sites with strains above 70  $\mu\epsilon$  were not considered perpetual but could become perpetual by applying additional asphalt surface material to the structure. This addition can effectively protect the AC base layer and make the pavement perpetual.

Based on those criteria, the asphalt pavement structures from Butler 129-22E, Delaware 23-17S, Hamilton 126-11E, Pike 32-19E, Pike 32-15W, Lucas 25-10S, and Clark 41-3N can be classified as perpetual. The Ross 35-1W structure was not classified as perpetual, but could be modified to meet the perpetual pavement requirements with a surface layer addition. The Champaign 68-2N and Greene 35-21E structures were considered to not be perpetual.

This research approach showed the condition of the AC base layer can be determined by FWD and IDT testing. Also, the higher performing pavements had similar IDT strength values as the rich bottom asphalt layer from WAY-30 designed perpetual pavement which shows the AC base layer of the older designs have maintained their structural integrity.

Empirical FWD equations that were based on FWD data were used to estimate the strain at the bottom of the AC base layer; those equations consistently under-estimated the strain. However, there was an excellent relationship between strain results from back-calculated strains and the empirically calculated strains. Therefore, strains can be quickly estimated by applying the loads and deflections to the Kim and Park (2002) AUPP equation and using the relationship found in the trend line to estimate the back-calculated results.

The Portable Seismic Property Analyzer (PSPA) was a very useful tool in quickly estimating the condition of the pavement; the seismic modulus can be used to estimate the resilient modulus of asphalt.

## 14 Status Update on Previous Perpetual Pavement Test Roads

### 14.1 US Route 30 Wayne County (WAY-30)

Construction of the US Route 30 bypass in Wayne County (WAY-30) was completed in 2005, and the road was built to demonstrate perpetual pavement concepts. Monitoring the test sections continued until 2010, last reported in a June 2010 report on a project titled “Monitoring And Modeling Of Pavement Response And Performance Task A: Ohio” (Sargand and Figueroa, 2010). At that point the perpetual AC pavement was performing well, with little or no distress. After June 2010, ODOT assumed responsibility for data collection from the test sections. To fulfill the requirements for this project, a forensic investigation trip was conducted with the assistance of ODOT personnel to the WAY-30 site in July 2014. At that time the ORITE team observed severe surface distress in the test pavement. Figure 107 through Figure 112 show examples of the surface distress observed on WAY-30. A check of the sensors in the test sections indicated that 90% of the gauges were non-functional as would be expected, given the life expectancy of a these gauges is listed as 2 to 3 years by the manufacturer, and since it had been 9 years since the installation of the sensors.



Figure 107. Surface distress at Station 876 of WAY-30, including test section and WIM.



**Figure 108. Surface distress at Sta. 876 of WAY-30.**



**Figure 109. Surface distress at Sta.876 of WAY-30.**





**Figure 110. Test section at Sta. 664 of WAY-30.**



**Figure 111. Surface distress at Sta. 664 of WAY-30.**



**Figure 112. Surface distress at Sta. 664 of WAY-30.**

Falling weight deflectometer (FWD) data collected by ODOT and included in the previous report (Sargand and Figueroa, 2010) showed that in October 2007, Section B (Station 884-889 WB) had an average spreadability (SPR) of 60.8% and average Df1/Df7 of 3.90. Section C (875-881 WB) from May 2008 had an average SPR of 60.2% and Df1/Df7 of 3.84 and Section E (661-667 WB) from May of 2008 had an average SPR of 63.7% and Df1/Df7 of 3.58. FWD data collected in April of 2014 are presented in Table 117 and show the average SPR for Section B is 57.3% and Average Df1/Df7 is 3.98, the average SPR for Section C is 55.2% and Df1/Df7 is 4.17 and the average SPR for Section E is 60.9% and Df1/Df7 is 4.32. Spreadability is correlated to the structural response of the entire pavement, and although these numbers show a small reduction between 4% to 8%, this likely reflects the surface condition and not necessarily the overall pavement condition.

**Table 117. Summary of FWD data from WAY-30.**

April 14, 2014 – AC Sections WAY-30 – FWD Summary								
Section ID	Pavement Surface Temperature		Right Wheel Path					
	(°F)	(°C)	Df1		Df7		Df1/Df7	SPR (%)
			(mil/kip)	(mm/MN)	(mil/kip)	(mm/MN)		
B	68.0	20.0	0.43	2.75	0.12	0.76	3.64	57.33
C	68.1	20.1	0.39	2.52	0.09	0.63	3.98	55.21
E	63.0	17.2	0.47	3.01	0.14	0.91	3.28	60.93

### 14.2177 Stark County (STA-77)

The I77 perpetual pavement section in Canton in Stark County (STA-77) was visited by the research team in September of 2011. A distress survey and FWD data collection was conducted. The pavement showed little rutting as shown in Figure 113, and the only major distresses are longitudinal cracks along the edge line as shown in Figure 114 and Figure 115. Falling Weight Deflectometer data collected during this visit is summarized in Table 118. Sections A and B represent a 500 ft (152 m) long test strip for each of the two test areas on STA-77, Section A at approximately mile marker 108.55 north bound, and Section B at approximately mile marker 112.8 north bound. The SPR and Df1/Df7 are similar to those on WAY30, even though these sections did not display any signs of surface distress, again reflecting the age of the sections and confirming the sections are still in a structurally sound condition. No previous FWD data were reported.

**Table 118. Summary of FWD data from STA-77.**

September 2011 – AC Sections STA-77 – FWD Summary								
Section ID	Pavement Surface Temperature		Right Wheel Path					
	(°F)	(°C)	Df1		Df7		Df1/Df7	SPR (%)
			(mil/kip)	(mm/MN)	(mil/kip)	(mm/MN)		
A	72.0	22.2	0.32	2.08	0.092	0.59	3.60	56.69
B	81.0	27.2	0.57	3.68	0.17	1.09	3.37	58.90



**Figure 113. Rutting measurement on STA-77.**



**Figure 114. Longitudinal cracks on STA-77.**



**Figure 115. Longitudinal cracks on STA-77.**

## 15 Conclusions and Recommendations

The primary objective of this study was to develop a procedure for the selection of the optimal design for perpetual pavements in Ohio. Other specific objectives of this project included:

- Investigate various perpetual pavement structure alternatives through varying the thickness and material properties of pavement layers in field test sections.
- Use data collected at the field test sections to verify the analysis results.
- Evaluate typical conventional asphalt pavement designs currently used in Ohio and develop an approach to retrofit existing conventional asphalt pavements in good condition to meet the perpetual pavement requirements.

The design of perpetual pavement is based on adjusting materials and thickness so that the maximum tensile strain at the bottom of the asphalt stays below the endurance limit, which prevents bottom-up fatigue cracking. Past projects, such as WAY-30 around Wooster and STA-77 in Canton, were designed based on an endurance limit of  $70\mu\epsilon$ . This is well-established as a conservative number. In this study, endurance limit was obtained following NCHRP Project 9-44A report (Witczak et al, 2013).

### 15.1 Major Conclusions

#### 15.1.1 DEL-23

All the data obtained from DEL-23 for all the loading conditions, speed, climate conditions, including worst case conditions, such as 5 mph (8 km/h) traffic under high temperature, were analyzed in conjunction with the NCHRP 9-44A endurance limit model. It was determined the thickness of 13 in (33 cm) or greater, constructed on a 6 in (15 cm) aggregate base and stabilized subgrade, met criteria for perpetual pavement, while the 11 in (28 cm) section on the same base and subgrade did not. It was also determined a pavement thickness of 15 in (38 cm) or greater, constructed on an aggregate base and compacted subgrade, also met perpetual pavement criteria.

With stabilized soil, both the stabilized soil and the ODOT Item 304 base will have increased stiffness (Sargand et al, 2014), thus the strains at the bottom of the asphalt pavement will be reduced and the deflection of the base and subgrade will also be low.

The worst case test conditions, 5 mph (8 km/h) heavy load will not produce a major discrepancy with static load. These conditions may lead to rutting in the surface course, but the rutting will be minimal in the base and stabilized subgrade due to their enhanced stiffness.

#### 15.1.2 Existing pavements

Using FWD back calculated moduli in elastic layer models predicted strain in bottom layer with reasonable accuracy when compared to finite element modeling, however empirical equations typically predicted lower strains.

Seven of the ten pavements studied met perpetual pavement criteria assuming an endurance limit of  $70\mu\epsilon$ , which observations and distress surveys confirmed. One pavement could be made perpetual with added AC layers, and the other two appeared to have damage and would require a substantial overlay to reduce strain to  $70\mu\epsilon$  or less.

ODOT can use the technique in the recommendations below (Section 15.3) to evaluate existing pavements to determine if they are perpetual or could be made perpetual with a designed overlay adding sufficient thickness to reduce the strain in the pavement below the endurance limit. If actual material properties data are not available, the  $70\mu\epsilon$  endurance limit can be used as a conservative value.

### **15.1.3 APLF**

Test lanes were constructed in the Accelerated Pavement Load Facility (APLF) which further evaluated thicknesses and included the use of high-polymer content binder, or highly modified asphalt (HiMA). On the built-up sections in the indoor facility, subgrade was stabilized, moisture increase in the subgrade soil typically experienced in the field did not occur, and construction quality was very high.

In the APLF, based on data collected, all sections satisfied NCHRP Project 9-44A criteria for perpetual pavement (Witczak et al, 2013). The 8 in (20 cm) thick well-constructed HiMA pavement on 304 and stabilized subgrade met perpetual pavement criteria in the highly controlled environment of the APLF.

Very little rutting was observed in the test pavements. Comparing HiMA with control sections there was significant improvement in rutting resistance using the high polymer asphalt.

### **15.1.4 Additional major conclusions**

Stabilization of subgrade appeared to have a significant impact on reducing strains in the FRL, based on data on DEL-23, where 13 in (33 cm) section on stabilized subgrade had lower FRL strains than 15 in (38 cm) section on non-stabilized subgrade.

Using the NCHRP 9-44A model, one of the key steps is determining the initial modulus  $E_0$  (Witczak et al, 2013). The MEPDG assumes  $E_0 = E^*$ , while Romanoschi, et al (2006) indicate  $E_0 = E^*/2$ . All DEL-23 sections satisfy perpetual criteria on the latter assumption; if  $E_0 = E^*$  only the 11 in (28 cm) section failed the perpetual pavement criterion, which matches the experimental findings.

For the mixes used on DEL-23 and in the APLF,  $E^*$  for the fatigue resistance layer and the asphalt base course (ODOT Item 302) were very similar in the laboratory tests. Thus in implementing NCHRP 9-44A, it is concluded the FRL can be replaced with an asphalt base course.

## **15.2 Detailed Conclusions from Various Tasks**

The controlled load testing on DEL-23 was conducted at speeds of 5 mph (8 km/h), representing heavily congested traffic, 30 mph (48 km/h) representing urban speeds, and 55 mph (89 km/h), representing rural areas. Temperature of the FRL on DEL-23 ranged between 40°F (4.4°C) to 45°F (7.2°C) during the late autumn weather testing and 97°F (36.1°C) to 86°F (30°C) during summer weather testing. The maximum measured horizontal strains in the FRL on US 23 were 68  $\mu\epsilon$ , 34  $\mu\epsilon$ , and 43  $\mu\epsilon$  during cold weather testing for the 11 in (28 cm), 13 in (33 cm), and 15 in (38 cm) asphalt thicknesses, respectively, and correspondingly 143  $\mu\epsilon$ , 85  $\mu\epsilon$ , and 102  $\mu\epsilon$  during warm weather testing for the 11 in (28 cm), 13 in (33 cm), and 15 in (38 cm) asphalt thicknesses, respectively. None of the pavements exceeded the 40°F (4.4°C) fatigue endurance limit, 80 $\mu\epsilon$ , during the cold weather testing. However, the 11 in (28 cm) thick pavement significantly exceeded, and the 15 in (38 cm) pavement barely exceeded the 100°F (37.8°C) fatigue endurance limit of 100  $\mu\epsilon$  during the warm weather testing. Thus the 11 in (28 cm) section was not perpetual. The 13 in (33 cm) design represents the minimum thickness perpetual

pavement on DGAB and stabilized subgrade, while the 15 in (38 cm) thickness is the minimum recommended for perpetual pavement on DGAB and compacted subgrade.

Using  $E_0 = E^*$ , the computed endurance limit strains were 68-70 $\mu\epsilon$  for 40°F (4.4°C), 79-80  $\mu\epsilon$  at 70°F (21.1°C) and 99-100 $\mu\epsilon$  at 100°F (37.8°C), with the narrow ranges describing the pavements at DEL-23 and the control and HiMA sections in the APLF.

All pavement responses measured, including longitudinal strain in the FRL and longitudinal and transverse strains in the base layer, tended to decrease as the truck testing speed was increased. This trend was least prevalent in the 13 in (33 cm) section for strain measurements obtained in both the FRL and base layer. Additionally, at higher tire pressures, the strain measured in the FRL and base layers of all three sections tended to stabilize between 30 mph (48 km/h) and 55 mph (89 km/h), although, as the pavement thickness increased, strain measurements continued to decrease between 30 mph (48 km/h) and 55 mph (89 km/h) even at higher tire pressures.

The computer simulations with PerRoad predicted lifespans for all sections which greatly exceeded 50 years. PerRoad predicted lifespans of 324 years for the 11 in (28 cm) section, 385 years for the 13 in (33 cm) section, and 402 years for the 15 in (38 cm) section. Pavement responses exceeded corresponding threshold limits less than 1% of the time, except horizontal strain in the FRL of the 11 in (28 cm) section was predicted to exceed the conservative 70 $\mu\epsilon$  threshold 2.28% of the time. The accuracy of PerRoad in Ohio should be validated before using it for pavement analysis.

Utilizing the available mechanistic properties of materials and the national calibration in the MEPDG software (AASHTOWare Pavement-ME Design), the simulated performance ranking of the test sections was similar to the results observed in the field test sections on DEL-23 and the APLF. However, only relative comparisons can be made because the ME Design software is not calibrated for Ohio.

### 15.3 Recommendations

New pavement designs which result in an asphalt thickness greater than 13 in (33 cm) on a 6 in (15 cm) dense graded aggregate base on stabilized subgrade or 15 in (38 cm) of asphalt on a 6 in (15 cm) dense graded aggregate base on compacted subgrade should be evaluated for perpetual performance using the following equation:

$$SR = 2.0844 - 0.1386 \cdot \log(E_0) - 0.4846 \cdot \log(\epsilon) - 0.2012 \cdot \log(N) + 1.4103 \cdot \tanh(0.8471 \cdot RP) + 0.0320 \cdot \log(E_0) \cdot \log(\epsilon) - 0.0954 \cdot \log(E_0) \cdot \tanh(0.7154 \cdot RP) - 0.4746 \cdot \log(\epsilon) \cdot \tanh(0.6574 \cdot RP) + 0.0041 \cdot \log(N) \cdot \log(E_0) + 0.0557 \cdot \log(N) \cdot \log(\epsilon) + 0.0689 \cdot \log(N) \cdot \tanh(0.259 \cdot RP)$$

Where:

$SR$  = stiffness ratio = stiffness measured at any load cycle during beam fatigue testing to the initial stiffness of the specimen

$E_0$  = initial flexural stiffness (ksi)

$\epsilon$  = applied tensile strain ( $\mu\epsilon$ )

$RP$  = rest period (sec)

$N$  = number of load cycles

The procedure is as follows:

- Measure or estimate the mechanical properties of the pavement layers and foundation soil.
  - The recent ODOT report entitled *Incorporating Chemical Stabilization of the Subgrade in Pavement Design and Construction Practices* (Sargand et al, 2014) provides a procedure for estimating the moduli of stabilized subgrade and compacted subgrade.
- Compute the endurance limit using the equation above, setting  $SR = 1$ , and determine  $\varepsilon_i$ . For the initial stiffness value,  $E_0$ , use the results of the beam fatigue test to provide the most accurate estimate.
  - If  $E_0$  from beam fatigue testing is not available,  $E^*$  obtained from AMPT (Asphalt Mixture Performance Test) or the Witczak equation can be used to estimate  $E_0$ .
- Use elastic layer software to estimate the horizontal strain at the bottom of the asphalt base and compare to the endurance limit determined in the previous step or to the currently used value of  $70 \mu\varepsilon$ , which appears to be a conservative and reasonable value based on testing completed for this project.

In-service flexible pavements programmed for overlays can be evaluated for perpetual performance by calculating the strain at the bottom of the asphalt layer using back calculated modulus values in elastic layer models. However, a quick estimate using the AUPP equation developed by Kim and Park (2002) may be used by pavement designers, keeping in mind that the AUPP equation results are about  $10 \mu\varepsilon$  lower than the back-calculated strain on average. Thus, the following steps are recommended for evaluating an existing flexible pavement's perpetual pavement status:

- Perform FWD test.
- Normalize all the deflections to be evaluated to a 9000 lb (40 kN) load.
- Insert deflection values for sensors  $D_0$ ,  $D_{12}$ ,  $D_{24}$ , and  $D_{36}$  into the equation below to calculate *AUPP*.

$$AUPP = (5D_0 - 2D_{12} - 2D_{24} - D_{36})/2$$

- Insert *AUPP* into the equation developed by Kim & Park (2002) to get a quick estimate of the strain at the bottom of the AC base layer,  $\varepsilon_{ac}$ .

$$\log(\varepsilon_{ac}) = 1.034 \log(AUPP) + 0.932$$

- Add  $10 \mu\varepsilon$  to obtain adjusted strain  $\varepsilon_{adj} = \varepsilon_{ac} + 10$  that matches back calculated value.
- If the adjusted strain  $\varepsilon_{adj}$  calculated is below  $70 \mu\varepsilon$ , then the pavement is considered perpetual.
  - If the adjusted strain  $\varepsilon_{adj}$  calculated is above  $70 \mu\varepsilon$  then the pavement is not considered perpetual, Reevaluate the AC pavement FWD results using Evercalc 5.0. Add thickness to the pavement structure until the strain at the bottom of the AC base layer is less than or equal to  $70 \mu\varepsilon$  on the Evercalc program.

Further research should be conducted to investigate the relationship between the initial modulus  $E_0$  as measured during the beam fatigue test and  $E^*$  measured with the AMPT.



## **15.4 Implementation**

ODOT can use the NCHRP 9-44A procedure to evaluate the endurance limit for an asphalt mix.

When designing perpetual pavement thickness, include global soil stabilization as per current policy. That will result in a significant reduction in asphalt thickness required to meet perpetual pavement design, particularly in combination with ODOT Item 302 base.

A procedure to evaluate the perpetual nature of in-service flexible pavement has been presented. ODOT should use this procedure when the FWD data is available to determine the thickness required to achieve perpetual performance.

An understanding of the  $E_0/E^*$  relationship may allow ODOT to reduce the thickness required for perpetual performance with confidence if the relationship developed by Romanoschi is valid for Ohio mixes.

## 16 References

- ABAQUS user's manual*, version 6.9. (2009). Simulia, Providence, RI
- Abbas, A., and Frankhouser, A. A. (2012). *Improved Characterization of Truck Traffic Volumes and Axle Loads for Mechanistic-Empirical Pavement Design*. Ohio Department of Transportation and U.S. Department of Transportation, Federal Highway Administration.
- Advanced Asphalt Technologies. (2008). Developing a Plan for Validating an Endurance Limit for HMA Pavements. HMA Endurance Limit Validation Study. Research Plan. NCHRP Project 9-44. Sterling, Virginia. November, 2008.
- Al-Qadi, I. L., Wang, H., Yoo, P. J., & Dessouky, S. H. (2008). Dynamic analysis and in situ validation of perpetual pavement response to vehicular loading. *Transportation Research Record: Journal of the Transportation Research Board*, 2087(1), 29–39.
- American Association of State Highway and Transportation Officials. (2007). *Standard method of test for resistance of compacted hot mix asphalt (HMA) to moisture-induced damage (AASHTO T 283)*. Washington, DC.
- Applied Research Associates, Inc. (2009). *Guidelines for Implementing NCHRP 1-37A*, State Job 134300. The Ohio Department of Transportation and U.S. Department of Transportation, Federal Highway Administration. In particular Volume 4, “MEPDG Models Validation and Recalibration”
- Asphalt Pavement Alliance. (2002). *Perpetual pavements: A synthesis*. (APA 101). Lanham, MD: National Asphalt Pavement Association, Asphalt Institute, State Asphalt Pavement Associations.
- Asphalt Pavement Association of Oregon. (2005). Perpetual pavement concept renders 20-year standard obsolete. *Centerline*, 4(2), 1–2.
- Asphalt Pavement Alliance. (2010). *Asphalt pavement: America rides on US*. (IM-41). Lanham, MD.
- Battaglia, I. K., Bischoff, D., Ryan, J., & Reichelt, S. (2010). *Evaluation of a hot mix asphalt perpetual pavement*. (FEP-01-10). Madison, WI: Wisconsin Department of Transportation
- Behbahani, H., Khaki, A. M., & Amini, A. A. (2009). *Assessment of perpetual pavement performance using mechanistic-empirical pavement design guide*. Iran University of Science and Technology, Narmak, Tehran, Iran.
- Bendana, J., Sargand, S. M., & Hernandez, J. A. (2009). Comparison between perpetual and standard asphalt concrete pavement sections on NY I-86. *Paper presented at the Proceedings for the International Conference on Perpetual Pavements*. Columbus, OH.
- Brown, E. R., Cooley, L. A., Hanson, D., Lynn, C., Powell, B., Prowell, B., & Watson, D. (2002). *NCAT test track design, construction, and performance*. (NCAT Report 02-12). Auburn, AL: National Center for Asphalt Technology.
- Buchner, M., Newcomb, D., & Huddleston, J. (2000). *Perpetual pavements*. Asphalt: The Magazine of the National Asphalt Institute, 15(3).
- Bushman, R., Pratt, A.J. (1998). Weigh in motion technology - Economics and performance. *Paper presented at the North American Travel Monitoring Exposition and Conference*, Charlotte, NC.
- Carpenter, S. H., & Shen, S. (2006). Fatigue characteristics of rich bottom bases (RBB) for structural design of perpetual pavements. *Paper presented at the Proceedings for the International Conference on Perpetual Pavements*, Columbus, OH.

- Carpenter, S. H., Ghuzlan, K. A., & Shen, S. (2003). A fatigue endurance limit for highway and airport pavements. *Paper presented at the Transportation Research Board 2003 Annual Meeting* (Paper No. 03-3428), Washinton, D.C.
- Estes, T. (2005). Oregon answers perpetual pavement analysis with a field test. *Maximum Asphalt*, 75(11), 56–61.
- Figuroa, J. (2004). *Long term monitoring of seasonal and weather stations and analysis of data from SHRP pavements*. Case Western Reserve University, Department of Civil Engineering, Cleveland, Ohio.
- Garg, Navneet, and Thompson, Marshall R. (1998). Mechanistic-Empirical Evaluation of the MN/Road Low Volume Road Test Sections. (Report No. FHWA-IL-UI-262 for Illinois Department of Transportation). Urbana IL, May, 1998.
- Geology (2013). *Ohio map collection*. Retrieved March 28, 2013, from <http://geology.com/state-map/ohio.shtml>
- Geomedia Research & Development. (2007). *PSPA and SPA manager manual*. El Paso, TX.
- Hatch, N. (2008). *Perpetual pavement: monitoring performance in real time*. (No. 0092-06-01). Madison, WI: Wisconsin Department of Transportation.
- Hernandez, J. A. (2010). *Evaluation of the response of perpetual pavement at accelerated pavement loading facility: Finite element analysis and experimental investigation*. (Unpublished MS thesis), Ohio University, Athens, OH.
- Hornyak, N. J. (2010). *Perpetual pavement analysis for the Marquette interchange instrumentation project*. (Unpublished MS thesis), Marquette University, Milwaukee, WI.
- Hornyak, N. J., & Croveti, J. A. (2008). *Marquette interchange perpetual pavement instrumentation project phase II final report*. (WHRP 08-04). Milwaukee, WI: Transportation Research Center, Marquette University.
- Huang, Y. H. (2004). *Pavement analysis and design* (2<sup>nd</sup> ed.). (M. Horton, Ed.) Upper Saddle River, New Jersey: Pearson Education, Inc.
- Jincheng, W., Lin, W., & Shijie, M. (2012). Modeling mechanical response of a perpetual pavement test road. *Journal of Performance of Contrusted Facilities*, 2(26), 153–161. doi:10.1061/(ASCE)CF.1943-5509.0000244.
- Kim, S., Sargand, S., Masada, T., & Hernandez, J. (2010). *Determination of mechanical properties of materials used in WAY-30 test pavements*. Ohio University, Civil Engineering Department, Athens, OH.
- Kim, Y. Richard, and Park, Heemun. (2002). *Use Of Falling Weight Deflectometer Multi-Load Data For Pavement Strength Estimation*. (Report No. FHWA/NC/2002-006 for the North Carolina Department of Transportation). Raleigh NC, June 2002.
- Liao, Y. (2007). *Viscoelastic FE modeling of asphalt pavements and its applications to U.S. 30 perpetual pavement*. (Unpublished Ph.D. dissertation), Ohio University, Civil Engineering Department, Athens, OH.
- Teruhisa Masada, Shad M. Sargand, Basel Abdalla and J. Ludwig Figuroa, (2004) *Materials Properties for Implementation of Mechanistic-Empirical (M-E) Pavement Design Procedures*, Final Report, ODOT/FHWA (February 2004).
- Morian, D., & Frith, D. J. (2009). *Consideration of design parameters for life long pavements*. Quality Engineering Solutions, Conneaut Lake, PA.
- National Atlas of the United States. (2013). *Transportation of the United States*. Retrieved May 13, 2013, from <http://nationalatlas.gov/transportation.html>

- National Cooperative Highway Research Program (NCHRP). (2008). *An experimental plan validation of an endurance limit for HMA pavements*. (Document 134). Sterling, VA: Advanced Asphalt Technologies.
- National Cooperative Highway Research Program (NCHRP). (2010). *Validating the fatigue endurance limit for hot mix asphalt*. (Report 646). Washington, DC: Transportation Research Board.
- Newcomb, D. E., & Hansen, K. R. (2006). *Mix type selection for perpetual pavements*. Lanham, MD: National Asphalt Pavement Association.
- Newcomb, D. E., Willis, R., & Timm, D. H. (2010). *Perpetual asphalt pavements a synthesis*. (IM 40) Lanham, MD: Asphalt Pavement Alliance.
- Ning, L. I., Molenaar, A. A. A., Van de Ven, M. F. C., & Shaopeng, W. U. (2010). Estimation of the fatigue endurance limit of HMAC for perpetual pavements. *Journal of Wuhan University of Technology-Mater*, 25(4), 645–649. doi:10.1007/s11595-010-0062-7
- Nunn, M., & Ferne, B. W. (2001). Design and assessment of long-life flexible pavements. *Transportation Research Circular*, 503, 32–49. ISSN: 0097-8515.
- Park, Hee Mun, and Kim, Y. Richard. (2003). “Use Of Falling Weight Deflectometer Multi-Load Data For Pavement Strength Estimation”. Paper 03-0684 presented at the Annual Meeting of the Transportation Research Board, January 2003.
- Portillo, M. M. (2008). *Measured and theoretical response of perpetual pavement structures*. (Unpublished MS thesis), University of Texas at Arlington, Arlington, TX.
- Priest, A. L., & Timm, D. H. (2006). *Methodology and calibration of fatigue transfer functions for mechanistic-empirical flexible pavement design*. (NCAT Report 06-03). Auburn, AL: National Center for Asphalt Technology.
- Prowell, B. D., & Brown, E. R. (2006). Methods for determining the endurance limit using beam fatigue tests. *Paper presented at the Proceedings for the International Conference on Perpetual Pavements, Columbus, OH*.
- Qin, J. (2010). *Predicting flexible pavement structural response using falling weight deflectometer deflections*. (Unpublished MS Thesis), Ohio University, Civil Engineering Department, Athens, OH.
- Retrepo-Velez, A. M. (2011). *Long-term performance of asphalt concrete perpetual pavement WAY-30 project*. (Unpublished MS thesis), Ohio University, Athens, OH.
- Robbins, M. M., & Timm, D. H. (2008). Temperature and velocity effects on a flexible perpetual pavement. *Paper presented at the 3rd International Conference on Accelerated Pavement Testing, Madrid, Spain*.
- Robbins, M. M., & Timm, D. H. (2009). *Effects of strain pulse duration on tensile strain in a perpetual pavement*. Proceedings from International Conference on Perpetual Pavement 2009, Columbus, OH.
- Romanello, M. T. (2007). *Load response analysis of the WAY-30 test pavements: US Route 30, Wayne County, Ohio*. (Unpublished MS thesis), Ohio University, Athens, OH.
- Romanoschi, S. A., Gisi, A. J., & Dumitru, C. (2006). The dynamic response of Kansas perpetual pavements under vehicle loading. *Paper presented at the Proceedings for the International Conference on Perpetual Pavements, Columbus, OH*.
- Romanoschi, S. A., Gisi, A. J., Portillo, M. M., & Dumitru, C. (2008). First findings from the Kansas perpetual pavements experiment. *Transportation Research Record*, 2068, 41–48.

- Sargand, S. M., Khoury, I. S., Romanello, M. T., & Figueroa, J. L. (2006). Seasonal and load response instrumentation of the WAY-30 perpetual pavements. *Paper presented at the Proceedings for the International Conference on Perpetual Pavements, Columbus, OH.*
- Sargand, S., Figueroa, J. L., & Romanello, M. (2008). *Instrumentation of the WAY-30 test pavements.* (Report No. FHWA/OH-2008/7). Athens, OH: Ohio Research Institute for Transportation and the Environment, Ohio Department of Transportation.
- Sargand, S., Figueroa, J. L., Edwards, W., & Al-Rawashdeh, A. S. (2009). *Performance assessment of warm mix asphalt (WMA) pavements.* (Report No. FHWA/OH-2009/08). Athens, OH: Ohio Research Institute for Transportation and the Environment, Ohio Department of Transportation.
- Sargand, S., Masada, T., Hernandez, J., and Kim, S.-S., (May 2010). *Determination of Mechanical Properties of Materials Used in WAY-30 Test Pavements.* (Report No. FHWA/OH-2010/9 for the Ohio Department of Transportation & Federal Highway Administration).
- Sargand, S. M., & Figueroa, J. L. (2010). *Monitoring and Modeling of Pavement Response and Performance Task A: Ohio.* (pp. 88–89). (Report No. FHWA/OH-2010/3A). Athens, OH: Ohio Research Institute for Transportation and the Environment, Ohio Department of Transportation.
- Sargand, S., and Edwards, W. (2010). with David Lankard, consultant. *Forensic Investigation of AC and PCC Pavements with Extended Service Life.* (Report No. FHWA/OH-2010/004 for the Ohio Department of Transportation & Federal Highway Administration).
- Sargand, S. M., Khoury, I. S., & Morrison, J. (2012). *Monitoring and Modeling of Pavement Response and Performance Task B: New York* (Vol. 1). (Report No. FHWA/OH-2012/08A). Athens, OH: Ohio Research Institute for Transportation and the Environment, Ohio Department of Transportation.
- Shad Sargand, Issam Khoury, Jayson Gray, and Anwer Al-Jhayyish, (2014), *Incorporating Subgrade Stabilization in Pavement Design and Construction*, Report FHWA/OH-2014/12 for Ohio Dept. of Transportation, October 2014.
- Scholz, T. V., Huddleston, J., Hunt, E. A., Lundy, J. R., & Shippen, N. C. (2006). Instrumentation and analysis of a perpetual pavement on an interstate freeway in Oregon. *Paper presented at the Proceedings for the International Conference on Perpetual Pavements, Columbus, OH.*
- Tarefder, R. A., & Bateman, D. (2009). Determining the optimal perpetual pavement structure. Ohio Research Institute for Transportation and the Environment. *Paper presented at the Proceedings for the International Conference on Perpetual Pavement. Columbus, OH.*
- Tarefder, R. A., & Bateman, D. (2012). Design of optimal perpetual pavement structure. *Journal of Transportation Engineering*, (February), 157–175. doi:10.1061/(ASCE)TE.1943-5436.0000259.
- Texas Department of Transportation. (2008). *Frequently asked questions about the falling weight deflectometer (FWD).* Construction and Bridge Divisions, Austin, Texas.
- Thompson, M. R., & Carpenter, S. H. (2006a). Perpetual pavement design: an overview. *Paper presented at the Proceedings for the International Conference on Perpetual Pavements, Columbus, OH.*
- Thompson, M. R., & Carpenter, S. H. (2006b). Considering hot-mix-asphalt fatigue endurance limit in full-depth mechanistic-empirical pavement design. *Paper presented at the Proceedings for the International Conference on Perpetual Pavements, Columbus, OH.*

- Thompson, M. R., & Carpenter, S. H. (2009). *Perpetual pavement design: An overview*. Proceedings from International Conference on Perpetual Pavement 2009, Columbus, OH.
- Timm, D. H., Robbins, M. M., Willis, J. R., Tran, N., & Taylor, A. J. (2013). *Field and Laboratory Study of High-Polymer Mixtures at the NCAT Test Track Final Report* (NCAT Report 13-03). Auburn, AL: National Center for Asphalt Technology.
- Timm, D. H. (2009). *Design, construction and instrumentation of the 2006 test track structural study*. (NCAT Report 09-01). Auburn, AL: National Center for Asphalt Technology.
- Timm, D. H., & Davis, K. P. (2009). Perpetual pavement design using the MEPDG and PerRoad. *Paper presented at the Proceedings for the International Conference on Perpetual Pavement, Columbus, OH.*
- Timm, D. H., & Newcomb, D. E. (2006). Perpetual pavement design for flexible pavements in the US. *International Journal of Pavement Engineering*, 7(2), 111–119. doi:10.1080/10298430600619182
- Timm, D. H., Robbins, M. M., Huber, G., & Yang, Y. (2010). Analysis of perpetual pavement experiment sections in china. *Paper presented at the 90th Annual Meeting of the Transportation Research Board, Washington, D.C.*
- Timm, D., Selvaraj, I., Brown, R., West, R. C., Priest, A., Powell, B., & Zhang, J. (2006). *Phase II NCAT test track results*. (NCAT Report 06-05). Auburn, AL: National Center for Asphalt Technology.
- The Weather Channel (2013). Monthly weather for Delaware. Retrieved from <http://www.weather.com/weather/wxclimatology/monthly/graph/USOH0252>.
- Von Quintus, H. L. (2006). Application of the endurance limit premise in mechanistic-empirical based pavement design procedures. *Paper presented at the Proceedings for the International Conference on Perpetual Pavements, Columbus, OH.*
- Washington State Department of Transportation. (2005). *Everseries user guide pavement analysis computer software and case studies*. Olympia, WA.
- Williams, R. R., & Nazarian, S. (2007). Correlation of Resilient and Seismic Modulus Test Results. *Journal of Materials in Civil Engineering*, 19, 1026-1032.
- Willis, J. R., & Timm, D. H. (2009). *Field-based strain thresholds for flexible perpetual pavement design*. (NCAT Report 09-09). Auburn, AL: National Center for Asphalt Technology.
- Willis, J.R. (2009), *Field-based Strain Thresholds for Flexible Perpetual Pavement Design*, Ph.D. Dissertation, Auburn University, Auburn AL, May 9, 2009. Available online at [http://etd.auburn.edu/etd/bitstream/handle/10415/1580/Willis\\_James\\_17.pdf?sequence=1](http://etd.auburn.edu/etd/bitstream/handle/10415/1580/Willis_James_17.pdf?sequence=1), viewed September 9, 2011.
- Willis, J.R. and Timm, D.H. (2009), “A Comparison of Laboratory Fatigue Thresholds to Measured Strains in Full-Scale Pavements”, Proceedings of the International Conference on Perpetual Pavement 2009, Columbus, Ohio, September 30-October 2, 2009.
- Willis, R., Timm, D., West, R., Powell, B., Robbins, M., Taylor, A., Smit, A., et al. (2009). *Phase III NCAT test track findings*. (NCAT Report 09-08). Auburn, AL: National Center for Asphalt Technology.
- Witczak, M., Mamlouk, M, Souliman, M., and Zeiada, W., 2013, *Laboratory Validation of an Endurance Limit for Asphalt Pavements*. NCHRP Report 762. Transportation Research Board. Washington, D.C.

- Wu, S., & Sargand, S. (2007). *Use of dynamic cone penetrometer in subgrade and base acceptance*. (Report No. FHWA/ODOT-2007/01 for the Ohio Department of Transportation & Federal Highway Administration).
- Yang, Y., Gao, X., Lin, W., Timm, D. H., Priest, A. L., Huber, G. A., & Andrews, D. A. (2006). Perpetual pavement design in China. *Paper presented at the Proceedings for the International Conference on Perpetual Pavements*. Columbus, OH.
- Yut, I., Nener-Plante, D., & Zofka, A. (2009). *Case study on perpetual pavement in connecticut*. Proceedings from International Conference on Perpetual Pavement 2009, Columbus, OH.

**Appendix A: LVDT calibration on DEL-23.**

**Table A.1 Calibration Data (LVDT 1-1 through 4-2)**

Displacement (in)	1-1 (V)	1-2 (V)	2-1 (V)	2-2 (V)	3-1 (V)	3-2 (V)	4-1 (V)	4-2 (V)
0	-8.12	-8.12	-8.29	-8.21	-8.37	-8.09	-8.03	-8.08
0.025	-7.84	-7.83	-8.00	-7.92	-8.12	-7.82	-7.77	-7.81
0.05	-7.55	-7.54	-7.71	-7.63	-7.84	-7.53	-7.48	-7.54
0.075	-7.25	-7.24	-7.41	-7.33	-7.55	-7.23	-7.19	-7.25
0.1	-6.95	-6.93	-7.11	-7.02	-7.25	-6.93	-6.89	-6.96
0.125	-6.65	-6.62	-6.80	-6.72	-6.95	-6.63	-6.59	-6.67
0.15	-6.34	-6.32	-6.50	-6.41	-6.65	-6.33	-6.29	-6.37
0.175	-6.04	-6.01	-6.19	-6.10	-6.35	-6.03	-5.99	-6.08
0.2	-5.74	-5.70	-5.89	-5.79	-6.04	-5.72	-5.68	-5.78
0.225	-5.43	-5.40	-5.58	-5.50	-5.74	-5.42	-5.38	-5.48
0.25	-5.13	-5.10	-5.28	-5.19	-5.44	-5.12	-5.08	-5.18
0.275	-4.82	-4.79	-4.97	-4.89	-5.14	-4.81	-4.77	-4.88
0.3	-4.52	-4.48	-4.67	-4.59	-4.83	-4.51	-4.47	-4.58
0.325	-4.22	-4.17	-4.37	-4.28	-4.53	-4.20	-4.16	-4.28
0.35	-3.91	-3.87	-4.06	-3.98	-4.22	-3.90	-3.86	-3.98
0.375	-3.61	-3.56	-3.76	-3.68	-3.92	-3.60	-3.56	-3.68
0.4	-3.30	-3.26	-3.45	-3.37	-3.61	-3.29	-3.26	-3.37
0.425	-2.99	-2.95	-3.14	-3.07	-3.30	-2.99	-2.95	-3.07
0.45	-2.69	-2.65	-2.84	-2.76	-3.00	-2.68	-2.65	-2.76
0.475	-2.38	-2.34	-2.53	-2.45	-2.69	-2.38	-2.34	-2.45
0.5	-2.07	-2.03	-2.22	-2.15	-2.39	-2.07	-2.04	-2.15
0.525	-1.76	-1.73	-1.92	-1.84	-2.08	-1.77	-1.73	-1.84
0.55	-1.45	-1.42	-1.61	-1.53	-1.78	-1.46	-1.42	-1.53
0.575	-1.04	-1.11	-1.30	-1.22	-1.47	-1.15	-1.12	-1.23
0.6	-0.83	-0.80	-0.99	-0.91	-1.16	-0.84	-0.81	-0.92
0.625	-0.52	-0.49	-0.69	-0.60	-0.85	-0.54	-0.50	-0.61
0.65	-0.21	-0.18	-0.38	-0.29	-0.54	-0.24	-0.19	-0.31
0.675	0.09	0.13	-0.07	0.01	-0.23	0.07	0.12	0.01
0.7	0.39	0.44	0.23	0.32	0.07	0.38	0.43	0.31
0.725	0.70	0.74	0.53	0.63	0.38	0.68	0.73	0.62
0.75	1.01	1.05	0.83	0.93	0.69	0.99	1.04	0.92
0.775	1.31	1.36	1.13	1.24	0.97	1.30	1.34	1.23
0.8	1.61	1.67	1.42	1.54	1.30	1.60	1.65	1.54
0.825	1.92	1.98	1.73	1.85	1.61	1.91	1.95	1.85
0.85	2.22	2.28	2.03	2.15	1.92	2.22	2.26	2.16
0.875	2.53	2.59	2.33	2.46	2.23	2.53	2.56	2.47
0.9	2.82	2.89	2.62	2.76	2.53	2.84	2.87	2.78
0.925	3.12	3.19	2.91	3.07	2.84	3.14	3.18	3.08
0.95	3.43	3.50	3.21	3.37	3.15	3.45	3.48	3.39
0.975	3.74	3.80	3.50	3.68	3.46	3.76	3.79	3.70
1	4.05	4.11	3.79	3.98	3.76	4.06	4.09	4.01
1.025	4.36	4.41	4.09	4.28	4.07	4.37	4.40	4.31
1.05	4.67	4.71	4.39	4.59	4.38	4.67	4.70	4.62
1.075	4.99	5.02	4.70	4.89	4.68	4.97	5.01	4.92
1.1	5.30	5.32	5.01	5.18	4.98	5.27	5.31	5.22
1.125	5.60	5.62	5.31	5.49	5.29			



Table A.2 Calibration Data (LVDT 5-1 through 8-2)

Displacement (in)	5-1 (V)	5-2 (V)	6-1 (V)	6-2 (V)	7-1 (V)	7-2 (V)	8-1 (V)	8-2 (V)
0	-8.23	-8.13	-8.10	-8.32	-8.00	-8.15	-8.29	-8.09
0.025	-7.96	-7.86	-7.82	-8.05	-7.71	-7.87	-8.03	-7.83
0.05	-7.66	-7.57	-7.53	-7.77	-7.43	-7.58	-7.75	-7.55
0.075	-7.36	-7.27	-7.24	-7.48	-7.14	-7.29	-7.45	-7.25
0.1	-7.06	-6.97	-6.94	-7.18	-6.85	-6.99	-7.15	-6.96
0.125	-6.75	-6.67	-6.64	-6.87	-6.55	-6.70	-6.85	-6.66
0.15	-6.44	-6.36	-6.34	-6.56	-6.25	-6.39	-6.54	-6.35
0.175	-6.13	-6.06	-6.04	-6.26	-5.95	-6.09	-6.24	-6.06
0.2	-5.83	-5.75	-5.73	-5.95	-5.64	-5.79	-5.94	-5.75
0.225	-5.51	-5.45	-5.43	-5.64	-5.34	-5.49	-5.63	-5.45
0.25	-5.21	-5.14	-5.13	-5.34	-5.04	-5.19	-5.33	-5.15
0.275	-4.90	-4.83	-4.83	-5.03	-4.73	-4.89	-5.02	-4.84
0.3	-4.60	-4.53	-4.52	-4.72	-4.42	-4.59	-4.71	-4.54
0.325	-4.30	-4.22	-4.22	-4.41	-4.12	-4.29	-4.41	-4.23
0.35	-3.99	-3.91	-3.91	-4.11	-3.81	-3.98	-4.10	-3.93
0.375	-3.68	-3.61	-3.60	-3.80	-3.50	-3.68	-3.79	-3.62
0.4	-3.37	-3.30	-3.29	-3.50	-3.20	-3.37	-3.49	-3.31
0.425	-3.07	-2.99	-2.98	-3.19	-2.89	-3.07	-3.18	-3.00
0.45	-2.76	-2.69	-2.67	-2.89	-2.58	-2.76	-2.87	-2.70
0.475	-2.46	-2.38	-2.36	-2.58	-2.27	-2.45	-2.56	-2.39
0.5	-2.15	-2.08	-2.05	-2.28	-1.96	-2.15	-2.25	-2.08
0.525	-1.85	-1.77	-1.74	-1.97	-1.65	-1.84	-1.94	-1.77
0.55	-1.54	-1.46	-1.43	-1.66	-1.34	-1.53	-1.64	-1.46
0.575	-1.23	-1.15	-1.11	-1.35	-1.03	-1.22	-1.33	-1.16
0.6	-0.92	-0.84	-0.80	-1.04	-0.73	-0.91	-1.03	-0.85
0.625	-0.61	-0.53	-0.49	-0.73	-0.42	-0.61	-0.72	-0.55
0.65	-0.30	-0.22	-0.18	-0.41	-0.11	-0.30	-0.42	-0.25
0.675	0.02	0.09	0.12	-0.10	0.19	0.09	-0.11	0.05
0.7	0.32	0.40	0.43	0.21	0.50	0.32	0.19	0.35
0.725	0.63	0.71	0.74	0.53	0.80	0.62	0.50	0.66
0.75	0.94	1.02	1.05	0.84	1.11	0.93	0.81	0.96
0.775	1.24	1.33	1.36	1.15	1.42	1.24	1.11	1.26
0.8	1.55	1.64	1.66	1.46	1.72	1.54	1.42	1.57
0.825	1.86	1.95	1.97	1.77	2.03	1.85	1.73	1.87
0.85	2.17	2.26	2.28	2.08	2.33	2.16	2.03	2.17
0.875	2.48	2.57	2.58	2.39	2.64	2.47	2.34	2.48
0.9	2.79	2.87	2.89	2.70	2.94	2.77	2.65	2.79
0.925	3.09	3.18	3.20	3.00	3.24	3.08	2.96	3.09
0.95	3.40	3.48	3.50	3.31	3.55	3.38	3.27	3.40
0.975	3.70	3.78	3.81	3.62	3.85	3.69	3.58	3.71
1	4.01	4.08	4.12	3.92	4.16	4.00	3.89	4.01
1.025	4.31	4.38	4.42	4.23	4.46	4.30	4.20	4.32
1.05	4.62	4.68	4.72	4.54	4.76	4.61	4.51	4.62
1.075	4.90	4.98	5.02	4.85	5.06	4.91	4.82	4.93
1.1	5.20	5.28	5.33	5.15	5.36	5.22	5.12	5.23
1.125		5.58	5.63		5.66	5.52		5.54

Table A.3 LVDT Calibration Factors

Sensor	Calibration Factor (V/in)	Calibration Factor (mil/mV)
LVDT 1-1	12.2309	0.081760
LVDT 1-2	12.2604	0.081563
LVDT 2-1	12.1265	0.082464
LVDT 2-2	12.2212	0.081825
LVDT 3-1	12.2268	0.081788
LVDT 3-2	12.2052	0.081932
LVDT 4-1	12.1972	0.081986
LVDT 4-2	12.1810	0.082095
LVDT 5-1	12.2793	0.081438
LVDT 5-2	12.2724	0.081484
LVDT 6-1	12.2858	0.081395
LVDT 6-2	12.3227	0.081151
LVDT 7-1	12.2209	0.081827
LVDT 7-2	12.2137	0.081875
LVDT 8-1	12.2526	0.081615
LVDT 8-2	12.1790	0.082109

**Appendix B: LVDT enclosure and reference rod diagrams for DEL-23.**

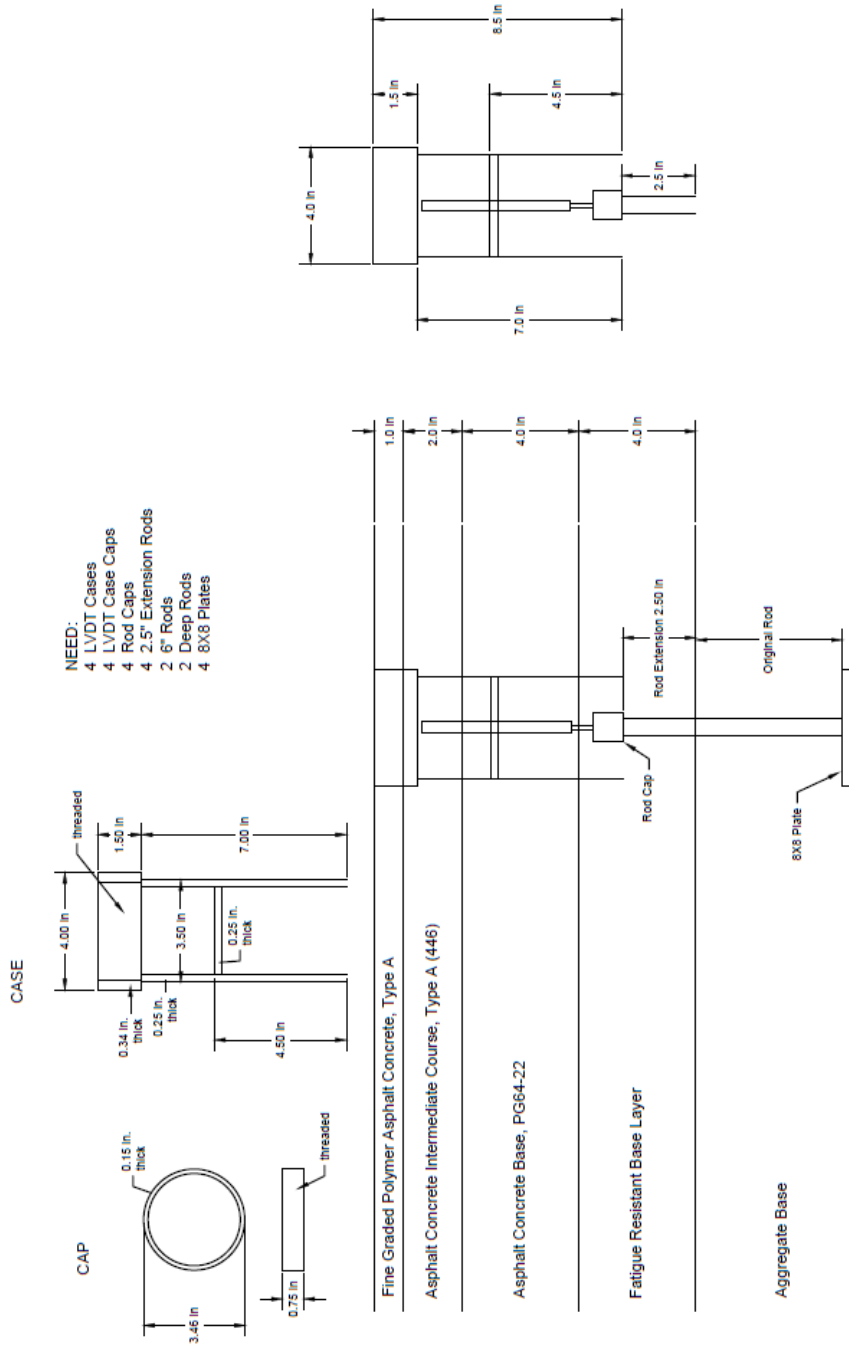


Figure B.1 11 in (28 cm) section LVDT enclosure and reference rod (1 in = 2.54 cm)

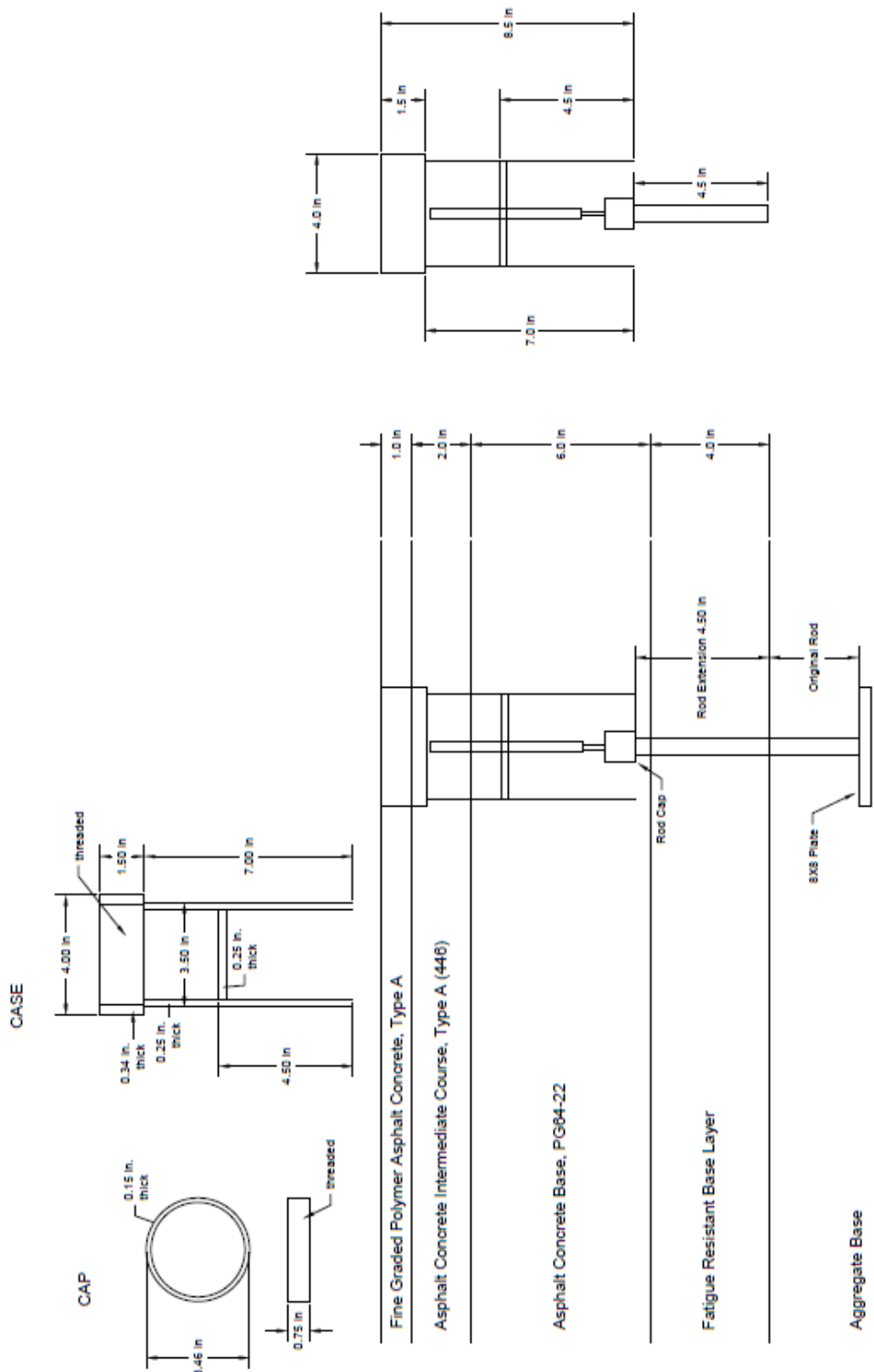


Figure B.2 13 in (33 cm) section LVDT enclosure and reference rod (1 in = 2.54 cm)

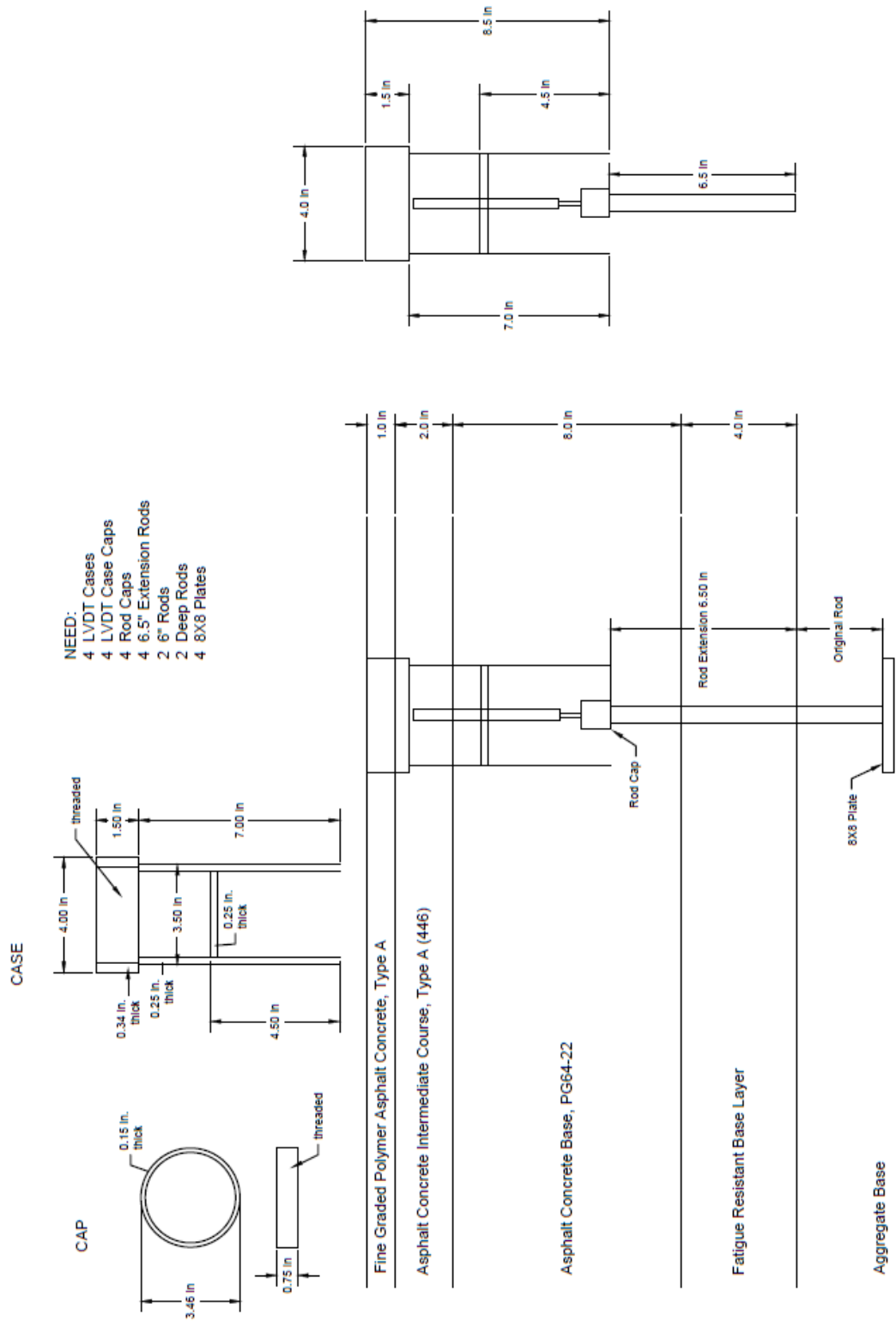


Figure B.3 15 in (38 cm) section LVDT enclosure and reference rod (1 in = 2.54 cm)

**Appendix C: Strain gage rosette hole diagrams for DEL-23.**

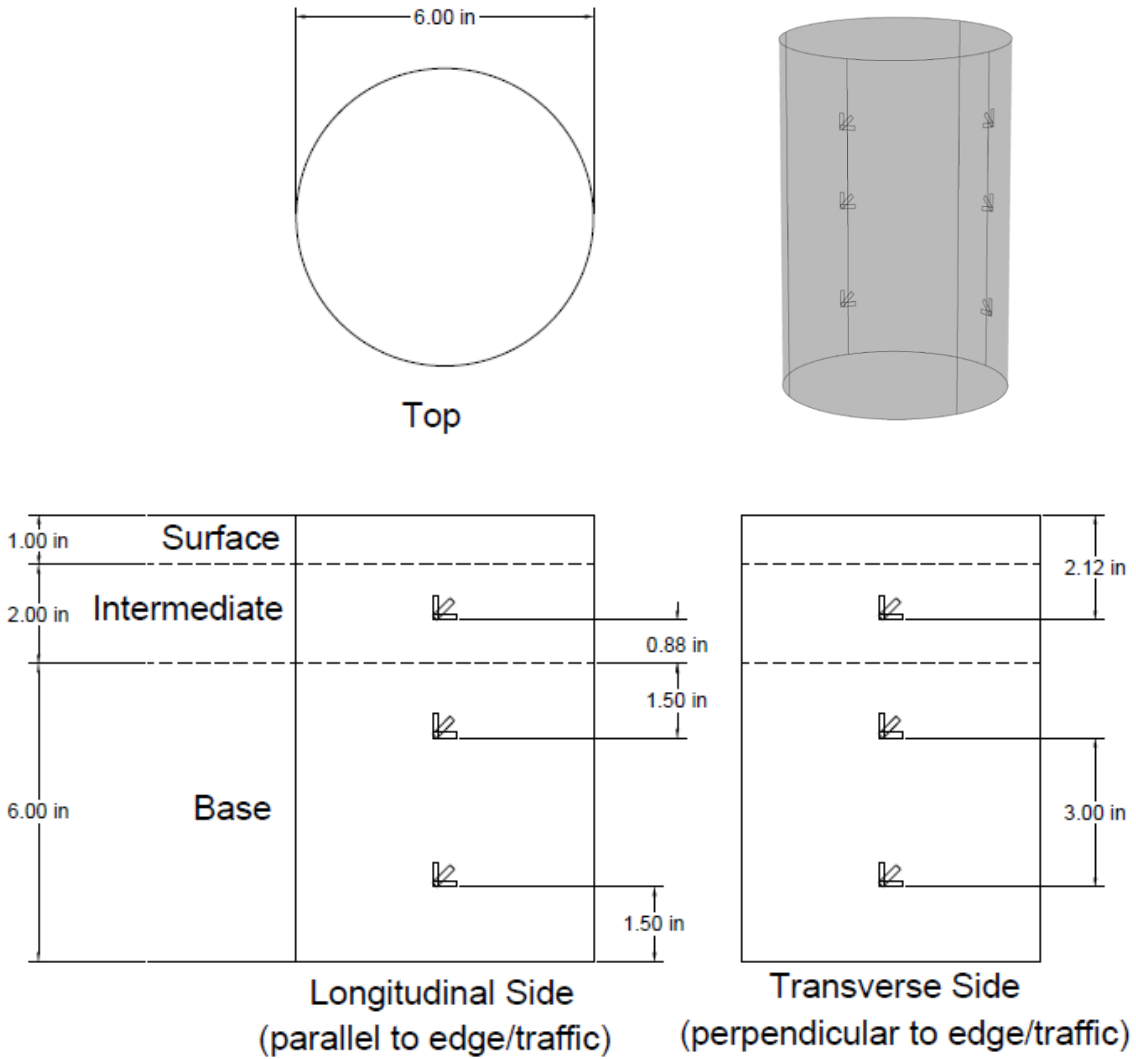


Figure C.1 13 in (33 cm) section round strain gage rosette hole (1 in = 2.54 cm)

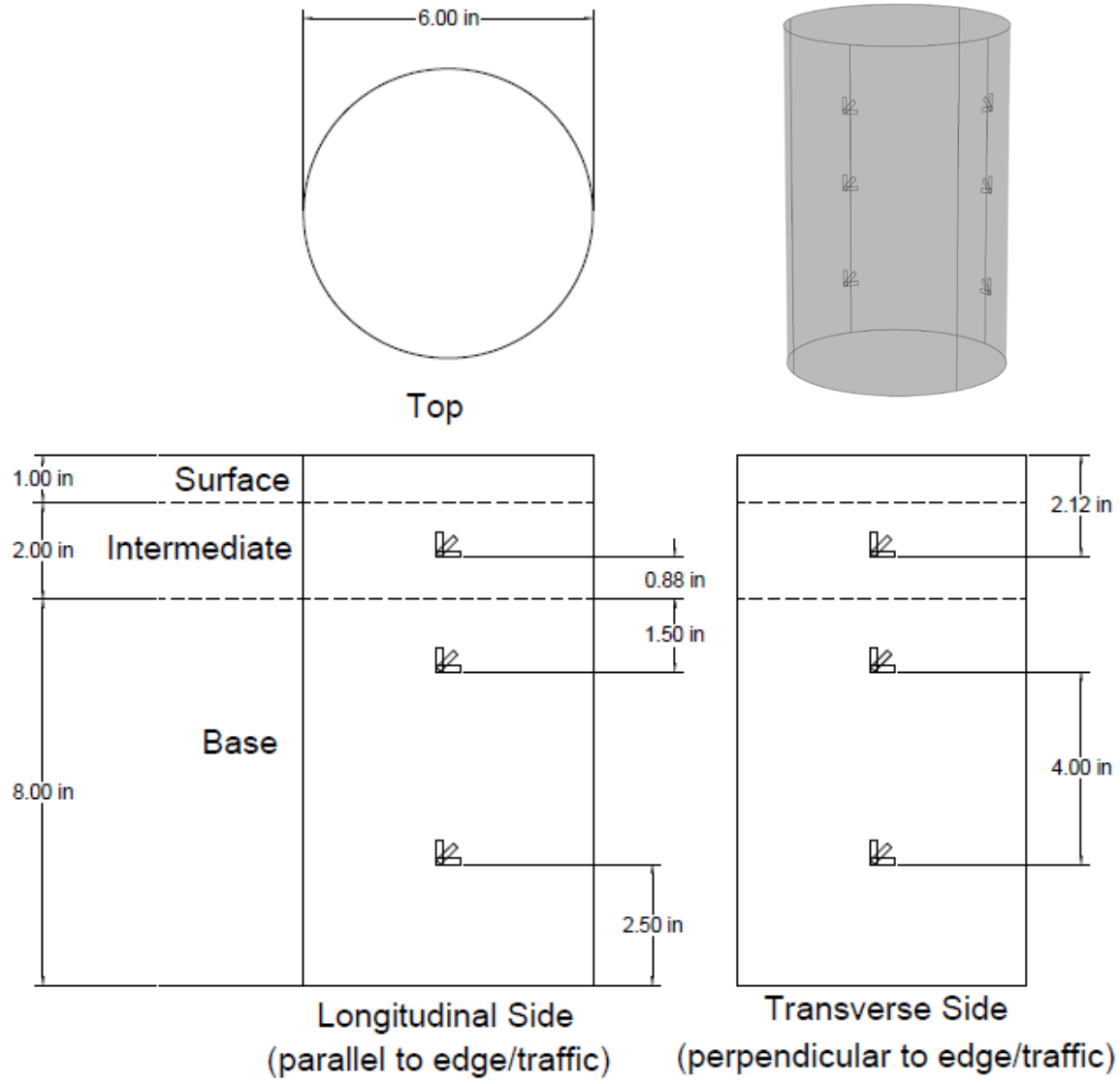
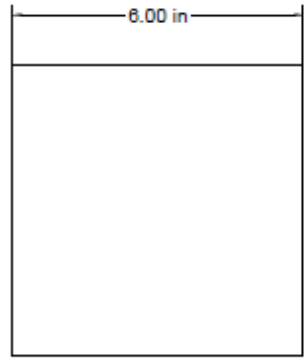


Figure C.2 15 in (38 cm) section round strain gage rosette hole (1 in = 2.54 cm)



Top

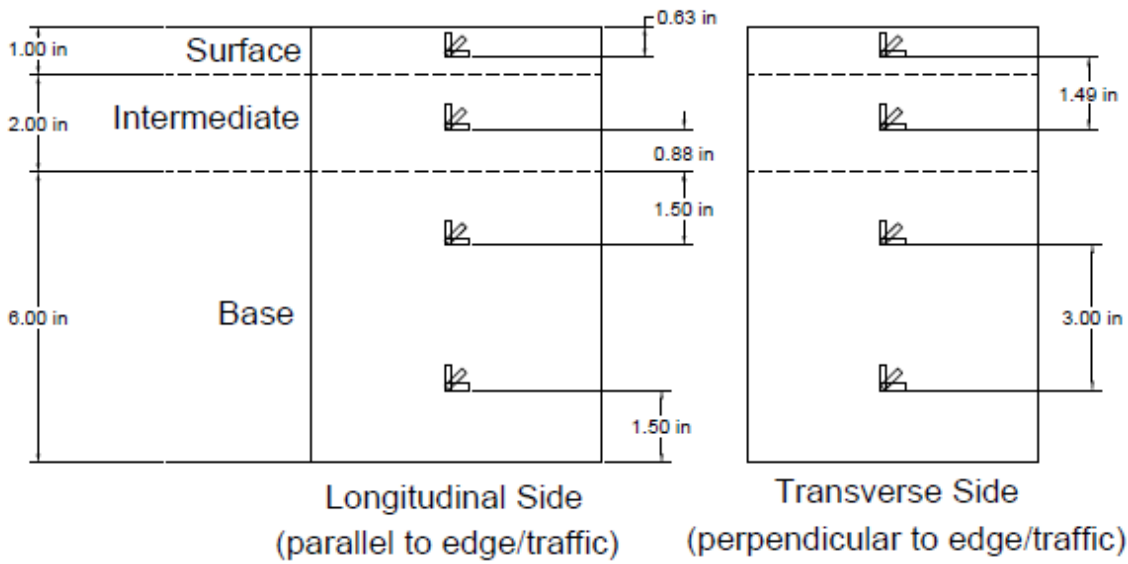
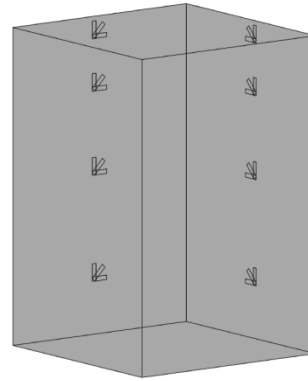
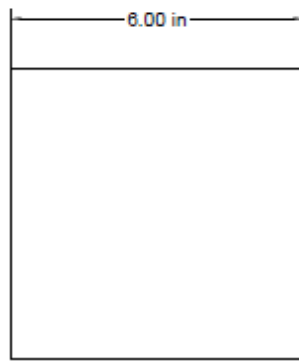


Figure C.3 13 in (33 cm) section square strain gage rosette hole (1 in = 2.54 cm)





Top

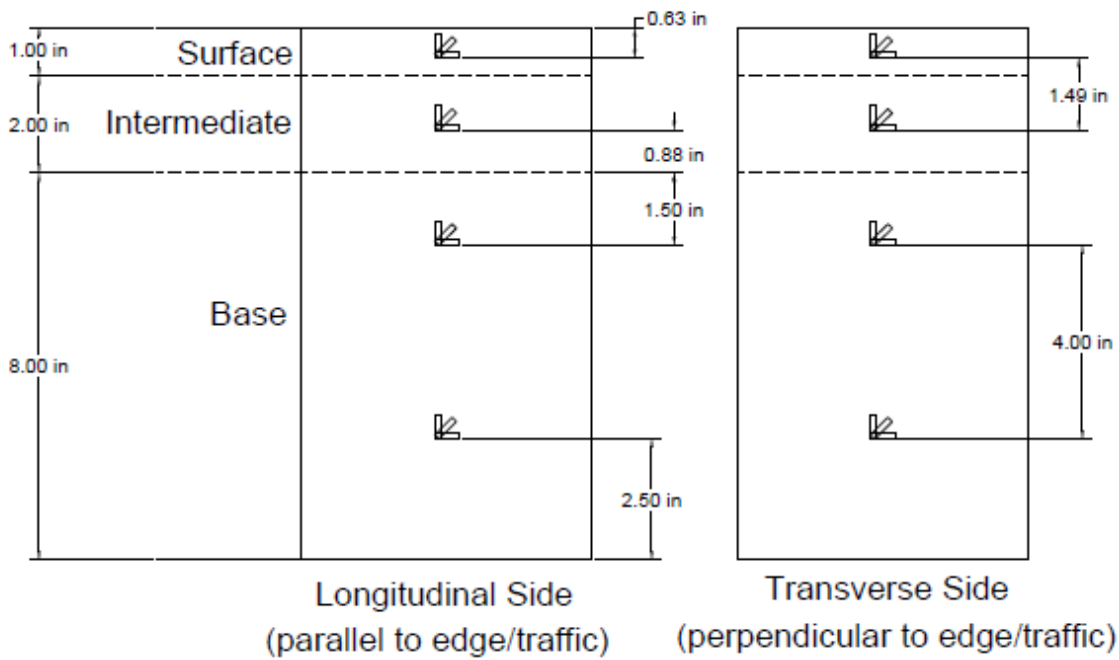
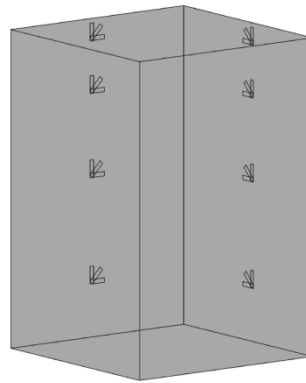


Figure C.4 15 in (38 cm) section square strain gage rosette hole (1 in = 2.54 cm)

Appendix D: Pavement instrumentation diagrams for DEL-23.

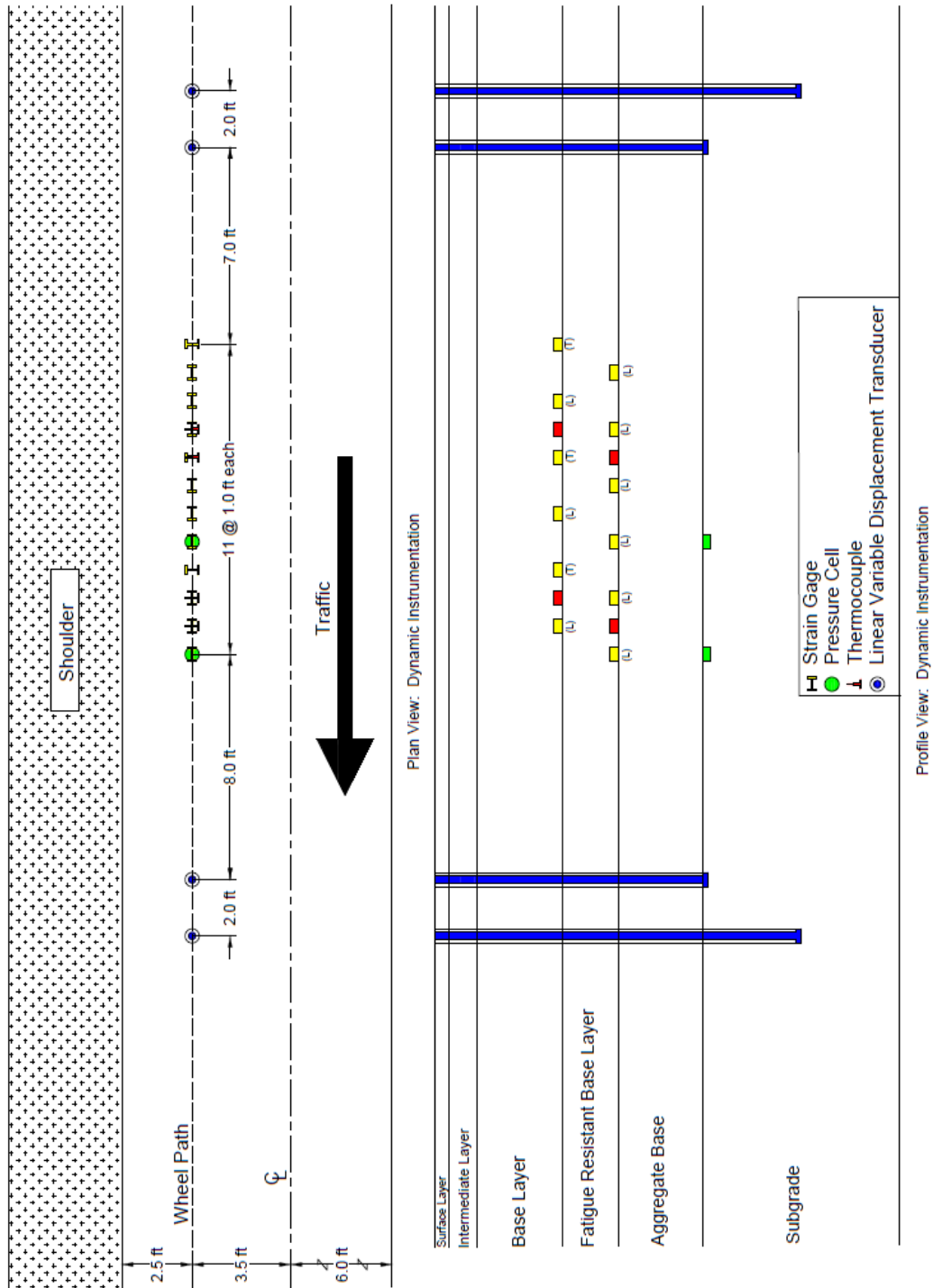


Figure D.1 11 in (28 cm) section instrumentation (1 ft = 0.305 m)

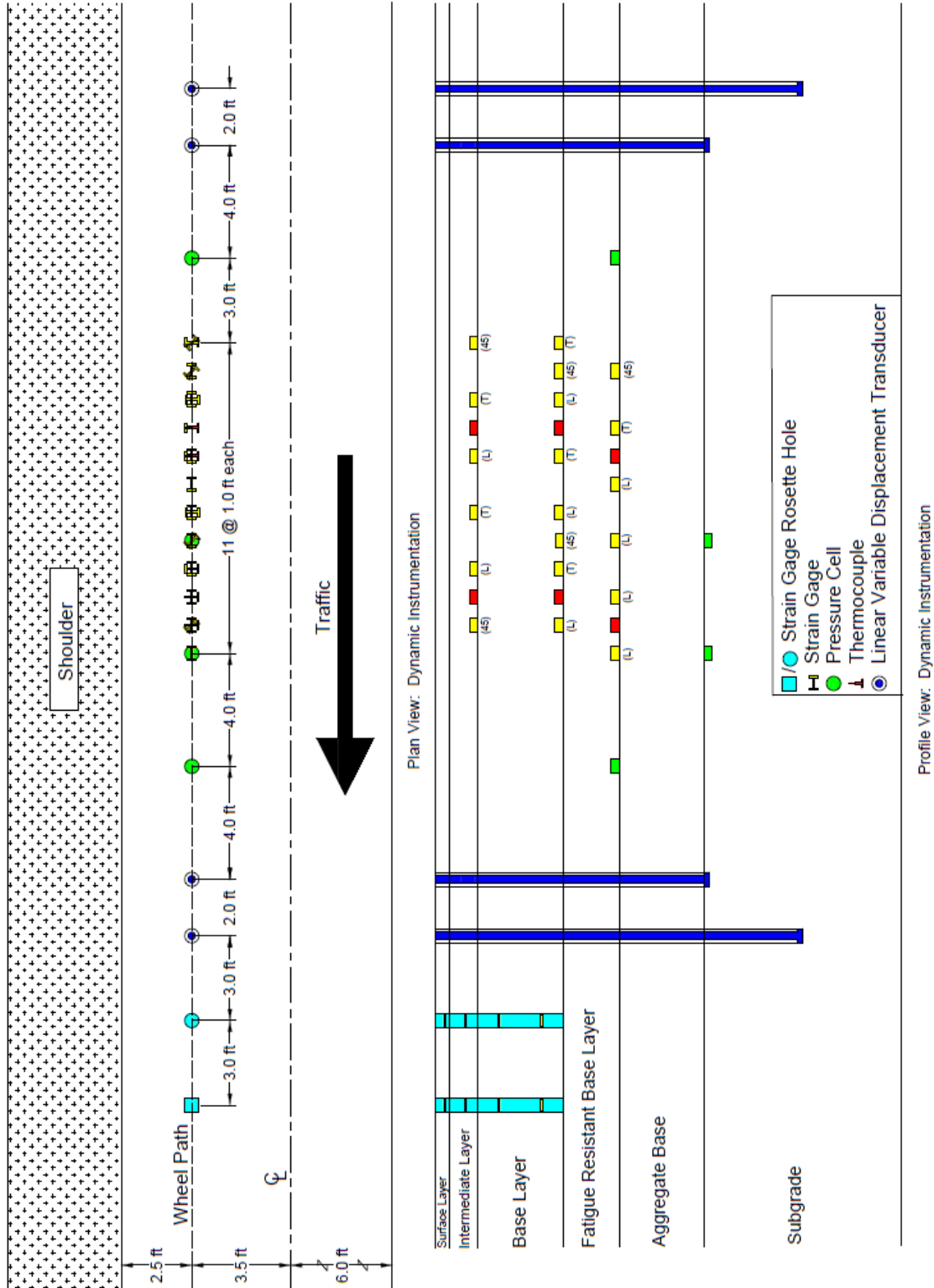


Figure D.2 13 and 15 in (38 cm) section instrumentation (1 ft = 0.305 m)

**Appendix E: Truck loads and dimensions for CVL tests on DEL-23**

Truck: T6-970 International Workstar 2545732

Rear Tires: Michelin 445/50 R22.5  
Cold Pressure: 100 psi

Front Tires: Continental 315/80 R22.5  
Cold Pressure: 100 psi

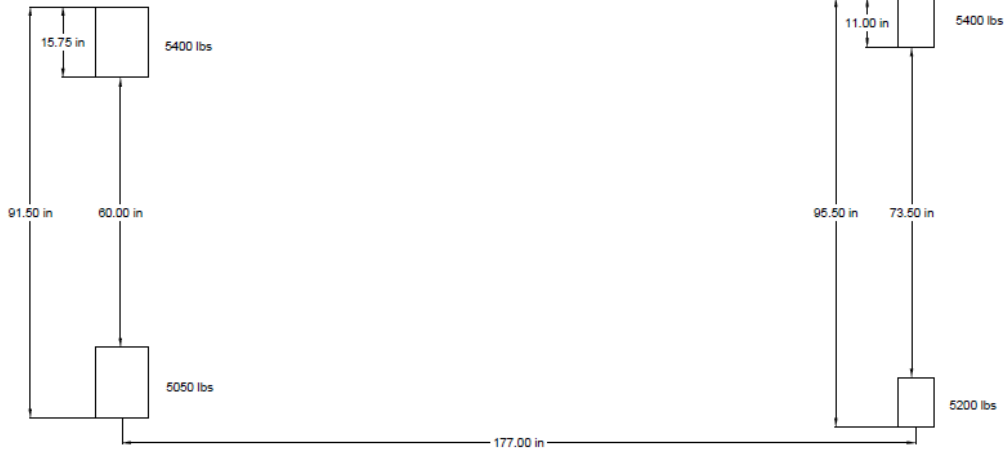


Figure E.1 Single axle wide-based tire (empty) (1 in = 2.54 cm, 1lb = 4.45 N, 100 psi = 689 kPa)

Truck: T6-970 International Workstar 2545732

Rear Tires: Michelin 445/50 R22.5  
Cold Pressure: 100 psi

Front Tires: Continental 315/80 R22.5  
Cold Pressure: 100 psi



Figure E.2 Single axle wide-based tire (max load) (1 in = 2.54 cm, 1lb = 4.45 N, 100 psi = 689 kPa)

Truck: T6-642 International Workstar 2560608

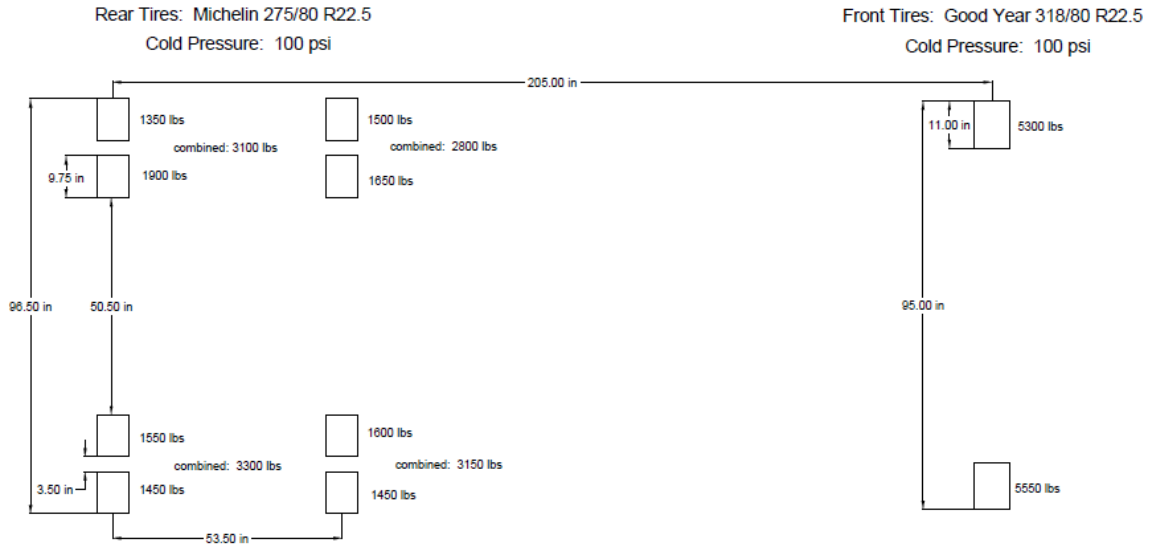


Figure E.3 Tandem axle dual tire (empty) (1 in = 2.54 cm, 1lb = 4.45 N, 100 psi = 689 kPa)

Truck: T6-642 International Workstar 2560608

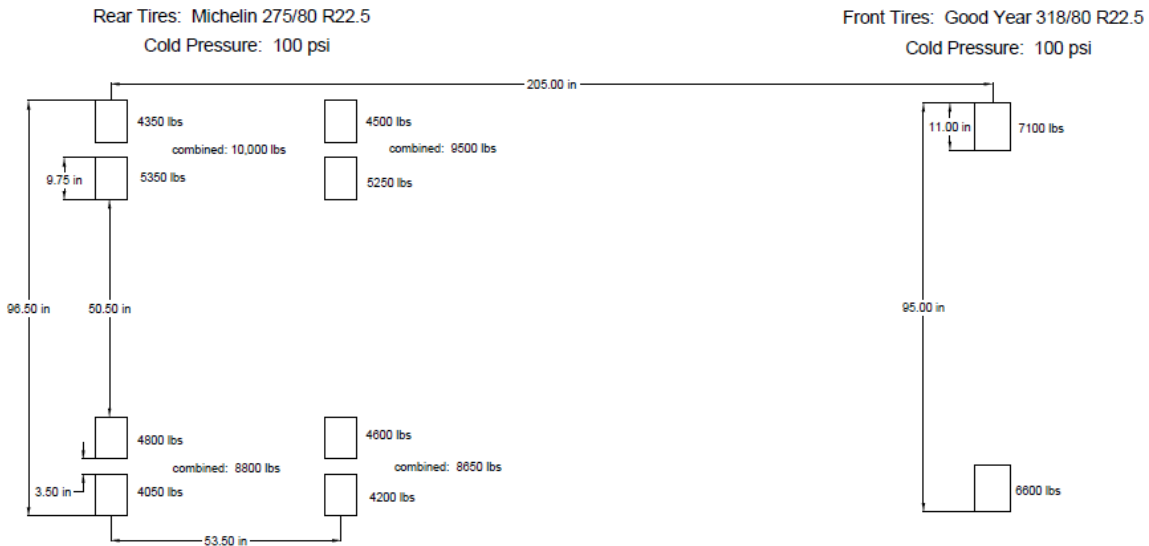


Figure E.4 Tandem axle dual tire (max load) (1 in = 2.54 cm, 1lb = 4.45 N, 100 psi = 689 kPa)

**Appendix F: Test day temperatures during CVL testing on DEL23.**

Table F.1 Test day temperatures for the 11 in (28 cm) section on 12/18/12

Time of Day	Air		TC1		TC2		TC3		TC4	
	(°C)	(°F)	(°C)	(°F)	(°C)	(°F)	(°C)	(°F)	(°C)	(°F)
10:20	4.22	39.59	6.91	44.44	6.92	44.45	6.68	44.02	6.44	43.58
10:30	4.77	40.59	6.62	43.92	6.62	43.92	6.43	43.57	6.23	43.21
10:40	5.33	41.59	6.58	43.85	6.58	43.85	6.40	43.51	6.16	43.08
10:50	5.98	42.76	6.56	43.80	6.55	43.79	6.36	43.44	6.17	43.11
11:00	5.85	42.52	6.93	44.47	6.91	44.44	6.72	44.09	6.47	43.65
11:10	5.96	42.72	6.81	44.26	6.79	44.22	6.60	43.87	6.38	43.49
11:20	5.70	42.25	6.86	44.35	6.85	44.34	6.65	43.98	6.46	43.63
11:30	5.25	41.45	6.78	44.21	6.80	44.24	6.60	43.88	6.42	43.55
11:40	5.42	41.75	6.21	43.17	6.19	43.15	6.04	42.87	5.86	42.55
11:50	5.93	42.68	6.48	43.66	6.49	43.69	6.37	43.46	6.19	43.14
12:00	5.82	42.47	6.65	43.96	6.63	43.94	6.46	43.63	6.26	43.26
12:10	7.19	44.94	5.99	42.79	5.97	42.74	5.78	42.41	5.61	42.11
12:20	8.96	48.13	5.96	42.72	5.94	42.70	5.78	42.41	5.62	42.12
12:30	9.74	49.53	6.30	43.34	6.30	43.34	6.15	43.07	6.00	42.81
12:40	8.70	47.66	6.96	44.53	6.96	44.54	6.83	44.29	6.64	43.95
12:50	8.35	47.03	6.75	44.15	6.71	44.07	6.57	43.82	6.41	43.53
13:00	8.80	47.84	7.09	44.76	7.06	44.71	6.89	44.40	6.64	43.95
13:10	9.14	48.45	6.67	44.00	6.64	43.95	6.53	43.76	6.40	43.53
13:20	10.15	50.27	6.40	43.52	6.40	43.52	6.33	43.39	6.22	43.20
13:30	9.90	49.82	6.72	44.09	6.68	44.02	6.58	43.84	6.46	43.62
13:40	9.84	49.71	6.79	44.23	6.78	44.21	6.72	44.10	6.63	43.93
13:50	9.88	49.78	6.50	43.70	6.50	43.69	6.45	43.60	6.38	43.48
14:00	9.84	49.71	6.47	43.65	6.47	43.64	6.46	43.63	6.44	43.58
14:10	9.73	49.51	6.59	43.87	6.59	43.86	6.61	43.89	6.59	43.86
14:20	9.83	49.69	6.74	44.14	6.70	44.07	6.68	44.02	6.64	43.95

Note: T1 and T2 were located in the FRL and T3 and T4 were located in the base layer

Table F.2 Test day temperatures for the 13 in (33 cm) section on 12/19/12

Time of Day	Air		TC1		TC2		TC3		TC4		TC5		TC6	
	(°C)	(°F)	(°C)	(°F)	(°C)	(°F)	(°C)	(°F)	(°C)	(°F)	(°C)	(°F)	(°C)	(°F)
10:20	6.28	43.30	6.86	44.35	6.88	44.38	6.72	44.09	6.55	43.79	6.35	43.44	6.11	43.00
10:30	6.00	42.79	6.74	44.14	6.72	44.10	6.65	43.97	6.53	43.75	6.31	43.36	6.07	42.92
10:40	5.79	42.43	6.79	44.22	6.82	44.28	6.69	44.04	6.53	43.75	6.33	43.39	6.11	42.99
10:50	5.63	42.13	6.75	44.16	6.81	44.25	6.68	44.03	6.50	43.70	6.31	43.36	6.09	42.97
11:00	5.53	41.95	6.75	44.14	6.74	44.13	6.64	43.94	6.50	43.69	6.30	43.34	6.10	42.98
11:10	5.56	42.01	6.68	44.02	6.69	44.05	6.58	43.84	6.48	43.66	6.30	43.33	6.07	42.93
11:20	5.77	42.38	6.66	43.98	6.66	43.99	6.60	43.88	6.49	43.68	6.27	43.29	6.06	42.92
11:30	5.93	42.68	6.71	44.07	6.72	44.10	6.61	43.89	6.47	43.65	6.30	43.34	6.12	43.02
11:40	6.20	43.15	6.65	43.96	6.70	44.05	6.60	43.87	6.46	43.62	6.31	43.35	6.13	43.04
11:50	6.75	44.16	6.66	43.99	6.71	44.08	6.63	43.93	6.50	43.70	6.36	43.45	6.18	43.13
12:00	7.27	45.09	6.63	43.93	6.68	44.02	6.65	43.97	6.53	43.76	6.41	43.54	6.27	43.28
12:10	7.83	46.09	6.71	44.08	6.75	44.14	6.68	44.02	6.53	43.76	6.43	43.57	6.32	43.37
12:20	8.11	46.60	6.79	44.21	6.83	44.29	6.74	44.14	6.60	43.89	6.54	43.78	6.45	43.62
12:30	8.26	46.87	6.86	44.36	6.90	44.41	6.80	44.24	6.66	44.00	6.65	43.97	6.57	43.83
12:40	8.32	46.98	6.84	44.32	6.86	44.34	6.82	44.27	6.69	44.03	6.68	44.02	6.64	43.96
12:50	8.25	46.85	6.86	44.35	6.90	44.41	6.81	44.26	6.69	44.04	6.72	44.10	6.73	44.11
13:00	8.17	46.71	6.86	44.34	6.89	44.40	6.81	44.25	6.71	44.08	6.77	44.18	6.79	44.22
13:10	8.11	46.60	6.83	44.29	6.87	44.37	6.81	44.26	6.71	44.08	6.78	44.20	6.83	44.29
13:20	7.97	46.35	6.88	44.39	6.92	44.45	6.87	44.36	6.75	44.15	6.82	44.27	6.89	44.39
13:30	8.14	46.65	6.79	44.23	6.84	44.31	6.77	44.19	6.65	43.97	6.77	44.19	6.87	44.37
13:40	8.47	47.25	6.82	44.28	6.87	44.37	6.81	44.26	6.71	44.08	6.83	44.29	6.92	44.45
13:50	8.71	47.68	6.78	44.20	6.85	44.32	6.84	44.31	6.73	44.12	6.88	44.39	6.99	44.58

Note: T1 and T2 were located in the FRL, T3 and T4 were located in the base layer, and T5 and T6 were located in the intermediate layer

Table F.3 Test day temperatures for the 15 in (38 cm) section on 11/29/12

Time of Day	Air		TC1		TC2		TC3		TC4		TC5		TC6	
	(°C)	(°F)	(°C)	(°F)	(°C)	(°F)	(°C)	(°F)	(°C)	(°F)	(°C)	(°F)	(°C)	(°F)
10:10	3.06	37.51	5.46	41.83	5.48	41.86	5.18	41.32	4.51	40.13	3.69	38.65	2.84	37.12
10:20	4.40	39.93	5.39	41.71	5.43	41.77	5.16	41.30	5.04	41.08	4.30	39.73	3.55	38.39
10:30	5.33	41.60	5.55	41.99	5.56	42.00	5.27	41.48	5.49	41.87	4.79	40.62	4.09	39.35
10:40	6.09	42.97	5.15	41.27	5.20	41.35	4.95	40.90	5.56	42.01	5.01	41.01	4.44	39.99
10:50	7.06	44.71	5.03	41.05	5.08	41.14	4.84	40.72	5.88	42.58	5.42	41.75	4.96	40.93
11:00	8.00	46.40	5.11	41.20	5.13	41.24	4.90	40.83	6.26	43.27	5.92	42.66	5.58	42.04
11:10	8.48	47.26	5.11	41.19	5.14	41.25	4.91	40.85	6.46	43.63	6.22	43.20	5.96	42.74
11:20	9.21	48.58	5.08	41.14	5.12	41.21	4.91	40.85	6.74	44.13	6.59	43.86	6.44	43.59
11:30	9.90	49.82	5.00	41.00	5.05	41.08	4.85	40.73	6.97	44.54	6.90	44.42	6.85	44.34
11:40	11.04	51.87	5.11	41.20	5.17	41.30	5.00	41.00	7.53	45.55	7.55	45.59	7.59	45.66
11:50	11.74	53.13	5.24	41.42	5.27	41.49	5.08	41.15	7.85	46.13	7.93	46.27	8.04	46.47
12:00	11.74	53.13	5.33	41.59	5.33	41.59	5.11	41.20	7.88	46.18	7.99	46.38	8.16	46.69
12:10	11.88	53.38	5.62	42.12	5.67	42.21	5.48	41.86	8.15	46.67	8.34	47.01	8.55	47.39
12:20	12.04	53.67	5.23	41.41	5.28	41.50	5.17	41.30	7.99	46.38	8.32	46.98	8.69	47.64
12:30	12.19	53.94	5.06	41.10	5.11	41.20	4.99	40.99	7.94	46.29	8.37	47.07	8.85	47.93
12:40	12.25	54.05	5.06	41.11	5.11	41.21	4.97	40.95	7.96	46.33	8.43	47.17	8.94	48.09
12:50	12.34	54.21	5.08	41.14	5.13	41.24	4.99	40.98	8.00	46.40	8.51	47.32	9.06	48.31
13:00	12.33	54.19	5.08	41.14	5.12	41.21	4.99	40.97	7.99	46.38	8.55	47.39	9.16	48.49
13:10	12.68	54.82	5.19	41.33	5.22	41.39	5.09	41.17	8.18	46.72	8.81	47.86	9.47	49.05
13:20	12.89	55.20	5.17	41.30	5.19	41.34	5.07	41.12	8.25	46.85	8.92	48.06	9.63	49.33
13:30	12.77	54.99	5.15	41.27	5.17	41.31	5.07	41.12	8.20	46.76	8.92	48.06	9.68	49.42
13:40	12.72	54.90	5.28	41.50	5.29	41.52	5.17	41.31	8.24	46.83	9.01	48.22	9.80	49.64
13:50	12.58	54.64	5.14	41.25	5.16	41.29	5.07	41.12	8.12	46.62	8.93	48.07	9.77	49.59
14:00	12.38	54.28	5.20	41.37	5.22	41.39	5.13	41.23	8.07	46.53	8.91	48.04	9.77	49.59
14:10	12.34	54.21	5.39	41.70	5.40	41.72	5.31	41.55	8.15	46.67	9.01	48.22	9.88	49.78

Note: T1 and T2 were located in the FRL, T3 and T4 were located in the base layer, and T5 and T6 were located in the intermediate layer



Table F.4 Test day temperatures for the 11 in (28 cm) section on 7/10/13

Time of Day	Air		TC1		TC2		TC3		TC4	
	(°C)	(°F)	(°C)	(°F)	(°C)	(°F)	(°C)	(°F)	(°C)	(°F)
10:40	37.03	98.65	26.06	78.91	26.09	78.96	26.16	79.09	26.28	79.30
10:50	38.95	102.11	25.96	78.73	25.98	78.76	26.13	79.03	26.25	79.25
11:00	40.61	105.10	25.99	78.78	25.99	78.78	26.17	79.11	26.47	79.65
11:10	42.44	108.39	26.20	79.16	26.22	79.20	26.46	79.63	26.75	80.15
11:20	43.64	110.55	26.58	79.84	26.59	79.86	26.90	80.42	27.27	81.09
11:30	43.30	109.94	26.61	79.90	26.63	79.93	27.02	80.64	27.37	81.27
11:40	43.54	110.37	26.47	79.65	26.47	79.65	26.95	80.51	27.39	81.30
11:50	44.33	111.79	26.50	79.70	26.52	79.74	26.99	80.58	27.51	81.52
12:00	45.33	113.59	26.61	79.90	26.63	79.93	27.20	80.96	27.75	81.95
12:10	45.98	114.76	26.48	79.66	26.51	79.72	27.14	80.85	27.76	81.97
12:20	45.80	114.44	26.76	80.17	26.81	80.26	27.51	81.52	28.09	82.56
12:30	44.97	112.95	26.83	80.29	26.92	80.46	27.61	81.70	28.26	82.87
12:40	45.08	113.14	26.96	80.53	27.03	80.65	27.76	81.97	28.42	83.16
12:50	45.35	113.63	26.82	80.28	26.91	80.44	27.71	81.88	28.43	83.17
13:00	46.07	114.93	26.53	79.75	26.61	79.90	27.50	81.50	28.31	82.96
13:10	46.29	115.32	26.59	79.86	26.69	80.04	27.56	81.61	28.36	83.05
13:20	46.05	114.89	26.72	80.10	26.81	80.26	27.73	81.91	28.58	83.44
13:30	45.89	114.60	27.06	80.71	27.15	80.87	28.07	82.53	28.88	83.98
13:40	44.46	112.03	27.51	81.52	27.55	81.59	28.43	83.17	29.20	84.56

Note: T1 and T2 were located in the FRL and T3 and T4 were located in the base layer

Table F.5 Test day temperatures for the 13 in (33 cm) section on 7/11/13

Time of Day	Air		TC1		TC2		TC3		TC4		TC5		TC6	
	(°C)	(°F)	(°C)	(°F)	(°C)	(°F)	(°C)	(°F)	(°C)	(°F)	(°C)	(°F)	(°C)	(°F)
10:20	29.89	85.80	27.06	80.71	26.96	80.53	26.78	80.20	26.62	79.92	26.99	80.58	27.23	81.01
10:30	31.45	88.61	27.23	81.01	27.10	80.78	26.90	80.42	26.75	80.15	27.25	81.05	27.59	81.66
10:40	32.31	90.16	27.27	81.09	27.14	80.85	26.98	80.56	26.89	80.40	27.47	81.45	27.92	82.26
10:50	33.95	93.11	27.52	81.54	27.36	81.25	27.12	80.82	27.02	80.64	27.67	81.81	28.17	82.71
11:00	35.45	95.81	27.55	81.59	27.41	81.34	27.20	80.96	27.12	80.82	27.87	82.17	28.47	83.25
11:10	36.10	96.98	27.46	81.43	27.34	81.21	27.21	80.98	27.19	80.94	28.07	82.53	28.81	83.86
11:20	34.72	94.50	27.46	81.43	27.36	81.25	27.25	81.05	27.25	81.05	28.24	82.83	29.08	84.34
11:30	35.08	95.14	27.34	81.21	27.23	81.01	27.13	80.83	27.13	80.83	28.17	82.71	29.11	84.40
11:40	34.64	94.35	27.50	81.50	27.39	81.30	27.35	81.23	27.38	81.28	28.44	83.19	29.40	84.92
11:50	34.83	94.69	27.54	81.57	27.42	81.36	27.39	81.30	27.46	81.43	28.56	83.41	29.58	85.24
12:00	36.12	97.02	27.56	81.61	27.41	81.34	27.33	81.19	27.41	81.34	28.59	83.46	29.65	85.37
12:10	36.21	97.18	27.63	81.73	27.53	81.55	27.47	81.45	27.55	81.59	28.79	83.82	29.87	85.77
12:20	35.83	96.49	27.79	82.02	27.71	81.88	27.72	81.90	27.82	82.08	29.14	84.45	30.30	86.54
12:30	35.80	96.44	27.54	81.57	27.50	81.50	27.56	81.61	27.72	81.90	29.13	84.43	30.39	86.70
12:40	38.15	100.67	26.94	80.49	26.96	80.53	27.09	80.76	27.36	81.25	28.93	84.07	30.36	86.65
12:50	39.10	102.38	27.40	81.32	27.41	81.34	27.56	81.61	27.84	82.11	29.46	85.03	30.95	87.71
13:00	39.00	102.20	27.41	81.34	27.44	81.39	27.59	81.66	27.91	82.24	29.61	85.30	31.15	88.07
13:10	37.63	99.73	27.40	81.32	27.45	81.41	27.65	81.77	27.92	82.26	29.66	85.39	31.27	88.29
13:20	38.69	101.64	27.56	81.61	27.58	81.64	27.81	82.06	28.11	82.60	29.85	85.73	31.49	88.68
13:30	38.84	101.91	27.39	81.30	27.48	81.46	27.72	81.90	28.05	82.49	29.87	85.77	31.57	88.83
13:40	39.19	102.54	27.45	81.41	27.51	81.52	27.74	81.93	28.10	82.58	29.97	85.95	31.68	89.02
13:50	37.84	100.11	27.62	81.72	27.65	81.77	27.88	82.18	28.23	82.81	30.14	86.25	31.89	89.40
14:00	40.38	104.68	27.64	81.75	27.66	81.79	27.93	82.27	28.30	82.94	30.23	86.41	31.95	89.51
14:10	40.85	105.53	27.68	81.82	27.72	81.90	27.99	82.38	28.41	83.14	30.45	86.81	32.27	90.09
14:20	40.20	104.36	27.74	81.93	27.76	81.97	28.10	82.58	28.57	83.43	30.71	87.28	32.67	90.81
14:30	38.90	102.02	27.99	82.38	28.03	82.45	28.34	83.01	28.75	83.75	30.85	87.53	32.78	91.00
14:40	40.67	105.21	27.90	82.22	27.93	82.27	28.23	82.81	28.68	83.62	30.84	87.51	32.82	91.08

Note: T1 and T2 were located in the FRL, T3 and T4 were located in the base layer, and T5 and T6 were located in the intermediate layer

Table F.6 Test day temperatures for the 15 in (38 cm) section on 7/1/13

Time of Day	Air		TC1		TC2		TC3		TC4		TC5		TC6	
	(°C)	(°F)	(°C)	(°F)	(°C)	(°F)	(°C)	(°F)	(°C)	(°F)	(°C)	(°F)	(°C)	(°F)
10:50	23.48	74.26	27.41	81.34	27.46	81.43	27.42	81.36	27.20	80.96	26.46	79.63	25.72	78.30
11:00	24.43	75.97	28.14	82.65	28.26	82.87	27.99	82.38	27.77	81.99	27.02	80.64	26.27	79.29
11:10	25.43	77.77	28.26	82.87	28.38	83.08	28.13	82.63	27.84	82.11	27.14	80.85	26.37	79.47
11:20	26.53	79.75	28.24	82.83	28.40	83.12	28.14	82.65	27.88	82.18	27.19	80.94	26.46	79.63
11:30	26.70	80.06	28.61	83.50	28.69	83.64	28.39	83.10	28.11	82.60	27.46	81.43	26.73	80.11
11:40	27.02	80.64	28.53	83.35	28.64	83.55	28.36	83.05	28.06	82.51	27.43	81.37	26.74	80.13
11:50	27.32	81.18	28.62	83.52	28.70	83.66	28.38	83.08	28.09	82.56	27.47	81.45	26.78	80.20
12:00	27.94	82.29	28.57	83.43	28.69	83.64	28.41	83.14	28.09	82.56	27.48	81.46	26.81	80.26
12:10	29.29	84.72	28.67	83.61	28.75	83.75	28.43	83.17	28.09	82.56	27.50	81.50	26.86	80.35
12:20	31.01	87.82	28.51	83.32	28.57	83.43	28.27	82.89	27.95	82.31	27.43	81.37	26.86	80.35
12:30	32.65	90.77	28.77	83.79	28.81	83.86	28.48	83.26	28.15	82.67	27.66	81.79	27.11	80.80
12:40	34.33	93.79	28.86	83.95	28.89	84.00	28.56	83.41	28.21	82.78	27.80	82.04	27.31	81.16
12:50	38.21	100.78	28.88	83.98	28.88	83.98	28.51	83.32	28.16	82.69	27.85	82.13	27.50	81.50
13:00	40.54	104.97	29.93	85.87	29.87	85.77	29.41	84.94	28.94	84.09	28.67	83.61	28.33	82.99
13:10	38.80	101.84	30.50	86.90	30.45	86.81	29.97	85.95	29.50	85.10	29.33	84.79	29.09	84.36
13:20	36.92	98.46	30.09	86.16	30.05	86.09	29.64	85.35	29.21	84.58	29.23	84.61	29.20	84.56
13:30	36.07	96.93	29.72	85.50	29.70	85.46	29.31	84.76	28.91	84.04	29.02	84.24	29.10	84.38
13:40	36.81	98.26	29.45	85.01	29.41	84.94	29.02	84.24	28.59	83.46	28.81	83.86	28.99	84.18
13:50	39.98	103.96	29.63	85.33	29.57	85.23	29.13	84.43	28.63	83.53	28.91	84.04	29.15	84.47
14:00	39.61	103.30	30.22	86.40	30.15	86.27	29.74	85.53	29.28	84.70	29.62	85.32	29.90	85.82
14:10	38.84	101.91	30.14	86.25	30.08	86.14	29.69	85.44	29.26	84.67	29.75	85.55	30.19	86.34
14:20	36.08	96.94	30.50	86.90	30.42	86.76	30.00	86.00	29.55	85.19	30.08	86.14	30.55	86.99
14:30	33.86	92.95	29.22	84.60	29.10	84.38	28.89	84.00	28.61	83.50	29.38	84.88	30.11	86.20

Note: T1 and T2 were located in the FRL, T3 and T4 were located in the base layer, and T5 and T6 were located in the intermediate layer

**Appendix G: Strain gauge data from CVL tests on DEL-23.**

Winter data

Table G.1 Maximum strains ( $\mu\epsilon$ ) for the 11 in (28 cm) section with tire pressure of 80 psi (552 kPa) – Winter data

Run	Longitudinal Strain Gages Located in the FRL						Longitudinal Strain Gages Located in the Base Layer			Transverse Strain Gages Located in the Base Layer		
	KM-001	KM-002	KM-003	PM-001	PM-002	PM-003	KM-004	KM-006	PM-005	KM-005	PM-004	PM-006
Single Axle 5 mph (8 km/h) Test Runs												
1	40.98	58.53	52.69	38.12	42.45	43.32	11.57	17.90	12.26	9.52	10.47	9.00
2	39.07	57.62	50.32	39.16	42.30	43.34	11.96	18.55	14.41	9.57	9.95	10.18
3	40.34	60.85	52.54	39.94	43.45	44.66	12.26	18.64	12.95	9.65	10.51	9.35
Tandem Axle 5 mph (8 km/h) Test Runs												
1	22.14	28.16	27.33	18.73	23.19	21.65	6.41	9.78	9.31	2.67	5.68	7.55
2	21.11	31.00	26.78	21.11	23.43	24.18	7.84	10.82	10.02	5.28	8.67	9.36
3	21.65	31.98	25.08	20.76	24.01	25.01	6.59	10.81	9.99	3.22	7.79	8.74
Single Axle 30 mph (48 km/h) Test Runs												
1	33.45	46.88	39.39	37.75	39.61	40.25	10.05	14.51	11.42	7.12	9.63	8.12
2	30.60	44.23	39.20	38.04	38.25	37.15	10.02	14.84	11.34	6.89	9.39	7.63
3	35.82	50.72	42.07	34.15	37.22	39.78	10.75	15.13	10.61	8.12	8.34	7.36
Tandem Axle 30 mph (48 km/h) Test Runs												
1	19.24	27.27	22.35	18.83	21.65	20.46	6.22	8.77	8.26	2.12	4.15	6.19
2	17.68	25.80	21.68	19.12	19.88	21.68	5.53	8.40	6.73	1.90	1.92	3.78
3	18.93	27.50	23.90	18.04	19.72	21.46	5.46	9.06	6.48	2.10	2.63	4.52
Single Axle 55 mph (89 km/h) Test Runs												
1	27.36	38.48	33.80	32.80	32.20	32.16	7.95	11.87	9.60	6.32	7.94	7.20
2	27.27	38.81	35.08	31.09	31.30	31.58	7.87	11.34	8.42	5.61	7.41	6.21
3	28.07	39.15	32.64	34.32	33.73	32.72	8.69	11.31	9.79	6.36	7.95	7.38
Tandem Axle 55 mph (89 km/h) Test Runs												
1	16.63	25.53	24.42	16.36	18.58	19.75	5.23	7.63	6.14	3.84	5.50	6.85
2	16.82	24.17	22.34	14.72	15.37	19.79	4.94	8.01	5.78	4.87	6.47	6.67
3	17.68	24.77	17.73	17.72	16.53	17.41	4.36	7.08	5.47	3.01	5.23	6.37

Table G.2 Maximum strains ( $\mu\epsilon$ ) for the 11 in (28 cm) section with tire pressure of 110 psi (758 kPa) – Winter data

Run	Longitudinal Strain Gages Located in the FRL						Longitudinal Strain Gages Located in the Base Layer			Transverse Strain Gages Located in the Base Layer		
	KM-001	KM-002	KM-003	PM-001	PM-002	PM-003	KM-004	KM-006	PM-005	KM-005	PM-004	PM-006
Single Axle 5 mph (8 km/h) Test Runs												
1	39.15	65.57	52.97	41.72	44.54	47.63	14.70	21.06	18.02	11.66	11.45	11.45
2	39.29	61.75	50.74	38.86	43.77	43.03	13.43	20.05	13.63	10.10	10.82	9.29
3	44.37	68.49	34.13	40.09	46.66	46.26	15.12	15.48	16.15	10.84	12.32	12.08
Tandem Axle 5 mph (8 km/h) Test Runs												
1	21.73	33.20	26.27	20.16	22.79	23.03	9.05	10.64	10.61	6.16	10.87	10.22
2	20.84	31.49	27.34	20.34	22.87	24.39	7.92	11.43	10.59	5.21	9.58	10.59
3	22.71	32.62	29.18	20.55	23.67	25.05	8.62	12.12	11.16	6.81	10.46	11.47
Single Axle 30 mph (48 km/h) Test Runs												
1	39.54	58.82	49.19	32.04	35.33	41.29	13.61	19.22	12.95	10.61	7.99	9.15
2	37.29	54.88	48.25	29.54	32.57	39.55	12.00	16.76	10.33	8.77	8.39	6.70
3	37.62	57.85	50.21	30.87	34.44	40.78	13.25	18.72	12.60	9.73	8.13	9.28
Tandem Axle 30 mph (48 km/h) Test Runs												
1	18.52	26.26	25.56	17.4	18.52	20.74	5.74	9.27	7.15	3.14	2.95	4.05
2	17.91	25.34	24.66	16.53	18.23	20.09	5.36	8.96	7.55	2.37	4.19	6.29
3	18.25	26.70	27.15	20.95	19.41	22.07	5.12	9.18	9.17	2.27	4.27	6.05
Single Axle 55 mph (89 km/h) Test Runs												
1	35.27	48.8	40.86	36.26	38.42	39.19	10.99	14.66	11.45	8.65	9.39	8.69
2	31.93	45.15	38.67	35.55	35.06	37.05	9.20	12.68	9.36	12.68	8.53	6.31
3	33.88	48.94	39.8	38.08	38.87	40.27	10.70	15.02	12.61	8.67	10.04	9.96
Tandem Axle 55 mph (89 km/h) Test Runs												
1	19.06	30.17	23.65	15.66	18.19	16.66	4.27	8.94	5.25	4.34	1.33	2.36
2	16.21	29.64	22.59	14.89	17.16	16.23	4.84	8.02	6.83	2.13	3.56	5.64
3	19.16	28.98	20.79	20.03	19.74	18.45	4.81	7.49	6.11	2.08	2.75	4.78

Table G.3 Maximum strains ( $\mu\epsilon$ ) for the 11 in (28 cm) section with tire pressure of 125 psi (862 kPa) – Winter data

Run	Longitudinal Strain Gages Located in the FRL						Longitudinal Strain Gages Located in the Base Layer			Transverse Strain Gages Located in the Base Layer		
	KM-001	KM-002	KM-003	PM-001	PM-002	PM-003	KM-004	KM-006	PM-005	KM-005	PM-004	PM-006
Single Axle 5 mph (8 km/h) Test Runs												
1	40.02	61.18	50.17	41.48	43.07	43.69	14.87	23.05	15.26	11.71	12.74	11.06
2	39.86	60.78	51.95	42.04	43.27	45.40	16.88	23.71	16.93	12.57	12.54	12.23
3	41.90	59.68	54.14	40.94	42.38	46.23	15.48	22.89	17.11	12.07	12.57	11.84
Tandem Axle 5 mph (8 km/h) Test Runs												
1	21.96	28.38	26.9	20.32	22.58	22.72	9.08	13.48	10.43	9.14	10.95	10.04
2	19.88	32.38	26.93	20.53	22.37	22.19	7.45	10.72	8.91	3.61	2.29	4.99
3	21.62	31.62	28.18	20.93	23.59	24.16	7.67	11.08	11.07	3.42	7.57	9.53
Single Axle 30 mph (48 km/h) Test Runs												
1	30.65	47.58	45.94	34.85	34.14	35.11	11.81	18.04	12.63	8.90	10.86	7.73
2	30.53	50.10	47.63	33.77	33.58	33.82	12.10	18.20	12.82	9.19	10.85	8.76
3	31.22	48.08	45.67	35.15	33.83	35.68	11.34	17.35	12.14	8.74	9.96	7.78
Tandem Axle 30 mph (48 km/h) Test Runs												
1	18.59	24.52	23.63	17.70	19.02	19.86	6.15	9.55	7.48	3.09	2.24	4.19
2	16.79	29.24	20.40	16.55	21.06	21.23	7.11	9.83	8.86	4.75	7.90	9.09
3	14.06	28.87	22.46	18.22	18.52	22.31	6.03	8.33	8.54	2.33	4.30	6.51
Single Axle 55 mph (89 km/h) Test Runs												
1	35.23	51.81	45.77	32.47	35.22	38.74	11.85	17.73	12.30	9.82	9.24	9.61
2	26.37	39.80	38.58	25.03	25.54	28.01	7.68	12.47	6.22	5.45	3.34	2.67
3	33.02	49.44	44.18	31.22	32.92	36.91	11.79	16.64	11.81	9.33	9.18	9.28
Tandem Axle 55 mph (89 km/h) Test Runs												
1	16.79	23.77	21.81	17.93	17.27	19.27	6.25	8.49	7.76	6.60	8.35	9.13
2	15.76	24.45	20.90	16.41	17.17	18.90	6.05	7.99	8.03	4.41	8.76	8.54
3	18.27	30.18	23.49	16.63	18.98	17.21	5.28	9.14	6.77	2.30	3.89	5.93

Table G.4 Maximum strains ( $\mu\epsilon$ ) for the 13 in (33 cm) section with tire pressure of 80 psi (552 kPa) – Winter data

Run	Longitudinal Strain Gages Located in the FRL				Longitudinal Strain Gages Located in the Base Layer			Transverse Strain Gages Located in the Base Layer		
	KM-001	KM-002	KM-003	PM-003	KM-005	KM-008	PM-005	KM-007	PM-004	PM-006
Single Axle 5 mph (8 km/h) Test Runs										
1	29.41	32.37	29.41	31.33	10.91	10.45	14.12	12.52	12.28	13.24
2	31.18	32.45	29.19	32.11	11.59	10.71	15.01	12.98	14.43	13.84
3	30.71	33.46	29.91	31.61	11.06	10.76	14.68	12.27	12.62	13.13
Tandem Axle 5 mph (8 km/h) Test Runs										
1	14.77	16.82	15.70	16.39	5.63	5.57	7.37	6.32	4.60	4.90
2	14.99	16.70	15.69	16.39	5.90	5.40	7.60	4.77	4.68	4.83
3	14.78	16.80	15.89	16.29	5.83	5.28	7.09	4.82	4.64	5.01
Single Axle 30 mph (48 km/h) Test Runs										
1	25.73	26.70	24.99	28.51	9.48	8.76	11.48	10.21	11.17	11.33
2	25.61	26.23	24.57	28.26	9.49	8.10	11.76	11.07	10.95	11.33
3	26.18	27.39	25.61	26.68	9.17	8.41	10.48	10.53	10.30	10.49
Tandem Axle 30 mph (48 km/h) Test Runs										
1	12.21	14.01	13.43	13.50	4.83	4.62	7.04	5.51	4.72	5.50
2	12.89	14.08	13.41	13.91	5.22	4.93	6.31	5.23	5.42	6.31
3	11.85	13.83	13.72	13.77	4.07	4.95	5.76	3.90	3.50	4.39
Single Axle 55 mph (89 km/h) Test Runs										
1	20.87	21.93	22.45	22.94	7.40	7.07	9.20	8.86	9.36	9.06
2	22.25	23.20	23.67	24.48	8.10	6.83	9.29	8.78	9.65	9.12
3	19.65	20.79	21.57	20.83	7.03	6.88	8.24	8.51	8.17	7.73
Tandem Axle 55 mph (89 km/h) Test Runs										
1	10.14	11.25	12.07	12.06	4.08	3.84	5.83	5.24	5.94	5.70
2	10.70	11.99	12.50	12.37	4.16	4.29	5.29	3.43	3.06	3.93
3	11.25	11.57	11.55	13.20	4.67	3.66	5.76	4.48	3.91	4.18

Table G.5 Maximum strains ( $\mu\epsilon$ ) for the 13 in (33 cm) section with tire pressure of 110 psi (758 kPa) – Winter data

Run	Longitudinal Strain Gages Located in the FRL				Longitudinal Strain Gages Located in the Base Layer			Transverse Strain Gages Located in the Base Layer		
	KM-001	KM-002	KM-003	PM-003	KM-005	KM-008	PM-005	KM-007	PM-004	PM-006
Single Axle 5 mph (8 km/h) Test Runs										
1	30.54	30.67	30.65	31.10	12.16	10.61	15.00	12.35	13.61	12.35
2	31.40	31.90	31.18	31.07	12.23	11.23	16.02	13.58	14.41	13.91
3	30.58	32.22	30.25	31.25	12.18	11.47	15.58	13.43	13.71	13.43
Tandem Axle 5 mph (8 km/h) Test Runs										
1	14.48	17.14	15.84	16.61	5.78	5.88	8.03	6.73	7.07	7.72
2	14.55	16.51	15.28	16.90	5.77	5.59	7.19	5.65	4.75	4.61
3	15.78	17.40	16.19	16.18	6.15	5.56	8.27	6.40	5.93	7.24
Single Axle 30 mph (48 km/h) Test Runs										
1	25.83	25.09	24.46	28.19	9.73	8.28	12.33	10.26	12.03	10.72
2	24.63	24.73	23.91	28.44	10.17	8.78	13.48	10.63	12.58	12.09
3	24.41	25.90	25.80	25.96	9.50	9.10	11.92	10.41	11.49	10.18
Tandem Axle 30 mph (48 km/h) Test Runs										
1	12.09	13.16	12.97	13.66	5.10	4.90	7.27	6.54	7.10	7.01
2	12.28	14.19	13.26	13.51	4.79	4.40	6.57	3.81	3.54	4.32
3	12.23	13.79	13.04	13.48	4.97	4.70	6.12	3.75	3.63	4.12
Single Axle 55 mph (89 km/h) Test Runs										
1	25.82	27.18	26.77	26.61	8.94	9.10	11.13	11.43	8.05	8.22
2	24.75	25.28	24.69	26.18	8.62	7.78	11.09	10.30	10.65	10.43
3	24.24	24.52	23.91	25.45	8.49	8.02	10.70	10.03	9.41	10.72
Tandem Axle 55 mph (89 km/h) Test Runs										
1	11.32	13.16	13.68	11.44	4.38	3.99	5.05	3.84	3.11	3.73
2	13.09	13.17	11.91	12.68	4.39	4.03	5.82	3.93	4.55	4.64
3	10.55	12.10	12.29	11.86	4.040	3.88	5.51	4.13	4.13	3.34



Table G.6 Maximum strains ( $\mu\epsilon$ ) for the 13 in (33 cm) section with tire pressure of 125 psi (862 kPa) – Winter data

Run	Longitudinal Strain Gages Located in the FRL				Longitudinal Strain Gages Located in the Base Layer			Transverse Strain Gages Located in the Base Layer		
	KM-001	KM-002	KM-003	PM-003	KM-005	KM-008	PM-005	KM-007	PM-004	PM-006
Single Axle 5 mph (8 km/h) Test Runs										
1	32.46	30.02	31.07	33.70	12.02	11.34	15.89	14.11	14.21	14.07
2	32.19	34.53	31.32	32.03	13.82	11.50	14.93	14.63	15.87	15.25
3	33.16	31.29	30.40	30.43	12.47	11.27	14.88	12.96	15.21	13.22
Tandem Axle 5 mph (8 km/h) Test Runs										
1	14.52	15.21	14.79	16.70	6.58	6.65	9.16	8.14	9.06	8.54
2	15.80	16.89	16.11	16.89	5.56	5.80	7.77	4.55	5.11	5.99
3	14.66	16.35	15.65	15.99	6.28	5.76	8.47	7.45	7.72	8.28
Single Axle 30 mph (48 km/h) Test Runs										
1	23.48	24.47	24.37	26.76	10.06	9.43	13.68	10.75	13.00	11.98
2	25.18	26.58	27.00	26.69	10.16	9.83	12.80	11.35	12.17	11.98
3	24.30	25.14	26.33	26.54	9.56	8.63	11.80	9.94	11.00	9.40
Tandem Axle 30 mph (48 km/h) Test Runs										
1	12.02	13.12	13.22	13.91	4.95	4.88	6.41	5.72	5.10	5.49
2	12.74	13.10	13.90	13.22	5.30	5.13	7.51	6.05	6.29	6.29
3	11.59	12.64	12.99	13.2	5.38	4.97	7.39	6.65	7.14	7.31
Single Axle 55 mph (89 km/h) Test Runs										
1	24.40	22.96	23.71	25.45	7.95	6.90	10.73	8.50	9.26	8.75
2	22.93	23.49	22.49	25.50	8.44	8.21	11.15	10.15	11.13	10.46
3	21.96	22.86	22.18	24.60	7.98	7.56	10.73	9.57	10.70	9.95
Tandem Axle 55 mph (89 km/h) Test Runs										
1	13.09	13.17	11.91	12.68	4.39	4.03	5.82	3.93	4.55	4.64
2	11.85	12.67	12.54	11.97	4.15	4.00	5.87	5.21	4.92	5.79
3	12.49	13.29	12.57	12.30	4.35	4.02	5.79	4.94	5.19	5.84

Table G.7 Maximum strains ( $\mu\epsilon$ ) for the 15 in (38 cm) section with tire pressure of 80 psi (552 kPa) – Winter data

Run	Longitudinal Strain Gages Located in the FRL				Longitudinal Strain Gages Located in the Base Layer			Transverse Strain Gages Located in the Base Layer		
	PM-001	PM-002	PM-003	KM-001	PM-005	KM-005	KM-008	PM-004	PM-006	KM-007
Single Axle 5 mph (8 km/h) Test Runs										
1	39.95	43.18	37.27	38.61	16.53	NA	11.37	11.88	14.70	11.22
2	40.78	40.84	38.88	38.29	16.65	NA	10.81	11.71	12.05	11.58
3	40.11	40.89	37.09	38.48	16.57	NA	10.52	12.37	15.23	11.62
Tandem Axle 5 mph (8 km/h) Test Runs										
1	24.58	24.80	20.63	20.18	9.04	NA	5.85	5.66	6.97	5.25
2	24.36	23.10	18.52	19.95	8.46	NA	5.75	5.80	7.33	5.66
3	24.29	25.12	20.20	20.8	9.16	NA	5.65	5.87	7.17	5.32
Single Axle 30 mph (48 km/h) Test Runs										
1	32.93	35.30	32.11	30.75	13.49	NA	8.63	8.81	12.23	9.06
2	30.60	32.85	30.50	31.09	12.72	NA	9.57	9.17	11.30	9.66
3	29.37	30.87	28.37	29.83	12.39	NA	9.12	8.67	10.77	9.84
Tandem Axle 30 mph (48 km/h) Test Runs										
1	18.61	20.63	18.07	17.26	7.35	NA	5.44	5.09	6.24	5.37
2	19.03	19.53	16.13	16.32	7.61	NA	5.43	5.41	6.46	4.60
3	21.83	22.81	17.28	16.01	9.47	NA	4.53	5.03	5.78	5.42
Single Axle 55 mph (89 km/h) Test Runs										
1	22.81	24.77	23.67	22.84	9.56	NA	7.14	6.79	7.83	7.60
2	25.84	28.57	28.48	27.91	11.18	NA	8.09	7.63	9.22	8.43
3	24.89	26.82	26.20	25.56	10.66	NA	7.56	6.88	9.62	8.47
Tandem Axle 55 mph (89 km/h) Test Runs										
1	13.92	18.37	15.96	14.68	6.00	NA	4.68	3.84	5.04	4.51
2	14.57	17.64	15.96	13.82	5.93	NA	4.54	4.27	6.13	3.82
3	14.78	18.27	16.58	14.55	6.22	NA	4.70	4.42	5.55	4.19

Table G.8 Maximum strains ( $\mu\epsilon$ ) for the 15 in (38 cm) section with tire pressure of 110 psi (758 kPa) – Winter data

Run	Longitudinal Strain Gages Located in the FRL				Longitudinal Strain Gages Located in the Base Layer			Transverse Strain Gages Located in the Base Layer		
	PM-001	PM-002	PM-003	KM-001	PM-005	KM-005	KM-008	PM-004	PM-006	KM-007
Single Axle 5 mph (8 km/h) Test Runs										
1	40.29	39.04	36.77	37.49	17.57	NA	11.68	12.70	15.35	11.97
2	38.88	40.34	38.24	37.54	18.10	NA	11.13	12.26	15.64	12.44
3	39.14	40.15	38.59	36.96	18.07	NA	11.51	12.04	15.28	11.82
Tandem Axle 5 mph (8 km/h) Test Runs										
1	23.55	22.82	20.11	19.24	9.23	NA	5.72	6.07	7.80	6.32
2	22.98	23.60	18.95	19.45	8.94	NA	5.68	5.71	6.91	5.41
3	23.66	23.02	19.81	19.45	9.45	NA	5.99	5.98	7.27	5.40
Single Axle 30 mph (48 km/h) Test Runs										
1	31.51	33.51	32.81	31.09	14.89	NA	9.25	9.98	12.53	10.28
2	30.78	33.69	33.17	31.88	13.88	NA	9.68	9.48	12.43	10.20
3	29.63	33.69	32.51	32.28	14.19	NA	9.65	9.52	12.58	10.64
Tandem Axle 30 mph (48 km/h) Test Runs										
1	18.84	21.24	16.48	16.97	7.80	NA	5.15	5.25	5.77	4.98
2	19.86	21.97	16.74	15.91	8.77	NA	5.24	5.76	6.30	4.87
3	18.62	20.58	15.87	15.64	8.43	NA	5.11	5.12	6.07	5.27
Single Axle 55 mph (89 km/h) Test Runs										
1	25.62	23.16	25.59	23.55	12.12	NA	6.43	7.75	7.48	6.63
2	25.81	26.18	26.07	24.4	11.50	NA	7.34	8.09	9.51	7.47
3	29.48	29.74	26.15	23.76	13.56	NA	6.73	10.05	10.01	7.61
Tandem Axle 55 mph (89 km/h) Test Runs										
1	23.08	22.31	13.89	13.62	9.82	NA	3.97	5.83	6.21	4.54
2	22.13	20.74	13.30	13.17	8.97	NA	4.78	5.61	5.88	4.66
3	20.96	22.14	14.51	13.04	8.68	NA	4.72	5.10	6.20	4.68

Table G.9 Maximum strains ( $\mu\epsilon$ ) for the 15 in (38 cm) section with tire pressure of 125 psi (862 kPa) – Winter data

Run	Longitudinal Strain Gages Located in the FRL				Longitudinal Strain Gages Located in the Base Layer			Transverse Strain Gages Located in the Base Layer		
	PM-001	PM-002	PM-003	KM-001	PM-005	KM-005	KM-008	PM-004	PM-006	KM-007
Single Axle 5 mph (8 km/h) Test Runs										
1	35.57	32.61	34.24	33.50	16.56	11.60	10.44	12.10	13.49	11.26
2	39.30	35.40	37.36	34.76	18.23	11.59	10.31	13.03	15.44	12.66
3	36.45	38.20	35.33	35.90	17.24	12.44	11.31	13.34	15.14	12.06
Tandem Axle 5 mph (8 km/h) Test Runs										
1	21.72	23.04	19.33	18.95	9.96	6.54	5.99	6.99	8.46	6.32
2	24.18	23.16	19.69	17.88	8.74	6.98	6.30	6.48	8.15	6.35
3	22.36	21.32	18.88	19.44	9.93	6.62	6.15	7.46	7.64	6.30
Single Axle 30 mph (48 km/h) Test Runs										
1	28.08	32.23	33.23	31.91	14.30	10.84	9.01	9.48	12.53	10.62
2	30.57	32.47	31.06	28.90	15.00	10.24	8.28	9.67	11.96	8.33
3	25.71	23.47	27.30	26.08	13.05	8.97	8.36	7.91	8.39	7.58
Tandem Axle 30 mph (48 km/h) Test Runs										
1	18.84	19.84	16.12	14.15	9.33	5.32	4.91	5.76	7.05	5.75
2	17.19	20.11	17.28	16.32	7.61	6.13	5.14	5.15	5.86	5.32
3	17.83	19.52	17.03	16.24	7.72	6.29	5.36	5.39	6.72	5.97
Single Axle 55 mph (89 km/h) Test Runs										
1	23.73	23.83	22.71	19.89	11.72	7.23	6.27	8.86	9.03	7.07
2	25.20	26.83	24.64	22.58	11.89	7.56	7.51	9.31	9.67	7.38
3	26.04	27.83	26.23	23.15	12.98	8.11	8.13	9.04	10.08	7.42
Tandem Axle 55 mph (89 km/h) Test Runs										
1	19.29	20.04	14.20	12.66	9.58	4.20	4.70	5.48	5.45	5.01
2	19.30	21.24	14.47	12.41	9.15	4.58	4.78	5.48	6.22	4.70
3	19.30	21.30	14.89	12.56	9.45	5.09	5.57	5.64	6.12	4.98

Table G.10 Maximum strains ( $\mu\epsilon$ ) during tandem axle testing on the 11 in (28 cm) section – Winter data

Run	Speed (mph)	Speed (km/h)	Longitudinal Strain Gages Located in the FRL						Longitudinal Strain Gages Located in the Base Layer			Transverse Strain Gages Located in the Base Layer		
			KM-001	KM-002	KM-003	PM-001	PM-002	PM-003	KM-004	KM-006	PM-005	KM-005	PM-004	PM-006
80 psi (552 kPa) Test Runs														
2	5	8	21.11	31.00	26.78	21.11	23.43	24.18	6.91	10.10	8.24	1.79	2.74	3.10
1	30	48	19.24	27.27	22.35	18.83	21.65	20.46	6.22	8.77	8.26	2.12	0.91	1.90
3	55	89	17.68	24.77	17.73	17.72	16.53	17.41	4.36	5.85	4.98	1.62	1.72	2.23
110 psi (758 kPa) Test Runs														
2	5	8	20.84	31.49	27.34	20.34	22.87	24.39	6.51	10.59	9.07	2.03	2.31	3.69
2	30	48	17.91	25.34	24.66	16.53	18.23	20.09	5.36	8.36	6.32	2.37	1.54	2.13
2	55	89	16.21	29.64	22.59	14.89	17.16	14.81	3.75	5.65	6.83	2.13	1.48	1.79
125 psi (862 kPa) Test Runs														
3	5	8	21.62	31.62	28.18	20.93	23.59	24.16	7.67	11.08	8.87	2.80	2.00	3.34
2	30	48	15.12	29.24	20.40	16.55	21.06	21.23	6.06	8.06	7.95	2.46	2.70	3.36
2	55	89	11.94	24.45	20.90	14.77	15.65	17.50	4.09	7.77	5.30	2.16	3.48	3.38

Table G.11 Maximum strains ( $\mu\epsilon$ ) during tandem axle testing on the 13 in (33 cm) section – Winter data

Run	Speed (mph)	Speed (km/h)	Longitudinal Strain Gages Located in the Base Layer			Transverse Strain Gages Located in the Base Layer		
			KM-005	KM-008	PM-005	KM-007	PM-004	PM-006
80 psi (552 kPa) Test Runs								
1	5	8	5.63	5.57	7.37	4.60	4.60	4.90
2	30	48	4.95	4.93	6.04	4.50	4.02	4.19
3	55	89	4.67	3.66	5.76	3.19	3.82	3.86
110 psi (758 kPa) Test Runs								
1	5	8	5.78	5.35	7.85	5.25	4.82	5.75
2	30	48	4.79	4.40	6.57	3.81	3.54	4.32
3	55	89	4.04	3.60	5.51	3.07	3.20	3.72
125 psi (862 kPa) Test Runs								
3	5	8	5.68	4.95	7.22	5.21	4.41	5.25
1	30	48	4.90	4.12	6.12	4.22	3.97	4.65
3	55	89	4.35	4.02	5.39	4.15	4.18	3.65

Table G.12 Maximum strains ( $\mu\epsilon$ ) during tandem axle testing on the 15 in (38 cm) section – Winter data

Run	Speed (mph)	Speed (km/h)	Longitudinal Strain Gages Located in the Base Layer			Transverse Strain Gages Located in the Base Layer		
			PM-005	KM-005	KM-008	PM-004	PM-006	KM-007
80 psi (552 kPa) Test Runs								
1	5	8	5.63	5.57	7.37	4.60	4.60	4.90
2	30	48	4.95	4.93	6.04	4.50	4.02	4.19
3	55	89	4.67	3.66	5.76	3.19	3.82	3.86
110 psi (758 kPa) Test Runs								
1	5	8	5.78	5.35	7.85	5.25	4.82	5.75
2	30	48	4.79	4.40	6.57	3.81	3.54	4.32
3	55	89	4.04	3.60	5.51	3.07	3.20	3.72
125 psi (862 kPa) Test Runs								
3	5	8	5.68	4.95	7.22	5.21	4.41	5.25
1	30	48	4.90	4.12	6.12	4.22	3.97	4.65
3	55	89	4.35	4.02	5.39	4.15	4.18	3.65

Table G.13 Additional maximum strains ( $\mu\epsilon$ ) during testing on the 13 in (33 cm) section – Winter data

Run	Speed (mph)	Speed (km/h)	Truck	FRL	Intermediate		Intermediate	
				Transverse	Longitudinal	Transverse		
				PM-002	KM-011	KM-013	KM-010	KM-012
80 psi (552 kPa) Test Runs								
3	5	8	Single	32.43	22.80	39.27	36.48	38.78
1	5	8	Tandem	18.21	10.34	14.34	27.11	32.92
3	30	48	Single	26.26	17.19	28.46	17.20	21.51
2	30	48	Tandem	14.59	8.39	12.75	23.12	26.61
1	55	89	Single	22.81	11.77	19.60	14.75	16.95
3	55	89	Tandem	13.80	6.03	8.00	20.19	21.65
110 psi (758 kPa) Test Runs								
1	5	8	Single	33.58	22.11	33.71	19.12	19.56
1	5	8	Tandem	17.95	20.50	15.00	30.25	33.77
2	30	48	Single	29.71	19.95	28.69	20.92	21.65
2	30	48	Tandem	15.00	9.04	10.10	17.25	20.75
1	55	89	Single	26.13	14.04	24.72	18.52	21.83
3	55	89	Tandem	13.05	5.32	7.22	19.10	21.21
125 psi (862 kPa) Test Runs								
1	5	8	Single	33.32	22.61	40.24	20.83	19.46
3	5	8	Tandem	17.49	9.61	14.50	27.62	31.26
2	30	48	Single	27.44	18.53	30.19	17.10	19.46
1	30	48	Tandem	14.58	6.82	10.45	21.24	24.65
2	55	89	Single	24.62	12.88	21.75	17.35	19.95
3	55	89	Tandem	13.28	5.55	9.55	17.31	19.24

Note: Tandem axle truck data refer to maximum strain produced by the tandem axle of the tandem axle truck.

Table G.14 Additional maximum strains ( $\mu\epsilon$ ) during testing on the 15 in (38 cm) section – Winter data

Run	Speed (mph)	Speed (km/h)	Truck	FRL Trans.	Intermediate Longitudinal		Intermediate Transverse		Surface Longitudinal	Surface Transverse
				KM-002	KM-013	KM-011	KM-010	KM-012	WFLM-043	WFLM-045
80 psi (552 kPa) Test Runs										
1	5	8	Single	42.78	31.02	41.35	30.59	24.57	38.78	42.82
3	5	8	Tandem	22.40	15.22	13.40	38.99	40.13	30.47	31.38
1	30	48	Single	34.08	23.36	29.27	21.82	19.41	48.54	47.65
3	30	48	Tandem	17.56	11.47	12.48	24.47	22.69	40.59	40.67
1	55	89	Single	27.80	16.06	17.31	13.43	13.27	55.32	58.50
3	55	89	Tandem	16.28	9.13	8.42	18.72	21.50	47.87	40.77
110 psi (758 kPa) Test Runs										
1	5	8	Single	41.94	30.76	39.75	26.10	21.70	29.19	40.46
1	5	8	Tandem	21.54	14.03	13.05	31.99	29.86	29.19	27.75
2	30	48	Single	36.41	24.60	29.42	18.84	18.70	37.84	41.53
1	30	48	Tandem	17.07	11.00	10.15	24.93	24.75	36.20	36.60
2	55	89	Single	26.67	16.36	19.36	14.47	12.88	50.23	49.88
3	55	89	Tandem	13.04	8.28	10.02	22.37	18.77	36.20	34.50
125 psi (862 kPa) Test Runs										
3	5	8	Single	39.44	26.86	34.22	22.27	19.30	30.56	40.32
2	5	8	Tandem	20.84	12.51	11.70	27.09	29.34	26.82	26.75
1	30	48	Single	34.05	22.17	26.15	15.64	16.59	39.26	47.99
2	30	48	Tandem	18.10	9.98	10.01	19.72	23.04	36.56	34.56
1	55	89	Single	22.70	12.10	14.52	10.86	9.63	38.61	48.81
1	55	89	Tandem	17.01	7.57	8.51	18.79	16.18	28.60	26.98

Note: Tandem axle truck data refers to maximum strain produced by the tandem axle of the tandem axle truck.



Table G.15 Maximum strains ( $\mu\epsilon$ ) from the steer axle of the tandem axle truck on the 13 in (33 cm) section – Winter data

Run	Speed (mph)	Speed (km/h)	Longitudinal Strain Gages Located in the Base Layer			Transverse Strain Gages Located in the Base Layer		
			KM-005	KM-008	PM-005	KM-007	PM-004	PM-006
80 psi (552 kPa) Test Runs								
1	5	8	5.30	5.19	6.88	6.23	NA	4.64
2	30	48	5.19	4.75	6.26	5.13	5.32	6.23
3	55	89	3.58	3.35	5.29	4.45	3.84	4.11
110 psi (758 kPa) Test Runs								
1	5	8	5.65	5.72	7.81	6.55	6.66	7.42
2	30	48	4.09	4.31	6.01	3.51	2.94	4.15
3	55	89	3.91	3.84	4.89	4.04	4.08	4.57
125 psi (862 kPa) Test Runs								
3	5	8	6.13	5.63	8.11	7.27	7.43	8.12
1	30	48	4.90	4.85	6.36	5.65	4.99	5.39
3	55	89	3.72	3.84	5.74	4.84	5.08	5.75

Table G.16 Maximum strains ( $\mu\epsilon$ ) from the steer axle of the tandem axle truck on the 15 in (38 cm) section – Winter data

Run	Speed (mph)	Speed (km/h)	Longitudinal Strain Gages Located in the Base Layer			Transverse Strain Gages Located in the Base Layer		
			PM-005	KM-005	KM-008	PM-004	PM-006	KM-007
80 psi (552 kPa) Test Runs								
1	5	8	6.80	NA	4.85	4.93	7.18	5.08
2	30	48	5.26	NA	4.03	4.80	5.78	5.43
3	55	89	5.40	NA	3.02	4.34	5.18	3.33
110 psi (758 kPa) Test Runs								
1	5	8	7.87	NA	4.88	5.98	7.65	6.23
2	30	48	5.37	NA	3.36	3.84	5.55	4.33
3	55	89	5.55	NA	2.89	4.68	5.37	3.23
125 psi (862 kPa) Test Runs								
3	5	8	7.32	NA	5.25	5.62	7.97	6.11
1	30	48	5.74	NA	3.47	4.13	5.01	4.18
3	55	89	5.07	NA	2.34	3.93	4.21	2.56

Table G.17 Additional maximum strains ( $\mu\epsilon$ ) from the steer axle of the tandem axle truck on the 13 in (33 cm) section – Winter data

Run	Speed (mph)	Speed (km/h)	FRL Transverse	Intermediate Longitudinal		Intermediate Transverse	
			PM-002	KM-011	KM-013	KM-010	KM-012
80 psi (552 kPa) Test Runs							
1	5	8	9.41	NA	19.05	26.14	26.36
2	30	48	12.11	NA	17.20	14.11	15.72
3	55	89	9.04	NA	11.53	12.80	15.87
110 psi (758 kPa) Test Runs							
1	5	8	15.01	NA	21.28	18.64	21.43
2	30	48	8.63	NA	12.66	21.29	23.14
3	55	89	8.63	4.98	NA	15.73	17.80
125 psi (862 kPa) Test Runs							
3	5	8	15.16	NA	23.22	17.42	18.05
1	30	48	10.56	NA	16.30	18.32	19.37
3	55	89	11.4	NA	11.33	12.14	13.71

Table G.18 Additional maximum strains ( $\mu\epsilon$ ) from the steer axle of the tandem axle truck on the 15 in (38 cm) section – Winter data

Run	Speed (mph)	Speed (km/h)	FRL Transverse	Intermediate Longitudinal		Intermediate Transverse		Surface Longitudinal	Surface Transverse
			KM-002	KM-013	KM-011	KM-010	KM-012	WFLM-043	WFLM-045
80 psi (552 kPa) Test Runs									
3	5	8	18.75	13.88	13.75	13.30	11.50	19.32	30.22
3	30	48	14.75	11.21	10.68	6.50	6.30	37.74	38.32
3	55	89	13.64	5.99	6.63	6.51	4.67	43.19	47.66
110 psi (758 kPa) Test Runs									
1	5	8	18.19	13.80	15.93	8.42	8.15	20.70	28.83
1	30	48	15.10	10.42	9.89	8.33	6.58	29.59	41.81
3	55	89	12.27	5.61	6.37	5.96	4.93	40.18	42.45
125 psi (862 kPa) Test Runs									
2	5	8	17.70	12.54	13.67	7.92	6.81	21.54	26.29
2	30	48	13.42	7.91	7.75	8.52	7.29	27.31	36.07
1	55	89	10.86	4.21	4.52	8.27	8.65	21.64	27.23

Summer data

Table G.19 Maximum strains ( $\mu\epsilon$ ) for the 11 in (28 cm) section with tire pressure of 80 psi (552 kPa) – Summer data

Run	Longitudinal Strain Gages Located in the FRL						Longitudinal Strain Gages Located in the Base Layer			Transverse Strain Gages Located in the Base Layer		
	KM-001	KM-002	KM-003	PM-001	PM-002	PM-003	KM-004	KM-006	PM-005	KM-005	PM-004	PM-006
Single Axle 5 mph (8 km/h) Test Runs												
1	106.55	137.69	119.03	80.00	96.15	102.80	58.22	73.71	61.15	38.31	42.69	40.37
2	103.01	135.23	110.13	78.80	93.40	97.58	54.92	69.60	62.58	32.41	39.77	38.94
3	73.38	104.92	86.78	57.72	69.74	74.19	26.35	40.98	34.75	18.79	20.21	19.95
Tandem Axle 5 mph (8 km/h) Test Runs												
1	82.63	106.26	88.74	65.02	74.18	79.97	30.33	42.14	42.00	21.49	23.81	24.37
2	83.00	104.12	91.07	62.50	72.22	77.88	35.66	44.17	49.97	-30.33	52.62	43.51
3	61.80	71.41	64.77	44.76	54.60	53.55	16.23	25.71	28.16	17.63	25.13	22.57
Single Axle 30 mph (48 km/h) Test Runs												
1	67.60	96.38	83.19	58.75	68.52	70.08	24.47	38.19	35.01	16.27	19.76	18.85
2	67.78	102.83	92.64	59.51	66.01	67.93	-23.77	39.38	31.46	18.58	22.70	17.89
3	63.51	85.39	68.37	58.60	69.71	68.81	17.37	25.05	20.87	14.26	16.68	15.73
Tandem Axle 30 mph (48 km/h) Test Runs												
1	54.94	76.18	58.50	45.03	56.02	57.69	15.06	25.49	19.63	-6.80	-8.70	-15.40
2	56.77	74.45	73.85	49.18	58.07	55.00	-17.41	28.48	18.90	10.76	-8.82	-9.09
3	43.34	65.14	60.30	36.33	51.37	54.65	10.68	18.97	12.11	-4.82	-12.08	-13.11
Single Axle 55 mph (89 km/h) Test Runs												
1	66.96	92.12	76.54	58.11	70.15	71.19	18.35	28.32	21.67	15.96	16.06	16.15
2	67.57	92.09	75.67	58.61	70.51	72.31	18.31	27.73	21.87	15.46	16.55	16.11
Tandem Axle 55 mph (89 km/h) Test Runs												
1	44.04	63.97	59.06	36.94	51.82	53.69	10.48	17.30	14.74	-12.28	-12.10	13.72
2	44.38	66.07	60.44	36.58	52.29	55.01	11.33	8.46	13.41	-4.83	-13.28	-14.27

Note: no third run at 55 mph (89 km/h)

Table G.20 Maximum strains ( $\mu\epsilon$ ) for the 11 in (28 cm) section with tire pressure of 110 psi (758 kPa) – Summer data

Run	Longitudinal Strain Gages Located in the FRL						Longitudinal Strain Gages Located in the Base Layer			Transverse Strain Gages Located in the Base Layer		
	KM-001	KM-002	KM-003	PM-001	PM-002	PM-003	KM-004	KM-006	PM-005	KM-005	PM-004	PM-006
Single Axle 5 mph (8 km/h) Test Runs												
1	96.70	138.67	109.64	79.55	95.30	94.58	54.10	65.47	52.27	42.50	54.67	47.97
2	101.90	140.14	125.44	83.23	98.48	99.04	63.14	74.85	64.74	40.80	46.47	41.36
3	105.32	143.25	119.04	84.70	98.52	103.47	64.71	81.40	68.96	48.52	50.21	44.56
Tandem Axle 5 mph (8 km/h) Test Runs												
1	79.04	102.22	85.63	58.88	70.76	73.31	43.04	56.31	54.62	44.26	58.81	55.32
2	70.21	99.51	89.04	58.40	66.73	68.09	37.15	49.73	44.43	43.21	53.21	44.53
3	80.02	105.32	87.61	61.84	72.15	77.07	29.83	42.87	43.93	-26.38	-25.51	-25.41
Single Axle 30 mph (48 km/h) Test Runs												
1	66.99	100.34	87.19	59.41	68.89	69.74	26.76	42.92	36.69	19.30	23.67	21.52
2	67.91	98.44	79.47	53.78	65.44	69.87	25.60	40.53	35.35	17.79	20.67	21.12
3	66.51	98.67	84.05	56.02	66.98	69.86	27.02	42.08	35.49	18.07	21.08	20.75
Tandem Axle 30 mph (48 km/h) Test Runs												
1	53.73	68.54	69.30	47.45	52.30	56.60	12.32	26.65	24.36	-11.08	-17.59	-17.85
2	56.37	72.71	56.74	43.49	50.57	54.37	17.19	26.92	19.36	-8.37	-10.59	-12.95
3	57.51	72.23	57.54	41.48	54.95	53.64	16.44	26.65	19.74	-7.03	-13.05	-14.47
Single Axle 55 mph (89 km/h) Test Runs												
1	60.27	89.41	78.33	48.92	59.06	62.06	17.78	30.03	19.49	17.86	16.88	15.60
2	54.12	80.56	68.87	44.76	55.41	56.45	15.44	26.84	20.67	9.95	12.91	15.64
3	60.71	89.02	77.71	48.65	59.30	62.56	18.70	29.70	20.26	17.26	16.04	16.51
Tandem Axle 55 mph (89 km/h) Test Runs												
1	49.73	69.56	48.05	43.85	46.70	47.65	10.60	17.28	15.78	-11.69	13.85	14.74
2	49.75	67.19	49.57	43.56	46.54	49.02	10.95	17.36	16.29	-13.00	14.83	16.03
3	47.22	66.81	49.63	43.51	46.02	49.39	10.41	17.56	16.25	-10.94	-13.01	13.29

Table G.21 Maximum strains ( $\mu\epsilon$ ) for the 11 in (28 cm) section with tire pressure of 125 psi (862 kPa) – Summer data

Run	Longitudinal Strain Gages Located in the FRL						Longitudinal Strain Gages Located in the Base Layer			Transverse Strain Gages Located in the Base Layer		
	KM-001	KM-002	KM-003	PM-001	PM-002	PM-003	KM-004	KM-006	PM-005	KM-005	PM-004	PM-006
Single Axle 5 mph (8 km/h) Test Runs												
1	80.97	108.01	102.02	73.44	86.14	91.41	42.80	59.82	39.00	43.35	31.73	21.44
2	107.46	138.15	115.93	83.51	99.76	105.85	62.57	83.58	70.44	44.23	53.18	47.72
3	100.64	138.56	119.50	79.84	95.76	99.10	63.41	75.88	65.72	53.07	53.44	52.38
Tandem Axle 5 mph (8 km/h) Test Runs												
1	72.83	91.63	79.71	56.76	65.83	68.17	40.56	48.22	54.10	33.49	61.08	56.90
2	76.40	99.37	80.06	58.12	69.91	72.19	38.24	52.74	54.04	26.42	50.90	52.44
3	73.20	94.54	81.44	56.39	67.44	70.00	33.60	46.33	51.06	-21.21	46.93	45.67
Single Axle 30 mph (48 km/h) Test Runs												
1	73.91	99.57	78.13	53.44	68.73	78.48	32.00	41.94	35.90	24.88	24.46	24.05
2	61.21	83.92	72.81	61.25	72.89	70.71	27.79	38.07	41.83	17.14	25.02	24.38
3	66.35	91.15	74.48	60.30	74.09	74.54	30.05	40.42	40.91	21.69	25.02	24.88
Tandem Axle 30 mph (48 km/h) Test Runs												
1	54.47	66.84	51.20	42.98	49.32	48.10	15.10	24.68	23.13	-8.79	-13.41	-12.28
2	58.41	61.87	56.62	37.51	51.09	45.55	17.17	29.94	20.31	12.21	-9.42	-4.15
3	55.66	60.94	63.69	39.53	50.94	45.61	18.92	26.76	30.03	-11.31	24.02	25.71
Single Axle 55 mph (89 km/h) Test Runs												
1	48.90	71.43	63.30	48.87	55.63	54.58	16.54	26.54	21.34	16.00	18.68	17.79
2	47.79	70.64	60.11	49.39	56.22	54.00	16.25	25.46	23.42	13.30	18.55	17.45
3	48.30	70.75	59.89	47.72	54.51	53.29	15.91	25.17	22.44	11.83	17.36	17.04
Tandem Axle 55 mph (89 km/h) Test Runs												
1	48.08	64.76	45.02	39.34	39.22	42.86	11.81	17.59	16.84	-10.42	15.80	16.94
2	48.43	64.63	47.23	40.85	43.97	44.99	11.14	18.65	14.30	-2.98	-10.65	-9.82
3	48.58	66.44	48.81	41.92	45.03	45.97	12.10	18.94	13.56	-3.41	-10.92	-10.34

Table G.22 Maximum strains ( $\mu\epsilon$ ) for the 13 in (33 cm) section with tire pressure of 80 psi (552 kPa) – Summer data

Run	Longitudinal Strain Gages Located in the FRL				Longitudinal Strain Gages Located in the Base Layer			Transverse Strain Gages Located in the Base Layer		
	KM-001	KM-002	KM-003	PM-003	KM-005	KM-008	PM-005	KM-007	PM-004	PM-006
Single Axle 5 mph (8 km/h) Test Runs										
1	76.16	80.77	1.29	61.84	35.91	31.02	37.69	37.99	65.94	33.03
2	83.97	85.04	1.11	64.39	39.01	34.11	41.46	43.68	70.19	35.86
3	77.81	83.25	1.35	62.09	35.62	30.81	37.80	40.27	66.04	32.87
Tandem Axle 5 mph (8 km/h) Test Runs										
1	52.11	57.12	3.58	44.49	21.51	18.93	26.97	28.73	47.68	25.48
2	54.81	61.89	1.43	43.60	22.06	20.82	26.02	28.93	51.16	26.93
3	55.18	60.40	1.58	45.95	21.13	20.19	23.40	7.84	42.30	12.42
Single Axle 30 mph (48 km/h) Test Runs										
1	42.57	45.24	1.81	42.55	17.97	14.81	21.97	10.45	43.74	15.45
2	46.14	50.92	0.77	44.74	18.80	16.94	23.85	15.91	46.38	17.94
3	40.34	44.89	1.46	40.42	16.27	14.75	22.94	11.55	45.63	15.15
Tandem Axle 30 mph (48 km/h) Test Runs										
1	38.42	38.70	1.33	34.66	14.31	11.50	20.12	19.72	39.92	20.63
2	36.49	39.09	1.91	35.43	12.21	11.20	17.26	11.83	35.09	14.60
3	37.00	38.58	1.60	34.60	12.98	11.04	17.07	9.32	33.07	13.02
Single Axle 55 mph (89 km/h) Test Runs										
1	36.30	39.86	1.02	37.48	12.37	12.65	17.31	10.60	40.40	13.24
2	40.65	42.15	1.25	40.42	14.58	12.71	19.61	14.16	42.66	15.86
3	39.91	42.06	363.49	40.11	14.21	11.80	19.01	13.68	44.43	16.84
Tandem Axle 55 mph (89 km/h) Test Runs										
1	30.82	33.81	1.27	30.15	9.66	9.83	11.05	4.65	29.02	7.77
2	31.76	33.97	1.93	29.68	10.64	9.75	12.21	5.27	26.05	7.03
3	30.91	33.93	1.49	29.35	10.34	8.48	12.77	14.34	29.62	15.32

Table G.23 Maximum strains ( $\mu\epsilon$ ) for the 13 in (33 cm) section with tire pressure of 110 psi (758 kPa) – Summer data

Run	Longitudinal Strain Gages Located in the FRL				Longitudinal Strain Gages Located in the Base Layer			Transverse Strain Gages Located in the Base Layer		
	KM-001	KM-002	KM-003	PM-003	KM-005	KM-008	PM-005	KM-007	PM-004	PM-006
Single Axle 5 mph (8 km/h) Test Runs										
1	69.26	71.36	1.27	56.86	36.51	27.39	36.47	43.24	62.03	32.86
2	74.02	77.14	1.20	59.97	39.00	31.40	40.97	45.39	66.41	38.14
3	74.82	73.38	1.88	59.78	35.88	31.06	40.70	45.03	68.10	37.70
Tandem Axle 5 mph (8 km/h) Test Runs										
1	46.27	50.47	1.56	41.11	24.66	19.40	23.73	14.04	38.55	18.33
2	48.41	54.74	1.55	41.29	25.45	21.38	29.91	34.65	48.89	30.48
3	48.79	52.98	1.42	41.79	22.80	20.27	29.35	30.13	49.55	29.35
Single Axle 30 mph (48 km/h) Test Runs										
1	48.03	48.54	1.10	49.62	23.21	17.68	27.97	24.48	50.88	25.13
2	41.73	45.50	1.10	43.74	20.10	17.89	27.16	20.80	49.63	23.77
3	42.51	46.06	1.33	44.60	20.23	17.54	26.10	18.79	45.93	21.58
Tandem Axle 30 mph (48 km/h) Test Runs										
1	29.05	32.62	1.75	30.29	12.13	10.70	14.49	6.58	27.17	7.54
2	29.87	34.58	2.39	30.37	14.15	12.34	19.69	20.39	36.25	20.65
3	32.49	34.40	1.44	29.57	12.65	9.76	14.26	7.89	30.69	10.51
Single Axle 55 mph (89 km/h) Test Runs										
1	32.78	36.00	1.52	34.98	13.11	11.46	19.45	13.54	37.80	16.00
2	36.02	39.75	1.05	38.15	15.02	12.83	20.49	15.33	42.47	17.73
3	40.01	41.26	1.70	39.64	16.31	12.97	19.79	20.55	44.30	19.28
Tandem Axle 55 mph (89 km/h) Test Runs										
1	30.40	27.07	1.47	27.48	11.13	7.82	11.48	5.86	26.12	8.50
2	30.55	26.10	1.13	28.78	11.29	6.82	12.49	7.19	28.24	9.56
3	28.14	25.01	1.12	27.54	12.00	8.87	12.48	10.56	26.88	12.19

Table G.24 Maximum strains ( $\mu\epsilon$ ) for the 13 in (33 cm) section with tire pressure of 125 psi (862 kPa) – Summer data

Run	Longitudinal Strain Gages Located in the FRL				Longitudinal Strain Gages Located in the Base Layer			Transverse Strain Gages Located in the Base Layer		
	KM-001	KM-002	KM-003	PM-003	KM-005	KM-008	PM-005	KM-007	PM-004	PM-006
Single Axle 5 mph (8 km/h) Test Runs										
1	62.65	73.99	25.56*	56.50	38.75	32.75	41.71	42.03	63.21	37.97
2	70.11	71.86	62.25*	57.61	38.52	31.97	42.67	46.89	63.96	39.97
3	70.67	72.11	115.8*	58.54	37.18	34.65	43.55	44.82	63.93	40.23
Tandem Axle 5 mph (8 km/h) Test Runs										
1	44.69	50.15	95.03*	36.64	20.62	18.80	25.13	20.77	37.18	22.43
2	47.23	52.06	48.34*	39.23	24.39	20.71	27.99	31.62	43.06	26.80
3	44.43	62.88	34.41*	38.45	22.49	20.38	23.89	16.63	37.54	17.35
Single Axle 30 mph (48 km/h) Test Runs										
1	39.05	43.63	1.39*	40.59	19.39	16.12	24.23	17.01	38.79	18.83
2	35.54	39.84	1.13*	39.24	18.18	15.10	23.73	14.67	40.99	19.16
3	38.47	42.72	1.45*	42.07	19.46	15.17	25.83	19.10	42.70	21.92
Tandem Axle 30 mph (48 km/h) Test Runs										
1	29.43	34.15	1.68*	29.99	13.13	11.10	17.56	15.53	32.33	16.49
2	28.28	33.55	1.53*	31.00	12.91	11.90	16.03	9.57	27.90	8.56
3	30.04	34.69	1.31*	31.02	11.92	10.82	15.53	8.99	30.12	8.93
Single Axle 55 mph (89 km/h) Test Runs										
1	36.34	39.71	1.19*	38.62	15.98	13.22	20.27	19.27	41.39	19.38
2	29.08	34.25	1.12*	31.52	12.63	11.04	15.98	11.77	32.49	12.94
3	36.85	40.23	1.64*	37.18	15.71	14.18	20.42	20.77	41.03	20.22
Tandem Axle 55 mph (89 km/h) Test Runs										
1	25.20	29.69	1.29*	25.68	10.12	9.40	10.65	8.92	23.41	7.75
2	24.85	29.25	1.20*	24.94	11.10	9.51	12.08	13.02	24.45	13.07
3	24.88	27.83	1.23*	26.48	10.54	8.94	13.16	9.97	24.76	10.87

\* Sensor KM-003 started giving bad readings



Table G.25 Maximum strains ( $\mu\epsilon$ ) for the 15 in (38 cm) section with tire pressure of 80 psi (552 kPa) – Summer data

Run	Longitudinal Strain Gages Located in the FRL				Longitudinal Strain Gages Located in the Base Layer			Transverse Strain Gages Located in the Base Layer		
	PM-001	PM-002	PM-003	KM-001	PM-005	KM-005	KM-008	PM-004	PM-006	KM-007
Single Axle 5 mph (8 km/h) Test Runs										
1	74.33	65.74	69.05	95.80	47.92	37.57	26.68	42.35	58.37	47.29
2	75.20	72.71	65.90	102.18	44.29	39.45	28.30	41.54	56.35	45.55
3	73.86	72.59	67.62	100.07	45.77	40.81	27.98	43.63	58.23	48.33
Tandem Axle 5 mph (8 km/h) Test Runs										
1	52.21	48.42	44.10	64.32	29.72	24.24	17.76	23.17	32.39	29.01
2	51.99	46.92	44.04	66.85	30.06	25.07	17.93	24.53	32.15	29.27
3	52.32	49.60	41.75	66.46	30.73	26.66	17.17	20.09	29.29	24.73
Single Axle 30 mph (48 km/h) Test Runs										
1	60.03	57.90	54.75	62.80	32.11	23.33	18.73	29.37	36.66	27.76
2	56.11	50.54	51.19	62.25	30.42	20.91	18.47	28.25	35.64	27.74
3	58.64	56.48	54.42	66.32	31.35	23.00	18.90	28.98	37.49	29.77
Tandem Axle 30 mph (48 km/h) Test Runs										
1	41.68	42.51	35.02	47.95	21.50	15.15	13.89	19.66	21.98	21.70
2	44.00	45.19	38.02	51.69	21.13	16.50	13.50	20.41	25.16	22.85
3	43.88	45.93	38.04	50.57	21.22	16.74	13.29	19.28	24.27	22.25
Single Axle 55 mph (89 km/h) Test Runs										
1	45.04	39.57	38.92	41.55	22.64	13.86	12.10	20.88	25.39	17.34
2	47.77	46.80	41.71	44.92	23.97	15.61	12.58	22.76	25.69	19.47
3	42.45	36.01	38.14	42.49	20.81	13.30	11.76	19.52	23.31	16.87
Tandem Axle 55 mph (89 km/h) Test Runs										
1	40.01	41.98	37.37	45.89	16.87	14.82	10.51	15.21	20.91	18.49
2	39.73	43.24	37.53	45.76	17.19	14.88	10.97	15.07	21.30	18.97
3	40.51	43.82	37.59	46.81	17.20	15.14	10.27	14.46	20.94	18.57

Table G.26 Maximum strains ( $\mu\epsilon$ ) for the 15 in (38 cm) section with tire pressure of 110 psi (758 kPa) – Summer data

Run	Longitudinal Strain Gages Located in the FRL				Longitudinal Strain Gages Located in the Base Layer			Transverse Strain Gages Located in the Base Layer		
	PM-001	PM-002	PM-003	KM-001	PM-005	KM-005	KM-008	PM-004	PM-006	KM-007
Single Axle 5 mph (8 km/h) Test Runs										
1	74.81	64.20	65.25	95.50	48.53	40.20	28.51	45.38	61.59	51.00
2	72.90	65.40	66.73	95.96	49.37	40.94	28.92	44.90	60.77	52.11
3	72.92	65.55	64.03	96.44	47.19	39.50	28.95	43.55	60.13	49.70
Tandem Axle 5 mph (8 km/h) Test Runs										
1	56.31	46.58	44.37	60.62	29.11	25.55	16.54	27.76	39.92	32.03
2	54.37	47.33	45.57	59.94	29.97	26.89	18.64	23.71	33.73	30.82
3	52.05	47.43	44.71	70.16	34.52	26.91	19.57	28.18	38.81	34.01
Single Axle 30 mph (48 km/h) Test Runs										
1	59.57	54.71	46.32	56.00	32.38	21.39	20.67	30.91	33.39	28.34
2	62.28	57.33	49.17	55.67	34.88	21.47	18.81	32.47	37.67	28.57
3	56.80	50.48	46.24	58.41	30.36	21.85	21.17	31.74	33.20	30.44
Tandem Axle 30 mph (48 km/h) Test Runs										
1	46.91	43.95	34.10	48.48	21.04	16.89	12.86	21.17	27.05	22.62
2	43.36	47.01	39.86	49.28	22.92	17.93	15.08	21.48	26.63	21.26
3	43.21	45.71	37.14	50.98	22.07	18.56	14.24	20.49	26.24	22.00
Single Axle 55 mph (89 km/h) Test Runs										
1	48.58	48.42	44.00	48.63	25.39	18.36	14.38	22.44	27.51	21.77
2	48.21	49.33	45.58	48.84	26.09	18.41	14.03	22.57	27.01	21.24
3	50.97	47.86	44.64	48.42	26.50	17.76	14.11	24.94	29.23	22.00
Tandem Axle 55 mph (89 km/h) Test Runs										
1	44.61	47.49	37.94	35.63	22.37	13.39	11.39	19.55	23.69	17.60
2	44.22	39.25	30.54	32.69	19.74	10.91	9.79	20.17	27.04	17.20
3	45.59	46.31	35.89	35.37	21.41	12.95	10.63	18.85	23.74	15.83

Table G.28 Maximum strains ( $\mu\epsilon$ ) for the 15 in (38 cm) section with tire pressure of 125 psi (862 kPa) – Summer data

Run	Longitudinal Strain Gages Located in the FRL				Longitudinal Strain Gages Located in the Base Layer			Transverse Strain Gages Located in the Base Layer		
	PM-001	PM-002	PM-003	KM-001	PM-005	KM-005	KM-008	PM-004	PM-006	KM-007
Single Axle 5 mph (8 km/h) Test Runs										
1	60.49	44.71	59.22	84.21	44.54	36.09	25.87	39.61	53.34	42.07
2	71.11	66.21	66.79	89.78	46.04	43.26	28.40	46.78	60.78	55.32
3	68.67	69.78	71.36	93.20	47.16	42.01	30.72	45.67	55.70	53.87
Tandem Axle 5 mph (8 km/h) Test Runs										
1	49.76	42.70	38.88	60.96	29.66	25.47	17.23	23.80	36.69	32.62
2	47.80	44.39	40.46	62.28	32.20	26.49	18.70	24.99	33.61	32.96
3	49.90	40.93	37.40	57.84	29.08	23.08	16.92	28.50	42.21	32.89
Single Axle 30 mph (48 km/h) Test Runs										
1	58.52	60.64	51.53	57.78	37.92	24.47	21.44	27.24	36.25	26.74
2	53.58	56.36	54.61	65.19	32.30	26.25	19.59	26.28	36.43	13.55
3	45.54	45.11	49.07	64.44	26.87	23.85	20.86	18.45	23.21	25.45
Tandem Axle 30 mph (48 km/h) Test Runs										
1	41.92	40.53	35.07	48.01	20.88	17.18	13.36	18.73	25.42	22.75
2	42.61	42.33	35.53	46.57	20.30	17.05	13.50	20.94	26.08	24.70
3	42.30	42.84	33.33	48.88	21.38	17.82	14.10	21.99	21.38	23.25
Single Axle 55 mph (89 km/h) Test Runs										
1	46.05	44.78	42.32	46.34	25.58	17.17	14.18	23.25	29.25	22.76
2	46.38	45.16	41.71	44.31	25.63	17.83	13.83	24.18	28.67	21.67
3	46.07	43.54	40.76	43.33	25.60	16.23	12.95	23.47	28.47	21.00
Tandem Axle 55 mph (89 km/h) Test Runs										
1	43.01	40.02	30.95	34.06	20.45	11.93	10.47	18.39	24.76	16.85
2	43.49	43.06	32.80	35.12	21.63	12.52	11.08	18.64	23.20	17.63
3	43.56	41.44	32.48	33.64	21.19	12.74	10.44	17.96	22.38	16.44

Table G.29 Maximum strains ( $\mu\epsilon$ ) during tandem axle testing on the 11 in (28 cm) section – Summer data

Run	Speed		Longitudinal Strain Gages Located in the FRL						Longitudinal Strain Gages Located in the Base Layer			Transverse Strain Gages Located in the Base Layer		
	(mph)	(km/h)	KM-001	KM-002	KM-003	PM-001	PM-002	PM-003	KM-004	KM-006	PM-005	KM-005	PM-004	PM-006
80 psi (552 kPa) Test Runs														
2	5	8	83.00	104.12	91.07	62.50	72.22	77.88	35.66	44.17	49.97	-30.33	52.62	43.51
3	30	48	43.34	65.14	60.30	36.33	51.37	54.65	10.68	18.97	12.11	-4.82	-12.08	-13.11
1	55	89	44.04	63.97	59.06	36.94	51.82	53.69	10.48	17.30	14.74	-12.28	-12.10	13.72
110 psi (758 kPa) Test Runs														
2	5	8	70.21	99.51	89.04	58.40	66.73	68.09	37.15	49.73	44.43	43.21	53.21	44.53
1	30	48	53.73	68.54	69.30	47.45	52.30	56.60	12.32	26.65	24.36	-11.08	-17.59	-17.85
1	55	89	49.73	69.56	48.05	43.85	46.70	47.65	10.60	17.28	15.78	-11.69	13.85	14.74
125 psi (862 kPa) Test Runs														
1	5	8	72.83	91.63	79.71	56.76	65.83	68.17	40.56	48.22	54.10	33.49	61.08	56.90
3	30	48	55.66	60.94	63.69	39.53	50.94	45.61	18.92	26.76	30.03	-11.31	24.02	25.71
1	55	89	48.08	64.76	45.02	39.34	39.22	42.86	11.81	17.59	16.84	-10.42	15.80	16.94

Table G.30 Maximum strains ( $\mu\epsilon$ ) during tandem axle testing on the 13 in (33 cm) section – Summer data

Run	Speed		Longitudinal Strain Gages Located in the Base Layer			Transverse Strain Gages Located in the Base Layer		
	(mph)	(km/h)	KM-005	KM-008	PM-005	KM-007	PM-004	PM-006
80 psi (552 kPa) Test Runs								
2	5	8	22.06	20.82	26.02	28.93	51.16	26.93
2	30	48	12.21	11.20	17.26	11.83	35.09	14.60
3	55	89	10.34	8.48	12.77	14.34	29.62	15.32
110 psi (758 kPa) Test Runs								
2	5	8	25.45	21.38	29.91	34.65	48.89	30.48
2	30	48	14.15	12.34	19.69	20.39	36.25	20.65
1	55	89	11.13	7.82	11.48	5.86	26.12	8.50
125 psi (862 kPa) Test Runs								
1	5	8	20.62	18.80	25.13	20.77	37.18	22.43
1	30	48	13.13	11.10	17.56	15.53	32.33	16.49
2	55	89	11.10	9.51	12.08	13.02	24.45	13.07

Table G.31 Maximum strains ( $\mu\epsilon$ ) during tandem axle testing on the 15 in (38 cm) section – Summer data

Run	Speed		Longitudinal Strain Gages Located in the Base Layer			Transverse Strain Gages Located in the Base Layer		
	(mph)	(km/h)	PM-005	KM-005	KM-008	PM-004	PM-006	KM-007
80 psi (552 kPa) Test Runs								
1	5	8	29.72	24.24	17.76	23.17	32.39	29.01
1	30	48	21.50	15.15	13.89	19.66	21.98	21.70
3	55	89	17.20	15.14	10.27	14.46	20.94	18.57
110 psi (758 kPa) Test Runs								
2	5	8	29.97	26.89	18.64	23.71	33.73	30.82
1	30	48	21.04	16.89	12.86	21.17	27.05	22.62
3	55	89	21.41	12.95	10.63	18.85	23.74	15.83
125 psi (862 kPa) Test Runs								
2	5	8	32.20	26.49	18.70	24.99	33.61	32.96
1	30	48	20.88	17.18	13.36	18.73	25.42	22.75
3	55	89	21.19	12.74	10.44	17.96	22.38	16.44

**Appendix H: LVDT and pressure cell data from CVL tests on DEL-23.**

Winter data

Table H.1a Maximum displacements and pressures on the 11 in (28 cm) section with tire pressure of 80 psi (552 kPa) – English units, Winter data

Run	Displacement (mil)				Pressure (psi)	
	LV-001	LV-002	LV-003	LV-004	PC-001	PC-002
<b>Single Axle 5 mph Test Runs</b>						
<b>1</b>	4.01	1.78	1.16	4.73	3.927	4.186
<b>2</b>	3.95	1.88	1.09	4.63	3.637	3.911
<b>3</b>	4.17	1.70	1.19	4.84	3.847	4.189
<b>Tandem Axle 5 mph Test Runs</b>						
<b>1</b>	2.77	1.31	0.67	3.16	2.046	2.172
<b>2</b>	3.02	1.17	0.69	3.43	1.998	2.116
<b>3</b>	3.04	0.87	0.69	3.67	2.069	2.211
<b>Single Axle 30 mph Test Runs</b>						
<b>1</b>	3.17	NA	0.85	4.13	2.851	2.594
<b>2</b>	3.61	NA	0.92	4.41	2.428	2.655
<b>3</b>	3.11	1.51	0.79	3.75	3.371	2.914
<b>Tandem Axle 30 mph Test Runs</b>						
<b>1</b>	2.84	1.45	0.50	3.03	1.891	1.701
<b>2</b>	2.93	0.79	0.50	3.06	1.750	1.595
<b>3</b>	2.89	0.57	0.51	2.88	1.844	1.842
<b>Single Axle 55 mph Test Runs</b>						
<b>1</b>	3.85	1.75	0.69	3.51	2.081	2.000
<b>2</b>	3.70	1.38	0.72	3.72	2.127	2.126
<b>3</b>	3.83	1.71	0.66	3.18	2.149	1.896
<b>Tandem Axle 55 mph Test Runs</b>						
<b>1</b>	2.10	0.43	0.46	2.50	1.743	1.921
<b>2</b>	2.23	0.86	0.46	2.56	1.603	1.702
<b>3</b>	2.37	NA	0.46	2.38	1.730	1.243

Note: LV-001 and LV-004 were deep LVDTs and LV-002 and LV-003 were shallow LVDTs

Table H.1b Maximum displacements and pressures on the 11 in (28 cm) section with tire pressure of (552 kPa) – metric units, Winter data

Run	Displacement ( $\mu\text{m}$ )				Pressure (kPa)	
	LV-001	LV-002	LV-003	LV-004	PC-001	PC-002
<b>Single Axle 8 km/h Test Runs</b>						
1	102	45	29	120	27.08	28.86
2	100	48	28	118	25.08	26.97
3	106	43	30	123	26.52	28.88
<b>Tandem Axle 8 km/h Test Runs</b>						
1	70	33	17	80	14.11	14.98
2	77	30	18	87	13.78	14.59
3	77	22	18	93	14.27	15.24
<b>Single Axle 48 km/h Test Runs</b>						
1	81	NA	22	105	19.66	17.89
2	92	NA	23	112	16.74	18.31
3	79	38	20	95	23.24	20.09
<b>Tandem Axle 48 km/h Test Runs</b>						
1	72	37	13	77	13.04	11.73
2	74	20	13	78	12.07	11.00
3	73	14	13	73	12.71	12.70
<b>Single Axle 89 km/h Test Runs</b>						
1	98	44	18	89	14.35	13.79
2	94	35	18	94	14.67	14.66
3	97	43	17	81	14.82	13.07
<b>Tandem Axle 89 km/h Test Runs</b>						
1	53	11	12	64	12.02	13.24
2	57	22	12	65	11.05	11.73
3	60	NA	12	60	11.93	8.57

Note: LV-001 and LV-004 were deep LVDTs and LV-002 and LV-003 were shallow LVDTs

Table H.2a Maximum displacements and pressures on the 11 in (28 cm) section with tire pressure of 110 psi (758 kPa) – English units, Winter data

Run	Displacement (mil)				Pressure (psi)	
	LV-001	LV-002	LV-003	LV-004	PC-001	PC-002
<b>Single Axle 5 mph Test Runs</b>						
<b>1</b>	4.12	2.09	1.22	4.57	3.508	4.178
<b>2</b>	4.02	1.53	1.14	4.67	3.621	3.754
<b>3</b>	4.13	2.19	1.11	4.36	3.703	2.858
<b>Tandem Axle 5 mph Test Runs</b>						
<b>1</b>	2.86	1.27	0.57	3.36	1.888	2.244
<b>2</b>	2.84	1.35	0.62	3.38	2.008	2.003
<b>3</b>	3.06	1.44	0.69	3.52	2.073	2.337
<b>Single Axle 30 mph Test Runs</b>						
<b>1</b>	3.44	1.24	0.78	3.30	3.812	3.460
<b>2</b>	3.54	1.76	0.74	3.17	3.407	3.451
<b>3</b>	3.70	1.96	0.85	3.40	3.610	3.789
<b>Tandem Axle 30 mph Test Runs</b>						
<b>1</b>	2.71	0.53	0.52	2.84	1.712	1.947
<b>2</b>	2.73	0.86	0.48	2.69	1.678	1.898
<b>3</b>	2.49	0.47	0.55	2.77	1.699	2.023
<b>Single Axle 55 mph Test Runs</b>						
<b>1</b>	3.33	1.51	0.71	3.26	2.937	2.518
<b>2</b>	3.22	1.14	0.71	3.26	2.635	2.324
<b>3</b>	3.42	1.58	0.70	3.19	2.949	2.468
<b>Tandem Axle 55 mph Test Runs</b>						
<b>1</b>	2.50	0.78	0.54	2.90	1.715	1.856
<b>2</b>	2.67	0.52	0.53	3.13	1.464	1.691
<b>3</b>	2.13	0.41	0.45	2.38	1.825	1.532

Note: LV-001 and LV-004 were deep LVDTs and LV-002 and LV-003 were shallow LVDTs



Table H.2b Maximum displacements and pressures on the 11 in (28 cm) section with tire pressure of 110 psi (758 kPa) – metric units, Winter data

Run	Displacement ( $\mu\text{m}$ )				Pressure (kPa)	
	LV-001	LV-002	LV-003	LV-004	PC-001	PC-002
<b>Single Axle 8 km/h Test Runs</b>						
1	105	53	31	116	24.19	28.81
2	102	39	29	119	24.97	25.88
3	105	56	28	111	25.53	19.71
<b>Tandem Axle 8 km/h Test Runs</b>						
1	73	32	14	85	13.02	15.47
2	72	34	16	86	13.84	13.81
3	78	37	18	89	14.29	16.11
<b>Single Axle 30 mph (48 km/h) Test Runs</b>						
1	87	31	20	84	26.28	23.86
2	90	45	19	81	23.49	23.79
3	94	50	22	86	24.89	26.12
<b>Tandem Axle 30 mph (48 km/h) Test Runs</b>						
1	69	13	13	72	11.80	13.42
2	69	22	12	68	11.57	13.09
3	63	12	14	70	11.71	13.95
<b>Single Axle 55 mph (89 km/h) Test Runs</b>						
1	85	38	18	83	20.25	17.36
2	82	29	18	83	18.17	16.02
3	87	40	18	81	20.33	17.02
<b>Tandem Axle 55 mph (89 km/h) Test Runs</b>						
1	64	20	14	74	11.82	12.80
2	68	13	13	80	10.09	11.66
3	54	10	11	60	12.58	10.56

Note: LV-001 and LV-004 were deep LVDTs and LV-002 and LV-003 were shallow LVDTs

Table H.3a Maximum displacements and pressures on the 11 in (28 cm) section with tire pressure of 125 psi (862 kPa) – English units, Winter data

Run	Displacement (mil)				Pressure (psi)	
	LV-001	LV-002	LV-003	LV-004	PC-001	PC-002
<b>Single Axle 5 mph Test Runs</b>						
<b>1</b>	3.98	2.15	1.17	4.42	3.750	3.638
<b>2</b>	4.00	2.12	1.18	4.48	3.783	3.719
<b>3</b>	3.95	2.13	1.14	4.54	3.678	3.834
<b>Tandem Axle 5 mph Test Runs</b>						
<b>1</b>	2.66	1.77	0.59	3.05	1.919	2.094
<b>2</b>	2.87	1.12	0.62	3.38	1.784	2.155
<b>3</b>	3.00	1.11	0.67	3.46	1.944	2.248
<b>Single Axle 30 mph Test Runs</b>						
<b>1</b>	3.50	1.83	0.96	4.12	2.356	3.250
<b>2</b>	3.75	1.39	0.97	3.90	2.427	3.629
<b>3</b>	3.46	1.83	0.89	3.93	2.524	3.206
<b>Tandem Axle 30 mph Test Runs</b>						
<b>1</b>	2.70	1.20	0.46	2.74	1.648	1.830
<b>2</b>	2.45	1.25	0.55	2.62	1.426	1.806
<b>3</b>	2.63	0.51	0.56	2.76	1.577	1.865
<b>Single Axle 55 mph Test Runs</b>						
<b>1</b>	3.01	1.07	0.85	3.74	3.127	3.261
<b>2</b>	2.83	1.69	0.73	3.77	2.083	2.593
<b>3</b>	2.97	1.10	0.83	3.56	2.768	2.960
<b>Tandem Axle 55 mph Test Runs</b>						
<b>1</b>	2.90	0.80	0.49	3.19	1.170	1.545
<b>2</b>	2.52	0.84	0.48	3.13	1.132	1.517
<b>3</b>	2.42	0.46	0.54	2.96	1.739	1.822

Note: LV-001 and LV-004 were deep LVDTs and LV-002 and LV-003 were shallow LVDTs

Table H.3b Maximum displacements and pressures on the 11 in (28 cm) section with tire pressure of 125 psi (862 kPa) – metric units, Winter data

Run	Displacement ( $\mu\text{m}$ )				Pressure (kPa)	
	LV-001	LV-002	LV-003	LV-004	PC-001	PC-002
<b>Single Axle 8 km/h Test Runs</b>						
1	101	55	30	112	25.86	25.08
2	102	54	30	114	26.08	25.64
3	100	54	29	115	25.36	26.43
<b>Tandem Axle 8 km/h Test Runs</b>						
1	68	45	15	77	13.23	14.44
2	73	28	16	86	12.30	14.86
3	76	28	17	88	13.40	15.50
<b>Single Axle 48 km/h Test Runs</b>						
1	89	46	24	105	16.24	22.41
2	95	35	25	99	16.73	25.02
3	88	46	23	100	17.40	22.10
<b>Tandem Axle 48 km/h Test Runs</b>						
1	69	30	12	70	11.36	12.62
2	62	32	14	67	9.83	12.45
3	67	13	14	70	10.87	12.86
<b>Single Axle 89 km/h Test Runs</b>						
1	76	27	22	95	21.56	22.48
2	72	43	19	96	14.36	17.88
3	75	28	21	90	19.08	20.41
<b>Tandem Axle 89 km/h Test Runs</b>						
1	74	20	12	81	8.07	10.65
2	64	21	12	80	7.80	10.46
3	61	12	14	75	11.99	12.56

Note: LV-001 and LV-004 were deep LVDTs and LV-002 and LV-003 were shallow LVDTs

Table H.4a Maximum displacements and pressures on the 13 in (33 cm) section with tire pressure of 80 psi (552 kPa) – English units, Winter data

Run	Displacement (mil)				Pressure (psi)	
	LV-001	LV-002	LV-003	LV-004	PC-001	PC-002
<b>Single Axle 5 mph Test Runs</b>						
1	NA	0.97	0.98	4.50	0.815	1.538
2	NA	0.99	0.89	4.35	0.862	1.572
3	NA	0.98	1.00	4.65	0.829	1.582
<b>Tandem Axle 5 mph Test Runs</b>						
1	NA	0.54	0.46	3.51	0.430	0.922
2	NA	0.58	0.48	3.64	0.443	0.927
3	NA	0.55	0.48	3.62	0.448	0.930
<b>Single Axle 30 mph Test Runs</b>						
1	NA	0.77	0.78	3.98	0.627	1.199
2	NA	8.00	0.73	3.78	0.638	1.170
3	NA	0.77	0.72	3.60	0.631	1.292
<b>Tandem Axle 30 mph Test Runs</b>						
1	NA	0.42	0.35	2.94	0.342	0.786
2	NA	0.44	0.35	3.12	0.367	0.807
3	2.07	0.43	0.34	3.03	0.346	0.795
<b>Single Axle 55 mph Test Runs</b>						
1	2.53	0.64	0.75	4.01	0.410	0.995
2	NA	0.58	0.64	3.49	0.482	1.054
3	2.43	0.61	0.76	3.96	0.386	0.941
<b>Tandem Axle 55 mph Test Runs</b>						
1	NA	0.41	0.39	3.14	0.284	0.708
2	2.04	0.37	0.37	3.15	0.294	0.703
3	NA	0.39	0.38	3.30	0.305	0.655

Note: LV-001 and LV-004 were deep LVDTs and LV-002 and LV-003 were shallow LVDTs

Table H.4b Maximum displacements and pressures on the 13 in (33 cm) section with tire pressure of 80 psi (552 kPa) – metric units, Winter data

Run	Displacement ( $\mu\text{m}$ )				Pressure (kPa)	
	LV-001	LV-002	LV-003	LV-004	PC-001	PC-002
<b>Single Axle 8 km/h Test Runs</b>						
1	NA	25	25	114	5.62	10.60
2	NA	25	23	110	5.94	10.84
3	NA	25	25	118	5.72	10.91
<b>Tandem Axle 8 km/h Test Runs</b>						
1	NA	14	12	89	2.96	6.36
2	NA	15	12	92	3.05	6.39
3	NA	14	12	92	3.09	6.41
<b>Single Axle 48 km/h Test Runs</b>						
1	NA	20	20	101	4.32	8.27
2	NA	203	19	96	4.40	8.07
3	NA	20	18	91	4.35	8.91
<b>Tandem Axle 48 km/h Test Runs</b>						
1	NA	11	9	75	2.36	5.42
2	NA	11	9	79	2.53	5.56
3	53	11	9	77	2.39	5.48
<b>Single Axle 89 km/h Test Runs</b>						
1	64	16	19	102	2.83	6.86
2	NA	15	16	89	3.32	7.27
3	62	15	19	101	2.66	6.49
<b>Tandem Axle 89 km/h Test Runs</b>						
1	NA	10	10	80	1.96	4.88
2	52	9	9	80	2.03	4.85
3	NA	10	10	84	2.10	4.52

Note: LV-001 and LV-004 were deep LVDTs and LV-002 and LV-003 were shallow LVDTs

Table H.5a Maximum displacements and pressures on the 13 in (33 cm) section with tire pressure of 110 psi (758 kPa) – English units, Winter data

Run	Displacement (mil)				Pressure (psi)	
	LV-001	LV-002	LV-003	LV-004	PC-001	PC-002
<b>Single Axle 5 mph Test Runs</b>						
1	NA	0.94	0.99	4.28	0.741	1.580
2	NA	0.98	1.02	4.36	0.782	1.571
3	NA	1.01	1.01	4.30	0.793	1.538
<b>Tandem Axle 5 mph Test Runs</b>						
1	NA	0.53	0.44	3.43	0.445	0.888
2	NA	0.49	0.46	3.52	0.418	0.921
3	NA	0.54	0.46	3.55	0.453	0.953
<b>Single Axle 30 mph Test Runs</b>						
1	NA	0.76	0.80	3.89	0.580	1.089
2	NA	0.79	0.88	3.99	0.555	1.044
3	NA	0.81	0.81	3.70	0.538	1.229
<b>Tandem Axle 30 mph Test Runs</b>						
1	NA	0.53	0.41	2.96	0.330	0.777
2	2.11	0.44	0.36	2.97	0.329	0.766
3	NA	0.44	0.36	3.01	0.338	0.759
<b>Single Axle 55 mph Test Runs</b>						
1	NA	0.61	0.74	3.46	0.581	1.226
2	NA	0.59	0.67	3.33	0.530	1.115
3	NA	0.60	0.67	3.37	0.511	1.074
<b>Tandem Axle 55 mph Test Runs</b>						
1	2.08	0.42	0.37	2.94	0.305	0.763
2	1.80	0.39	0.37	2.98	0.340	0.694
3	1.92	0.36	0.34	3.03	0.290	0.690

Note: LV-001 and LV-004 were deep LVDTs and LV-002 and LV-003 were shallow LVDTs

Table H.5b Maximum displacements and pressures on the 13 in (33 cm) section with tire pressure of 110 psi (758 kPa) – metric units, Winter data

Run	Displacement ( $\mu\text{m}$ )				Pressure (kPa)	
	LV-001	LV-002	LV-003	LV-004	PC-001	PC-002
<b>Single Axle 8 km/h Test Runs</b>						
1	NA	24	25	109	5.11	10.89
2	NA	25	26	111	5.39	10.83
3	NA	26	26	109	5.47	10.60
<b>Tandem Axle 8 km/h Test Runs</b>						
1	NA	13	11	87	3.07	6.12
2	NA	12	12	89	2.88	6.35
3	NA	14	12	90	3.12	6.57
<b>Single Axle 48 km/h Test Runs</b>						
1	NA	19	20	99	4.00	7.51
2	NA	20	22	101	3.83	7.20
3	NA	21	21	94	3.71	8.47
<b>Tandem Axle 48 km/h Test Runs</b>						
1	NA	13	10	75	2.28	5.36
2	54	11	9	75	2.27	5.28
3	NA	11	9	76	2.33	5.23
<b>Single Axle 89 km/h Test Runs</b>						
1	NA	15	19	88	4.01	8.45
2	NA	15	17	85	3.65	7.69
3	NA	15	17	86	3.52	7.40
<b>Tandem Axle 89 km/h Test Runs</b>						
1	53	11	9	75	2.10	5.26
2	46	10	9	76	2.34	4.78
3	49	9	9	77	2.00	4.76

Note: LV-001 and LV-004 were deep LVDTs and LV-002 and LV-003 were shallow LVDTs

Table H.6a Maximum displacements and pressures on the 13 in (33 cm) section with tire pressure of 125 psi (862 kPa) – English units, Winter data

Run	Displacement (mil)				Pressure (psi)	
	LV-001	LV-002	LV-003	LV-004	PC-001	PC-002
<b>Single Axle 5 mph Test Runs</b>						
<b>1</b>	3.13	1.11	1.19	4.27	0.807	1.562
<b>2</b>	2.95	1.13	1.11	4.52	0.780	1.519
<b>3</b>	3.26	0.95	1.08	4.36	0.807	1.482
<b>Tandem Axle 5 mph Test Runs</b>						
<b>1</b>	2.38	0.62	0.49	3.34	0.415	0.921
<b>2</b>	2.57	0.54	0.51	3.48	0.448	0.882
<b>3</b>	2.40	0.53	0.46	3.32	0.416	0.912
<b>Single Axle 30 mph Test Runs</b>						
<b>1</b>	2.50	0.83	0.88	3.75	0.507	1.080
<b>2</b>	2.67	0.87	0.83	3.62	0.566	1.226
<b>3</b>	2.64	0.83	0.75	3.42	0.529	1.224
<b>Tandem Axle 30 mph Test Runs</b>						
<b>1</b>	2.12	0.39	0.36	2.81	0.318	0.713
<b>2</b>	1.88	0.42	0.35	2.75	0.309	0.766
<b>3</b>	1.96	0.46	0.41	2.71	0.308	0.708
<b>Single Axle 55 mph Test Runs</b>						
<b>1</b>	2.22	0.59	0.61	3.26	0.492	1.018
<b>2</b>	2.33	0.67	NA	3.56	0.467	0.960
<b>3</b>	2.40	0.68	0.72	3.60	0.434	0.872
<b>Tandem Axle 55 mph Test Runs</b>						
<b>1</b>	1.80	0.39	0.37	2.98	0.340	0.694
<b>2</b>	1.76	0.36	0.32	2.71	0.323	0.718
<b>3</b>	1.84	0.36	0.32	2.70	0.347	0.761

Note: LV-001 and LV-004 were deep LVDTs and LV-002 and LV-003 were shallow LVDTs



Table H.6b Maximum displacements and pressures on the 13 in (33 cm) section with tire pressure of 125 psi (862 kPa) – metric units, Winter data

Run	Displacement ( $\mu\text{m}$ )				Pressure (kPa)	
	LV-001	LV-002	LV-003	LV-004	PC-001	PC-002
<b>Single Axle 8 km/h Test Runs</b>						
1	80	28	30	108	5.56	10.77
2	75	29	28	115	5.38	10.47
3	83	24	27	111	5.56	10.22
<b>Tandem Axle 8 km/h Test Runs</b>						
1	60	16	12	85	2.86	6.35
2	65	14	13	88	3.09	6.08
3	61	13	12	84	2.87	6.29
<b>Single Axle 48 km/h Test Runs</b>						
1	64	21	22	95	3.50	7.45
2	68	22	21	92	3.90	8.45
3	67	21	19	87	3.65	8.44
<b>Tandem Axle 48 km/h Test Runs</b>						
1	54	10	9	71	2.19	4.92
2	48	11	9	70	2.13	5.28
3	50	12	10	69	2.12	4.88
<b>Single Axle 89 km/h Test Runs</b>						
1	56	15	15	83	3.39	7.02
2	59	17	NA	90	3.22	6.62
3	61	17	18	91	2.99	6.01
<b>Tandem Axle 89 km/h Test Runs</b>						
1	46	10	9	76	2.34	4.78
2	45	9	8	69	2.23	4.95
3	47	9	8	69	2.39	5.25

Note: LV-001 and LV-004 were deep LVDTs and LV-002 and LV-003 were shallow LVDTs

Table H.7a Maximum displacements and pressures on the 15 in (38 cm) section with tire pressure of 80 psi (552 kPa) – English units, Winter data

Run	Displacement (mil)				Pressure (psi)	
	LV-001	LV-002	LV-003	LV-004	PC-001	PC-002
<b>Single Axle 5 mph Test Runs</b>						
<b>1</b>	7.36	1.45	1.41	4.38	1.882	2.034
<b>2</b>	7.54	1.41	1.36	4.40	1.841	1.985
<b>3</b>	7.38	1.41	1.37	4.39	1.883	2.066
<b>Tandem Axle 5 mph Test Runs</b>						
<b>1</b>	6.30	0.74	0.75	3.60	1.529	1.701
<b>2</b>	6.13	0.76	0.73	3.55	1.489	1.725
<b>3</b>	6.24	0.74	0.71	3.58	1.525	1.731
<b>Single Axle 30 mph Test Runs</b>						
<b>1</b>	6.04	1.10	1.07	3.69	1.686	1.777
<b>2</b>	6.44	1.18	1.03	3.45	1.664	1.907
<b>3</b>	6.79	1.22	1.06	3.66	1.602	1.925
<b>Tandem Axle 30 mph Test Runs</b>						
<b>1</b>	5.34	0.67	0.59	2.89	1.443	1.663
<b>2</b>	4.94	0.64	0.58	2.68	1.345	1.712
<b>3</b>	5.22	0.62	0.69	2.96	1.408	1.442
<b>Single Axle 55 mph Test Runs</b>						
<b>1</b>	5.45	0.89	0.97	3.52	1.284	1.559
<b>2</b>	4.81	0.82	0.89	3.19	1.567	1.763
<b>3</b>	4.96	0.84	0.91	3.31	1.460	1.669
<b>Tandem Axle 55 mph Test Runs</b>						
<b>1</b>	5.25	0.48	0.58	2.77	1.282	1.560
<b>2</b>	5.11	0.52	0.58	2.86	1.248	1.531
<b>3</b>	5.27	0.49	0.57	2.80	1.281	1.575

Note: LV-001 and LV-004 were deep LVDTs and LV-002 and LV-003 were shallow LVDTs

Table H.7b Maximum displacements and pressures on the 15 in (38 cm) section with tire pressure of 80 psi (552 kPa) – metric units, Winter data

Run	Displacement ( $\mu\text{m}$ )				Pressure (kPa)	
	LV-001	LV-002	LV-003	LV-004	PC-001	PC-002
<b>Single Axle 8 km/h Test Runs</b>						
1	187	37	36	111	12.98	14.02
2	192	36	35	112	12.69	13.69
3	187	36	35	112	12.98	14.24
<b>Tandem Axle 8 km/h Test Runs</b>						
1	160	19	19	91	10.54	11.73
2	156	19	19	90	10.27	11.89
3	158	19	18	91	10.51	11.93
<b>Single Axle 48 km/h Test Runs</b>						
1	153	28	27	94	11.62	12.25
2	164	30	26	88	11.47	13.15
3	172	31	27	93	11.05	13.27
<b>Tandem Axle 48 km/h Test Runs</b>						
1	136	17	15	73	9.95	11.47
2	125	16	15	68	9.27	11.80
3	133	16	18	75	9.71	9.94
<b>Single Axle 89 km/h Test Runs</b>						
1	138	23	25	89	8.85	10.75
2	122	21	23	81	10.80	12.16
3	126	21	23	84	10.07	11.51
<b>Tandem Axle 89 km/h Test Runs</b>						
1	133	12	15	70	8.84	10.76
2	130	13	15	73	8.60	10.56
3	134	12	14	71	8.83	10.86

Note: LV-001 and LV-004 were deep LVDTs and LV-002 and LV-003 were shallow LVDTs

Table H.8a Maximum displacements and pressures on the 15 in (38 cm) section with tire pressure of 110 psi (758 kPa) – English units, Winter data

Run	Displacement (mil)				Pressure (psi)	
	LV-001	LV-002	LV-003	LV-004	PC-001	PC-002
<b>Single Axle 5 mph Test Runs</b>						
<b>1</b>	7.14	1.44	1.39	4.21	1.802	1.959
<b>2</b>	7.11	1.47	1.35	4.27	1.782	1.967
<b>3</b>	7.06	1.47	1.38	4.22	1.781	1.940
<b>Tandem Axle 5 mph Test Runs</b>						
<b>1</b>	6.08	0.74	0.81	3.36	1.415	1.635
<b>2</b>	5.96	0.68	0.67	3.55	1.453	1.651
<b>3</b>	6.19	0.70	0.64	3.40	1.473	1.646
<b>Single Axle 30 mph Test Runs</b>						
<b>1</b>	6.07	1.07	1.18	3.36	1.668	1.661
<b>2</b>	6.34	1.21	1.10	3.39	1.709	1.793
<b>3</b>	6.21	1.14	1.13	3.51	1.704	1.795
<b>Tandem Axle 30 mph Test Runs</b>						
<b>1</b>	5.44	0.58	0.57	2.82	1.346	1.573
<b>2</b>	5.49	0.63	0.60	2.72	1.311	1.531
<b>3</b>	5.42	0.63	0.62	2.74	1.300	1.483
<b>Single Axle 55 mph Test Runs</b>						
<b>1</b>	4.48	0.73	0.80	2.64	1.360	1.384
<b>2</b>	5.10	0.87	0.95	3.06	1.343	1.463
<b>3</b>	5.46	0.99	0.80	2.90	1.354	1.299
<b>Tandem Axle 55 mph Test Runs</b>						
<b>1</b>	3.65	0.49	0.62	3.34	1.248	1.081
<b>2</b>	3.82	0.54	0.59	3.07	1.281	1.214
<b>3</b>	4.08	0.45	0.51	2.78	1.251	1.312

Note: LV-001 and LV-004 were deep LVDTs and LV-002 and LV-003 were shallow LVDTs

Table H.8b Maximum displacements and pressures on the 15 in (38 cm) section with tire pressure of 110 psi (758 kPa) – metric units, Winter data

Run	Displacement ( $\mu\text{m}$ )				Pressure (kPa)	
	LV-001	LV-002	LV-003	LV-004	PC-001	PC-002
<b>Single Axle 8 km/h Test Runs</b>						
1	181	37	35	107	12.42	13.51
2	181	37	34	108	12.29	13.56
3	179	37	35	107	12.28	13.38
<b>Tandem Axle 8 km/h Test Runs</b>						
1	154	19	21	85	9.76	11.27
2	151	17	17	90	10.02	11.38
3	157	18	16	86	10.16	11.35
<b>Single Axle 48 km/h Test Runs</b>						
1	154	27	30	85	11.50	11.45
2	161	31	28	86	11.78	12.36
3	158	29	29	89	11.75	12.38
<b>Tandem Axle 48 km/h Test Runs</b>						
1	138	15	14	72	9.28	10.85
2	139	16	15	69	9.04	10.56
3	138	16	16	70	8.96	10.22
<b>Single Axle 89 km/h Test Runs</b>						
1	114	19	20	67	9.38	9.54
2	130	22	24	78	9.26	10.09
3	139	25	20	74	9.34	8.96
<b>Tandem Axle 89 km/h Test Runs</b>						
1	93	12	16	85	8.60	7.45
2	97	14	15	78	8.83	8.37
3	104	11	13	71	8.63	9.05

Note: LV-001 and LV-004 were deep LVDTs and LV-002 and LV-003 were shallow LVDTs

Table H.9a Maximum displacements and pressures on the 15 in (38 cm) section with tire pressure of 125 psi (862 kPa) – English units, Winter data

Run	Displacement (mil)				Pressure (psi)	
	LV-001	LV-002	LV-003	LV-004	PC-001	PC-002
<b>Single Axle 5 mph Test Runs</b>						
<b>1</b>	6.46	1.23	1.27	3.76	1.628	1.817
<b>2</b>	7.07	1.28	1.24	3.74	1.643	1.863
<b>3</b>	6.59	1.34	1.30	3.91	1.693	1.858
<b>Tandem Axle 5 mph Test Runs</b>						
<b>1</b>	6.17	0.77	0.79	3.17	1.371	1.591
<b>2</b>	6.24	0.74	0.68	3.21	1.417	1.610
<b>3</b>	6.24	0.87	0.86	3.34	1.419	1.588
<b>Single Axle 30 mph Test Runs</b>						
<b>1</b>	6.05	1.14	0.99	3.34	1.649	1.653
<b>2</b>	5.70	1.04	0.98	3.40	1.512	1.548
<b>3</b>	5.08	0.87	1.04	3.05	1.416	1.618
<b>Tandem Axle 30 mph Test Runs</b>						
<b>1</b>	4.95	0.70	0.67	2.80	1.207	1.487
<b>2</b>	5.09	0.60	0.56	2.72	1.335	1.424
<b>3</b>	5.08	0.59	0.57	2.71	1.315	1.507
<b>Single Axle 55 mph Test Runs</b>						
<b>1</b>	5.10	0.96	0.93	3.07	1.114	1.234
<b>2</b>	5.09	0.94	0.88	3.00	1.248	1.412
<b>3</b>	4.97	0.91	0.82	2.78	1.311	1.340
<b>Tandem Axle 55 mph Test Runs</b>						
<b>1</b>	3.75	0.39	0.52	2.66	1.160	1.261
<b>2</b>	3.83	0.37	0.54	2.63	1.178	1.292
<b>3</b>	3.86	0.40	0.56	2.69	1.226	1.311

Note: LV-001 and LV-004 were deep LVDTs and LV-002 and LV-003 were shallow LVDTs

Table H.9b Maximum displacements and pressures on the 15 in (38 cm) section with tire pressure of 125 psi (862 kPa) – metric units, Winter data

Run	Displacement ( $\mu\text{m}$ )				Pressure (kPa)	
	LV-001	LV-002	LV-003	LV-004	PC-001	PC-002
<b>Single Axle 8 km/h Test Runs</b>						
1	164	31	32	96	11.22	12.53
2	180	33	31	95	11.33	12.84
3	167	34	33	99	11.67	12.81
<b>Tandem Axle 8 km/h Test Runs</b>						
1	157	20	20	81	9.45	10.97
2	158	19	17	82	9.77	11.10
3	158	22	22	85	9.78	10.95
<b>Single Axle 48 km/h Test Runs</b>						
1	154	29	25	85	11.37	11.40
2	145	26	25	86	10.42	10.67
3	129	22	26	77	9.76	11.16
<b>Tandem Axle 48 km/h Test Runs</b>						
1	126	18	17	71	8.32	10.25
2	129	15	14	69	9.20	9.82
3	129	15	14	69	9.07	10.39
<b>Single Axle 89 km/h Test Runs</b>						
1	130	24	24	78	7.68	8.51
2	129	24	22	76	8.60	9.74
3	126	23	21	71	9.04	9.24
<b>Tandem Axle 89 km/h Test Runs</b>						
1	95	10	13	68	8.00	8.69
2	97	9	14	67	8.12	8.91
3	98	10	14	68	8.45	9.04

Note: LV-001 and LV-004 were deep LVDTs and LV-002 and LV-003 were shallow LVDTs

Summer data

Table H.10a Maximum displacements and pressures on the 11 in (28 cm) section with tire pressure of 80 psi (552 kPa) – English units, Summer data

Run	Displacement (mil)				Pressure (psi)	
	LV-001	LV-002	LV-003	LV-004	PC-001	PC-002
Single Axle 5 mph Test Runs						
1	10.41	4.02	4.43	7.98	11.12	10.71
2	10.53	3.66	4.04	7.85	10.18	9.62
3	7.32	2.34	2.54	5.95	7.36	7.93
Tandem Axle 5 mph Test Runs						
1	8.08	2.66	2.47	5.86	7.47	7.88
2	8.31	2.75	2.71	5.76	7.60	7.87
3	5.91	1.69	1.65	4.26	5.73	5.99
Single Axle 30 mph Test Runs						
1	7.66	2.43	2.46	5.81	6.17	7.70
2	7.35	2.61	3.08	6.49	6.41	9.84
3	5.50	1.72	2.33	5.37	6.51	5.86
Tandem Axle 30 mph Test Runs						
1	6.43	1.75	2.19	5.28	5.49	5.37
2	7.60	2.13	2.27	5.14	5.16	6.15
3	5.60	1.47	1.43	3.89	4.63	6.73
Single Axle 55 mph Test Runs						
1	6.04	1.94	2.15	5.01	7.40	7.29
2	5.99	1.93	2.19	5.10	7.39	7.11
Tandem Axle 55 mph Test Runs						
1	4.94	1.41	1.34	3.87	4.54	6.62
2	5.68	1.47	1.48	4.00	4.63	6.70

Note: LV-001 and LV-004 were deep LVDTs and LV-002 and LV-003 were shallow LVDTs  
There was no third run at 55 mph



Table H.10b Maximum displacements and pressures on the 11 in (28 cm) section with tire pressure of (552 kPa) – metric units, Summer data

Run	Displacement ( $\mu\text{m}$ )				Pressure (kPa)	
	LV-001	LV-002	LV-003	LV-004	PC-001	PC-002
Single Axle 8 km/h Test Runs						
1	264	102	113	203	77	74
2	267	93	103	199	70	66
3	186	59	65	151	51	55
Tandem Axle 8 km/h Test Runs						
1	205	68	63	149	52	54
2	211	70	69	146	52	54
3	150	43	42	108	40	41
Single Axle 48 km/h Test Runs						
1	195	62	62	148	43	53
2	187	66	78	165	44	68
3	140	44	59	136	45	40
Tandem Axle 48 km/h Test Runs						
1	163	44	56	134	38	37
2	193	54	58	131	36	42
3	142	37	36	99	32	46
Single Axle 89 km/h Test Runs						
1	153	49	55	127	51	50
2	152	49	56	130	51	49
Tandem Axle 89 km/h Test Runs						
1	125	36	34	98	31	46
2	144	37	38	102	32	46

Note: LV-001 and LV-004 were deep LVDTs and LV-002 and LV-003 were shallow LVDTs  
There was no third run at 89 km/h

Table H.11a Maximum displacements and pressures on the 11 in (28 cm) section with tire pressure of 110 psi (758 kPa) – English units, Summer data

Run	Displacement (mil)				Pressure (psi)	
	LV-001	LV-002	LV-003	LV-004	PC-001	PC-002
Single Axle 5 mph Test Runs						
1	10.05	3.92	4.27	7.70	9.82	11.00
2	10.07	3.81	4.22	7.61	10.23	11.68
3	11.19	4.12	4.63	8.15	10.69	10.92
Tandem Axle 5 mph Test Runs						
1	7.38	2.64	2.78	5.66	7.13	7.95
2	7.07	2.68	2.66	5.21	6.18	7.40
3	7.82	2.54	2.36	5.86	7.49	7.68
Single Axle 30 mph Test Runs						
1	7.03	2.42	2.63	5.78	6.28	8.30
2	6.79	2.04	2.25	5.47	6.71	6.86
3	6.53	2.13	2.28	5.65	6.33	7.78
Tandem Axle 30 mph Test Runs						
1	5.77	1.70	1.72	4.32	5.25	6.60
2	6.02	1.70	1.86	4.75	4.98	5.57
3	6.02	1.66	1.75	4.58	5.13	5.58
Single Axle 55 mph Test Runs						
1	6.40	2.09	1.89	4.68	6.04	7.74
2	5.63	1.63	1.36	4.10	5.12	6.50
3	6.56	2.02	1.79	4.57	6.12	7.69
Tandem Axle 55 mph Test Runs						
1	4.74	1.44	1.06	3.73	5.55	4.80
2	4.41	1.42	1.08	3.74	5.66	4.97
3	4.77	1.44	1.09	3.77	5.46	4.98

Note: LV-001 and LV-004 were deep LVDTs and LV-002 and LV-003 were shallow LVDTs

Table H.11b Maximum displacements and pressures on the 11 in (28 cm) section with tire pressure of 110 psi (758 kPa) – metric units, Summer data

Run	Displacement ( $\mu\text{m}$ )				Pressure (kPa)	
	LV-001	LV-002	LV-003	LV-004	PC-001	PC-002
Single Axle 8 km/h Test Runs						
1	255	100	108	196	68	76
2	256	97	107	193	71	81
3	284	105	118	207	74	75
Tandem Axle 8 km/h Test Runs						
1	187	67	71	144	49	55
2	180	68	68	132	43	51
3	199	65	60	149	52	53
Single Axle 30 mph (48 km/h) Test Runs						
1	179	61	67	147	43	57
2	172	52	57	139	46	47
3	166	54	58	144	44	54
Tandem Axle 30 mph (48 km/h) Test Runs						
1	147	43	44	110	36	46
2	153	43	47	121	34	38
3	153	42	44	116	35	39
Single Axle 55 mph (89 km/h) Test Runs						
1	163	53	48	119	42	53
2	143	41	35	104	35	45
3	167	51	45	116	42	53
Tandem Axle 55 mph (89 km/h) Test Runs						
1	120	37	27	95	38	33
2	112	36	27	95	39	34
3	121	37	28	96	38	34

Note: LV-001 and LV-004 were deep LVDTs and LV-002 and LV-003 were shallow LVDTs

Table H.12a Maximum displacements and pressures on the 11 in (28 cm) section with tire pressure of 125 psi (862 kPa) – English units, Summer data

Run	Displacement (mil)				Pressure (psi)	
	LV-001	LV-002	LV-003	LV-004	PC-001	PC-002
Single Axle 5 mph Test Runs						
1	8.57	3.42	3.48	NA	8.03	8.97
2	10.48	3.85	4.08	NA	10.84	10.41
3	10.92	4.01	4.23	NA	10.03	11.47
Tandem Axle 5 mph Test Runs						
1	6.99	2.24	2.82	NA	6.84	7.76
2	6.98	2.52	2.13	NA	6.85	7.33
3	6.91	2.32	2.08	NA	6.69	7.63
Single Axle 30 mph Test Runs						
1	7.08	2.17	2.53	NA	7.78	6.46
2	7.03	2.27	2.00	4.52	5.36	6.32
3	7.09	2.25	2.09	4.95	6.24	6.48
Tandem Axle 30 mph Test Runs						
1	4.89	1.39	1.42	NA	5.02	5.26
2	5.87	1.50	1.83	3.99	5.32	4.98
3	5.12	1.44	1.47	3.53	5.33	5.54
Single Axle 55 mph Test Runs						
1	6.04	1.79	1.96	4.90	4.12	5.50
2	5.84	1.66	1.89	4.85	4.08	5.21
3	5.89	1.62	1.81	4.79	4.14	5.20
Tandem Axle 55 mph Test Runs						
1	4.42	1.44	1.03	3.65	4.72	4.90
2	4.80	1.45	1.10	3.78	4.80	4.98
3	4.71	1.51	1.11	3.89	4.90	5.22

Note: LV-001 and LV-004 were deep LVDTs and LV-002 and LV-003 were shallow LVDTs

Table H.12b Maximum displacements and pressures on the 11 in (28 cm) section with tire pressure of 125 psi (862 kPa) – metric units, Summer data

Run	Displacement ( $\mu\text{m}$ )				Pressure (kPa)	
	LV-001	LV-002	LV-003	LV-004	PC-001	PC-002
Single Axle 8 km/h Test Runs						
1	218	87	88	NA	55	62
2	266	98	104	NA	75	72
3	277	102	107	NA	69	79
Tandem Axle 8 km/h Test Runs						
1	178	57	72	NA	47	53
2	177	64	54	NA	47	51
3	176	59	53	NA	46	53
Single Axle 48 km/h Test Runs						
1	180	55	64	NA	54	45
2	179	58	51	115	37	44
3	180	57	53	126	43	45
Tandem Axle 48 km/h Test Runs						
1	124	35	36	NA	35	36
2	149	38	46	101	37	34
3	130	37	37	90	37	38
Single Axle 89 km/h Test Runs						
1	153	45	50	124	28	38
2	148	42	48	123	28	36
3	150	41	46	122	29	36
Tandem Axle 89 km/h Test Runs						
1	112	37	26	93	33	34
2	122	37	28	96	33	34
3	120	38	28	99	34	36

Note: LV-001 and LV-004 were deep LVDTs and LV-002 and LV-003 were shallow LVDTs

Table H.13a Maximum displacements and pressures on the 13 in (33 cm) section with tire pressure of 80 psi (552 kPa) – English units, Summer data

Run	Displacement (mil)				Pressure (psi)	
	LV-001	LV-002	LV-003	LV-004	PC-001	PC-002
Single Axle 5 mph Test Runs						
1	6.02	NA	4.59	8.49	2.81	4.42
2	6.82	NA	5.09	9.04	3.04	4.81
3	6.25	NA	4.84	8.80	2.70	4.48
Tandem Axle 5 mph Test Runs						
1	4.37	NA	3.48	6.92	1.99	3.46
2	4.44	NA	3.25	7.01	2.11	3.68
3	4.84	NA	2.56	7.20	2.03	3.52
Single Axle 30 mph Test Runs						
1	3.66	NA	2.19	5.56	1.48	1.99
2	4.14	NA	2.77	5.92	1.61	2.60
3	3.64	NA	2.46	5.40	1.37	2.22
Tandem Axle 30 mph Test Runs						
1	3.83	NA	2.24	5.70	1.32	2.53
2	3.46	NA	1.71	5.70	1.36	2.55
3	3.42	NA	1.73	5.75	1.36	2.59
Single Axle 55 mph Test Runs						
1	3.58	NA	2.10	5.34	1.25	1.96
2	3.39	NA	2.26	5.47	1.44	2.19
3	3.46	NA	2.28	5.54	1.38	2.09
Tandem Axle 55 mph Test Runs						
1	3.04	NA	1.68	5.45	1.24	2.32
2	3.34	NA	1.80	5.29	1.28	2.37
3	3.34	NA	1.80	5.31	1.20	2.55

Note: LV-001 and LV-004 were deep LVDTs and LV-002 and LV-003 were shallow LVDTs

Table H.13b Maximum displacements and pressures on the 13 in (33 cm) section with tire pressure of 80 psi (552 kPa) – metric units, Summer data

Run	Displacement ( $\mu\text{m}$ )				Pressure (kPa)	
	LV-001	LV-002	LV-003	LV-004	PC-001	PC-002
Single Axle 8 km/h Test Runs						
1	153	NA	117	216	19	30
2	173	NA	129	230	21	33
3	159	NA	123	224	19	31
Tandem Axle 8 km/h Test Runs						
1	111	NA	88	176	14	24
2	113	NA	83	178	15	25
3	123	NA	65	183	14	24
Single Axle 48 km/h Test Runs						
1	93	NA	56	141	10	14
2	105	NA	70	150	11	18
3	92	NA	62	137	9	15
Tandem Axle 48 km/h Test Runs						
1	97	NA	57	145	9	17
2	88	NA	43	145	9	18
3	87	NA	44	146	9	18
Single Axle 89 km/h Test Runs						
1	91	NA	53	136	9	13
2	86	NA	57	139	10	15
3	88	NA	58	141	10	14
Tandem Axle 89 km/h Test Runs						
1	77	NA	43	138	9	16
2	85	NA	46	134	9	16
3	85	NA	46	135	8	18

Note: LV-001 and LV-004 were deep LVDTs and LV-002 and LV-003 were shallow LVDTs

Table H.14a Maximum displacements and pressures on the 13 in (33 cm) section with tire pressure of 110 psi (758 kPa) – English units, Summer data

Run	Displacement (mil)				Pressure (psi)	
	LV-001	LV-002	LV-003	LV-004	PC-001	PC-002
Single Axle 5 mph Test Runs						
1	5.24	NA	3.95	7.65	2.33	4.20
2	5.56	NA	4.11	7.94	2.54	4.32
3	5.45	NA	4.16	7.82	2.59	4.22
Tandem Axle 5 mph Test Runs						
1	3.92	NA	2.71	6.82	1.83	2.94
2	4.12	NA	2.77	6.27	1.81	3.21
3	4.09	NA	2.08	6.46	1.84	3.15
Single Axle 30 mph Test Runs						
1	4.09	NA	2.77	6.14	1.60	2.18
2	3.54	NA	2.47	5.40	1.34	2.19
3	3.87	NA	2.49	5.46	1.48	2.11
Tandem Axle 30 mph Test Runs						
1	3.12	NA	1.67	5.11	1.11	1.92
2	3.14	NA	1.61	5.18	1.16	2.23
3	3.03	NA	1.34	4.88	1.14	1.99
Single Axle 55 mph Test Runs						
1	3.02	NA	1.62	4.62	1.10	1.65
2	3.12	NA	2.02	5.28	1.22	1.83
3	3.43	NA	2.29	5.65	1.30	2.16
Tandem Axle 55 mph Test Runs						
1	2.85	NA	1.35	4.62	1.07	2.14
2	3.06	NA	1.64	4.81	1.09	2.05
3	2.94	NA	1.95	4.86	1.01	1.72

Note: LV-001 and LV-004 were deep LVDTs and LV-002 and LV-003 were shallow LVDTs



Table H.14b Maximum displacements and pressures on the 13 in (33 cm) section with tire pressure of 110 psi (758 kPa) – metric units, Summer data

Run	Displacement ( $\mu\text{m}$ )				Pressure (kPa)	
	LV-001	LV-002	LV-003	LV-004	PC-001	PC-002
Single Axle 8 km/h Test Runs						
1	133	NA	100	194	16	29
2	141	NA	104	202	17	30
3	138	NA	106	199	18	29
Tandem Axle 8 km/h Test Runs						
1	100	NA	69	173	13	20
2	105	NA	70	159	12	22
3	104	NA	53	164	13	22
Single Axle 48 km/h Test Runs						
1	104	NA	70	156	11	15
2	90	NA	63	137	9	15
3	98	NA	63	139	10	15
Tandem Axle 48 km/h Test Runs						
1	79	NA	42	130	8	13
2	80	NA	41	132	8	15
3	77	NA	34	124	8	14
Single Axle 89 km/h Test Runs						
1	77	NA	41	117	8	11
2	79	NA	51	134	8	13
3	87	NA	58	144	9	15
Tandem Axle 89 km/h Test Runs						
1	72	NA	34	117	7	15
2	78	NA	42	122	8	14
3	75	NA	50	123	7	12

Note: LV-001 and LV-004 were deep LVDTs and LV-002 and LV-003 were shallow LVDTs

Table H.15a Maximum displacements and pressures on the 13 in (33 cm) section with tire pressure of 125 psi (862 kPa) – English units, Summer data

Run	Displacement (mil)				Pressure (psi)	
	LV-001	LV-002	LV-003	LV-004	PC-001	PC-002
Single Axle 5 mph Test Runs						
1	5.11	NA	3.51	7.02	2.32	3.65
2	5.14	NA	3.77	7.34	2.43	3.90
3	5.21	NA	3.78	7.53	2.54	3.79
Tandem Axle 5 mph Test Runs						
1	3.58	NA	1.99	5.93	1.84	2.69
2	3.76	NA	1.99	6.13	1.85	3.07
3	4.04	NA	1.96	6.13	1.79	2.97
Single Axle 30 mph Test Runs						
1	3.13	NA	2.05	4.82	1.39	1.78
2	3.18	NA	1.73	4.38	1.23	1.81
3	3.25	NA	2.14	4.66	1.31	1.92
Tandem Axle 30 mph Test Runs						
1	2.87	NA	1.26	4.75	1.19	2.10
2	2.94	NA	1.51	5.06	1.14	2.06
3	3.07	NA	1.60	5.01	1.09	2.03
Single Axle 55 mph Test Runs						
1	2.94	NA	1.85	4.89	1.21	1.79
2	2.74	NA	1.40	4.40	1.02	1.58
3	3.21	NA	2.11	5.31	1.21	2.06
Tandem Axle 55 mph Test Runs						
1	2.99	NA	1.36	4.47	1.07	2.06
2	2.79	NA	1.09	4.23	1.09	2.14
3	3.05	NA	1.79	4.70	1.02	1.85

Note: LV-001 and LV-004 were deep LVDTs and LV-002 and LV-003 were shallow LVDTs

Table H.15b Maximum displacements and pressures on the 13 in (33 cm) section with tire pressure of 125 psi (862 kPa) – metric units, Summer data

Run	Displacement ( $\mu\text{m}$ )				Pressure (kPa)	
	LV-001	LV-002	LV-003	LV-004	PC-001	PC-002
Single Axle 8 km/h Test Runs						
1	130	NA	89	178	16	25
2	131	NA	96	186	17	27
3	132	NA	96	191	17	26
Tandem Axle 8 km/h Test Runs						
1	91	NA	51	151	13	19
2	96	NA	51	156	13	21
3	103	NA	50	156	12	20
Single Axle 48 km/h Test Runs						
1	80	NA	52	122	10	12
2	81	NA	44	111	8	12
3	83	NA	54	118	9	13
Tandem Axle 48 km/h Test Runs						
1	73	NA	32	121	8	14
2	75	NA	38	129	8	14
3	78	NA	41	127	7	14
Single Axle 89 km/h Test Runs						
1	75	NA	47	124	8	12
2	70	NA	36	112	7	11
3	82	NA	54	135	8	14
Tandem Axle 89 km/h Test Runs						
1	76	NA	35	114	7	14
2	71	NA	28	107	8	15
3	77	NA	45	119	7	13

Note: LV-001 and LV-004 were deep LVDTs and LV-002 and LV-003 were shallow LVDTs

Table H.16a Maximum displacements and pressures on the 15 in (38 cm) section with tire pressure of 80 psi (552 kPa) – English units, Summer data

Run	Displacement (mil)				Pressure (psi)	
	LV-001	LV-002	LV-003	LV-004	PC-001	PC-002
Single Axle 5 mph Test Runs						
1	NA	6.56	5.03	10.89	1.59	2.78
2	NA	6.75	4.52	10.62	1.65	2.75
3	NA	6.77	4.98	11.23	1.63	2.78
Tandem Axle 5 mph Test Runs						
1	NA	3.47	2.29	10.36	1.65	2.96
2	NA	4.06	2.70	10.98	1.68	2.97
3	NA	2.99	2.05	10.83	1.78	3.14
Single Axle 30 mph Test Runs						
1	NA	3.96	2.81	7.80	1.21	2.21
2	NA	3.85	2.99	7.52	1.21	2.34
3	NA	4.00	2.93	7.79	1.28	2.37
Tandem Axle 30 mph Test Runs						
1	NA	2.39	1.47	7.89	1.38	2.87
2	NA	2.62	2.24	9.14	1.48	2.69
3	NA	2.34	2.39	9.03	1.46	2.60
Single Axle 55 mph Test Runs						
1	NA	2.71	2.30	7.55	0.90	1.75
2	NA	3.01	2.21	7.70	0.92	1.76
3	NA	2.61	2.36	7.70	0.92	1.78
Tandem Axle 55 mph Test Runs						
1	NA	1.45	1.55	7.70	1.40	2.46
2	NA	1.52	1.80	7.80	1.41	2.51
3	NA	1.38	1.45	7.58	1.43	2.49

Note: LV-001 and LV-004 were deep LVDTs and LV-002 and LV-003 were shallow LVDTs

Table H.16b Maximum displacements and pressures on the 15 in (38 cm) section with tire pressure of 80 psi (552 kPa) – metric units, Summer data

Run	Displacement ( $\mu\text{m}$ )				Pressure (kPa)	
	LV-001	LV-002	LV-003	LV-004	PC-001	PC-002
Single Axle 8 km/h Test Runs						
1	NA	167	128	277	11	19
2	NA	171	115	270	11	19
3	NA	172	126	285	11	19
Tandem Axle 8 km/h Test Runs						
1	NA	88	58	263	11	20
2	NA	103	69	279	12	20
3	NA	76	52	275	12	22
Single Axle 48 km/h Test Runs						
1	NA	101	71	198	8	15
2	NA	98	76	191	8	16
3	NA	102	74	198	9	16
Tandem Axle 48 km/h Test Runs						
1	NA	61	37	200	10	20
2	NA	67	57	232	10	19
3	NA	59	61	229	10	18
Single Axle 89 km/h Test Runs						
1	NA	69	58	192	6	12
2	NA	76	56	196	6	12
3	NA	66	60	196	6	12
Tandem Axle 89 km/h Test Runs						
1	NA	37	39	196	10	17
2	NA	39	46	198	10	17
3	NA	35	37	193	10	17

Note: LV-001 and LV-004 were deep LVDTs and LV-002 and LV-003 were shallow LVDTs

Table H.17a Maximum displacements and pressures on the 15 in (38 cm) section with tire pressure of 110 psi (758 kPa) – English units, Summer data

Run	Displacement (mil)				Pressure (psi)	
	LV-001	LV-002	LV-003	LV-004	PC-001	PC-002
Single Axle 5 mph Test Runs						
1	NA	5.12	3.69	9.87	1.56	2.70
2	NA	5.05	3.46	9.90	1.56	2.75
3	NA	4.76	3.62	9.78	1.56	2.64
Tandem Axle 5 mph Test Runs						
1	NA	3.67	2.21	9.97	1.71	2.80
2	NA	2.57	1.78	9.55	1.67	2.90
3	NA	3.78	1.91	10.45	1.69	3.04
Single Axle 30 mph Test Runs						
1	NA	2.97	2.02	5.98	1.03	2.35
2	NA	2.92	2.35	6.37	1.05	2.15
3	NA	3.21	2.20	6.32	1.09	2.45
Tandem Axle 30 mph Test Runs						
1	NA	2.07	1.42	7.72	1.34	2.58
2	NA	2.07	1.44	8.22	1.36	2.68
3	NA	1.95	1.44	7.91	1.39	2.64
Single Axle 55 mph Test Runs						
1	NA	2.36	1.78	6.65	0.97	1.76
2	NA	2.37	1.75	6.59	0.97	1.72
3	NA	2.46	2.00	6.93	0.99	1.77
Tandem Axle 55 mph Test Runs						
1	NA	1.36	1.51	8.56	1.28	1.93
2	NA	2.08	1.80	8.76	1.22	1.87
3	NA	1.24	1.43	8.55	1.28	1.95

Note: LV-001 and LV-004 were deep LVDTs and LV-002 and LV-003 were shallow LVDTs

Table H.17b Maximum displacements and pressures on the 15 in (38 cm) section with tire pressure of 110 psi (758 kPa) – metric units, Summer data

Run	Displacement ( $\mu\text{m}$ )				Pressure (kPa)	
	LV-001	LV-002	LV-003	LV-004	PC-001	PC-002
Single Axle 8 km/h Test Runs						
1	NA	130	94	251	11	19
2	NA	128	88	251	11	19
3	NA	121	92	248	11	18
Tandem Axle 8 km/h Test Runs						
1	NA	93	56	253	12	19
2	NA	65	45	243	11	20
3	NA	96	49	265	12	21
Single Axle 48 km/h Test Runs						
1	NA	75	51	152	7	16
2	NA	74	60	162	7	15
3	NA	82	56	161	7	17
Tandem Axle 48 km/h Test Runs						
1	NA	53	36	196	9	18
2	NA	53	37	209	9	18
3	NA	50	37	201	10	18
Single Axle 89 km/h Test Runs						
1	NA	60	45	169	7	12
2	NA	60	44	167	7	12
3	NA	62	51	176	7	12
Tandem Axle 89 km/h Test Runs						
1	NA	35	38	217	9	13
2	NA	53	46	223	8	13
3	NA	31	36	217	9	13

Note: LV-001 and LV-004 were deep LVDTs and LV-002 and LV-003 were shallow LVDTs

Table H.18a Maximum displacements and pressures on the 15 in (38 cm) section with tire pressure of 125 psi (862 kPa) – English units, Summer data

Run	Displacement (mil)				Pressure (psi)	
	LV-001	LV-002	LV-003	LV-004	PC-001	PC-002
Single Axle 5 mph Test Runs						
1	NA	NA	NA	NA	1.48	2.72
2	NA	NA	NA	NA	1.46	2.81
3	NA	NA	NA	NA	1.52	2.76
Tandem Axle 5 mph Test Runs						
1	NA	NA	NA	NA	1.59	2.82
2	NA	NA	NA	NA	1.56	2.87
3	NA	NA	NA	NA	1.56	2.78
Single Axle 30 mph Test Runs						
1	NA	3.11	1.82	7.04	1.07	2.35
2	NA	3.05	2.15	6.73	1.21	2.08
3	NA	2.75	1.56	6.29	1.15	2.22
Tandem Axle 30 mph Test Runs						
1	NA	1.88	1.32	7.59	1.41	2.51
2	NA	2.27	1.94	8.10	1.36	2.45
3	NA	2.08	1.71	7.90	1.33	2.56
Single Axle 55 mph Test Runs						
1	NA	2.13	1.77	6.52	0.94	1.68
2	NA	2.18	1.75	6.56	0.92	1.66
3	NA	2.14	1.81	6.57	0.91	1.63
Tandem Axle 55 mph Test Runs						
1	NA	1.49	1.29	7.89	1.19	1.81
2	NA	1.29	1.44	8.18	1.25	1.92
3	NA	1.18	1.23	7.99	1.22	1.88

Note: LV-001 and LV-004 were deep LVDTs and LV-002 and LV-003 were shallow LVDTs



Table H.18b Maximum displacements and pressures on the 15 in (38 cm) section with tire pressure of 125 psi (862 kPa) – metric units, Summer data

Run	Displacement ( $\mu\text{m}$ )				Pressure (kPa)	
	LV-001	LV-002	LV-003	LV-004	PC-001	PC-002
Single Axle 8 km/h Test Runs						
1	NA	NA	NA	NA	10	19
2	NA	NA	NA	NA	10	19
3	NA	NA	NA	NA	11	19
Tandem Axle 8 km/h Test Runs						
1	NA	NA	NA	NA	11	19
2	NA	NA	NA	NA	11	20
3	NA	NA	NA	NA	11	19
Single Axle 48 km/h Test Runs						
1	NA	79	46	179	7	16
2	NA	77	55	171	8	14
3	NA	70	40	160	8	15
Tandem Axle 48 km/h Test Runs						
1	NA	48	34	193	10	17
2	NA	58	49	206	9	17
3	NA	53	43	201	9	18
Single Axle 89 km/h Test Runs						
1	NA	54	45	166	6	12
2	NA	55	44	167	6	11
3	NA	54	46	167	6	11
Tandem Axle 89 km/h Test Runs						
1	NA	38	33	200	8	12
2	NA	33	37	208	9	13
3	NA	30	31	203	8	13

Note: LV-001 and LV-004 were deep LVDTs and LV-002 and LV-003 were shallow LVDTs

**Appendix I: Lateral tire offset data from CVL testing on DEL-23.**

Table I.1a Average lateral tire offset – English units ( in), Winter data

Run	11 in (28 cm) Section			13 in (33 cm) Section			15 in (38 cm) Section		
	Pressure (psi)								
	80	110	125	80	110	125	80	110	125
Single Axle 5 mph Test Runs									
1	0.13	3.51	0.38	3.76	1.63	1.00	1.38	3.13	1.51
2	1.88	1.88	0.88	3.38	1.38	1.13	3.38	0.50	3.01
3	0.00	1.26	0.50	3.01	2.26	1.13	3.26	2.76	5.13
Tandem Axle 5 mph Test Runs									
1	0.88	0.37	3.25	1.25	0.75	0.75	1.50	0.88	2.50
2	0.00	0.00	3.50	3.13	1.25	2.25	0.25	1.25	3.00
3	0.50	1.00	0.63	2.00	0.63	0.01	0.13	0.00	2.50
Single Axle 30 mph Test Runs									
1	0.38	1.63	0.88	1.38	1.38	1.63	0.88	1.25	3.38
2	0.13	1.25	1.00	1.13	0.13	0.26	1.13	0.76	5.88
3	1.25	0.88	1.63	0.13	0.13	1.50	1.88	1.50	4.38
Tandem Axle 30 mph Test Runs									
1	1.88	3.13	2.63	0.62	3.25	0.38	0.12	0.63	1.87
2	3.13	1.50	0.75	0.00	2.00	0.25	0.50	0.75	1.38
3	3.38	2.50	1.25	2.25	2.50	0.12	0.00	1.37	8.00
Single Axle 55 mph Test Runs									
1	1.26	0.51	1.88	0.13	1.32	3.50	0.13	0.51	1.25
2	0.50	1.88	5.13	2.25	1.38	2.38	0.38	1.38	2.26
3	1.26	3.01	1.88	1.01	2.76	2.76	0.50	0.63	0.38
Tandem Axle 55 mph Test Runs									
1	0.63	5.25	2.25	1.37	2.25	1.63	1.25	0.62	0.62
2	1.37	1.50	1.00	1.13	1.38	1.50	1.00	0.63	0.00
3	0.38	2.63	2.00	0.25	0.25	1.12	0.37	0.88	4.75

Table I.1b Average lateral tire offset – metric units (cm), Winter data

Run	11 in (28 cm) Section			13 in (33 cm) Section			15 in (38 cm) Section		
	Pressure (kPa)								
	552	758	862	552	758	862	552	758	862
Single Axle 8 km/h Test Runs									
1	0.33	8.92	0.97	9.55	4.14	2.54	3.51	7.95	3.84
2	4.78	4.78	2.24	8.59	3.51	2.87	8.59	1.27	7.65
3	0.00	3.20	1.27	7.65	5.74	2.87	8.28	7.01	13.03
Tandem Axle 8 km/h Test Runs									
1	2.24	0.94	8.26	3.18	1.91	1.91	3.81	2.24	6.35
2	0.00	0.00	8.89	7.95	3.18	5.72	0.64	3.18	7.62
3	1.27	2.54	1.60	5.08	1.60	0.03	0.33	0.00	6.35
Single Axle 48 km/h Test Runs									
1	0.97	4.14	2.24	3.51	3.51	4.14	2.24	3.18	8.59
2	0.33	3.18	2.54	2.87	0.33	0.66	2.87	1.93	14.94
3	3.18	2.24	4.14	0.33	0.33	3.81	4.78	3.81	11.13
Tandem Axle 48 km/h Test Runs									
1	4.78	7.95	6.68	1.57	8.26	0.97	0.30	1.60	4.75
2	7.95	3.81	1.91	0.00	5.08	0.64	1.27	1.91	3.51
3	8.59	6.35	3.18	5.72	6.35	0.30	0.00	3.48	20.32
Single Axle 89 km/h Test Runs									
1	3.20	1.30	4.78	0.33	3.35	8.89	0.33	1.30	3.18
2	1.27	4.78	13.03	5.72	3.51	6.05	0.97	3.51	5.74
3	3.20	7.65	4.78	2.57	7.01	7.01	1.27	1.60	0.97
Tandem Axle 89 km/h Test Runs									
1	1.60	13.34	5.72	3.48	5.72	4.14	3.18	1.57	1.57
2	3.48	3.81	2.54	2.87	3.51	3.81	2.54	1.60	0.00
3	0.97	6.68	5.08	0.64	0.64	2.84	0.94	2.24	12.07

Table I.2a Average lateral tire offset – English units ( in), Summer data

Run	11 in (28 cm) Section			13 in (33 cm) Section			15 in (38 cm) Section		
	Tire pressure (psi)								
	80	110	125	80	110	125	80	110	125
Single Axle 5 mph Test Runs									
1	2.13	0.88	2.88	3.38	0.38	4.00	0.63	0.50	3.88
2	3.88	1.63	1.50	2.13	0.75	2.13	2.63	1.00	0.63
3	3.50	0.50	0.63	1.63	1.50	1.50	1.50	0.88	0.88
Tandem Axle 5 mph Test Runs									
1	0.63	2.75	2.00	0.88	2.88	1.38	0.63	2.13	2.25
2	0.50	2.88	2.38	0.00	0.50	1.75	2.25	0.63	1.00
3	0.75	0.13	2.25	1.00	0.88	1.38	1.00	1.13	3.50
Single Axle 30 mph Test Runs									
1	4.13	2.75	0.63	8.88	5.75	6.88	0.00	1.63	4.88
2	1.63	4.38	0.63	6.13	5.38	6.63	1.25	0.25	3.38
3	1.50	4.25	3.50	7.38	5.88	6.75	1.75	0.88	5.88
Tandem Axle 30 mph Test Runs									
1	2.38	0.63	0.88	2.50	3.63	1.00	1.50	1.13	0.25
2	2.88	3.13	4.00	0.25	1.50	2.38	2.50	1.50	3.50
3	1.75	2.25	1.00	0.25	1.75	3.00	2.50	1.50	2.50
Single Axle 55 mph Test Runs									
1	2.13	0.88	2.25	6.88	6.63	5.38	3.75	2.13	0.50
2	1.88	5.63	3.63	5.25	5.00	8.00	1.50	2.50	1.13
3	7.88	2.38	4.00	6.38	2.63	3.13	3.50	0.25	0.25
Tandem Axle 55 mph Test Runs									
1	0.13	0.25	0.88	2.38	1.63	3.25	3.00	2.38	2.50
2	1.25	1.13	1.75	3.25	3.75	0.50	2.63	4.63	1.75
3	11.50	0.50	1.38	1.25	6.00	4.75	1.75	1.88	0.50

Table I.2b Average lateral tire offset – metric units (cm), Summer data

Run	11 in (28 cm) Section			13 in (33 cm) Section			15 in (38 cm) Section		
	Tire pressure (kPa)								
	552	758	862	552	758	862	552	758	862
Single Axle 8 km/h Test Runs									
1	5.40	2.22	7.30	8.57	0.95	10.16	1.59	1.27	9.84
2	9.84	4.13	3.81	5.40	1.91	5.40	6.67	2.54	1.59
3	8.89	1.27	1.59	4.13	3.81	3.81	3.81	2.22	2.22
Tandem Axle 8 km/h Test Runs									
1	1.59	6.99	5.08	2.22	7.30	3.49	1.59	5.40	5.72
2	1.27	7.30	6.03	0.00	1.27	4.45	5.72	1.59	2.54
3	1.91	0.32	5.72	2.54	2.22	3.49	2.54	2.86	8.89
Single Axle 48 km/h Test Runs									
1	10.48	6.99	1.59	22.54	14.61	17.46	0.00	4.13	12.38
2	4.13	11.11	1.59	15.56	13.65	16.83	3.18	0.64	8.57
3	3.81	10.80	8.89	18.73	14.92	17.15	4.45	2.22	14.92
Tandem Axle 48 km/h Test Runs									
1	6.03	1.59	2.22	6.35	9.21	2.54	3.81	2.86	0.64
2	7.30	7.94	10.16	0.64	3.81	6.03	6.35	3.81	8.89
3	4.45	5.72	2.54	0.64	4.45	7.62	6.35	3.81	6.35
Single Axle 89 km/h Test Runs									
1	5.40	2.22	5.72	17.46	16.83	13.65	9.53	5.40	1.27
2	4.76	14.29	9.21	13.34	12.70	20.32	3.81	6.35	2.86
3	20.00	6.03	10.16	16.19	6.67	7.94	8.89	0.64	0.64
Tandem Axle 89 km/h Test Runs									
1	0.32	0.64	2.22	6.03	4.13	8.26	7.62	6.03	6.35
2	3.18	2.86	4.45	8.26	9.53	1.27	6.67	11.75	4.45
3	29.21	1.27	3.49	3.18	15.24	12.07	4.45	4.76	1.27

**Appendix J. PerRoad input values for DEL-23.**

Table K.1 DEL-23 yearly volume by classification

<b>Class</b>	<b>2012</b>	<b>2011</b>	<b>2010</b>	<b>%AADTT</b>
<b>4</b>	15355	20410	17644	1.85%
<b>5</b>	88011	133875	194358	14.41%
<b>6</b>	20629	34935	33899	3.10%
<b>7</b>	19765	39726	29546	3.08%
<b>8</b>	28322	45967	48003	4.23%
<b>9</b>	513809	731327	770020	69.74%
<b>10</b>	6052	8912	10063	0.87%
<b>11</b>	15656	23102	24031	2.17%
<b>12</b>	3805	4995	5126	0.48%
<b>13</b>	665	578	842	0.07%

Table K.2 Average monthly temperature in Delaware, Ohio

Month	Average temperature	
	(°F)	(°C)
January	29	-1.7
February	33	0.6
March	42	5.6
April	54	12.2
May	63	17.2
June	72	22.2
July	75	23.9
August	73	22.8
September	67	19.4
October	55	12.8
November	44	6.7
December	33	0.6





---

ORITE • 151 Stocker Center • Athens, Ohio 45701-2979 • 740-593-1470  
Fax: 740-593-0625 • orite@ohio.edu • <http://www.ohio.edu/orite/>